UiT The Arctic University of Norway

Faculty of Science and Technology, Department of Chemistry

New Corrole Analogues: Isocorroles and Azulicorrole

Simon Larsen

A dissertation for the degree of Philosophiae Doctor, December 2019

A dissertation for the degree of Philosophiae Doctor

New Corrole Analogues: Isocorroles and Azulicorrole

Simon Larsen

Department of Chemistry

Faculty of Science and Technology

UiT – The Arctic University of Norway

Tromsø, Norway

Acknowledgements

I wish to express my deepest gratitude to my advisor Prof. Abhik Ghosh for giving me the opportunity to work in his lab as a PhD student. I also particularly appreciate the faith he bestowed in me when he assigned me a highly exploratory line of work and full freedom to pursue my own ideas, without a great deal of expectations for short-term results. His guidance and expertise have assisted and motivated me ever since I joined his lab as a bachelor student.

My sincere thanks also go to the senior members of our group, Dr. Abraham Alemayehu and Dr. Kolle Thomas. As for a number of other members in our group, they took me under their wing and taught me all I needed to know to become a successful corrole scientist. I shall be forever in their debt.

I also wish to extend my deepest appreciation to my fellow group members and close friends Ivar, Rune, Hans-Kristian, Sumit, Hugo, and Jan, with whom I have shared many laughs and wonderful conversations. A special thanks also goes to Janosch Kettner, who helped me explore trifluoromethylation reactions on corroles, during his stay as an exchange student.

I wish to thank our collaborators Dr. Laura J. McCormick-McPherson, Dr. Simon Teat, Dr. Cina Foroutan-Nejad, and Prof. Jeanet Conradie for their specific contributions to this work. I am also grateful to Truls, Jostein, Fred, Arnfinn, and Johan at my own department for their assistance with spectroscopic analyses and administrative tasks.

Finally, I want to express my deepest appreciation and gratitude to my wonderful family, particularly my fiancé Lill Miriam, my father Steinar, and my late mother Aslaug. If not for their unfaltering support and encouragement, I would not have been able to accomplish what is described in this thesis.

Preface

Porphyrins play a crucial role in life as a key part of several biomolecules, most notably as the heme cofactor in metalloproteins such as hemoglobin and in cytochrome P450. Synthetic analogues of porphyrins understandably also enjoy a variety of applications. Preeminent among these analogues are corroles, whose chemistry has grown by leaps and bounds in the last quarter-century. The focus of this thesis is the synthesis and characterization of *corrole analogues*, namely isocorroles and the new macrocycle azulicorrole.

My interest in isocorroles was piqued by pure chance. Attempts at condensing a highly fluorinated benzaldehyde with pyrrole led to the isolation of a macrocycle whose identity eluded me, owing to low yield and solubility issues. Surprisingly, I isolated analogous products via the interaction of simple corroles and pyrrole in the presence of DDQ. The larger quantity of products available by the latter route allowed their X-ray crystallographic characterization and identification as pyrrole-appended isocorroles.

As part of my coursework, I studied the field of perfluoroalkylation and became intrigued by the possibility of electrophilic trifluoromethylation of corroles. Surprisingly, the use of a Togni reagent led to the isolation of a *meso*-trifluoromethylated isocorrole.

Experimenting with solutions of pyrrole, benzaldehydes, and azulene led me to realize that azulene might be able to compete with pyrrole in cyclocondensation reactions with benzaldehydes. Attempting to steer the condensations towards corrole, using a solvent-free method due to Gryko *et al*., resulted in the formation of minuscule amounts of azulicorrole. Careful optimization of the reaction conditions raised the yield to the point where the macrocycle, along with its copper and gold complexes, could be isolated and characterized. Further optimization of the synthesis as well as new routes to the novel macrocycle remain as key goals for the future.

The above compounds all exhibit strong absorption in the near-infrared, promising potential applications in photodynamic therapy.

The organization of the thesis is as follows:

Chapter 1 provides a general introduction to the realm of porphyrinoids, with emphasis on porphyrins and corroles. Important synthetic methods are discussed, as well as aspects of structure and spectroscopy. Additionally, a brief introduction to the concept of photodynamic

therapy is provided. This Chapter serves as a point of reference, enabling comparisons with the types of macrocycles discussed later in the thesis.

Chapters 2 and **3** are devoted to isoporphyrins and isocorroles, respectively. **Chapter 2** discusses the synthesis, properties and applications of isoporphyrins. **Chapter 3** starts with the synthesis and properties of known isocorroles and concludes with my own new unpublished synthetic studies on isocorroles.

Chapter 4 reviews the field of azuliporphyrin, starting with synthesis and properties of free-base azuliporphyrin and continues discussing the synthesis and properties of metal complexes. **Chapter 5** gives a brief discussion on azulicorrole, as introduction to **Papers C** and **D**.

List of publications and of my contributions therein

Paper A: "Rapid one-pot synthesis of pyrrole-appended isocorroles." Larsen, S.; McCormick, L. J.; Ghosh, A. *Organic & Biomolecular Chemistry* **2019**, 17, 3159-3166.

I synthesized pyrrole-appended isocorroles and their copper complexes and characterized these with ESI-MS, NMR, UV-vis, and cyclic voltammetry experiments. I grew single crystals of two of the compounds, which were solved by Dr. Laura J. McCormick-McPherson at Advanced Light Source, Lawrence Berkeley National Laboratory in Berkeley.

Paper B: "Isocorroles as Homoaromatic NIR-Absorbing Chromophores: A First Quantum Chemical Study." Foroutan-Nejad, C.; Larsen, S.; Conradie, J.; Ghosh, A. *Scientific Reports* **2018**, 8, 11952.

I prepared two new *meso*-methoxy isocorroles, and the nickel complex of one of these, and characterized them with MALDI-TOF MS, NMR, and UV-vis. I participated in the original line of questioning that preceded the study and in the interpretation of the results. The calculations were performed by Dr. Cina Foroutan-Nejad and Prof. Jeanet Conradie.

Paper C: "Azulicorrole." Larsen, S.; McCormick-McPherson, L. J.; Teat, S. J.; Ghosh, A. *ACS Omega* **2019**, 4, 6737-6745.

I prepared the first and only known azulicorrole and its copper and gold complexes and characterized these with ESI-MS, NMR, UV-vis, and cyclic voltammetry experiments. I grew single crystals of two of the compounds, which were solved by Dr. Laura J. McCormick-McPherson and Dr. Simon Teat at Advanced Light Source, Lawrence Berkeley National Laboratory in Berkeley.

Paper D: "Local versus global aromaticity in azuliporphyrin and benziporphyrin derivatives." Ghosh, A.; Larsen, S.; Conradie, J.; Foroutan-Nejad, C. *Organic & Biomolecular Chemistry* **2018**, 16, 7964-7970

I played a major role in the selection of compounds to be studied and in the interpretation of the results. The calculations themselves were performed by Dr. Cina Foroutan-Nejad and Prof. Jeanet Conradie.

Table of contents

List of abbreviations

ATP	adenosine triphosphate
COD	1,5-cyclooctadiene
DBU	1,8-Diazabicyclo[5.4.0]undec-7-ene
DCM	dichloromethane
DDQ	2,3-dichloro-5,6-dicyanobenzoquinone
DFT	density functional theory
DMA	*N*,*N*-dimethylaniline
DMF	*N*,*N*-dimethylformamide
DSSC	dye-sensitized solar cell
EPR	electron paramagnetic resonance
ESI-MS	electron spray ionization mass spectroscopy
IC	internal conversion
ISC	intersystem crossing
MALDI-TOF	matrix-assisted laser desorption-ionization time over flight mass spectrometer
*m*CPBA	*meta*-chloroperoxybenzoic acid
NADPH	nicotinamide adenine dinucleotide phosphate
NBS	*N*-bromosuccinimide
Near-IR	near-infrared
Near-UV	near-ultraviolet
NICS	nucleus independent chemical shift
NMR	nuclear magnetic resonance
PDT	photodynamic therapy

TBACl	tetrabutylammonium chloride
TDDFT	time-dependent density functional theory
TFA	trifluoroacetic acid
THF	tetrahydrofuran
TPC	triphenylcorrole
TPP	tetraphenylporphyrin
UV-vis	ultraviolet-visible

Chapter 1. Porphyrins and corroles

1.1. Introduction to porphyrins and corroles

Porphyrins are an important class of aromatic compounds that are abundant in nature and paramount to all forms of life. Preeminent examples include hemes, iron porphyrins that play a major role in oxygen transport (hemoglobin), oxygen storage (myoglobin), and electron transport in ATP synthesis (cytochromes).[1] Magnesium complexes of reduced porphyrins occur as the photosynthetic pigments of plants (chlorophylls) and of photosynthetic bacteria (bacteriochlorophylls).

True porphyrins consist of four pyrrole units linked via four "methine bridges". The "methine bridges" are referred to as *meso*-carbons while the outer pyrrole carbons are called *β*-carbons (**Figure 1.1**). The aromaticity of porphyrins is sometimes represented as arising out of an [18]-annulene substructure, although theoretical calculations indicate a somewhat different picture involving the entire *π*-system.[2] Doubly deprotonated porphyrins act as dianionic ligands for nearly all metals and metalloids.

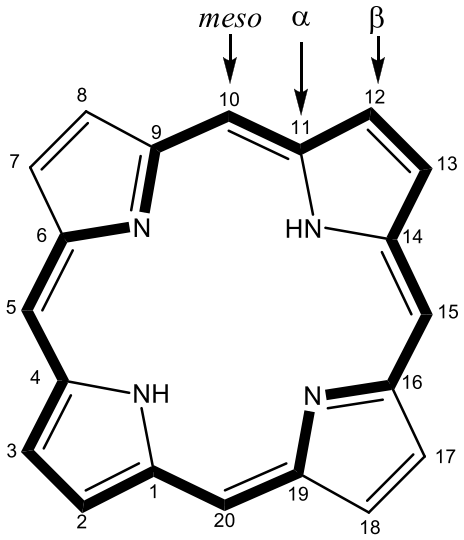

Figure 1.1. The structure of porphine with atom numbering, the [18]-annulene substructure is marked in bold.

Corroles are the fully aromatic analogues of corrins, which are extensively saturated contracted porphyrins that serve as the macrocyclic ligand for cobalt in vitamin B_{12}. Corroles are thus similar to porphyrins, but lack one of the *meso*-carbons (**Figure 1.2**). This structural difference results in a contracted core, with three NH protons that are readily deprotonated. As trianionic ligands, corroles are known to stabilize metals in unusually high oxidation

states. In recent years, however, many of these complexes have been shown to be noninnocent, i.e., the corrole ligand transfers an electron to the metal and is best described as a dianion-radical.[3-9]

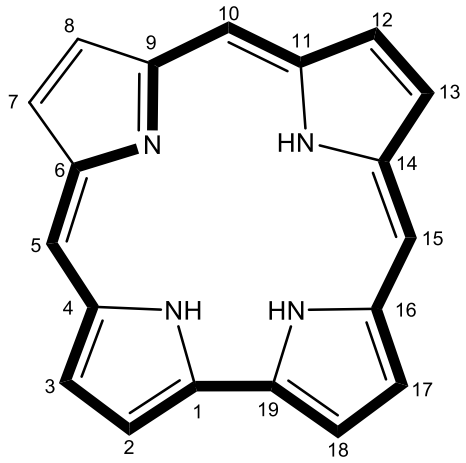

Figure 1.2. The structure of corrole with atom numbering, the [18]-annulene substructure is marked in bold.

The intriguing properties of corroles and porphyrins have led to applications including catalysis, gas sensing, dyes for dye-sensitized solar cells and photosensitizers in photodynamic therapy, among others.[10-12]

1.2. Synthesis of porphyrins

Hans Fischer prepared the first synthetic porphyrin by heating dipyrromethene salts in different organic acids (**Figure 1.3**).[13,14] Despite poor yields, many different porphyrins were prepared this way.[13-15] A milder procedure, involving the cyclization of formyl-substituted dipyrromethanes in the presence of an acid catalyst, was reported in 1960 by MacDonald.[16] Much more recently, the group of Momenteau reported an acid catalyzed cyclization of tripyrranes with pyrrole-2,5-dicarbaldehydes (**Figure 1.4**).[17,18] These two methods, often referred to as the "2 + 2" and "3 + 1" syntheses, turned out to be a game changer for porphyrin synthesis, since they allowed the synthesis of a wide variety of porphyrin type molecules.[19]

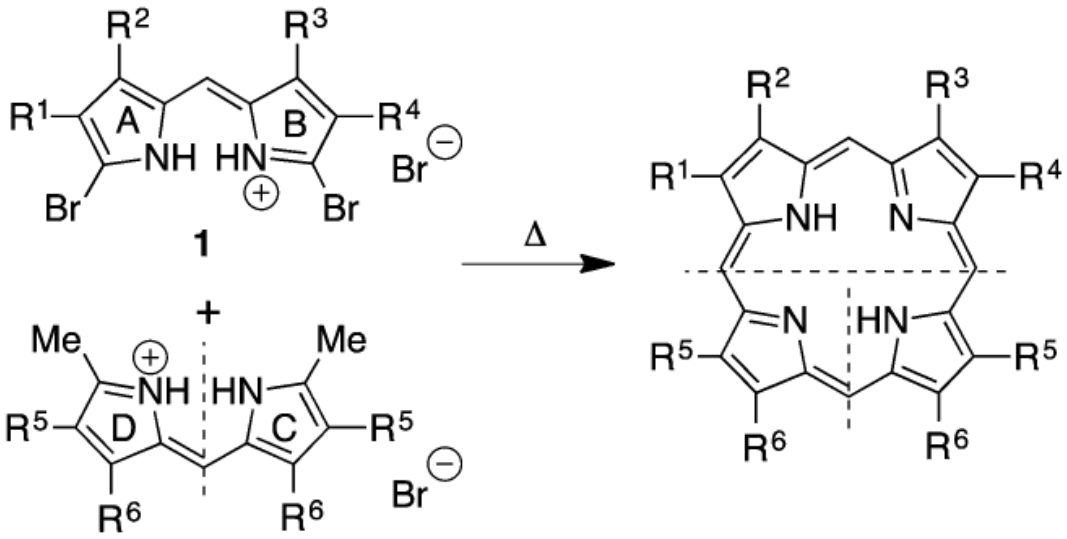

Figure 1.3. Fischer synthesis of porphyrins starting from dipyrromethene salts. Adapted with permission from ref 20. Copyright 2016 Royal Society of Chemistry.

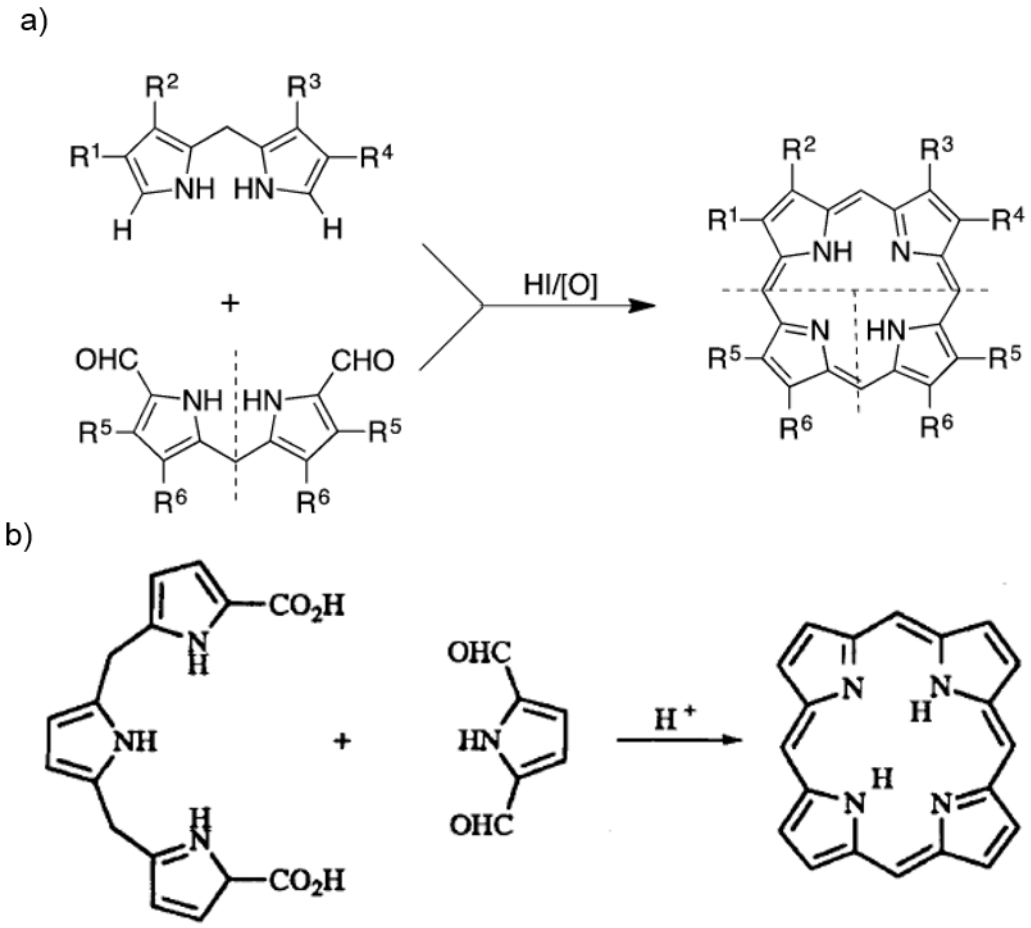

Figure 1.4. a) MacDonald "2 + 2" synthesis, adapted with permission from ref 20. Copyright 2016 Royal Society of Chemistry. b) MacDonald "3 + 1" synthesis, developed by Momenteau, adapted with permission from ref 17. Copyright 1996 Royal Society of Chemistry.

During the 1960s, cyclizations of *b*-oxobilanes, *b*-bilenes and *a*,*c*-biladienes led to the synthesis of several unsymmetrical porphyrins (**Figure 1.5**).[20] Cyclization of *a*,*c*-biladienes also resulted in isolation of the first corrole (*vide infra*).

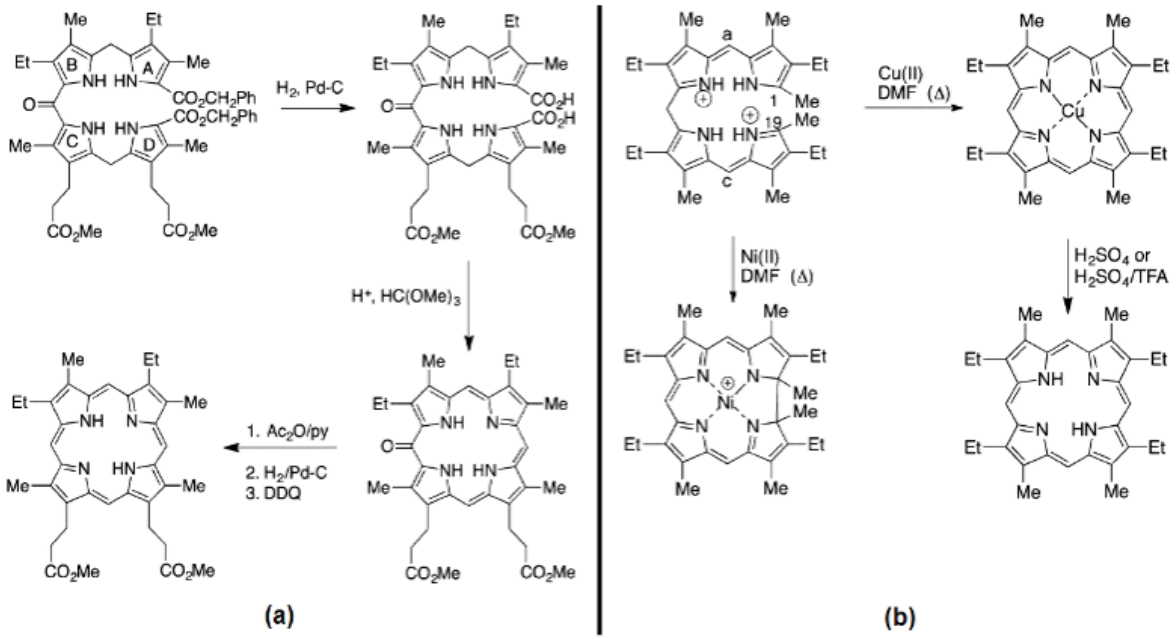

Figure 1.5. Porphyrin synthesis via cyclization of *b*-oxobilane (a) and *a,c*-biladiene (b), adapted with permission from ref 20. Copyright 2016 Royal Society of Chemistry.

Another important facet of porphyrins synthesis consists of the popular one-pot protocols. In 1935, Rothemund prepared several porphyrins by reacting pyrrole and aldehydes in pyridine at high temperatures.[21-25] Low yields and long reaction times, were a major limitation of the Rothemund method. In a major improvement, Adler and Longo obtained tetraphenylporphyrin (approx. 25% yield) by refluxing equimolar amounts of pyrrole and benzaldehyde in propionic acid.[26] Besides higher yields, the method was also applicable to several substituted aldehydes.

A major advance in porphyrin synthesis occurred when the group of Lindsey reported a one-pot, two-step synthesis that produced porphyrins in unprecedented, up to 40% yields.[27,28] Equimolar amounts of pyrrole and aldehyde were dissolved in dry dichloromethane in the presence of catalytic amounts of $BF_3{\cdot}Et_2O$ or TFA. After an hour of stirring, the porphyrinogen intermediate that had formed was oxidized by *p*-chloranil or DDQ to the corresponding porphyrin (**Figure 1.6**). This method also proved amenable to larger scale synthesis.[29]

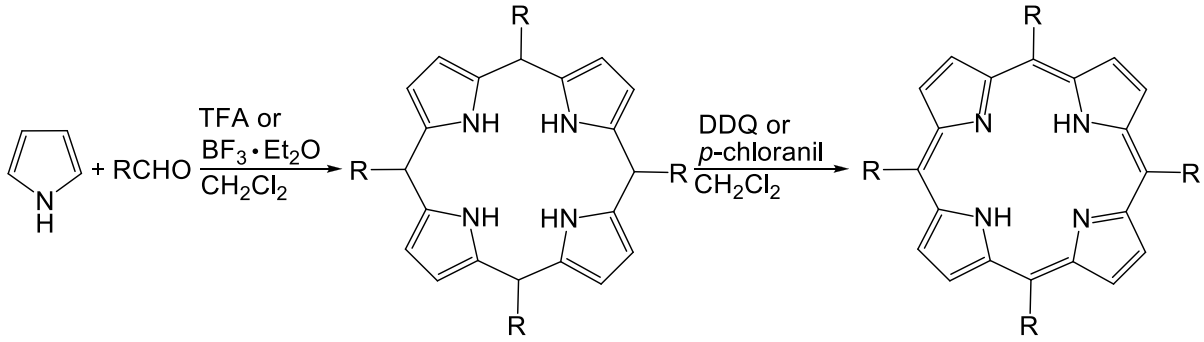

Figure 1.6. The Lindsey synthesis of porphyrins.

1.3. Synthesis of corroles

The first corrole was synthesized in 1965 by Johnson and Kay via photocyclization of *a*,*c*-biladiene dihydrobromides in alkaline methanol solutions (**Figure 1.7**).[30,31]

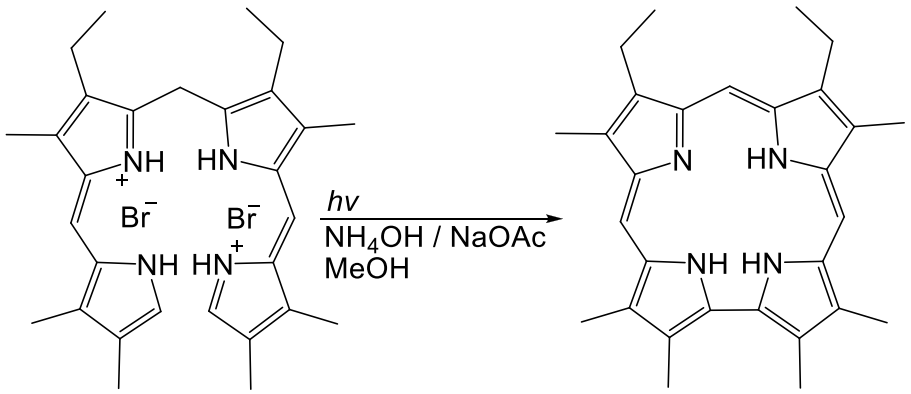

Figure 1.7. First synthesis of corrole by Johnson and Kay

Following Johnson and Kay's synthesis, the field of corroles essentially lay dormant until the turn of the century when the Paolesse[32,33] and Gross[34,35] groups simultaneously published two different one-pot protocols towards triarylcorroles (**Figure 1.8**). By refluxing mixtures of pyrrole and benzaldehydes (3:1 ratio) in acetic acid, Paolesse and coworkers synthesized corroles in decent yields.

Gross's method involved synthesis on a solid support in the absence of both solvent and catalyst (**Figure 1.8**). The method was initially believed to only work for electron-poor benzaldehydes. The Ghosh group, however, demonstrated that the method did indeed work for electron-rich benzaldehydes, albeit at lower yields.[36] A few years later, the Gryko group demonstrated that stirring pyrrole and benzaldehydes, in the absence of solvent, with catalytic amounts of TFA improved the yield of corroles from electron-poor benzaldehydes (**Figure**

1.9). Three different protocols were devised, based on the reactivity and steric bulk of the benzaldehyde in question.[37]

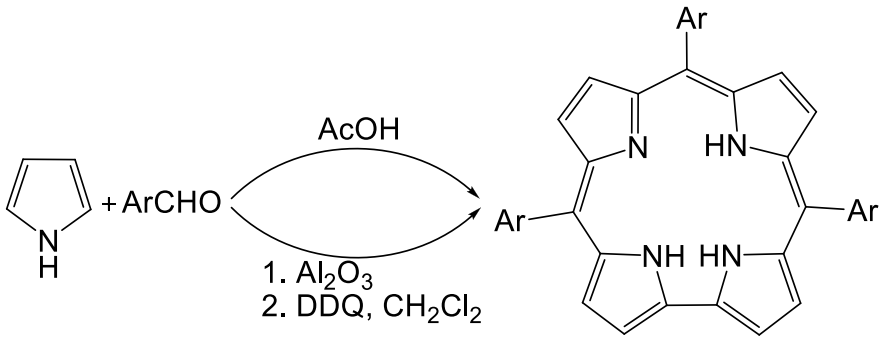

Figure 1.8. One-pot methods developed by Paolesse (top arrow) and Gross (bottom arrow).

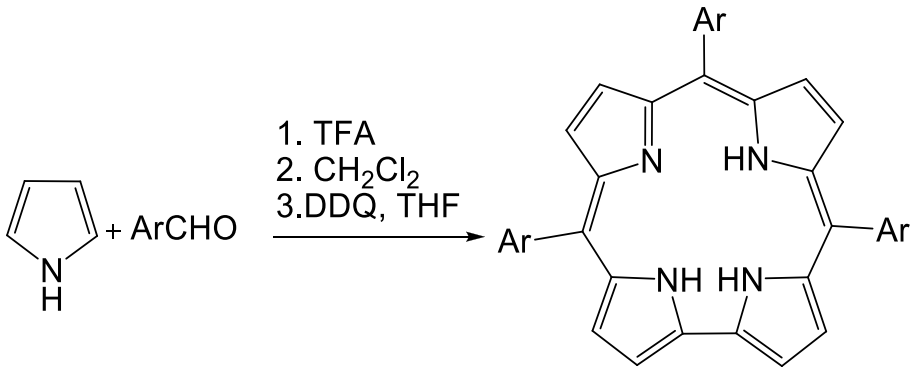

Figure 1.9. The solvent free method developed by Gryko *et al.*

A major development came in 2006 when the Gryko group reported the water/methanol method, which allowed the synthesis of a wide range of corroles in unprecedented yields (**Figure 1.10**).[38] Inspired by the work of Kral on dipyrromethane synthesis in water,[39] Gryko envisioned a strategy where the differences in solubility between the starting materials and bilanes (the corrole precursor) resulted in the precipitate of the latter and thereby helped drive the reaction forward. Extraction of the bilane with chloroform, followed by oxidation with *p*-chloranil, produced the corroles.

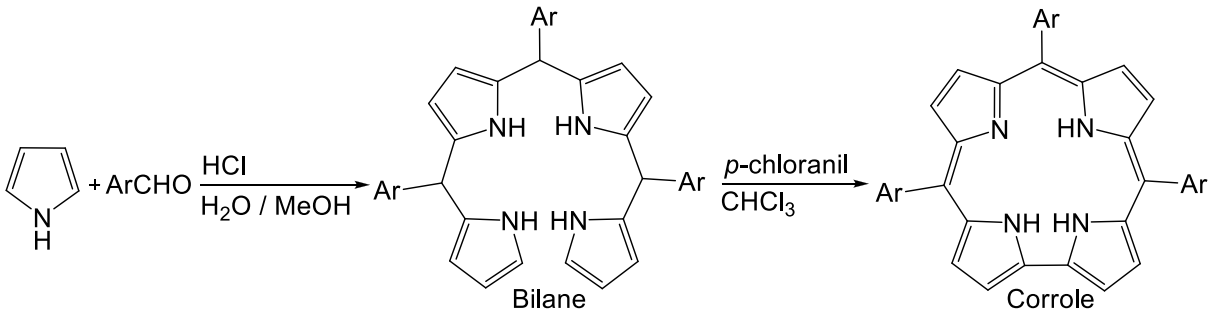

Figure 1.10. The water/methanol method developed by the group of Gryko.

1.4. Nonplanarity in porphyrins

Despite being aromatic compounds, both porphyrins and corroles may exhibit conformations that deviate significantly from planarity (**Figure 1.11**). In fact, the heme groups of many, if not most, heme proteins are nonplanar.[40,41] Nonplanar conformations result from a number of factors including size mismatches between the macrocyclic core and a coordinated element, bulky substituents around the periphery of the macrocycle, axial ligation, and specific metal ligand orbital interactions.

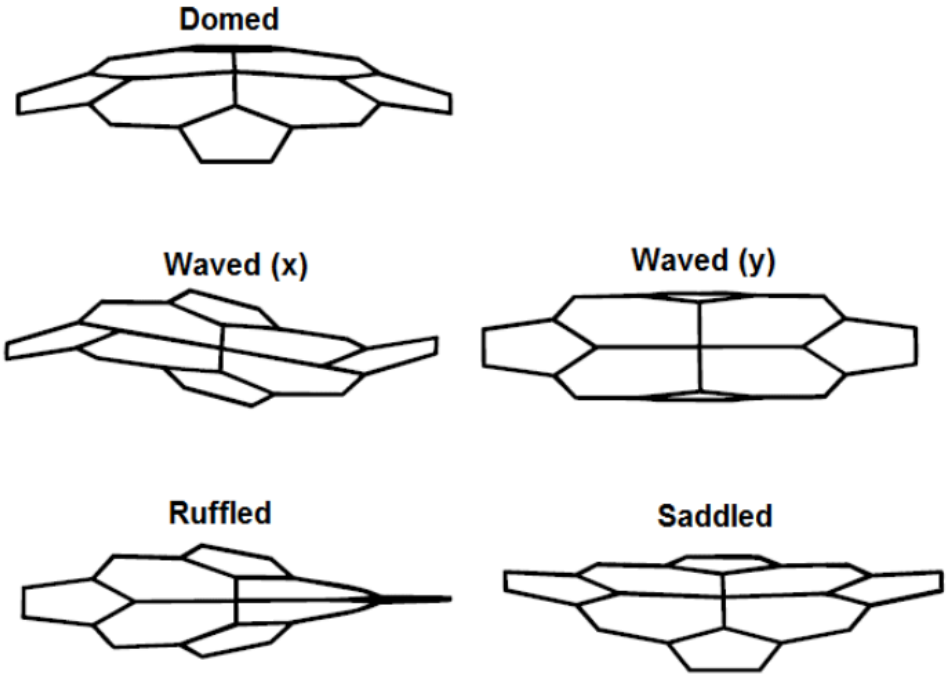

Figure 1.11. Nonplanar conformations of porphyrins and corroles, adapted with permission from ref 42. Copyright 1998 Elsevier.

Domed conformations are often the result of porphyrins binding metals that are too large for their cores to accommodate. As a result, the metal is displaced above the mean macrocyclic plane while the β-carbons are displaced below. Examples of domed complexes include those of thallium[43] and lead.[44]

The wave conformation is characterized by tilting of an opposite pair of pyrrole rings above and below the plane, while the other pair remains relatively in plane. Examples of porphyrins exhibiting the waved conformation include 5,10,15,20-tetrakis(2-thienylporphyrinato)zinc(II)[45] and β-octakis(4-fluorophenyl)-5,10,15,20-tetrakis(pentafluorophenyl)porphyrin.[46]

In the ruffled conformation, the *meso*-carbons deviate alternatively above and below the mean plane. The conformation is typically observed when a porphyrin binds a small ion (e.g., nickel,[47] phosphorous[48] and certain low spin iron(III) porhyrins[49]) that forces the ring to contract and thus distort. Another cause of ruffling is bulky *meso*-substituents.[50,51]

Saddling is the alternative tilting above and below the plane of the pyrrole rings and is commonly observed for porphyrins with bulky groups around their periphery.[52-54]

1.5. Nonplanarity in corroles

While free-base corroles may deviate significantly from planarity due to steric repulsion between the core protons,[55] metallocorroles are far less structurally diverse than porphyrins, and most of them are either planar or mildly domed. Interestingly, some complexes are essentially planar even with considerable crowding around their periphery. An example is a gold corrole with trifluoromethyl groups on all β-carbons.[56] Examples of domed corroles include oxo-complexes of molybdenum,[57] technetium[58] and rhenium[59] as well as nitrido-complexes of osmium[60] and ruthenium.[61]

Copper corroles are inherently saddled.[3] In contrast to porphyrins where saddling is the result of steric crowding, even sterically unhindered copper corroles are saddled. The saddling is the result of an orbital interaction between a corrole π-orbital and a copper d-orbital. While steric crowding is not a prerequisite for saddling it does enhance it.[62] Another metallocorrole that adopts the saddled conformation is that of silver. In the case of silver, however, peripheral crowding is necessary to induce saddling, as β-unsubstituted silver corroles does not.[63]

The wave and ruffled conformations are rare for corroles. The wave conformation has yet to be observed, and DFT calculations suggest that corroles should not be able to ruffle.[64] Nonetheless, a phosphorous corrole has been reported to exhibit a mildly ruffled conformation.[65]

1.6. Electronic absorption spectra of porphyrins and corroles

Both porphyrins and corroles are vividly colored chromophores that absorb light in the near-UV and visible regions of the electromagnetic spectrum. In the UV-vis spectrum, they both exhibit strong absorptions around 400 nm, called the Soret band, and several weaker features between 500 and 700 nm, called Q bands. Examples of corrole and porphyrin UV-vis spectra are presented in **Figure 1.12**.

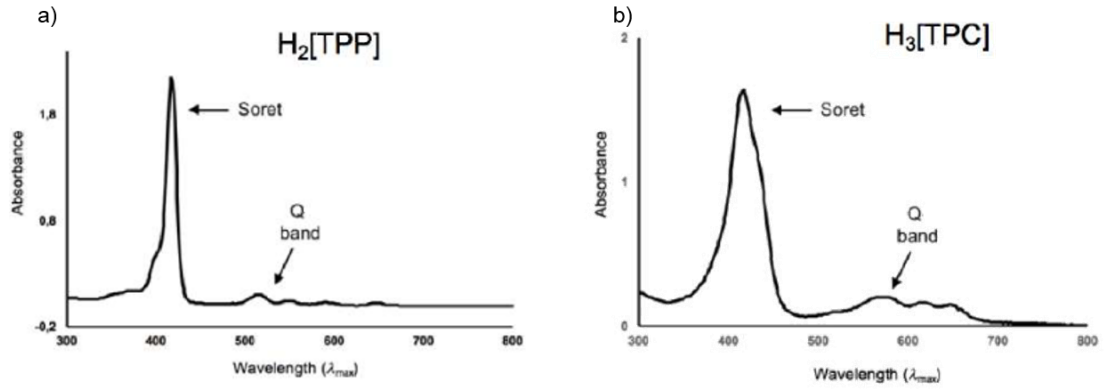

Figure 1.12. UV-visible spectra of a) tetraphenylporphyrin and b) triphenylcorrole.

The electronic absorption spectra of porphyrins have been rationalized in terms of Gouterman`s four orbital model.[66-68] According to the model, the frontier orbitals of porphyrins consist of two near-degenerate HOMOs [$b_1(a_{2u})$ and $b_2(a_{1u})$] and two degenerate LUMOs [$c_1(e_g)$ and $c_2(e_g)$] (**Figure 1.13**), which are energetically well separated from the remainder of the molecular orbitals.

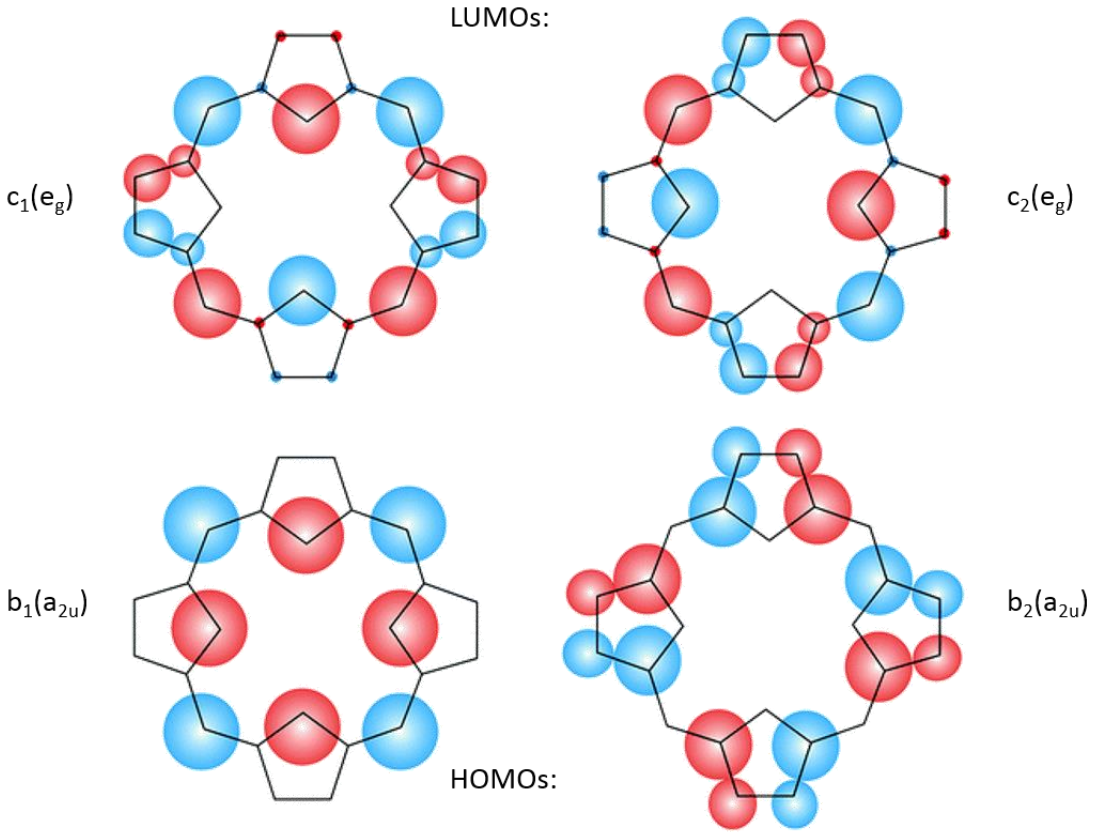

Figure 1.13. The four frontier orbitals of porphyrin, adapted with permission from ref 68. Copyright 2014 Royal Society of Chemistry.

The four possible transitions between the HOMOs and LUMOs give rise to two degenerate pairs of excited states, of which the lower-energy state corresponds to the Q band and the higher-energy state corresponds to the Soret band (**Figure 1.14**).

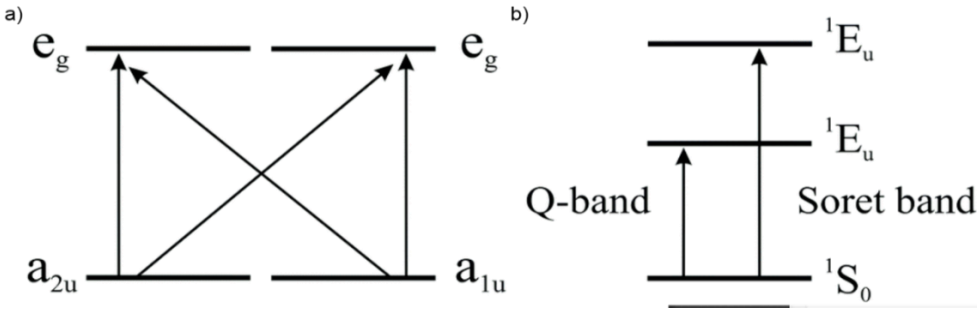

Figure 1.14. a) The possible transitions between the HOMOs and LUMOs and b) the two excited states that gives rise to the Soret and Q bands, adapted with permission from ref 68. Copyright 2014 Royal Society of Chemistry.

As shown in **Figure 1.13**, the a_{2u} HOMO has amplitudes at the *meso*-carbons and pyrrole nitrogens, whereas the a_{1u} HOMO has amplitudes at the pyrrole α- and β-carbons. Thus, binding of an electropositive metal ion increases the energy of the a_{2u} HOMO, reduces the energy of the excited state, and redshifts the Soret band. Similarly, substituents at the *meso*- and β-carbons are expected to affect the energies of the electronic transitions.

Quantum chemical calculations have shown that Gouterman's four orbital model is applicable to corroles.[69] While the lower symmetry of corroles affect the formal symmetries of the orbitals, the qualitative shape of the orbitals remain similar, and as such similar arguments may be applied to explain spectral shifts as a function of changing substituents.

1.7. Photodynamic therapy

Photodynamic therapy (PDT) is a form of phototherapy where light, a photosensitizer, and molecular oxygen are used to destroy cancerous tissue/cells and/or microorganisms. Particularly in cancer treatment, it is recognized as a minimally invasive and toxic form of treatment. Both porphyrins and corroles have shown promise as photosensitizers for PDT[70,71] and a number of porphyrin based photosensitizers are already in clinical use.[70,72]

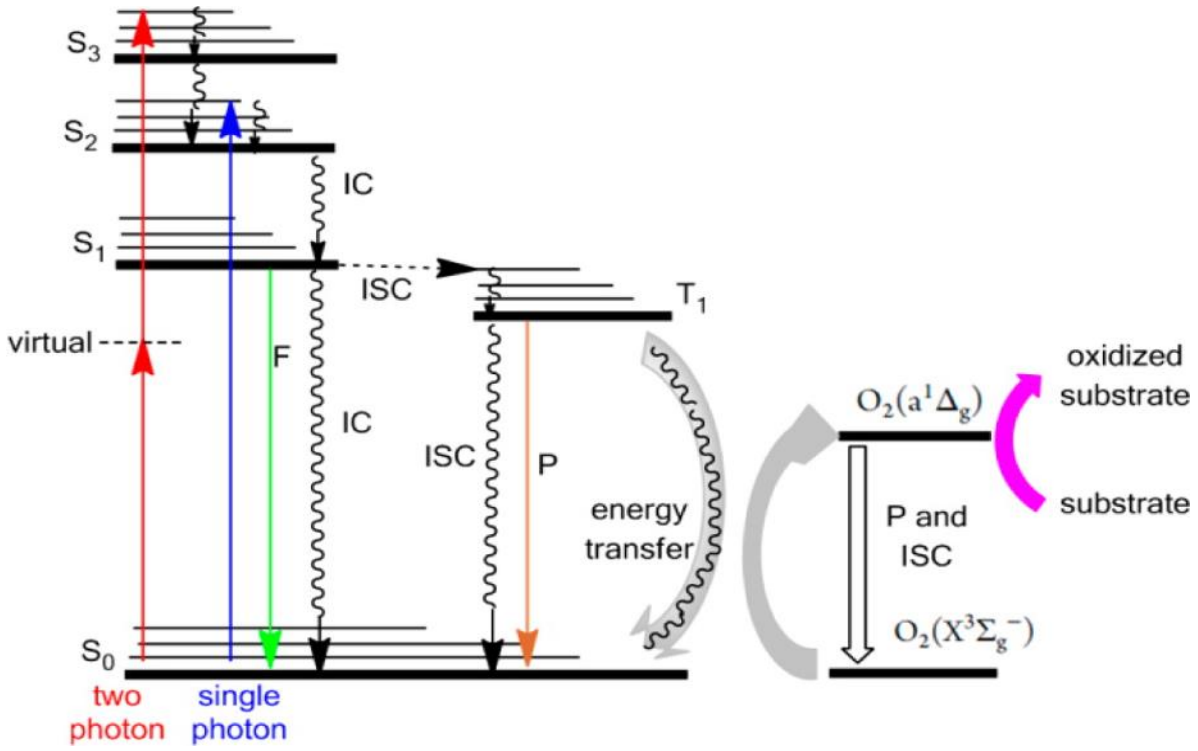

Figure 1.15. Jablonski diagram depicting the photophysical states of a photosensitizer and the transitions between them, adapted from ref 73. Copyright 2013 American Chemical Society.

Central to PDT is the generation of singlet oxygen, the active species responsible for destroying the malignant tissue (**Figure 1.15**). In a typical scenario, a photosensitizer absorbs light and is excited from its singlet ground state S_0 to a singlet excited state S_n, from which it relaxes to its lowest singlet excited state S_1 by internal conversion (IC) or loss of thermal energy. In the S_1 state, the photosensitizer may relax further to its ground state by further loss of thermal energy or by emission of light, known as fluorescence (F). Alternatively, the photosensitizer may undergo intersystem crossing (ISC) to a long-lived triplet state T_1. It is from the triplet state that the photosensitizer is able to transfer energy to oxygen, a ground-state triplet, to generate singlet oxygen. In the absence of oxygen, the T_1 state will relax to the singlet ground state, either by the emission of light known as phosphorescence (P) or by thermal deactivation.

Intersystem crossing, the crucial step that is necessary for singlet oxygen generation, is promoted by closed-shell metal ions and heavy atoms. As such, good examples of porphyrin phosphors are complexes of zinc,[74] palladium,[74] platinum[75] and iridium.[76] Examples of corrole phosphors are complexes of gold,[71] osmium-nitrido,[77] rhenium-oxo,[78] iridium,[79] and platinum.[80]

Chapter 2. Isoporphyrins

2.1 Introduction

Isoporphyrins are porphyrin tautomers, where a core proton has migrated to a *meso*-carbon, changing its hybridization to sp^3 and disrupting the macrocyclic conjugation (**Figure 2.1**).[81] Isoporphyrins are monoanionic ligands, which form cationic complexes with divalent metals. A prominent feature of isoporphyrins, compared to porphyrins, is the redshifted Q-bands in the near-IR region. As a result, isoporphyrins have shown promise in photovoltaic polymers[82] and the redshifted Q-bands have allowed their detection in biomimetic studies by UV-vis spectroscopy.[83-85]

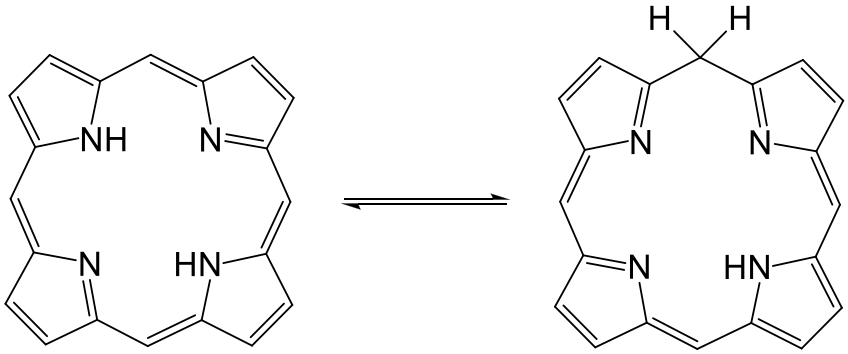

Figure 2.1. Isoporphyrin-porphyrin tautomerization

2.2 Synthesis of isoporphyrins

The first mention of isoporphyrins was by R. B. Woodward, as possible intermediates in the total synthesis of chlorophyll.[86] A few years later, Dolphin and coworkers discovered that adding water or methanol to solutions of electrochemically generated π-dications of ZnTPP, caused the solutions to instantly change color, resulting in the corresponding hydroxy or methoxy isoporphyrin cations (**Figure 2.2**).[87]

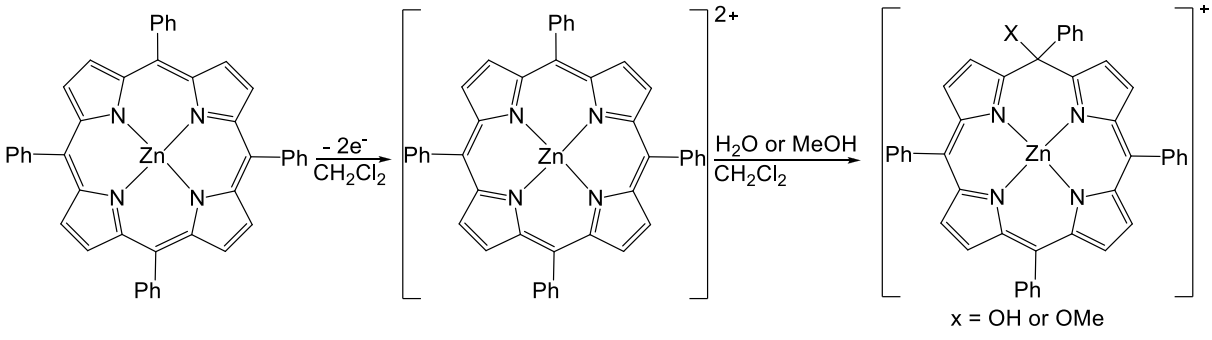

Figure 2.2. Isoporphyrins from nucleophilic attack of methanol or water on electrochemically generated porphyrin π-dications.

Porphyrin π-dications readily form isoporphyrins in the presence of nucleophiles, as evidenced by spectroelectrochemical experiments.[88-90] In addition to oxidation by electrochemical means,[87,91] hydroperoxides react with iron,[92] zinc,[93] cobalt,[94] and chromium porphyrins[95] to generate the corresponding *meso*-hydroperoxo isoporphyrins. Ceric ammonium nitrate, in the presence of methanol, produces *meso*-methoxy isoporphyrins from zinc tetraarylporphyrins.[96] In aqueous solution, photochemical oxidation of zinc tetraarylporphyrins result in formation of the corresponding *meso*-hydroxy isoporphyrins,[97,98] while the ozonide derived from styrene and ozone was found to transform a chromium porphyrin to the corresponding *meso*-hydroxy isoporphyrin.[99]

Porphyrin π-cation radicals readily add nucleophiles. Octaalkylporphyrins form the appropriate *meso*-substituted products, presumably via isoporphyrin intermediates.[100-104] Tetraphenylporphyrins predominantly form β-substituted products,[105] expect for the π-cation radicals FeCl(TPP$^{+\bullet}$)[106] and Zn(TPP$^{+\bullet}$),[105] which formed isoporphyrins in the presence of pyridine and methanol, respectively. In both instances, disproportionation of the π-cation radical to the π-dication and the neutral ligand, likely preceded isoporphyrin formation.

Bubbling NO_2 through a solution containing ZnTPP produced the corresponding *meso*-hydroxy isoporphyrin via a *meso*-NO_2 intermediate.[107] Initially, NO_2 oxidized ZnTPP to its π-cation radical, after which another NO_2 added by radical coupling.[108,109] Hydrolysis of the *meso*-NO_2 intermediate resulted in the final product. In a similar fashion, NO_2 reacted with iron tetraarylporphyrins to produce the corresponding *meso*-hydroxy isoporphyrins.[110,111]

Condensing dipyrromethane-5,5-dimethyl-1,9-dicarboxylic acid and 1,9-diformyldipyrromethane (MacDonald 2+2 method) in the presence of zinc acetate led to a zinc 5,5-dimethylisoporphyrin (**Figure 2.3**).[112] Although the reaction needed six days to finish, the dimethyl moiety imparted the isoporphyrin with unprecedented stability, which allowed crystallographic,[113] electrochemical,[114] and photophysical[115] studies of an isoporphyrin for the first time. Demetalation with TFA resulted in the first free-base isoporphyrin.[116] Unstable, however, the free base did not survive attempts at chromatography and as such was only partially characterized. Exposing the free base to zinc acetate regenerated the zinc complex. Attempts at inserting other metals, however, failed.

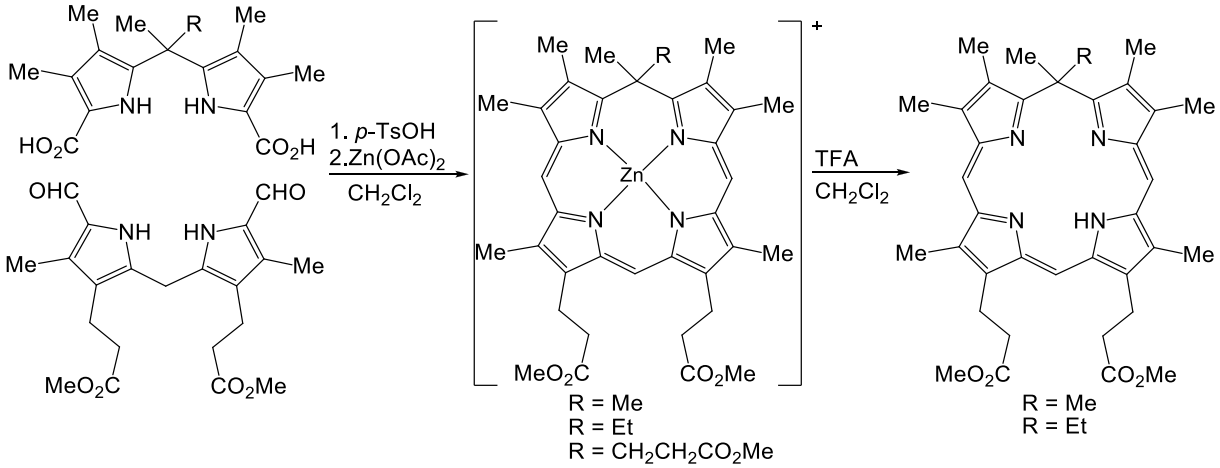

Figure 2.3. MacDonald 2+2 synthesis of isoporphyrins.

Cyclizations of *a,c*-biladienes resulted in stable isoporphyrins in higher yields and with considerably shorter reaction times, compared to the above mentioned MacDonald 2+2 approach.[117,118] Starting from a *b*-bilene hydrochloride, reaction with TFA followed by $Zn(OAc)_2$ and 2,2-dimethoxypropane resulted in a free-base isoporphyrin after 24 hours. Likewise, addition of TFA, followed by either α-ketoesters or α-diketones, and $Zn(OAc)_2$ resulted in various zinc complexes in just a few hours, following oxidation with DDQ. (**Figure 2.4**). The free base proved amenable to copper complexation, resulting in the first copper isoporphyrin.

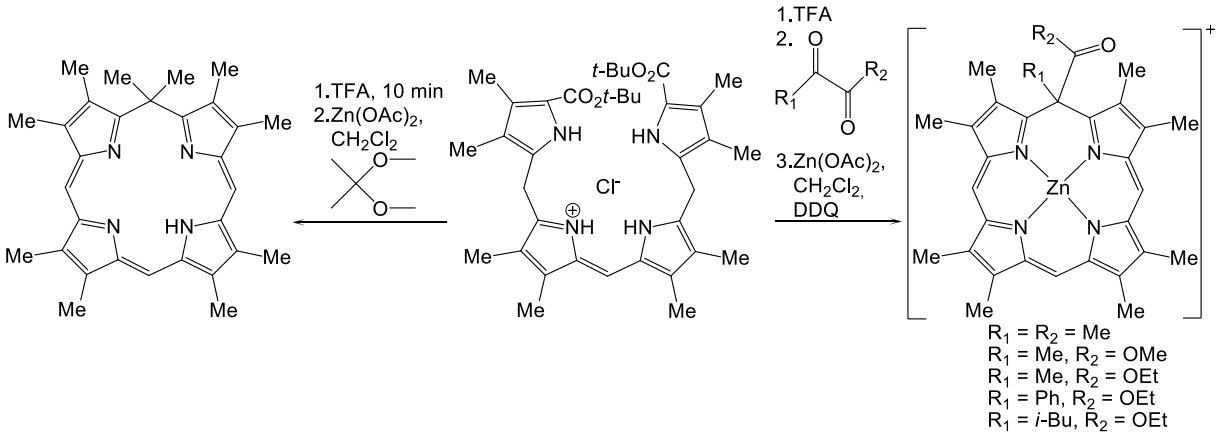

Figure 2.4. Synthesis of free-base and zinc isoporphyrins starting from a *b*-bilene hydrochloride salt.

By adding zinc or cadmium acetate to the oxidation step of an otherwise standard Gryko water/methanol synthesis of corrole, Bröring and coworkers managed to isolate metal-complexed isoporphyrins bearing pyrrole and dipyrromethane moieties at their *meso*-carbons (**Figure 2.5**).[119] The simplicity of the reaction allowed for the isolation of up to 250 mg of isoporphyrins in a single day. Adding TFA to one of the pyrrole-appended zinc complexes

produced the free base, which could be complexed to copper with $Cu(OAc)_2$ in near-quantitative yield.

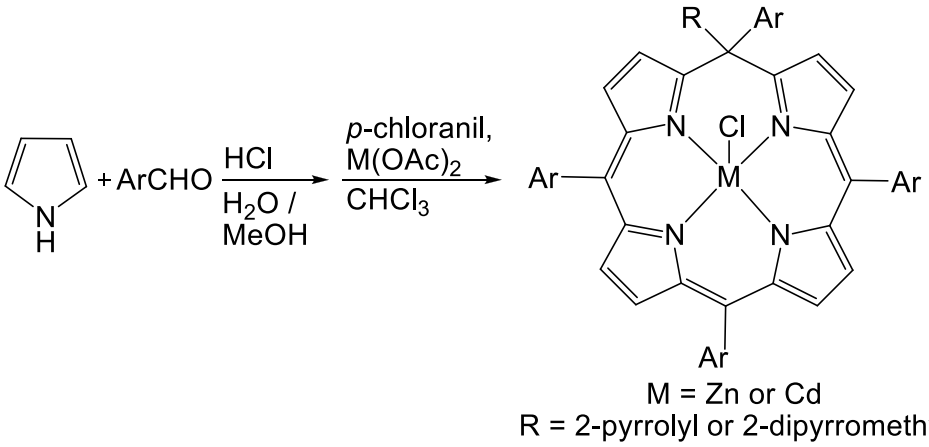

Figure 2.5. One-pot synthesis of pyrrole- and dipyrromethane-appended isoporphyrins.

Adding TFA and tetrabutylammonium chloride (TBACl) to an ozone-generated ferryl porphyrin produced an Fe(III) porphyrin π-dication, which readily picked up a chloride ion to form a *meso*-chlorinated isoporphyrin (**Figure 2.6**).[120] Later, it was demonstrated the Fe(III) porphyrin π-dication was stable for hours at low temperatures, allowing isoporphyrins to form via addition of cyanide, azide, and 3,4-dimethylimidazole.[83]

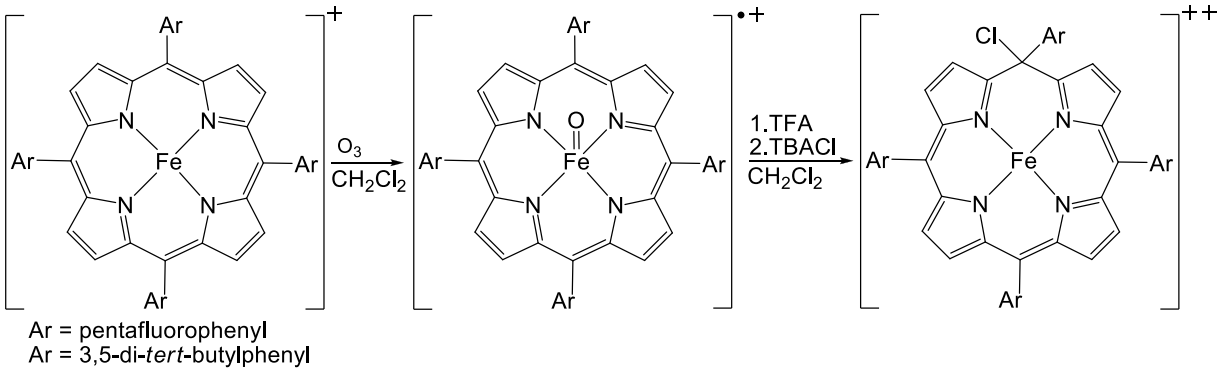

Figure 2.6. Synthesis of *meso*-chlorinated isoporphyrins from adding TFA and TBACl to a ferryl porphyrin.

2.3 Electronic absorption spectra of isoporphyrins

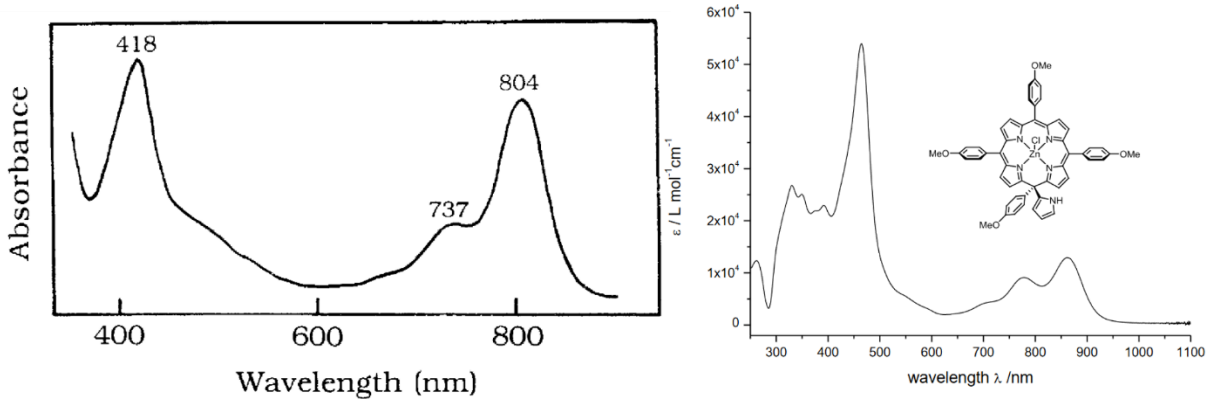

Figure 2.7. UV-vis spectra of Zn[13,17-bis(2-methoxycarbonylethyl)-2,3,5,5,7,8,12,18-octamethylisoporphyrin]chloride (left, adapted with permission from ref 112, copyright 1992 Elsevier) and Zn[5(2-pyrrolyl)-5,10,15,20-tetraanisylisoporphyrin]chloride (right, adapted with permission from ref 119, copyright 2016 John Wiley & Sons).

Figure 2.7 depicts typical electronic absorptions for *meso*-unsubstituted (left) and *meso*-aryl (right) isoporphyrins. M*eso*-unsubstituted complexes exhibit sharp Soret transitions in the 410-450 nm region accompanied by a shouldered Q band in the 800-840 nm region. Tetraaryl analogues exhibit more richly featured spectra, with several peaks in the 300-500 nm region, in addition to double-humped Q bands in the 700-950 nm region.

Compared to porphyrins, the most prominent feature of the electronic absorption of isoporphyrins is the redshifted Q bands, which serve as a diagnostic tool to detect the formation of isoporphyrins that are too unstable to be isolated. The redshifted Q bands result from stabilization of both the HOMO and the LUMO,[107] compared to porphyrins.[121] The LUMO, however, is stabilized to a greater extent, resulting in a narrower HOMO-LUMO gap.

2.4 Aromaticity of isoporphyrins

Proton NMR spectra of diamagnetic metalloisoporphyrins reflect the broken conjugation at the saturated *meso*-carbon. In diamagnetic complexes, i.e., zinc complexes of *meso*-unsubstituted isoporphyrins[112,116-118] and zinc,[87,96,107,119] cadmium,[119] and nickel[122] complexes of tetraaryl isoporphyrins, the *meso*- and *β*-protons resonate ~2-3 ppm upfield compared to zinc porphine[123] and ZnTPP,[87,124] respectively. The upfield shift is a result of reduced diamagnetic currents and indirectly of reduced macrocyclic aromaticity.

The interruption of macrocyclic conjugation, with concomitant loss of aromaticity, is also apparent from the molecular structures of two zinc isoporphyrins.[107,113] Bond lengths to carbons adjacent to the saturated *meso*-carbon are elongated to >1.5 Å, indicative of single bonds, and the bond angle between the saturated *meso*-carbon and the adjacent *β*-carbons is reduced from ~125 to ~117-118 degrees, thus approaching a tetrahedral geometry. Both structures show the zinc as pentacoordinated, with an axially bound water molecule, and it is slightly displaced from the mean plane of the macrocycle, while the macrocycle itself is slightly ruffled.

Although X-ray structures and NMR spectroscopy suggests a nonaromatic macrocycle, DFT calculations of magnetically induced current densities tell a more nuanced story.[125] The calculations revealed diatropic ring currents that circulate around the macrocycle of both free-base isoporphyrin and its zinc complex (**Figure 2.8**), with net current strengths of 6.7-7.0 nAT^{-1} and 10.1 nAT^{-1}, respectively. For comparison, the calculated current strength of benzene is 11.8 nAT^{-1} and that of ZnTPP is 26.6 nAT^{-1}. The current pathway in the free base splits at each pyrrole ring into an outer and an inner route. The outer route is preferred and sustains a stronger current than the inner route. The pyrrole ring bearing a proton sustained a local ring current. As for the free base, the ring current of the zinc complex splits at each pyrrole, with the outer route sustaining a stronger current compared to the inner route. The six-membered ring between the zinc and the saturated *meso*-carbon sustains a weak local diatropic ring current.

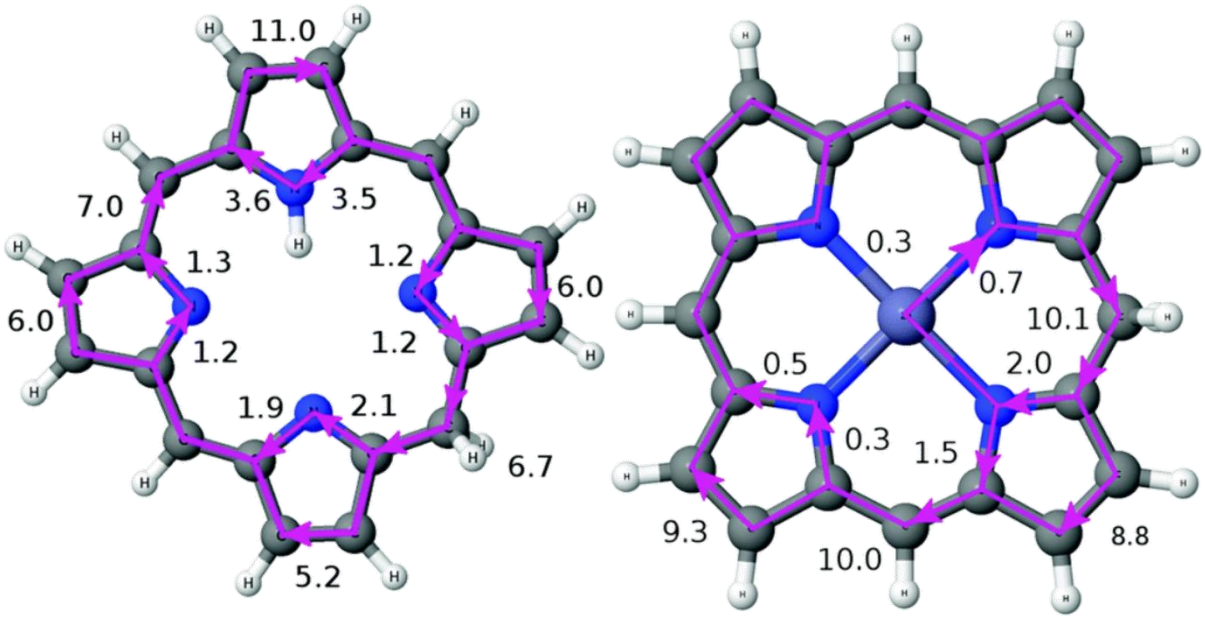

Figure 2.8. Current density pathways and calculated current strengths (in nAT^{-1}) passing through selected bonds, calculated 1 bohr above the molecular plane of free-base isoporphyrin (left) and zinc isoporphyrin (right). Adapted with permission from ref 125. Copyright 2017 Royal Society of Chemistry.

As for paramagnetic complexes, the *β*-protons of FeCl tetraarylisoporphyrin resonate around 70-80 ppm,[92] typical of high spin Fe(III) porphyrins.[92,106] Further evidence comes from EPR studies, with g values of ~2 and ~6.[83,92,120] Similarly, a chromium(III) isoporphyrin derived from a chromium(III) porphyrin revealed nearly identical ^{1}H chemical shifts.[95]

2.5 Electrochemistry of isoporphyrins

Cyclic voltammetry studies of zinc 13,17-bis(2-methoxycarbonylethyl)-2,3,5,5,7,8,12,18-octamethylisoporphyrin, the first stable isoporphyrin to be synthesized, revealed a reversible one-electron oxidation at 0.62 V vs. Ag/Ag^{+} in DCM and two reversible one-electron reductions at -0.76 and -1.11 V vs. Ag/Ag^{+} in DMSO.[114] The redox behavior was solvent dependent as oxidation in DMSO and reduction in DCM was irreversible. Compared to zinc octaethylporphyrin,[126] the first reduction occurs at significantly higher potential while the oxidation occurs at slightly lower potential, resulting in an electrochemical HOMO-LUMO gap of 1.38 V compared to 2.25 V for the porphyrin, in agreement with the redshifted Q bands of the isoporphyrins. Cyclic voltammetry studies of *meso*-hydroxy[107] and *meso*-methoxy[96] zinc tetraarylisoporphyrins revealed reversible one-electron oxidations for both

compounds; both, however, also exhibited irreversible one-electron reductions at intriguingly high potentials, i.e., -0.12 V and -0.13 V vs Ag/Ag^+, respectively. The difference in reduction potential correlates the relative stability of the compounds in question. While zinc 13,17-bis(2-methoxycarbonylethyl)-2,3,5,5,7,8,12,18-octamethylisoporphyrin is stable for months, due to the 5,5-dimethyl moiety, trace amounts of mild reducing agents are enough to revert the *meso*-hydroxy and *meso*-methoxy isoporphyrins back to the parent porphyrins. The stability of the complexes may be correlated to the nature of the substituents at the saturated carbon. Relatively good leaving groups, such as methoxy and hydroxy, result in unstable isoporphyrins that readily reduce to porphyrins.[96,107]

2.6 Applications of isoporphyrins

Cellular studies of a series of zinc isoporphyrins and a copper isoporphyrin,[117] prepared from *b*-bilene salts, exhibited rapid uptake in human epithelial type 2 (HEp2) cells. The isoporphyrins possessing bulky groups (e.g., phenyl and isobutyl) accumulated the most, likely due to decreased aggregation. While the compounds displayed relatively low dark toxicities, all zinc isoporphyrins exhibited significantly higher toxicities upon light activation. The top performing zinc isoporphyrin (R_1 = *i*-Bu, R_2 = OEt, **Figure 2.4**), demonstrated a phototoxic IC_{50} value of 11 μM. Coupled with the recent facile synthesis of water-soluble zinc isoporphyrins[96] and the ubiquitous near-IR absorptions of isoporphyrins, the results of the cellular studies demonstrate significant potential for isoporphyrins in photodynamic therapy.

The *meso*-chlorinated isoporphyrin, derived from addition of TFA and TBACl to a ferryl porphyrin (**Figure 2.6**), turned out to be a chlorinating agent.[120] Adding 1,3,5-trimethyxobenzene, anisole, or cyclohexene to mixtures containing the *meso*-chlorinated isoporphyrin resulted in chlorine transfer to the substrate. Kinetic studies suggested electrophilic aromatic substitution as the mechanism of chlorine transfer, as did the absence of secondary reaction products, i.e., products resulting from reaction with chlorine radicals. The *meso*-chlorinated isoporphyrin could also be employed catalytically, with catalyst loading of 1 mol %. Accordingly, vigorous stirring of aqueous hydrogen peroxide with a mixture containing the *meso*-chlorinated isoporphyrin, TFA, TBACl, and 1,3,5-trimethoxybenzene resulted in chlorination of the arene in 85 % yield.

Electropolymerization of a zinc-5,15-bis(*p*-tolyl)porphyrin in the presence of a viologen, i.e., 1,1´´-(1,3-propanediyl)bis-4,4´-bipyridinium hexafluorophosphate salt, resulted in the

deposition of, depending on the applied voltage, isoporphyrin or porphyrin copolymers on indium tin oxide (ITO) electrodes.[82] Photovoltaic measurements on both revealed the isoporphyrin copolymer to be about 2.5 times more efficient than the porphyrin analogue, a difference that was attributed to the broader Soret band and the near-IR absorptions of the isoporphyrin.

2.7 Biomimetic studies: Isoporphyrins in heme oxygenase and cytochrome *c* oxidase

Heme oxygenase enzymes (HO) catalyze the breakdown of heme. The process proceeds via *meso*-hydroxyheme and verdoheme before yielding biliverdin and free iron ions (**Figure 2.9**). In the first step, two-electron reduction of oxygen to hydroperoxide affords a ferrous hydroperoxide intermediate that inserts the terminal oxygen into the *meso*-position to generate *meso*-hydroxyheme. Monitoring the reaction of heme with O_2 and NADPH in the presence of human heme oxygenase-1 (hHO-1) with UV-vis demonstrated immediate formation of a ferrous-oxo species, which over the course of 20 minutes decayed to verdoheme and ultimately biliverdin.[85] Exposing *meso*-arylhemes to the same conditions also resulted in ferrous-oxo species. However, detection of an additional transient species for the *meso*-arylhemes, with absorptions in the near-IR region, indicated an isoporphyrin intermediate. Similarly, when exposed to hydrogen peroxide, the hHO-1 heme complex resulted in verdoheme, while the *meso*-arylhemes generated the presumed isoporphyrin. Unambiguous proof of isoporphyrin generation came from HPLC and LC-ESI-MS analysis. The results demonstrated that an isoporphyrin intermediate is part of the catalytic cycle of heme oxygenase, but in the absence of *meso*-substituents the transient species deprotonates instantly, rendering it undetectable.

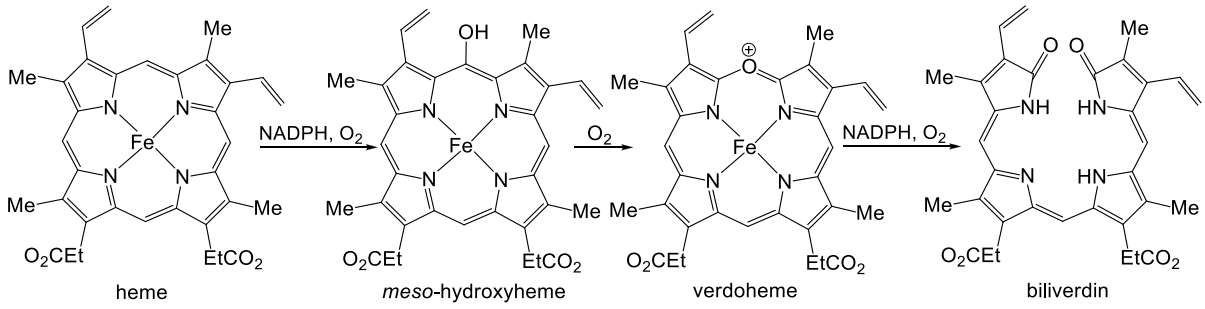

Figure 2.9. Heme oxygenase catalyzed degradation of heme.

Further evidence of isoporphyrin intermediates in the catalytic breakdown of heme came from oxidation of ferrous tetraarylporphyrins to verdohemes with ceric ammonium nitrate.[84] Exposing ferrous tetraarylporphyrins to an excess of ceric ammonium nitrate in CH_3CN/H_2O

resulted in the immediate formation of an isoporphyrin, evidenced by near-IR absorptions in the optical spectrum. Over time, the isoporphyrin decayed to an iron benzoyl-biliverdin complex and ultimately to verdoheme.

Cytochrome *c* oxidase, found in the mitochondrial electron transport chain, catalyzes the reduction of dioxygen to water, which ultimately drives ATP synthase to synthesize ATP. In the active site of the enzyme, a histidine residue binds a tyrosine, a modification to the active site that occurs post-translationally. The Karlin group suggested this modification proceeds via an isoporphyrin intermediate,[83] analogous to the synthesis of a *meso*-chlorinated isoporphyrin (*vide supra*).[120] To acquire evidence for their hypothesis, the authors prepared a ferryl porphyrin from ferric [tetrakis(2,6-difluorophenyl)porphyrin] with *meta*-chloroperoxybenzoic acid (*m*CPBA). TFA converted the ferryl porphyrin to a ferric porphyrin π-dication, from which an isoporphyrin formed by nucleophilic attack of 4,5-dimethylimidazole. Finally, addition of electron rich phenolic substrates resulted in nucleophilic attack on the imidazole moiety, resulting in covalently linked imidazole-phenol adducts, in addition to regenerating the starting iron porphyrin (**Figure 2.10**).

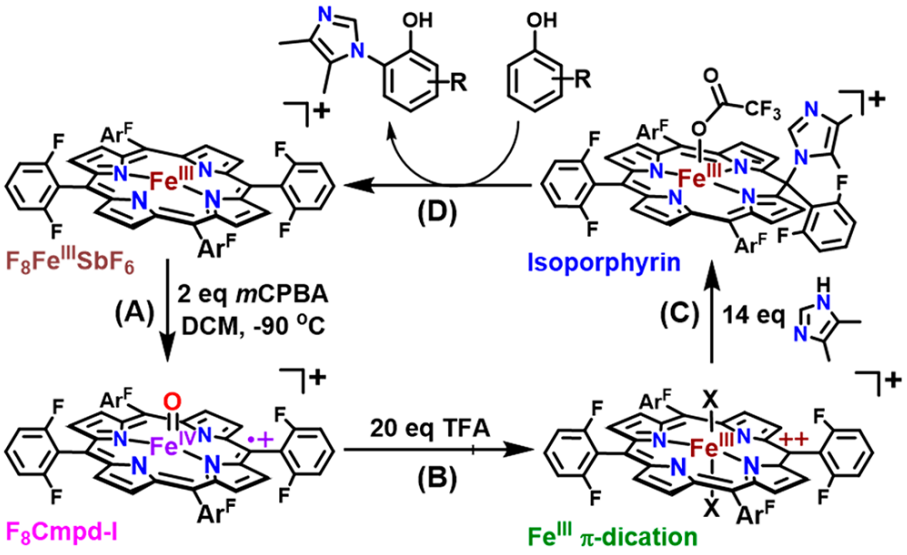

Figure 2.10. Imidazole-phenol linking via an isoporphyrin intermediate, to emulate the histidine-tyrosine cross-link that forms prior to catalytic activity in cytochrome *c* oxidase. Adapted with permission from ref 83. Copyright 2019 American Chemical Society.

Chapter 3. Isocorroles

3.1 Introduction

Isocorroles are corrole isomers with a saturated *meso*-carbon. They are fascinating hybrid ligands, which combine key characteristics of both porphyrins and corroles (**Figure 3.1**). Thus, like porphyrins, they act as dianionic ligands, while sharing a contracted N4 core with corroles.

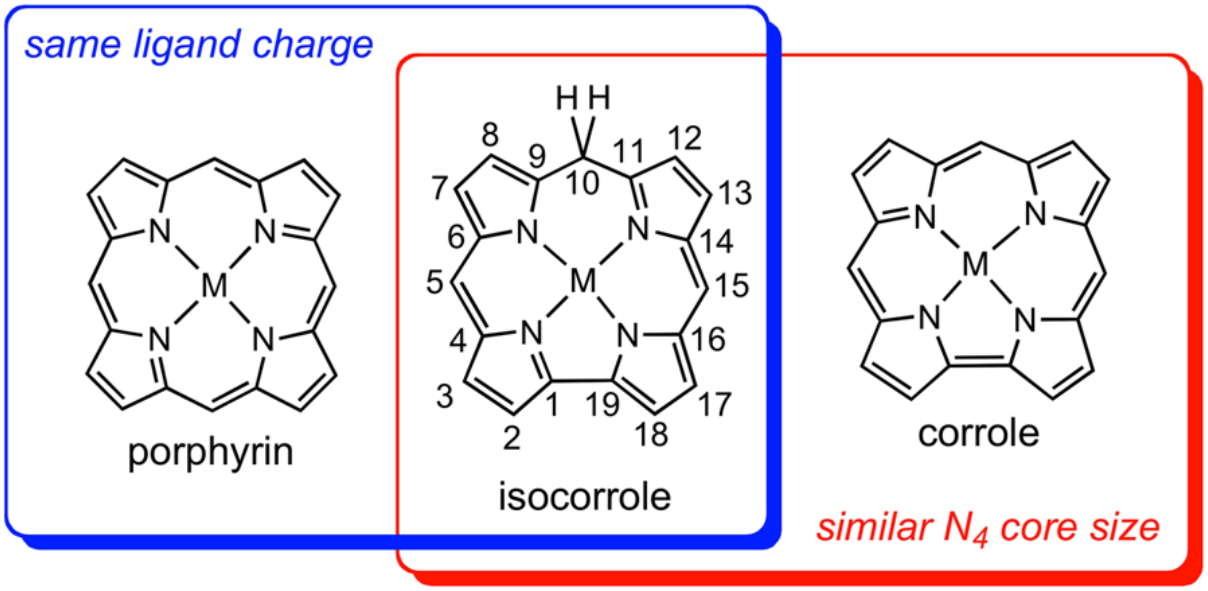

Figure 3.1. Isocorroles, with atom numbering, as hybrid ligands with characteristics of both porphyrins and corroles. Adapted with permission from ref 127. Copyright 2018 Springer Nature.

The saturated *meso*-carbon bestows isocorroles with qualities similar to isoporphyrins, such as near-IR absorptions. Although there are no reports of isocorrole applications yet, their stability and relative ease of formation surely promise applications in areas such as photodynamic therapy.

3.2 Synthesis of isocorroles

β-Octabromination of a free-base corrole resulted in the first recognized formation of an isocorrole, when the product revealed unexpected characteristics in both NMR (internal protons at δ = 13) and UV-vis (broad absorptions at 440 nm and 600-800 nm).[128] The authors, Paolesse *et al.*, theorized the unusual characteristics were the result of a tautomeric shift of an internal hydrogen to a *me*so-carbon, interrupting the macrocyclic aromaticity. Unable to attain suitable crystals of the new compound, they attempted to coordinate it to cobalt, which

induced a rearomatization of the macrocycle to yield a cobalt corrole complex (**Figure 3.2**). Later, the authors corrected the assignment of the *meso*-substituent to a hydroxy group, instead of a hydrogen.[129]

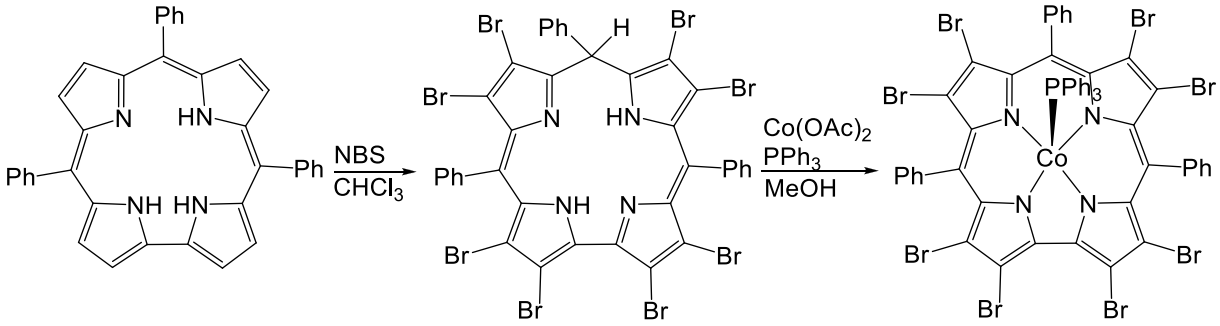

Figure 3.2. Synthesis of the first isocorrole.

A few years later, the Vogel group treated an *a*,*c*-biladiene dihydrobromide salt with nickel acetate followed by *p*-chloranil to form a nickel isocorrole.[130] The Bröring group used Vogel's method to produce nickel, palladium, and copper complexes starting from two different biladiene type salts (**Figure 3.3**).[131]

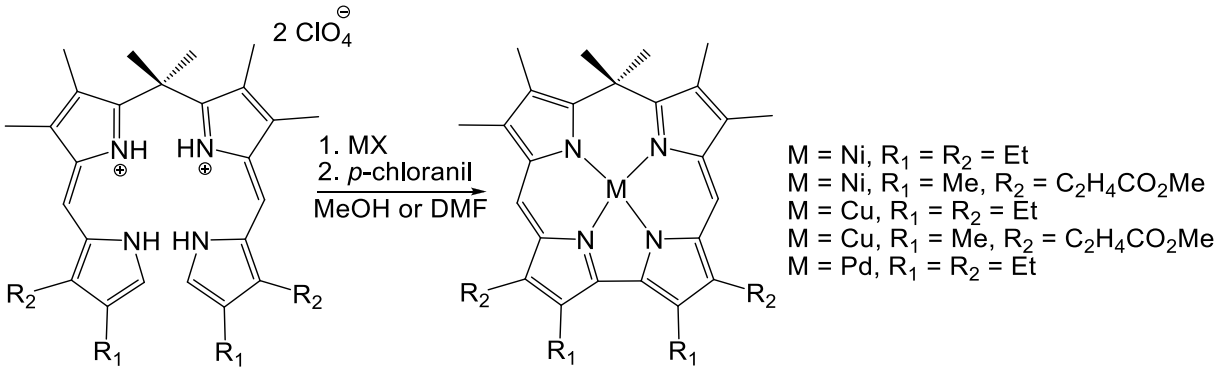

Figure 3.3. Synthesis of isocorrole complexes from biladiene type salts.

Through the interaction of *gem*-dimethyl-2,2´-bis(6-phenylazafulvenyl)methane and 3,3´-di-*iso*-butyl-4,4´-dimethyl-2,2´-bipyrrole, following oxidation with DDQ, Setsune and coworkers were able to isolate the first free-base isocorrole in 27.8 % yield (**Figure 3.4**).[132,133] The authors employed their isocorrole to prepare no less than eight metal complexes (**Figure 3.5**).[134] Adding methanol solutions of $Cu(OAc)_2$, $Ni(OAc)_2$, $FeCl_2$, or $MnCl_2$ to dichloromethane solutions of the free base led to the corresponding Cu(II), Ni(II), Fe(III)Cl, and Mn(III)Cl complexes after stirring at room temperature. Vigorous stirring of the FeCl complex with aqueous NaOH resulted in the μ-oxo bridged complex denoted $(Fe)_2O$. Refluxing the free-base with $[Rh(COD)Cl]_2$ and pyridine produced the RhCl(py)

complex while stirring with $[Rh(CO)_2Cl]_2$ resulted in the immediate formation of the $Rh(CO)_2$ complex. Subjecting the $Rh(CO)_2$ complex to another round of $[Rh(CO)_2Cl]_2$ produced the $Rh_2(CO)_4$ complex.

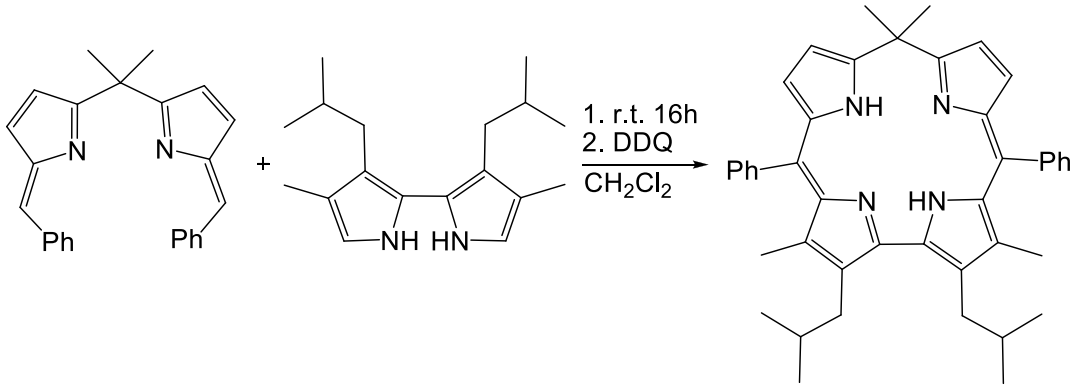

Figure 3.4. Synthesis of the first free-base isocorrole.

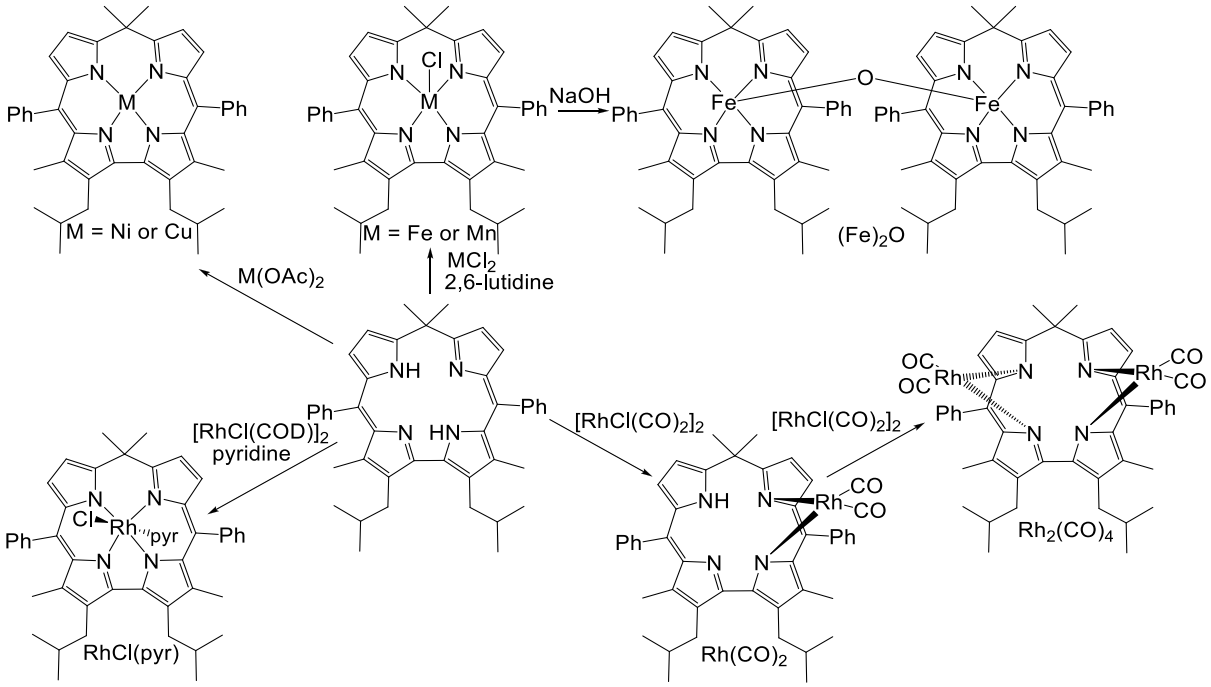

Figure 3.5. Synthesis of metal complexes from Setsune's free-base isocorrole.

While attempting to prepare a phlorin from a dipyrromethane and a dipyrromethanedi-carbinol, the Geier group observed low quantities of a corresponding 5-isocorrole. Intrigued, the authors redesigned their synthesis to favor the isocorrole and, after an extensive survey of reaction conditions, arrived at a method that produced 5,5-dimethyl-10,15-bis(pentafluorophenyl)isocorrole in 37 % yield (**Figure 3.6**).[135] Interactions with copper or zinc acetate produced the corresponding copper and zinc complexes in yields greater than 75 %.[136]

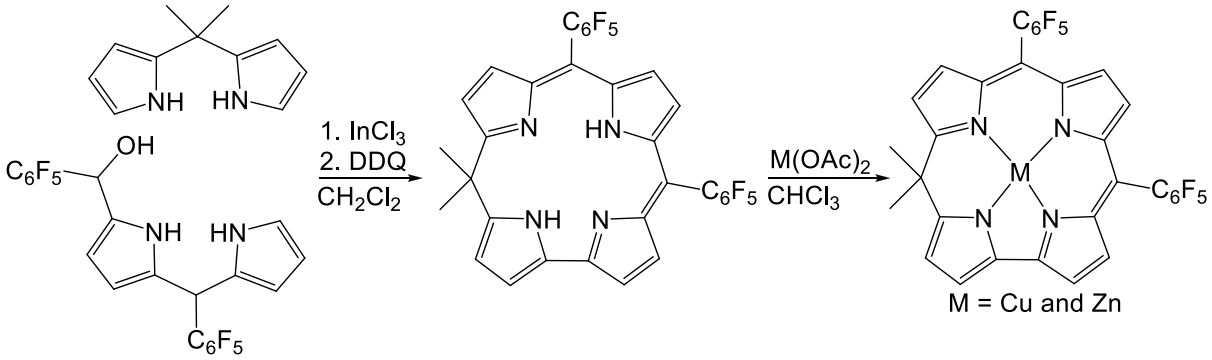

Figure 3.6. Synthesis of free-base, copper and zinc 5,5-dimethyl-10,15-bis(pentafluorophenyl)isocorroles.

Inspired by the development of simple and high-yielding one-pot procedures in corrole synthesis,[35,38,128,137,138] the Paolesse group sought to develop methods that allowed facile synthesis of isocorroles. Considering the first isoporphyrin formed from the reaction of an oxidized porphyrin with methanol, the authors wished to explore a similar route towards isocorroles. Accordingly, *meso*-methoxy isocorroles, both 5- and 10-isomers, were made by briefly stirring triarylcorroles and DDQ in methanol.[139] Electron-rich corroles produced isocorroles in excellent yields of ~75%, while only traces were made starting from electron-poor corroles. Copper and nickel complexes, of both isomers, were made by reactions with the appropriate metal acetates.[140] The authors later demonstrated that their method could be expanded to different nucleophiles, such as a Grignard reagent. Reacting tritolylcorrole with DDQ followed by EtMgBr in toluene resulted in 5-ethyl- and 10-ethyltritolylisocorroles. These results potentially foreshadowed a facile and general approach towards isocorroles where oxidation of corrole, followed by attack of a nucleophile, would afford a variety of isocorroles (**Figure 3.7**).[141]

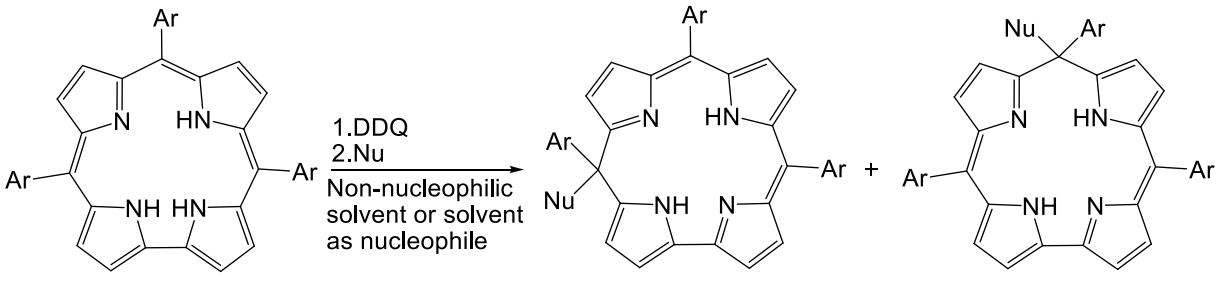

Figure 3.7. A potentially general approach towards isocorroles.

While searching for conditions that would effectively demetalate copper corroles, the Paolesse group learned that 5-hydroxy and 10-hydroxy isocorroles formed as byproducts when TFA/$CHCl_3$ or concentrated H_2SO_4 were employed as reaction mediums.[129] The

authors were able to demetalate without isocorrole side-products, but only when concentrated H_2SO_4 was added dropwise to chloroform solutions containing the copper corrole. Employing the latter method to a *β*-octabromo complex once again resulted in isocorrole byproducts. In this instance, only the 10-hydroxy isomer was isolated. The Ghosh group , however, demonstrated that sonicating the suspension allowed both isomers to form in decent yields.[142] Demetalation of copper undecaarylcorroles, employing similar conditions, also led to 5- and 10-hydroxy isocorroles, with the former dominating.[143]

Demetalation of a copper *β*-octakis(trifluoromethyl)corrole resulted in a hydrated corrole, where the elements of water added across two *meso*-carbons (5-OH and 10-H).[142] Cobalt insertion caused the more labile OH group to leave, resulting in a cobalt complexed 10-H isocorrole (**Figure 3.8**).

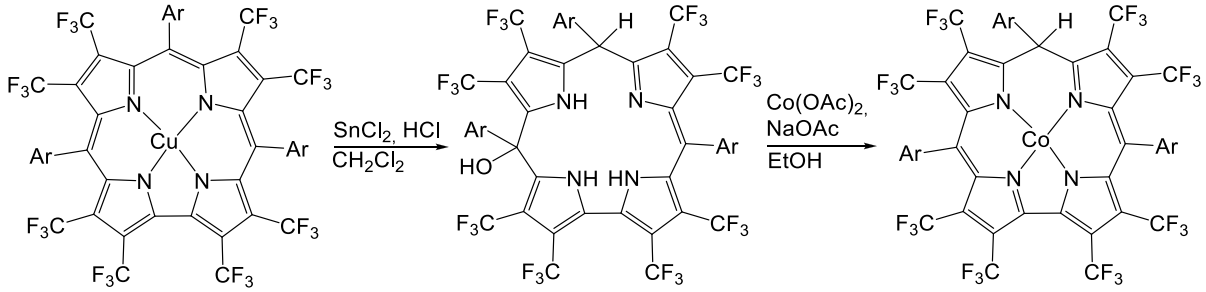

Figure 3.8. Demetalation of a copper *β*-octakis(trifluoromethyl)corrole, followed by cobalt insertion to yield a 10-H isocorrole.

Under acidic conditions, silver corroles demetalated to yield *meso*-hydroxy isocorroles. Triarylcorroles yielded both isomers, while 3-nitro substituted corroles exclusively produced the 5-isomer, presumably due to hydrogen bonding between the hydroxy and nitro groups.[144]

There are several examples of isocorrole to corrole conversion, induced by interactions with metals like copper,[140] gold,[143] manganese,[140] and cobalt.[128,140] The first report was one by the Paolesse group, where interactions with Co(II) ions caused a 10-hydroxy isocorrole to lose the hydroxy substituent and form a Co(III) corrole.[128] Interestingly, in the hands of the Ghosh group, the very same isocorrole retained the hydroxy substituent and formed a Co(II) isocorrole upon interactions with Co(II) ions.[142] A closer inspection of the reaction conditions revealed that the Ghosh group performed their complexation at lower temperatures, suggesting the isocorrole to corrole conversion was thermally induced. This notion was corroborated by Kadish and Paolesse *et al*., when they demonstrated that *meso*-methoxy isocorroles, upon copper complexation, formed small amounts of copper corroles.[140] The

yield for the isocorrole to corrole conversion increased with increasing temperature and/or reaction time, to the point where copper corrole was the main product and only traces of copper isocorrole remained.

The nature of the *meso*-substituent might also affect the stability of isocorroles against complexation. Setsune's 10,10-dimethylisocorrole coordinated manganese in excellent yield when exposed to $MnCl_2$,[134] in sharp contrast to Kadish and Paolesse's methoxyisocorrole, which led to manganese corrole as the only isolable product.[140] It stands to reason that methoxy substituents are better leaving groups than methyl substituents. However, in this case, the former reaction was commenced at lower temperatures, which could also explain the differences in reactivity.

β-Monobromination of a 3-NO_2-triarylcorrole resulted in a 2-Br-15-OH-17-NO_2-triarylisocorrole.[145] While formation of a *meso*-hydroxy isocorrole upon bromination of a corrole is not unprecendented,[128] bromination of the 2-position is indeed unexpected, as corroles tend to favor substitution at the 3-position.[146] This result led the authors to postulate that isocorrole formation preceded bromination. Brominating a pre-made isocorrole and inserting silver into the corrole to prevent isocorrole formation confirmed their hypothesis, as the results demonstrated that the isocorrole formed the 2-Br product and the corrole formed the 3-Br product exclusively (**Figure 3.9**). The authors also demonstrated that, in addition to interactions with metal cations, isocorrole to corrole conversion could be achieved by reduction with $NaBH_4$. Thus, while they are interesting in their own right, isocorroles also show promise as intermediates in corrole functionalization, allowing transformations that are otherwise not possible.

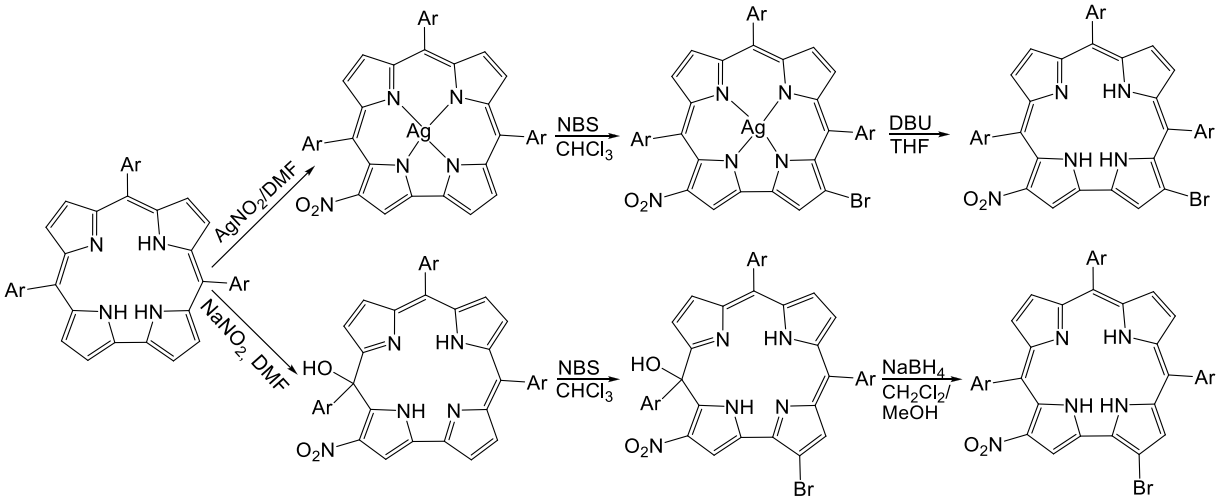

Figure 3.9. Bromination of isocorrole and corrole, demonstrating the difference in regioselectivity.

3.3 Electronic absorption spectra of isocorroles

Despite the interrupted macrocyclic conjugation, isocorroles exhibit surprisingly "porphyrin-like" electronic absorption spectra. **Figure 3.10** depicts examples of isocorrole UV-vis spectra. The left spectrum displays the isomers of a free-base isocorrole, while the right spectrum depicts a free-base isocorrole and two of its metal complexes.

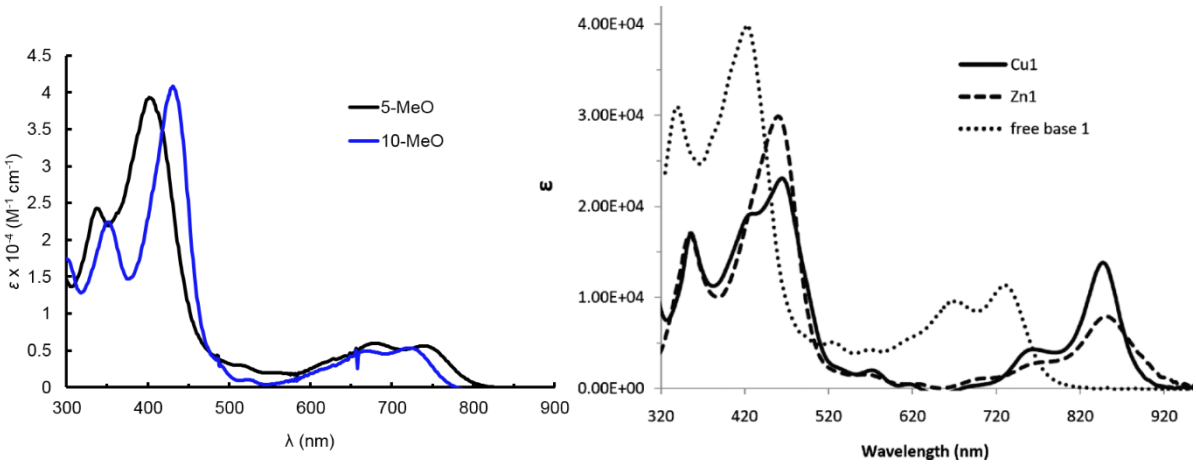

Figure 3.10. UV-vis spectra of 5/10-methoxy-5,10,15-triphenylisocorrole (left) and free-base, zinc and copper complexes of 5,5-dimethyl-10,15,bis(pentafluorophenyl)isocorrole (right). The right spectrum is adapted with permission from ref 136. Copyright 2011 The Royal Society of Chemistry.

Free-base isocorroles exhibit a strong Soret band in the 400-450 nm region, as well as sharp post-Soret absorptions in the near-UV. The relatively strong Q bands are broad, double-

humped features plateauing within 600-750 nm. Both the 5- and 10-isomer of a given isocorrole display similar UV-vis spectra. The only discernible difference is that the Soret band is slightly redshifted, and the Q bands slightly blueshifted, in the 10-isomers relative to the 5-isomers.

Metal complexation brings about a broadening of the Soret band (this effect is most pronounced in 5-isocorroles) and a redshift of the peak by several tens of nm. The Q bands are significantly redshifted and pushed well into the near-IR, absorbing in the 700-1000 nm region, depending on the metal. The Q bands retain their double-humped feature and the higher wavelength "hump" is significantly sharpened.

3.4 Molecular structure of isocorroles

Structurally, isocorroles resemble to corroles, with regard to their reluctance to deviate from planarity, which is thought to be a consequence of the rigidity of the direct pyrrole-pyrrole linkage.

Square planar complexes of nickel,[130,131,134,142] copper[131,136,140] and palladium[131] revealed essentially planar macrocycles where the metal was situated almost in the same plane as the four N atoms. The same was true for a six-coordinate RhCl(py) complex.[134] In five-coordinate complexes (i.e., FeCl, Fe_2O, and MnCl) the metal is slightly displaced from the macrocyclic plane while the macrocycle itself remains mostly flat.[134] The reluctance to assume nonplanar distortions is illustrated by two cobalt complexes bearing either bromines or aryl groups on all β-carbons;[142] both are planar despite significant peripheral crowding.

Macrocycle planarity is the norm for free-base isocorroles as well,[136,139,141] as for simple tetraphenylporphyrins,[147,148] but in sharp contrast to corroles that buckle under the pressure of having three core hydrogens.[55] Even in the presence of considerable steric crowding, i.e., β-octabromo and β-octaaryl derivatives, free-base isocorroles retain a planar macrocycle.[142,143]

A few examples of nonplanar isocorroles do exist. A zinc isocorrole crystallized with an axial solvent molecule to give a five-coordinate domed structure.[136] Two free-base β-nitro 5-hydroxy isocorroles exhibited slightly saddled structures, most likely due to hydrogen bonding between the nitro and hydroxy groups.[144,145] A dirhodium complex revealed a structure where two units of rhodium ($Rh(CO)_2$) bound the isocorrole on opposite sides, forcing the pyrroles on each side to tilt in the opposite direction of the rhodium moiety.[134]

3.5 Electrochemistry of isocorroles

Cyclic voltammetry studies of free-base, nickel, and copper tritolylisocorroles, bearing methoxy groups at either the 5- or the 10-position, all exhibit two reversible one-electron oxidations and one or two irreversible one-electron reductions.[140] While stable on the cyclic voltammetry time scale during the oxidative sweep, electron addition resulted in a chemical reaction, postulated as an elimination of the methoxy substituent followed by isocorrole to corrole conversion. Spectroelectrochemical experiments confirmed the hypothesis.

Cyclic voltammetry studies of nickel, palladium and copper complexes of a 10,10-dimethyl isocorrole revealed stable compounds that all exhibited three reversible one-electron processes, i.e., one reduction and two oxidations.[131] The oxidations and reduction occurred at similar potentials, across the three complexes, which pointed to ligand-centered redox processes.

3.6 New isocorrole ligands 1: Synthesis via the "oxidation-nucleophile" approach

In the remainder of this Chapter, I shall describe my own efforts in developing isocorrole chemistry. Parts of these efforts are also described in **Papers A** and **B** appended in this thesis.

Pyrrole-appended isocorroles

Attempts at synthesizing a corrole with long perfluoroalkyl chains consistently produced a compound where ESI-MS indicated a macrocycle with five units of pyrrole and three *meso*-carbons, initially suspected to be an isosmaragdyrin. While full characterization was hampered by low yield and solubility issues, the conditions responsible for the formation of the new macrocycle were theorized, and successfully applied to simpler triarylcorroles in much greater yield (**Figure 3.11**). Incidentally, the conditions that led to success were similar to the one-pot procedure for isocorrole synthesis developed by the Paolesse group (**Figure 3.7**).[141,149] With larger quantities available, the macrocycle could be identified by NMR and single-crystal X-ray structure analysis as a pyrrole-appended isocorrole. Pyrrole-appended isocorroles, both 5- and 10-isomers, were made starting from four different *meso*-tris(*para*-X-phenyl)corroles where X = CF_3, H, CH_3 and OCH_3, by adding pyrrole to a stirred solution of the corrole and DDQ in dichloromethane. The free-base isocorrole ligands could all be complexed to copper with $Cu(OAc)_2 \cdot H_2O$ in chloroform/methanol. Further details are available in **Paper A:** "Rapid one-pot synthesis of pyrrole-appended isocorroles."

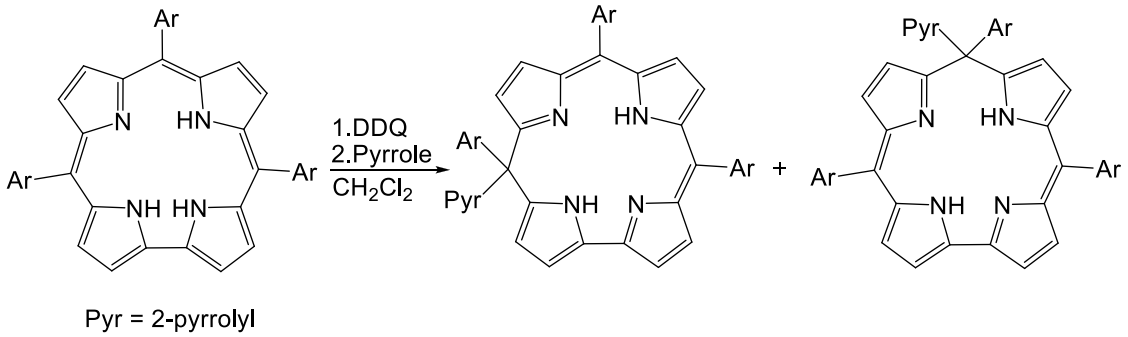

Figure 3.11. Synthesis of pyrrole-appended isocorroles

The successful coupling of pyrrole and corrole prompted an investigation into the scope of the method. First, I investigated furan and thiophene, due to their similarities to pyrrole. Unfortunately, no products were detected from adding furan or thiophene to a stirred solution of triarylcorrole and DDQ in dichloromethane. Heating the reaction to reflux did not work, nor did changing the solvent to chloroform. Finally, the reactions were commenced in refluxing furan or thiophene, but to no avail. The reduced reactivity of the two heterocycles, coupled with their relatively low boiling points, likely caused the reactions to fail.

Aryl-appended isocorroles

The synthesis of a *meso*-alkyl isocorrole, employing a Grignard reagent,[141] inspired the use of phenylmagnesiumbromide to prepare isocorroles. A solution of triphenylcorrole and DDQ in dichloromethane was briefly stirred before a solution of phenylmagnesiumbromide in THF was added. After about 50 minutes of stirring, the reaction was worked up, and 5,5,10,15-tetraphenylisocorrole was isolated, albeit in extremely low yields. The low yield was likely due to interactions between the Grignard and the solvent. Replacing dichloromethane with toluene led to a significant improvement. While still low-yielding (8.7 %), the reaction yielded enough for characterization. A nickel chelate of the tetraphenylisocorrole was prepared via the interaction with $Ni(OAc)_2 \cdot 4H_2O$ in chloroform/methanol.

The most striking features of the two tetraphenylisocorroles are their electronic absorption spectra. **Figure 3.12** depicts their UV-vis-NIR spectra where the typical double-humped Q bands are replaced by an even wider “single humped” absorption that ranges 600-900 nm for the free base and 700-1000 nm for the nickel complex.

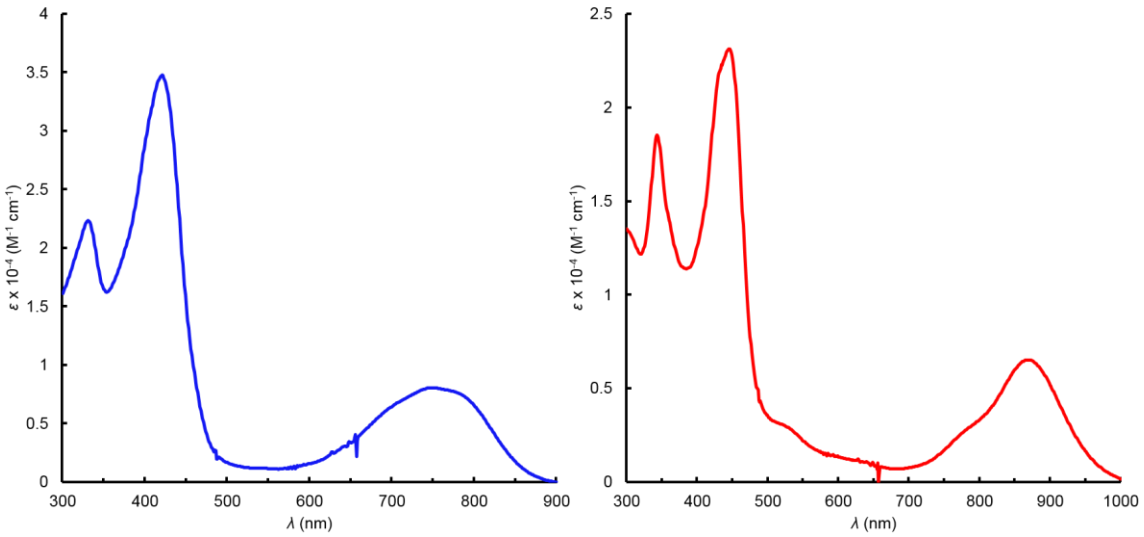

Figure 3.12. UV-vis spectra of 5,5,10,15-tetraphenylisocorrole (left) and Ni[5,5,10,15-tetraphenylisocorrole] (right)

The low yield of tetraphenylisocorrole rendered its synthesis largely impractical. Its intriguing absorption properties, however, inspired the continued quest for aryl-appended isocorroles. As more reactive nucleophiles, anilines and phenols were of obvious interest. To avoid reactions at the nitrogen and oxygen, however, *N*,*N*-dimethylaniline (DMA) and anisole were employed as reactants.

Thus, to a stirred solution of tritolylcorrole in dichloromethane and DMA, I added DDQ. After a few minutes of stirring, the reaction was worked up to reveal that, surprisingly, no isocorroles had formed and most of the tritolylcorrole was recovered. Upon closer inspection it became evident that DDQ reacted instantly with DMA, presumably to DMA polymers. Changing the order of additions, DDQ to oxidize the corrole before adding DMA, allowed the DMA-appended isocorroles to form (**Figure 3.13**), albeit in low yields (~20% for both isomers). Both isomers exhibited electronic absorptions typical of isocorroles.

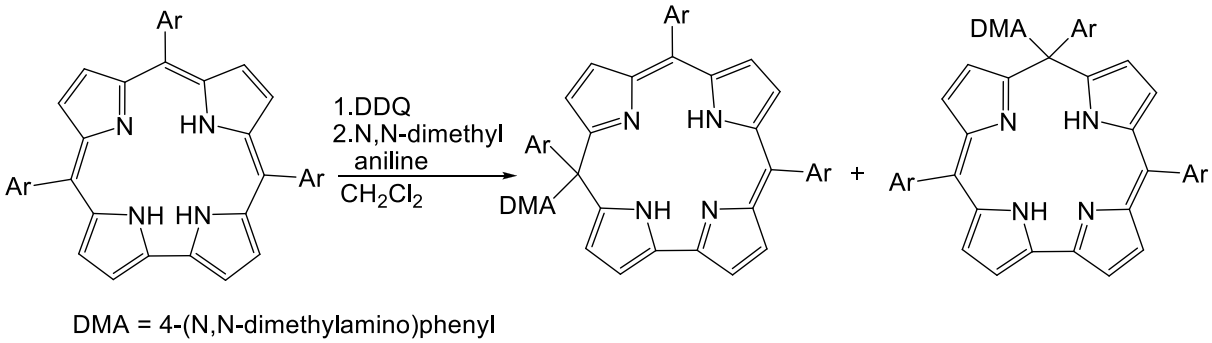

Figure 3.13. Synthesis of dimethylaniline-appended isocorroles.

Next, I experimented with anisole. To prevent *ortho*-substitution, 2,6-dimethylanisole (referred to simply as anisole) was employed. Adding anisole to a stirred solution of a triarylcorrole and DDQ in dichloromethane did not result in any reaction. Nor did refluxing the solution or employing higher boiling solvents like chloroform, toluene or DMSO. Purifying the starting corroles were unsuccessful, as were using fresh bottles of DDQ and anisole. Finally, triarylcorrole and DDQ were refluxed in pure anisole. An isocorrole product was detectable in ESI-MS, however, all attempts at isolating the product failed. In hindsight, it seems the steps taken to prevent *ortho*-substitution were ultimately responsible for the failure of the reaction. The isocorrole formed at elevated temperatures, however, it could not be isolated at room temperature, which likely means the increased steric strain from the *ortho*-methyl groups caused the anisole group to be labile, and too unstable to exist at room temperature.

3.7 New isocorrole ligands 2: Synthesis via radical coupling

Gold corroles have shown considerable potential as photoactive materials, particularly in photodynamic therapy and dye-sensitized solar cells (DSSCs).[71] In our group, it was postulated that electron-withdrawing groups on the gold corrole *β*-positions would further improve their efficiencies in DSSCs. To that end, two electrophilic trifluoromethylating reagents, 3,3-dimethyl-1-(trifluoromethyl)-1,2-benziodoxole (Togni reagent)[150] and 5-(trifluoromethyl)dibenzothiophenium tetrafluoroborate (Umemoto reagent)[151], should allow corroles to add CF_3 groups to their *β*-positions via electrophilic aromatic substitution.

Initial results were baffling. A free-base corrole, trianisylcorrole, did indeed pick up a CF_3 group from the Togni reagent. The product was not, however, a *β*-CF_3 corrole, but rather a *meso*-CF_3 isocorrole. It quickly became evident that the hypervalent-iodine nature of the Togni reagent likely caused it to oxidize the corrole instead of transferring a CF_3 group. After

a proton exchange, the Togni radical eliminated a CF_3 radical that coupled with the corrole radical. **Figure 3.14** depicts the suggested mechanism. An important aspect of this reaction is that it represents a potential new route to isocorroles that compliments the oxidation-nucleophile approach developed by Paolesse *et al.*[139,141] Single-electron oxidation, followed by coupling with radicals, could open up a new avenue of attack where in principle any radical could be added to the *meso*-carbon of a corrole.

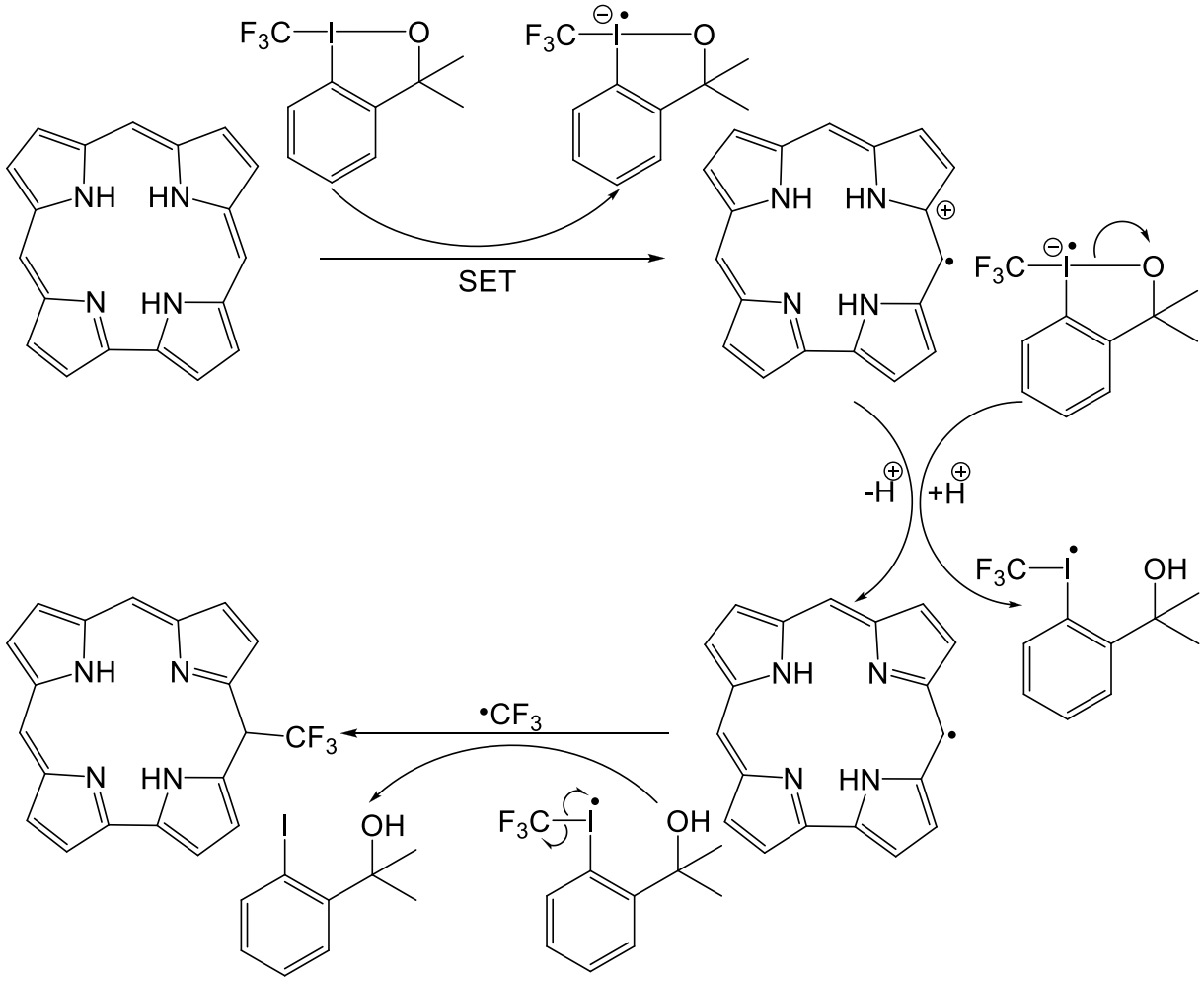

Figure 3.14. Proposed mechanism of *meso*-CF_3 isocorrole formation. Aryl groups have been omitted for clarity.

ESI-MS evidence indicated that both trifluoromethylating reagents acted upon free-base and copper tritolylcorrole to form *meso*-CF_3 isocorrole. Interestingly, the two reagents reacted with gold tritolylcorrole to yield *β*-CF_3 products, presumably due to the higher oxidation potential of gold corroles.[152] Interestingly, reacting the gold corrole with Umemoto's reagent at 80°C produced two isomers, 2-CF_3 and 3-CF_3, indicative of an isocorrole reactive intermediate.[145] While no isocorrole was isolated, reducing the temperature of the reaction to

40°C allowed detection of the gold isocorrole in the ESI-MS. Knowing that gold insertion to an isocorrole may induce rearomatization to corrole,[143] it is indeed possible that a short-lived gold isocorrole formed *in situ*, and existed long enough to trifluoromethylate its 2-position, before reverting to the corrole.

3.8 Palladium isocorroles

As for isoporphyrins, the near-IR absorptions of isocorroles herald potential applications as photosensitizers in PDT. Whereas stable isoporphyrins require lengthy synthesis, stable isocorroles are readily available, particularly with the discovery of pyrrole- and other aryl-appended isocorroles.

As zinc and palladium porphyrins are known phosphors,[74] attempts at preparing the corresponding complexes from pyrrole-appended isocorroles were made. While zinc complexation failed, briefly heating a DMF solution of a pyrrole-appended isocorrole and $Pd(OAc)_2$ to reflux, resulted in the corresponding palladium complex. Similarly, palladium complexes of a DMA-appended isocorrole and 10-CF_3 isocorrole were prepared.

Interestingly, palladium insertion into a mixture of 5-CF_3 and 10-CF_3 isocorroles revealed an intriguing selectivity. While both free bases were isolated in reasonable yields, only the 10-CF_3 isomer proved readily amenable to palladium insertion. No traces of a 5-CF_3 palladium complex was detected, and most of the free base was recovered. This is the second account of such peculiar selectivity. The first was for nickel insertion into a mixture of 5- and 10-MeO isocorroles, which exclusively produced the nickel complex of the 10-isomer (for details see **Paper B**: "Isocorroles as Homoaromatic NIR-Absorbing Chromophores: A First Quantum Chemical Study.")

Unfortunately, no emissions were detected during preliminary phosphorescence measurements on the pyrrole-appended palladium complex.

3.9 Aromaticity of isocorroles

Much like isoporphyrins, the proton NMR of isocorroles exhibit upfield shifted *β*-protons compared to corrole.[33] While clearly an indicator of reduced aromatic properties, due to the saturated *meso*-carbon, the proton NMR also exhibits unusually downfield shifted core protons. Whereas corrole core protons resonate around -3 ppm, the core protons of isocorroles resonate between 13 and 17 ppm, indicative of antiaromatic properties.

DFT calculations of magnetically induced current densities revealed a net diatropic ring current circulates the periphery of an unsubstituted nickel isocorrole. The current strength was calculated to ~9.8 nAT^{-1}, comparable to that of an unsubstituted zinc isoporphyrin.[125] Like other porphyrinoid systems,[2] diatropic currents circulate around the outer rim of the macrocycle while paratropic ones flow around the inner $C_{11}N_4$ framework. Whereas the contribution from diamagnetic currents are an order of magnitude greater than the paramagnetic currents in the case of porphine,[2] the nature of the net global currents in isocorroles depend on the nature of the *meso*-substituent (**Figure 3.15**). Fluoride substituents quench the diamagnetic currents, and the calculations show that Ni[10-F_2-isoCor] sustains a net paratropic current of -6.8 nAT^{-1}. On the other hand, trimethylsilyl groups enhance the diamagnetic currents, and Ni[10-$(Me_3Si)_2$-isoCor] sustains a net diamagnetic current of 15.6 nAT^{-1}.

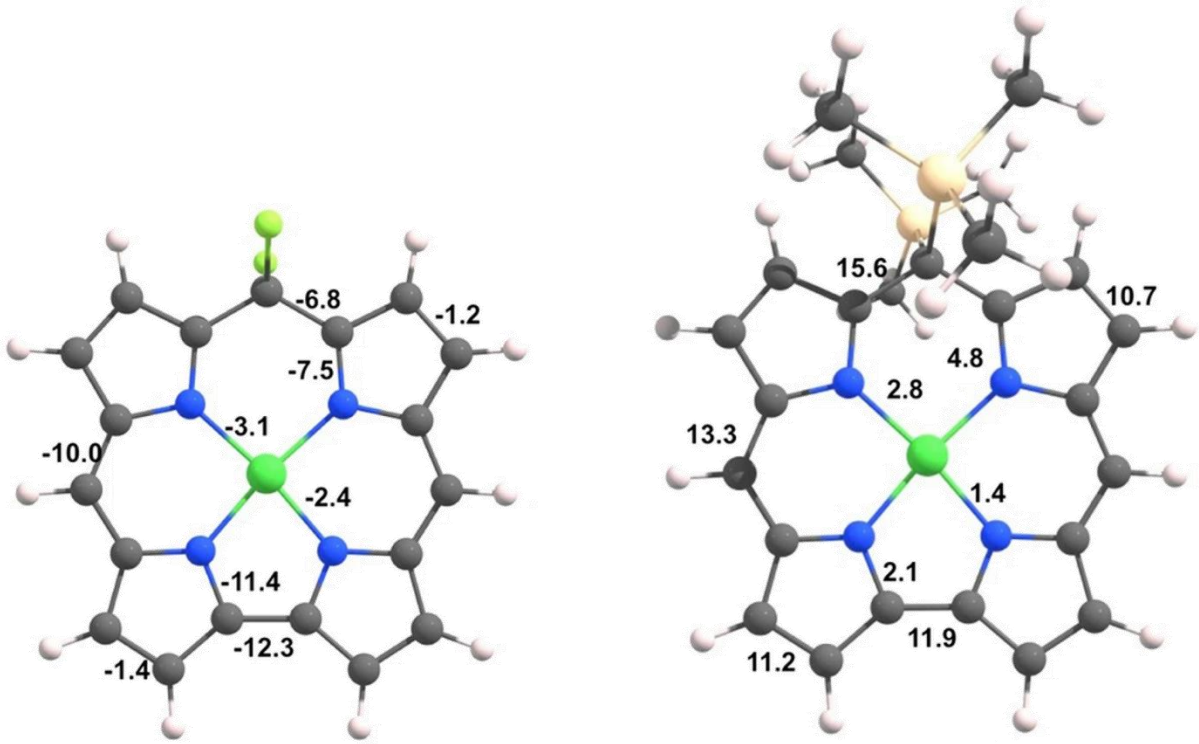

Figure 3.15. Calculated current densities (in nAT^{-1}) passing through selected bonds of Ni[10-F_2-isoCor] (left) and Ni[10-$(Me_3Si)_2$-isoCor] (right), calculated 1 bohr above the molecular plane. Adapted with permission from ref 127. Copyright 2018 Springer Nature.

The above results are clear indications of homoaromaticity and homoantiaromaticity, i.e., the presence of a ring current in organic molecules where conjugation is broken by an sp^3 atom.[153,154] TDDFT calculations provided conclusive proof. The calculations revealed four π-

type occupied MOs and the LUMO as having significant hyperconjugative interactions, i.e., significant amplitudes at the saturated *meso*-carbon. Whereas hyperconjugation through a $C(SiMe_3)_2$ moiety contributes two "pseudo" electrons to the π-system, the electron-withdrawing effect of the fluorides means a CF_2 moiety does not. Applying Hückel's rule, the former results in 22 π-electrons, and hence an aromatic macrocycle, while the latter results in 20 π-electrons and an antiaromatic system.[155]

For further details see **Paper B**: "Isocorroles as Homoaromatic NIR-Absorbing Chromophores: A First Quantum Chemical Study".

3.10 Experimental section

Materials

All free-base corroles were synthesized via the now standard water-methanol method.[38] Gold corroles were prepared according to a literature procedure.[152] All reagents, except pyrrole, were purchased from Sigma-Aldrich and used as received. Pyrrole was passed through basic alumina (aluminium oxide 60, active basic activity I, 0.063-0.200 mm particle size, 70-230 mesh, Merck) and stored in the freezer. Silica gel 60 (0.04-0.063 mm particle size, 230-400 mesh, Merck) was employed for flash chromatography. Silica gel 60 preparative thin-layer chromatographic plates (20 cm x 20 cm x 0.5 mm, Merck) were used for final purification of all compounds.

General instrumental methods

UV-visible spectra were recorded on an HP 8453 spectrophotometer. ^{1}H NMR spectra were recorded on a 400 MHz Bruker Avance III HD spectrometer equipped with a 5 mm BB/1H SmartProbe and referenced to either residual CH_2Cl_2 at 5.32 ppm or residual $CHCl_3$ at 7.26 ppm. High-resolution electrospray-ionization (HR-ESI) mass spectra were recorded on an LTQ Orbitrap XL spectrometer, using methanolic solutions and typically in positive ion mode.

Synthetic methods

Synthesis of 5,5,10,15-tetraphenylisocorrole: To a stirred solution of triphenylcorrole (54 mg) and DDQ (23.1 mg, ~1eq) in dry toluene (25 mL) was added a solution of phenylmagnesiumbromide 1.0 M in THF (0.47 mL, 5 eq), under argon. After 50 minutes of stirring, the solvents were removed under vacuum and the resulting solids passed through a plug of silica with dichloromethane. All fractions were collected, the solvents removed under vacuum, and the solids purified by preparative thin-layer chromatography employing dichloromethane/*n*-hexane 2:1 as solvent. A green fraction (R_f = 0.34) was collected and purified again by preparative thin-layer chromatography employing *n*-hexane/ethyl acetate 5:1 as solvent to give the product as an olive-green band. Yield: 8.5 mg (13.7 %); UV-Vis (CH_2Cl_2): λ_{max} (nm), [ϵ x 10^{-4} ($M^{-1}cm^{-1}$)]: 331 (2.2), 421 (3.5), 747 (0.8); ^{1}H NMR (400 MHz, $CDCl_3$, δ): 14.68 (s, 1H, NH), 13.30 (s, 1H, NH), 7.61 – 7.52 (m, 3H, overlapping *β*-H and Ph), 7.47 – 7.26 (m, 16H, Ph), 7.24 (d, *J* = 7.5 Hz, 2H, Ph), 6.55 (d, *J* = 4.6 Hz, 1H, *β*-H), 6.45 (d, *J* = 5.5 Hz, 1H, *β*-H), 6.33 (d, *J* = 4.9 Hz, 1H, *β*-H), 6.30 (d, *J* = 5.4 Hz, 1H, *β*-H), 6.18 (d, *J* = 3.9 Hz, 1H, *β*-H), 6.13 (d, *J* = 4.6 Hz, 1H, *β*-H), 6.01 (d, *J* = 3.8 Hz, 1H, *β*-H); MS (MALDI-TOF): m/z calcd for $C_{43}H_{30}N_4H$: 603.2548 [$M+H^+$]; found: 603.2346

Synthesis of Ni[5,5,10,15-tetraphenylisocorrole]: To a solution of 5,5,10,15-tetraphenylisocorrole (3.6 mg) in chloroform (10 mL) was added a solution of $Ni(OAc)_2 \cdot 4 H_2O$ (14.3 mg, 10 eq) in MeOH (2 mL) and the resulting solution was stirred at room temperature overnight. The solvents were removed under vacuum and the solids passed through a plug of silica with dichloromethane. All fractions were collected, the solvents removed under vacuum, and the solids purified by preparative thin-layer chromatography employing *n*-hexane/ethyl acetate 10:1 as solvent, to give the product as a brown band. Yield: 1.6 mg (38.8 %); UV-Vis (CH_2Cl_2): λ_{max} (nm), [ϵ x 10^{-4} ($M^{-1}cm^{-1}$)]: 343 (1.85), 445 (2.31), 868 (0.65); ^{1}H NMR (400 MHz, $CDCl_3$, δ): 7.60 (d, *J* = 5.4 Hz, 1H, *β*-H), 7.57 – 7.51 (m, 3H, Ph), 7.50 – 7.31 (m, 14H, Ph), 7.25 – 7.15 (m, 3H, Ph), 6.96 (d, *J* = 5.2 Hz, 1H, *β*-H), 6.85 (d, *J* = 5.1 Hz, 1H, *β*-H), 6.81 (d, *J* = 4.8 Hz, 1H, *β*-H), 6.73 (d, *J* = 4.1 Hz, 1H, *β*-H), 6.52 – 6.45 (m, 3H, *β*-H); MS (MALDI-TOF): m/z calcd for $C_{43}H_{28}N_4Ni$: 658.1667 [M^+]; found: 658.2018

Synthesis of 5/10-[4-(*N*,*N*-dimethylamino)phenyl]-5,10,15-tris(4-methylphenyl)isocorrole: To a solution of 5,10,15-tris(4-methylphenyl)corrole (44.8 mg) in dichloromethane (20 mL) was added DDQ (18 mg, 1 eq) and *N*,*N*-dimethylaniline (499 μL,

50 eq) in succession. After 5 minutes stirring, the solvents were removed under vacuum and the solids passed through a plug of silica with dichloromethane to yield the crude product as a mixture of the 5- and 10-isomers. Separation of the two regioisomers was accomplished with preparative thin-layer chromatography employing dichloromethane/*n*-hexane 2:1 as solvent. Yields and analytical details are as follows:

5-[4-(*N*,*N*-dimethylaminophenyl)]-5,10,15-tris(4-methylphenyl)isocorrole: Yield 10.1 mg (18.6 %); UV-Vis (CH_2Cl_2) λ_{max} (nm) [ϵ x 10^{-4} ($M^{-1}cm^{-1}$)]: 343 (1.75), 416 (3.24), 678 (0.40), 736 (0.39); ^{1}H NMR (400 MHz, CD_2Cl_2, δ): 15.08 (s, 1H, NH), 14.96 (s, 1H, NH), 7.45 (d, *J* = 7.9 Hz, 2H, 15-*o*-Ph), 7.35 (d, *J* = 6.9, 2H, 10-*o*-Ph), 7.30 (d, *J* = 7.6 Hz, 2H, 15-*m*-Ph), 7.26 – 7.21 (m, 4H, overlapping 5-*o*-Ph and 10-*m*-Ph), 7.16 [d, *J* = 8.6 Hz, 2H, 3-(*N*,*N*-dimethylaminophenyl)], 7.07 (d, *J* = 7.9 Hz, 2H, 5-*m*-Ph), 7.03 (d, *J* = 4.5 Hz, 1H, *β*-H), 6.96 (d, *J* = 4.5 Hz, 1H, *β*-H), 6.64 – 6.56 [m, 4H, overlapping 2-(*N*,*N*-dimethylaminophenyl) and *β*-H], 6.43 (dd, *J* = 4.3, 1.9 Hz, 1H, *β*-H), 6.40 (d, *J* = 4.6 Hz, 1H, *β*-H), 6.23 (dd, *J* = 4.3, 2.4 Hz, 1H, *β*-H), 5.83 (dd, *J* = 3.6, 2.2 Hz, 1H, *β*-H), 2.91 [s, 6H, (*N*,*N*-dimethylaminophenyl)-CH_3], 2.44 (s, 3H, 15-*p*-CH_3), 2.43 (s, 3H, 10-*p*-CH_3), 2.32 (s, 3H, 5-*p*-CH_3). MS (ESI): m/z calcd for $C_{48}H_{41}N_5H$: 688.3435 [$M+H^+$]; found: 688.3433.

10-[4-(*N*,*N*-dimethylaminophenyl)]-5,10,15-Tris(4-methylphenyl)isocorrole: Yield 0.95 mg (1.8 %); UV-Vis (CH_2Cl_2) λ_{max} (nm) [ϵ x 10^{-4} ($M^{-1}cm^{-1}$)]: 358 (1.76), 438 (3.14), 671 (0.32), 718 (0.35); ^{1}H NMR (400 MHz, $CDCl_3$, δ): 14.95 (s, 2H, NH), 7.48 (d, *J* = 8.0 Hz, 4H, 5/15-*o*-Ph), 7.28 – 7.23 (m, 4H, 5/15-*m*-Ph), 7.08 – 7.02 (m, 4H, overlapping 10-*o*-Ph and 10-*m*-Ph), 6.98 [d, *J* = 8.9 Hz, 2H, 2-(*N*,*N*-dimethylaminophenyl)], 6.68 (d, *J* = 4.1 Hz, 2H, *β*-H), 6.65 (d, *J* = 4.1 Hz, 2H, *β*-H), 6.61 [d, *J* = 8.7 Hz, 2H, 3-(*N*,*N*-dimethylaminophenyl)], 6.54 (d, *J* = 4.3 Hz, 2H, *β*-H), 5.96 (d, *J* = 4.3 Hz, 2H, *β*-H), 2.92 [s, 6H, (*N*,*N*-dimethylaminophenyl)-CH_3], 2.44 (s, 6H, 5/15-*p*-CH_3), 2.32 (s, 3H, 10-*p*-CH_3); MS (ESI): m/z calcd for $C_{48}H_{41}N_5H$: 688.3435 [$M+H^+$]; found: 688.3434.

Synthesis of 5/10-CF_3-5,10,15-tris(4-methoxyphenyl)isocorrole: To a solution of 5,10,15-tris(4-methoxyphenyl)corrole (21.6 mg) in dry dichloromethane (10 mL) was added 3,3-dimethyl-1-(trifluoromethyl)-1,2-benziodoxole (20.4 mg, ~1.8 eq). After stirring under argon for 1.5 h, the solvent was removed under vacuum and the resulting solids passed through silica with dichloromethane/*n*-hexane 1:1 as solvent to yield the crude product as a mixture of the 5- and 10-isomers. Separation of the two regioisomers was accomplished with preparative

thin-layer chromatography employing dichloromethane/*n*-pentane 1:1 as solvent. Yields and analytical details are as follows:

5-CF_3-5,10,15-tris(4-methoxyphenyl)isocorrole: Yield 5.2 mg (21.7 %); UV-Vis (CH_2Cl_2) λ_{max} (nm) [ϵ x 10^{-4} ($M^{-1}cm^{-1}$)]: 335 (1.59), 354 (1.63), 413 (4.75), 660 (0.63), 716 (0.62); ^{1}H NMR (400 MHz, $CDCl_3$, δ): 14.93 (s, 1H, NH), 14.79 (s, 1H, NH), 7.51 (d, J = 8.3 Hz, 2H, 5/15-*o*-Ph), 7.42 (dd, J = 18.5, 8.7 Hz, 2H, 5/15-*o*-Ph), 7.35 (d, J = 8.6 Hz, 2H, 10-*o*-Ph), 7.09 (d, J = 4.5 Hz, 1H, *β*-H), 7.04 – 6.92 (m, 5H, overlapping 5,15-*m*-Ph and *β*-H), 6.82 (d, J = 4.5 Hz, 2H, 10-*m*-Ph), 6.69 (d, J = 4.6 Hz, 1H, *β*-H), 6.65 – 6.62 (m, 1H, *β*-H), 6.51 (dd, J = 4.3, 1.9 Hz, 1H, *β*-H), 6.38 (dd, J = 4.3, 2.5 Hz, 1H, *β*-H), 6.35 (d, J = 4.6 Hz, 1H, *β*-H), 6.05 – 6.02 (m, 1H, *β*-H), 3.90 (s, 3H, 5/15-*p*-OCH_3), 3.89 (s, 3H, 5/15-*p*-OCH_3), 3.79 (s, 3H, 10-*p*-OCH_3); MS (ESI): m/z calcd for $C_{41}H_{31}N_4F_3O_3H$: 685.2421 [$M+H^+$]; found: 685.2429.

10-CF_3-5,10,15-tris(4-methoxyphenyl)isocorrole: Yield 3.3 mg (13.8 %); UV-Vis (CH_2Cl_2) λ_{max} (nm) [ϵ x 10^{-4} ($M^{-1}cm^{-1}$)]: 427 (3.35), 657 (0.56), 699 (0.60); ^{1}H NMR (400 MHz, $CDCl_3$, δ): 14.59 (s, 2H, NH), 7.50 (d, J = 8.4 Hz, 4H, 5/15-*o*-Ph), 7.28 (d, J = 8.6 Hz, 2H, 10-*o*-Ph), 6.93 (d, J = 8.7 Hz, 4H, 5,15-*m*-Ph), 6.82 (d, J = 9.0 Hz, 2H, 10-*m*-Ph), 6.77 (d, J = 4.2 Hz, 2H, *β*-H), 6.73 (d, J = 4.2 Hz, 2H, *β*-H), 6.55 (d, J = 4.3 Hz, 2H, *β*-H), 5.90 (d, J = 4.3 Hz, 2H, *β*-H), 3.83 (s, 6H, 5/15-*p*-OCH_3), 3.76 (s, 3H, 10-*p*-OCH_3); MS (ESI): m/z calcd for $C_{41}H_{31}N_4F_3O_3H$: 685.2421 [$M+H^+$]; found: 685.2428.

Synthesis of palladium isocorroles: A solution of free-base isocorrole (10-15 mg) and $Pd(OAc)_2$ (1.5 eq) in dry DMF (10 mL) was heated to reflux and immediately cooled down to room temperature. The solvent was removed under vacuum, and the solids passed through a silica plug with dichloromethane. The solvent was removed under vacuum and the resulting solids purified by preparative thin-layer chromatography. Solvents employed, yields, and analytical details are as follows:

Pd[5-(2-pyrrolyl)-5,10,15-tris(4-methoxyphenyl)isocorrole]: Prep-TLC (dichloromethane/n-hexane 9:1); yield 1.8 mg (12.4 %); UV-Vis (CH_2Cl_2) λ_{max} (nm) [ϵ x 10^{-4} ($M^{-1}cm^{-1}$)]: 389 (1.05), 443 (2.12), 587 (0.26), 630 (0.24), 821 (0.28), 904 (0.36); ^{1}H NMR (400 MHz, $CDCl_3$, δ): 8.13 (s, 1H, 1-pyrrolyl), 7.45 – 7.40 (m, 4H, overlapping 5-*o*-Ph and 15-*o*-Ph), 7.21 (d, J = 9.0 Hz, 2H, 10-*o*-Ph), 7.00 – 6.93 (m, 4H, overlapping 5-*m*-Ph and 15-*m*-Ph), 6.80 – 6.74 (m, 4H, overlapping 10-*m*-Ph and *β*-H), 6.72 – 6.69 (m, 2H, overlapping *β*-H), 6.60 – 6.53 (m, 3H, overlapping 5-pyrrolyl and *β*-H), 6.47 (d, J = 4.6 Hz, 1H, *β*-H),

6.21 – 6.18 (m, 1H, 4-pyrrolyl), 6.10 – 6.07 (m, 1H, 3-pyrrolyl), 5.92 (d, J = 3.8 Hz, 1H, *β*-H), 3.90 – 3.86 (m, 6H, overlapping 5- and 15-*p*-OCH_3), 3.78 (s, 3H, 10-*p*-OCH_3); MS (ESI): m/z calcd for $C_{44}H_{33}N_5O_3Pd$: 785.1628 [M^+]; found: 785.1646.

Palladium 5-[4-(*N*,*N*-dimethylaminophenyl)]-5,10,15-tris(4-methylphenyl)isocorrole: Prep-TLC (dichloromethane/n-hexane 2:1); yield 2.1 mg (18.1 %); UV-Vis (CH_2Cl_2) λ_{max} (nm) [ϵ x 10^{-4} ($M^{-1}cm^{-1}$)]: 372 (2.53), 446 (4.37), 589 (0.55), 635 (0.48), 837 (0.57), 928 (0.85); ^{1}H NMR (400 MHz, $CDCl_3$, δ): δ 7.39 – 7.33 (m, 6H, 5/10/15-*o*-Ph), 7.31 [d, *J* = 8.4 Hz, 2H, 3-(*N*,*N*-dimethylaminophenyl)], 7.24 (d, *J* = 7.8 Hz, 2H, 5/10/15-*m*-Ph), 7.20 (d, *J* = 7.7 Hz, 2H, 5/10/15-*m*-Ph), 7.02 (d, *J* = 8.0 Hz, 2H, 5/10/15-*m*-Ph), 6.74 – 6.70 (m, 2H, overlapping *β*-H), 6.64 (d, *J* = 3.9 Hz, 1H, *β*-H), 6.61 – 6.54 [m, 3H, overlapping *β*-H and 2-(*N*,*N*-dimethylaminophenyl)], 6.52 – 6.46 (m, 3H, overlapping *β*-H), 5.89 (d, *J* = 4.0 Hz, 1H, *β*-H), 2.92 [s, 6H, (*N*,*N*-dimethylaminophenyl)-CH_3)], 2.43 (s, 3H, 5/10/15-*p*-CH_3), 2.42 (s, 3H, 5/10/15-*p*-CH_3), 2.31 (s, 3H, 5/10/15-*p*-CH_3); MS (ESI): m/z calcd for $C_{48}H_{39}N_5Pd$: 791.2252 [M^+]; found: 791.2300.

Pd[10-CF_3-5,10,15-tris(4-methoxyphenyl)isocorrole]: Prep-TLC (dichloromethane/n-hexane 2:1); yield 3 mg (16.5 %); UV-Vis (CH_2Cl_2) λ_{max} (nm) [ϵ x 10^{-4} ($M^{-1}cm^{-1}$)]: 431 (4.28), 547 (1.14), 767 (0.38), 848 (0.94); ^{1}H NMR (400 MHz, $CDCl_3$, δ): 7.46 – 7.37 (m, 4H 5,15-*o*-Ph, 7.24 (d, J = 8.6 Hz, 2H, 10-*o*-Ph), 6.94 – 6.86 (m, 4H, 5,15-*m*-Ph), 6.76 (d, J = 9.2 Hz, 2H, 10-*m*-Ph), 6.56 – 6.52 (m, 4H, *β*-H), 6.50 (d, J = 4.3 Hz, 2H, *β*-H), 6.02 – 5.98 (m, 2H, *β*-H), 3.82 (s, 6H, 5,15-*p*-OCH_3), 3.72 (s, 3H, 10-*p*-OCH_3); MS (ESI): m/z calcd for $C_{41}H_{29}N_4F_3O_3PdNa$: 811.1134 [M+$Na^+$]; found: 811.1159.

Synthesis of Au[2-CF_3-5,10,15-tris(4-methylphenyl)corrole] and Au[3-CF_3-5,10,15-tris(4-methylphenyl)corrole]: Two reaction mixtures, one with Au[5,10,15-tris(4-methylphenyl)corrole] (19.8 mg) and 5-(trifluoromethyl)dibenzothiophenium tetrafluoroborate (23.1 mg, ~2.5 eq) in dry acetonitrile (10 mL). The other with Au[5,10,15-tris(4-methylphenyl)corrole] (14.5 mg) and 5-(trifluoromethyl)dibenzothiophenium tetrafluoroborate (16.5 mg, ~2.5 eq) in dry acetonitrile (10 mL), were stirred at 80°C for 3 h. The reaction mixtures were combined, the solvents dried under vacuum, and the solids passed through a silica column with dichloromethane/*n*-pentane 1:2 to yield the crude product as a mixture of the 2- and 3-isomers. Separation of the two regioisomers was accomplished with preparative thin-layer chromatography employing dichloromethane/*n*-pentane 1:4 as solvent. Yields and analytical details are as follows:

Au[2-CF_3-5,10,15-tris(4-methylphenyl)corrole]: Yield 1.3 mg (3 %); UV-Vis (CH_2Cl_2) λ_{max} (nm) [ϵ x 10^{-4} ($M^{-1}cm^{-1}$)]: 416 (2.49), 563 (0.69), 581 (0.93); ^{1}H NMR (400 MHz, $CDCl_3$, δ): 9.20 (d, J = 4.3Hz, 1H, *β*-H), 9.03 – 8.96 (m, 3H, overlapping *β*-H), 8.84 (d, J = 4.2Hz, 1H, *β*-H), 8.77 – 8.72 (m, 2H, overlapping *β*-H), 8.17 – 8.12 (m, 4H, overlapping 5-*o*-Ph and 15-*o*-Ph), 8.04 (d, J = 7.7Hz, 2H, 10-*o*-Ph), 7.65 – 7.60 (m, 4H, overlapping 5-*m*-Ph and 15-*m*-Ph), 7.58 (d, J = 7.7Hz, 2H, 10-*m*-Ph), 2.70 (s, 6H, 5,15-*p*-CH_3), 2.69 (s, 3H, 10-*p*-CH_3); MS (ESI): m/z calcd for $C_{41}H_{28}N_4F_3Au$: 830.19 [M^+]; found: 830.1941.

Au[3-CF_3-5,10,15-tris(4-methylphenyl)corrole]: Yield 1.6 mg (4 %); UV-Vis (CH_2Cl_2) λ_{max} (nm) [ϵ x 10^{-4} ($M^{-1}cm^{-1}$)]: 416 (5.35), 563 (1.48), 577 (1.77); ^{1}H NMR (400 MHz, $CDCl_3$, δ): 9.50 (s, 1H, *β*-H), 9.12 (d, J = 4.5Hz, 1H, *β*-H), 9.00 (d, J = 5.0Hz, 1H, *β*-H), 8.83 (d, J = 4.6Hz, 1H, *β*-H), 8.75 (d, J = 5.0Hz, 1H, *β*-H), 8.67 (d, J = 4.9Hz, 1H, *β*-H), 8.61 (d, J = 5.0Hz, 1H, *β*-H), 8.15 (d, J = 7.8Hz, 2H, 5-*o*-Ph), 8.02 (d, J = 7.7Hz, 2H, 10-*o*-Ph), 7.96 (d, J = 7.6Hz, 2H, 15-*o*-Ph), 7.62 (d, J = 7.7Hz, 2H, 5-*m*-Ph), 7.56 (d, J = 7.8Hz, 2H, 10-*m*-Ph), 7.48 (d, J = 7.7Hz, 2H, 15-*m*-Ph), 2.70 (s, 3H, 5-*p*-CH_3), 2.69 (s, 6H, 10,15-*p*-CH_3). MS (ESI): m/z calcd for $C_{41}H_{28}N_4F_3Au$: 830.19 [M^+]; found: 830.1939.

3.11 Supporting information

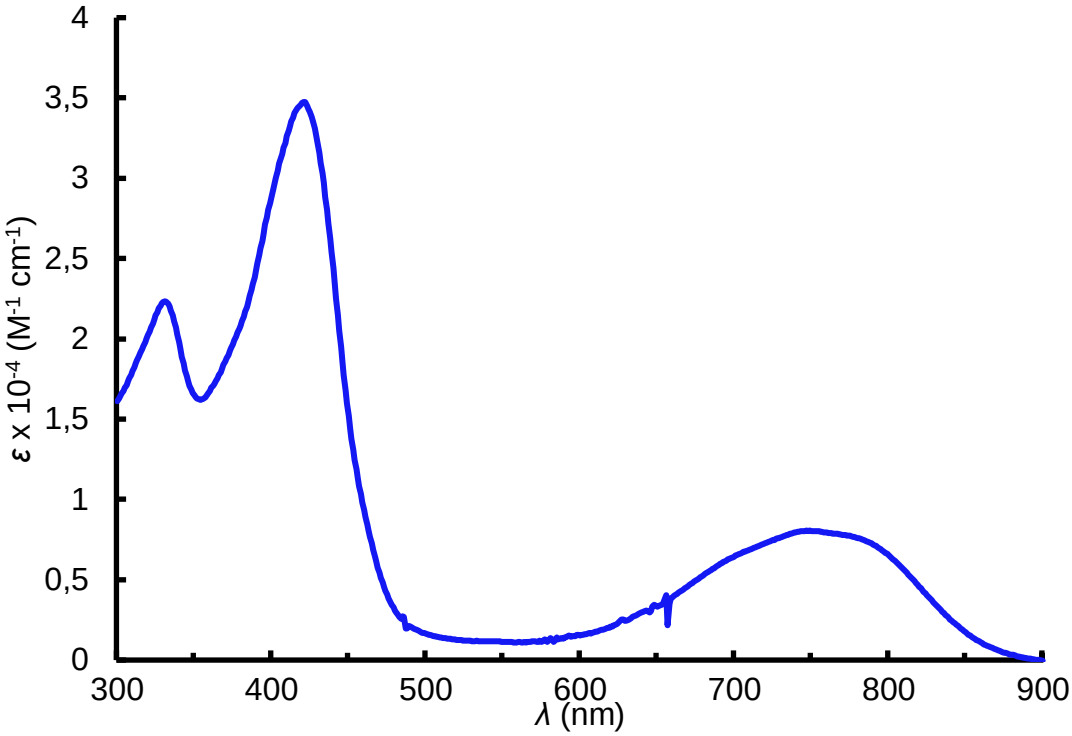

Figure 3.16. UV-vis spectrum of 5,5,10,15-tetraphenylisocorrole.

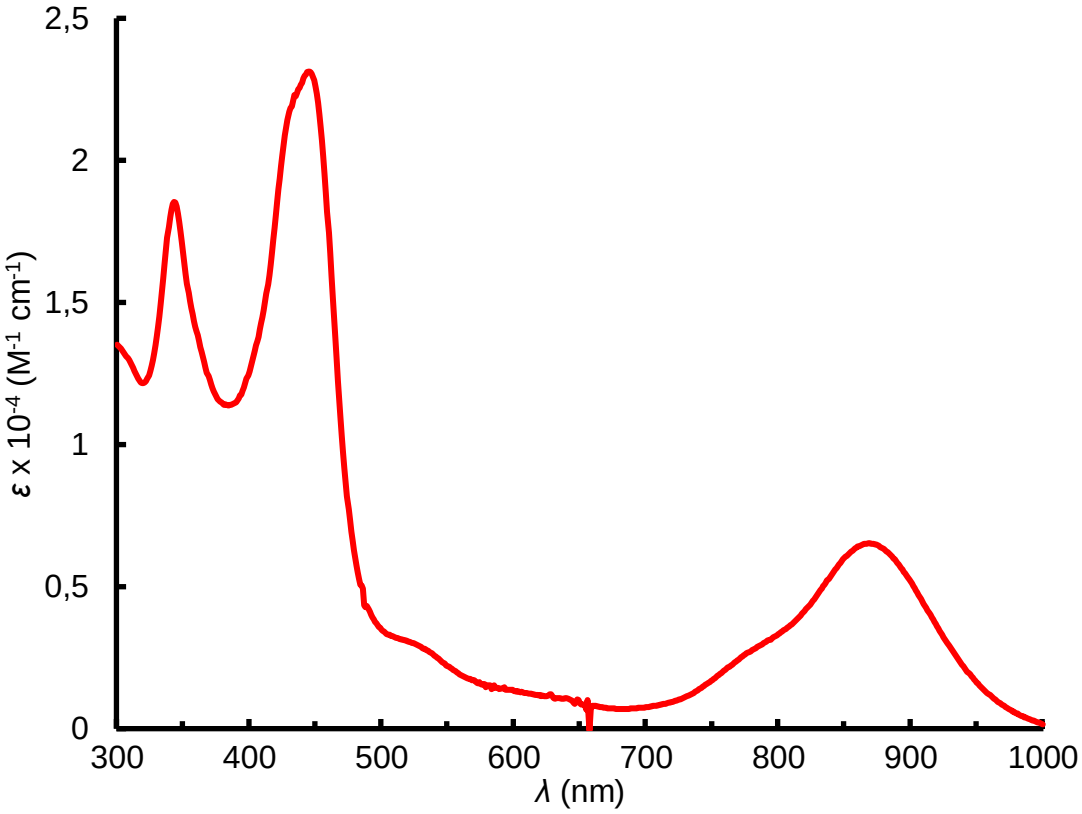

Figure 3.17. UV-vis spectrum of Ni[5,5,10,15-tetraphenylisocorrole].

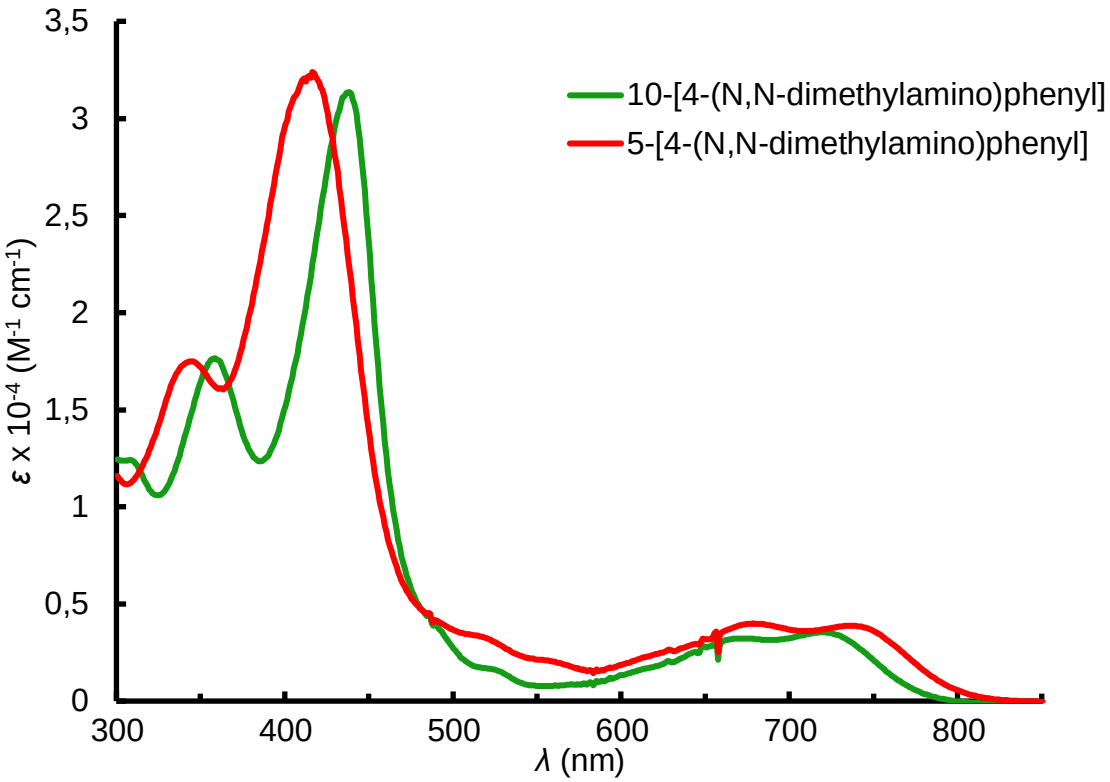

Figure 3.18. UV-vis spectra of 5/10-[4-(*N*,*N*-dimethylamino)phenyl]-5,10,15-tris(4-methylphenyl)isocorrole.

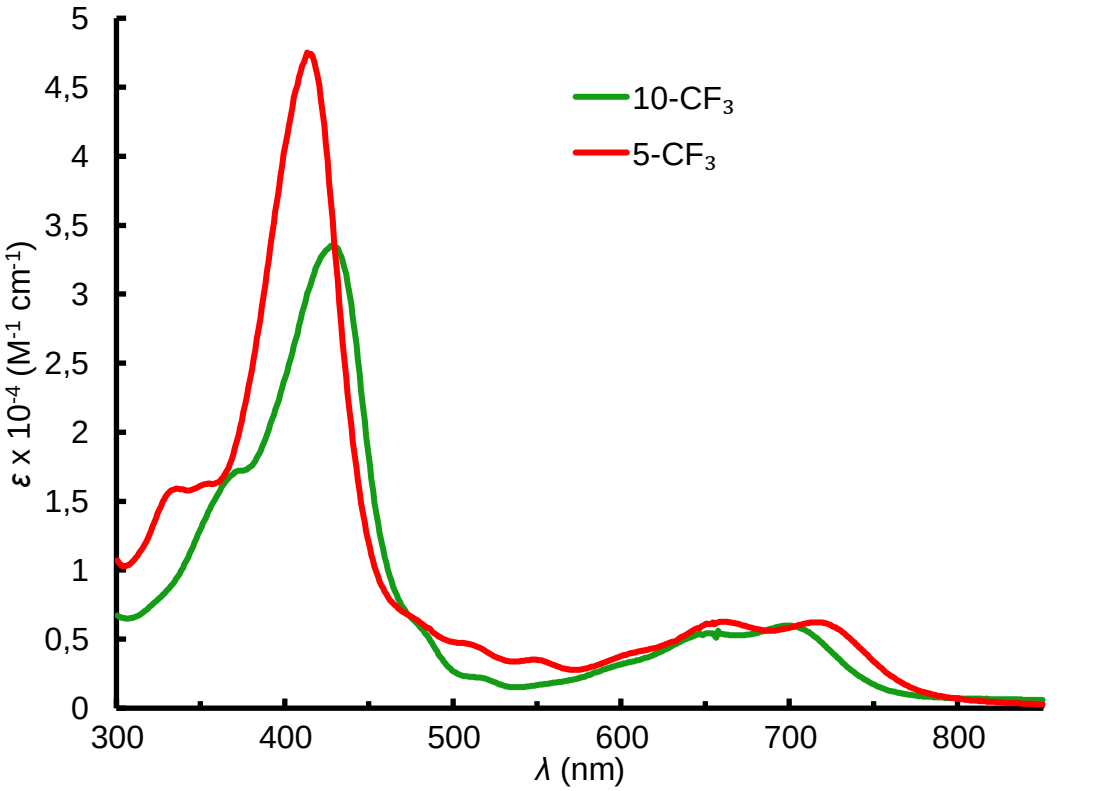

Figure 3.19. UV-vis spectra of 5/10-CF_3-5,10,15-tris(4-methoxyphenyl)isocorrole.

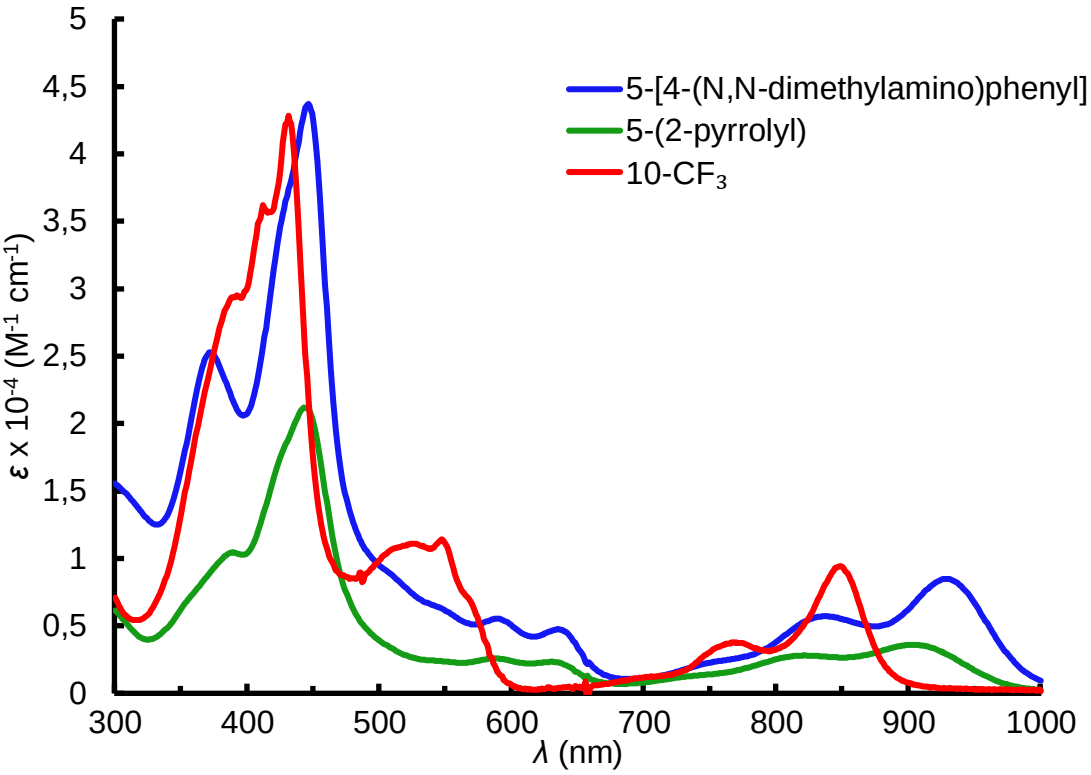

Figure 3.20. UV-vis spectra of palladium isocorroles.

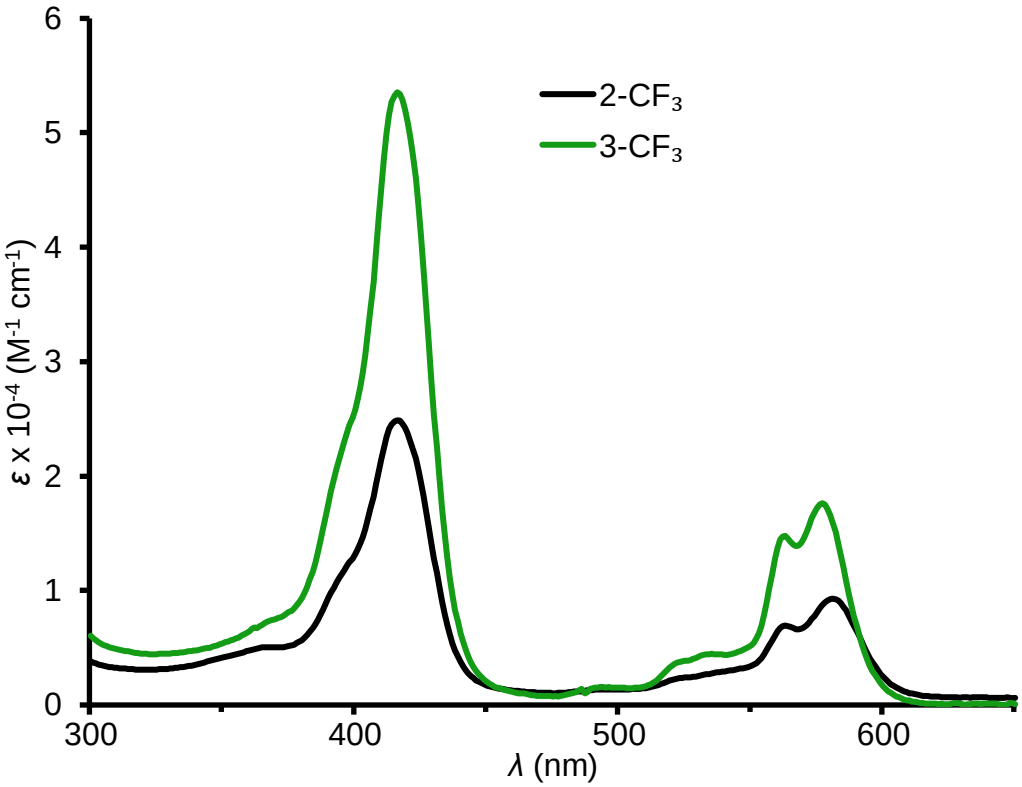

Figure 3.21. UV-vis spectra of Au[2-CF3-5,10,15-tris(4-methylphenyl)corrole] and Au[2-CF3-5,10,15-tris(4-methylphenyl)corrole].

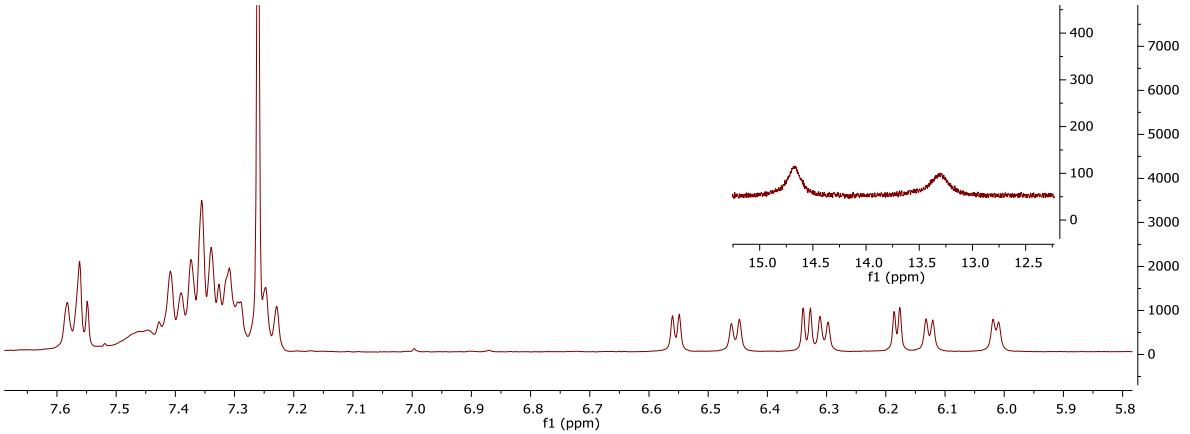

Figure 3.22. ^{1}H NMR spectrum of 5,5,10,15-tetraphenylisocorrole, inset displays core protons.

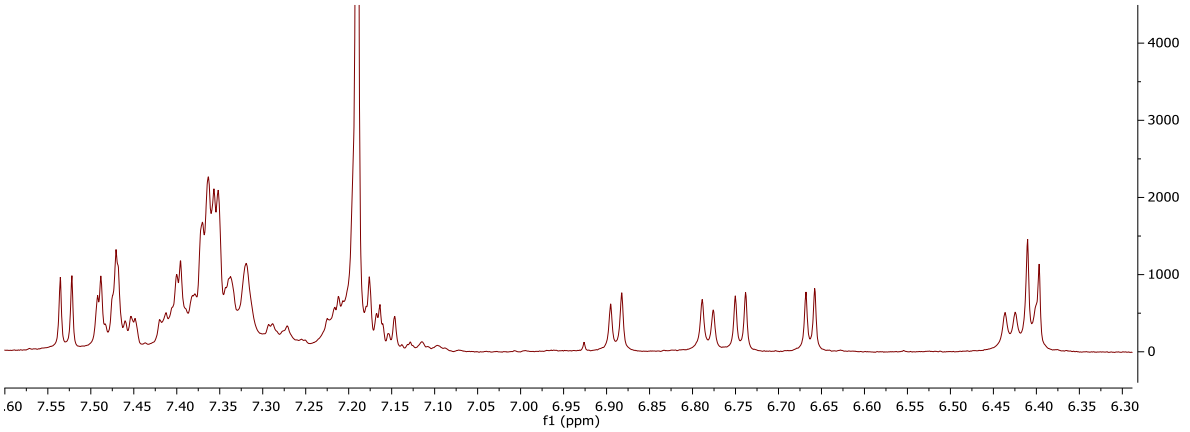

Figure 3.23. ^{1}H NMR spectrum of Ni[5,5,10,15-tetraphenylisocorrole].

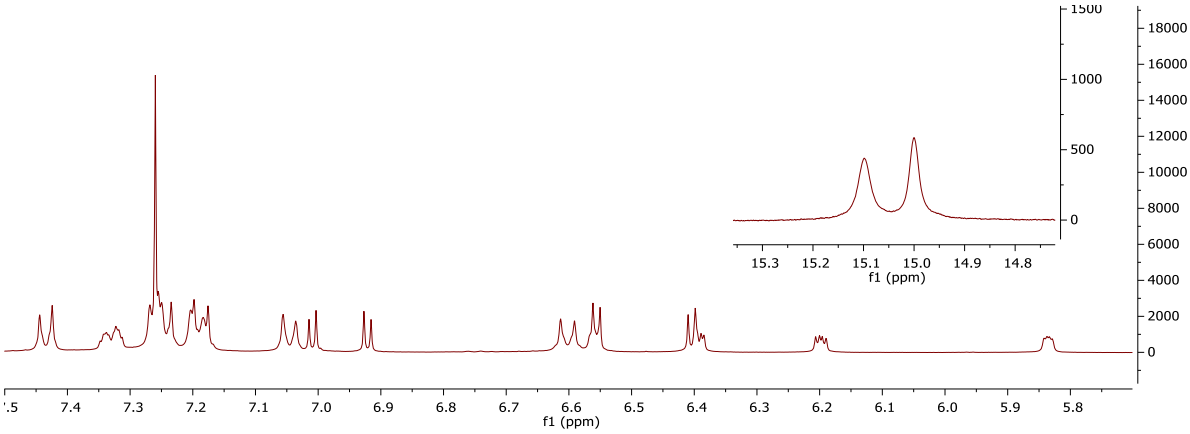

Figure 3.24. ^{1}H NMR spectrum of 5-[4-(*N*,*N*-dimethylamino)phenyl]-5,10,15-tris(4-methylphenyl)isocorrole, inset displays core protons.

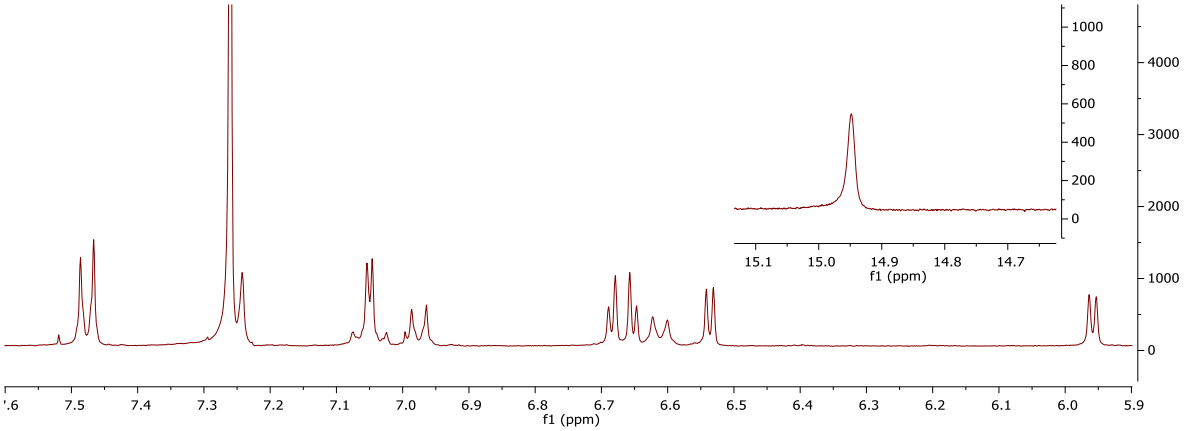

Figure 3.25. ^{1}H NMR spectrum of 10-[4-(*N*,*N*-dimethylamino)phenyl]-5,10,15-tris(4-methylphenyl)isocorrole, inset displays core protons.

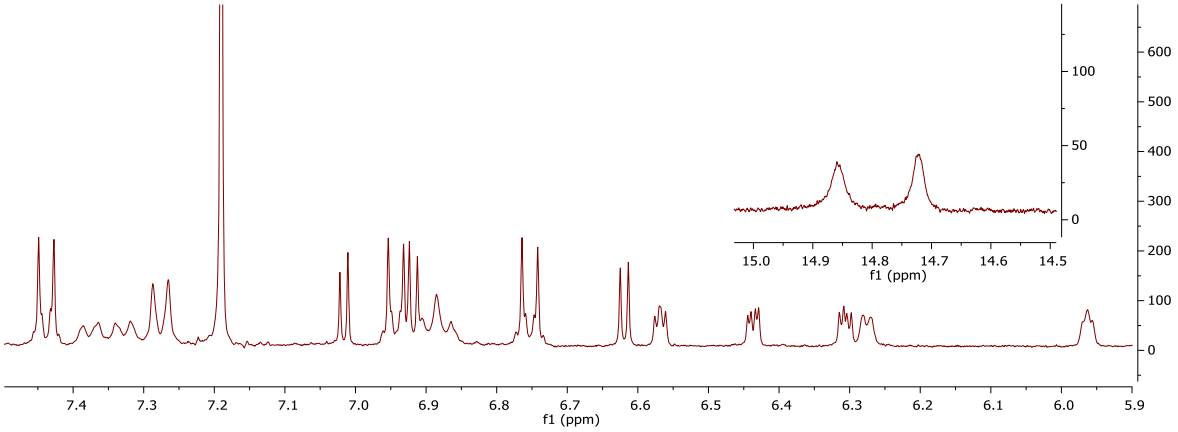

Figure 3.26. ^{1}H NMR spectrum of 5-CF_3-5,10,15-tris(4-methoxyphenyl)isocorrole, inset displays core protons.

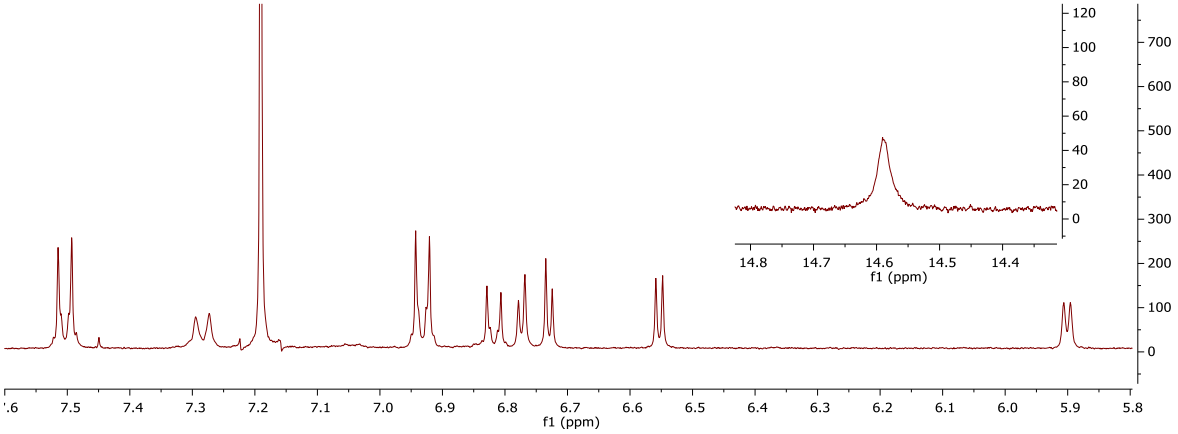

Figure 3.27. ^{1}H NMR spectrum of 10-CF_3-5,10,15-tris(4-methoxyphenyl)isocorrole, inset displays core protons.

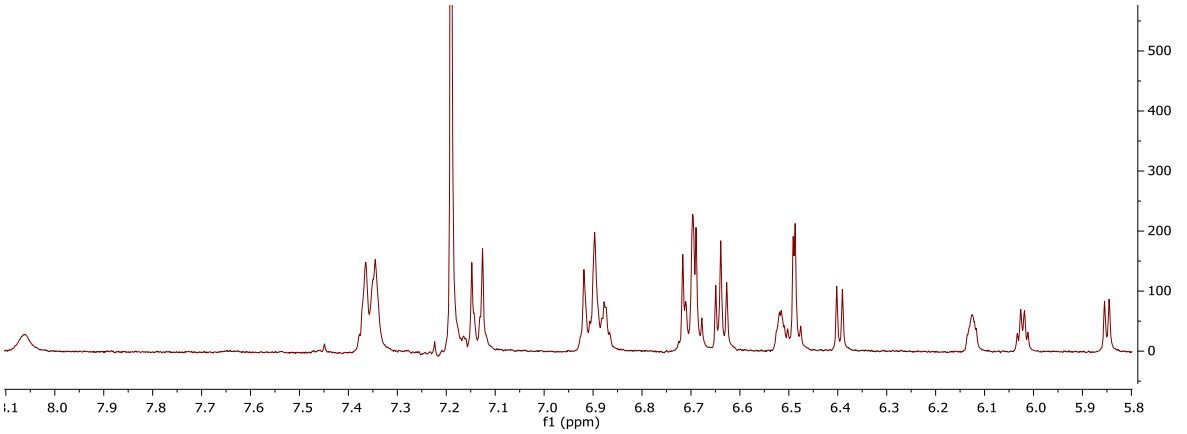

Figure 3.28. ^{1}H NMR spectrum of Pd[5-(2-pyrrolyl)-5,10,15-tris(4-methoxyphenyl)isocorrole].

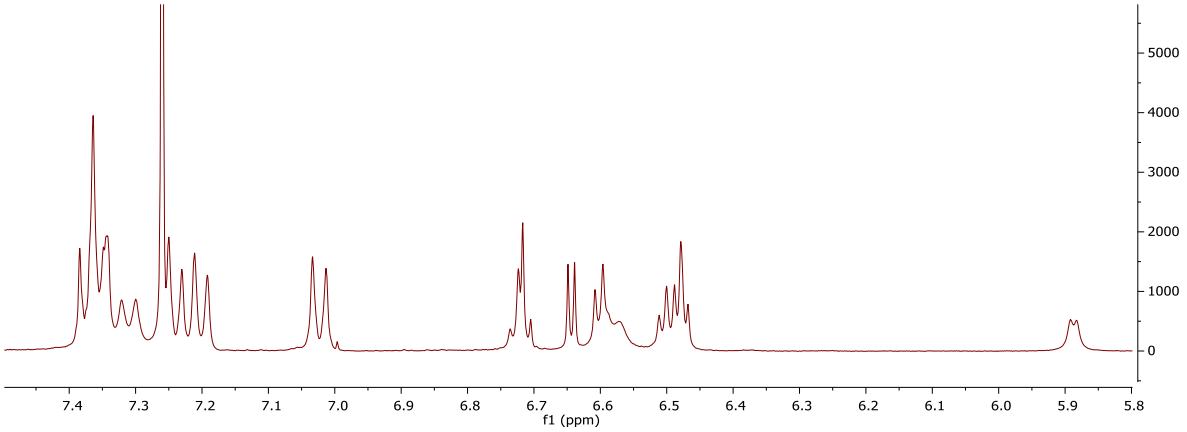

Figure 3.29. ^{1}H NMR spectrum of palladium 5-[4-(*N*,*N*-dimethylaminophenyl)]-5,10,15-tris(4-methylphenyl)isocorrole.

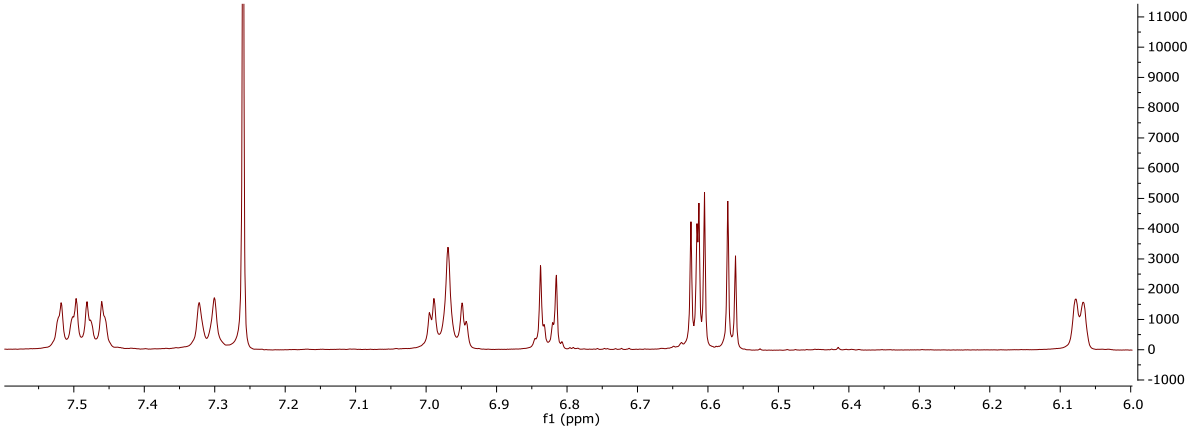

Figure 3.30. ^{1}H NMR spectrum of Pd[10-CF3-5,10,15-tris(4-methoxyphenyl)isocorrole].

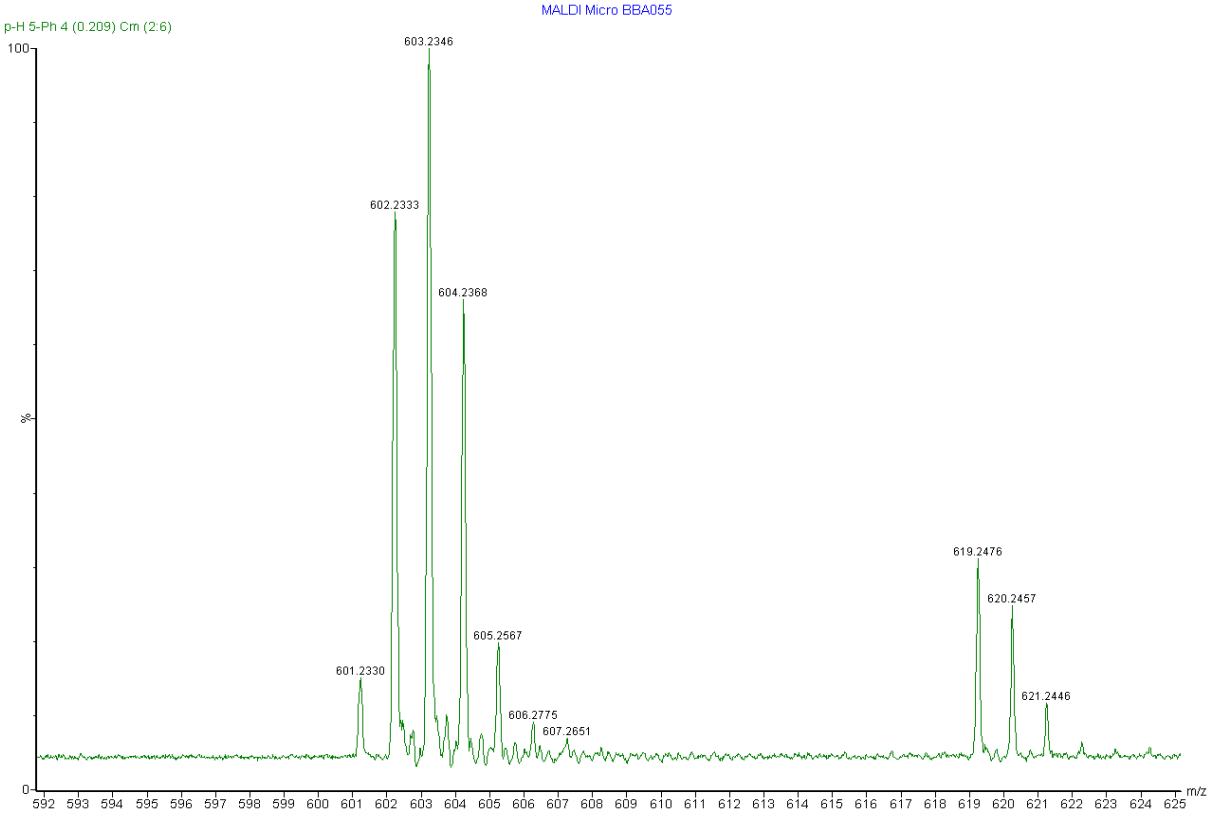

Figure 3.31. MALDI-TOF MS spectrum of 5,5,10,15-tetraphenylisocorrole.

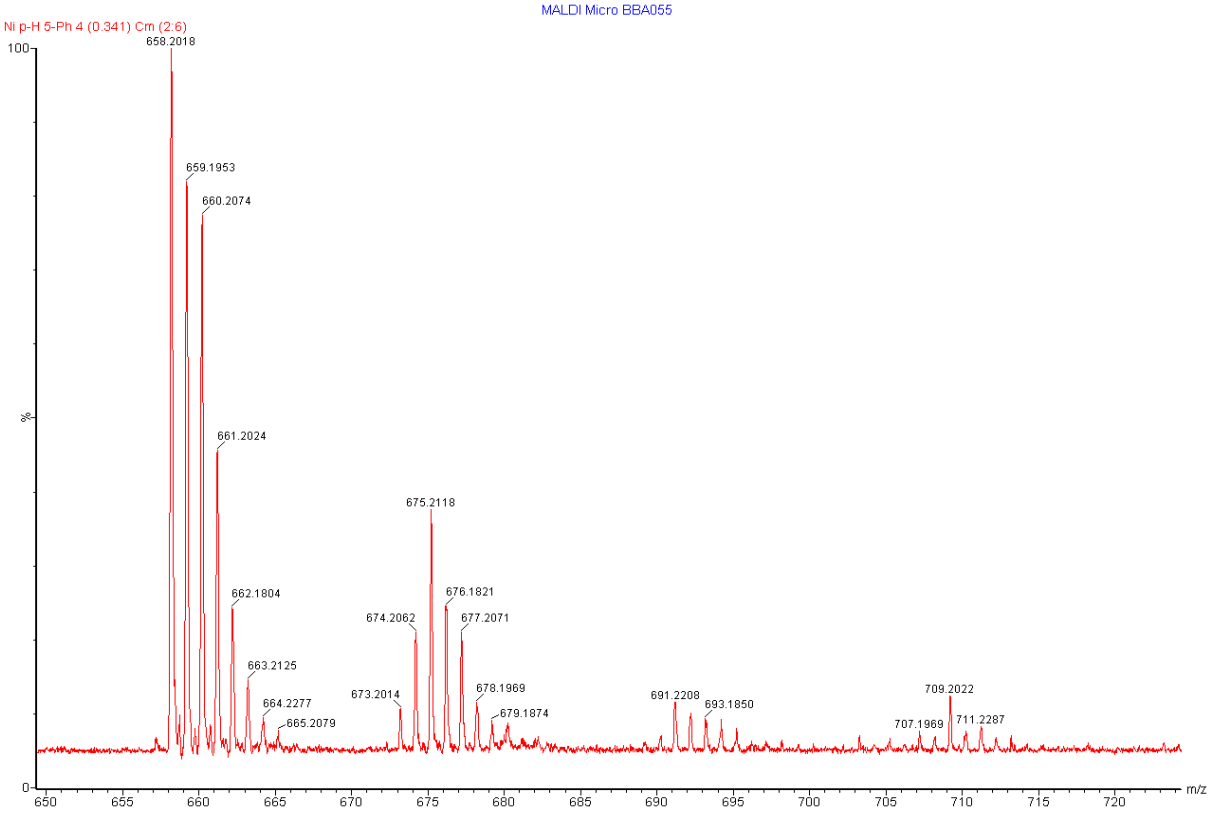

Figure 3.32. MALDI-TOF MS spectrum of Ni[5,5,10,15-tetraphenylisocorrole].

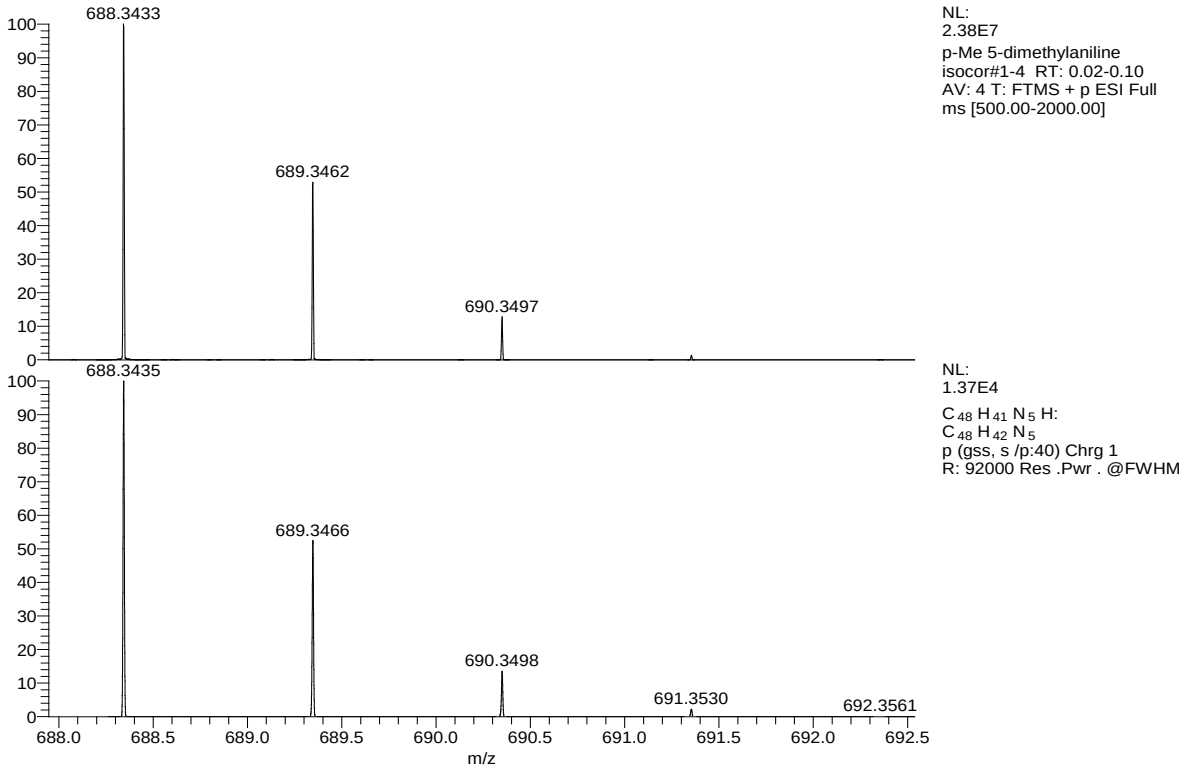

Figure 3.33. ESI-MS spectrum of 5-[4-(*N*,*N*-dimethylaminophenyl)]-5,10,15-tris(4-methylphenyl)isocorrole.

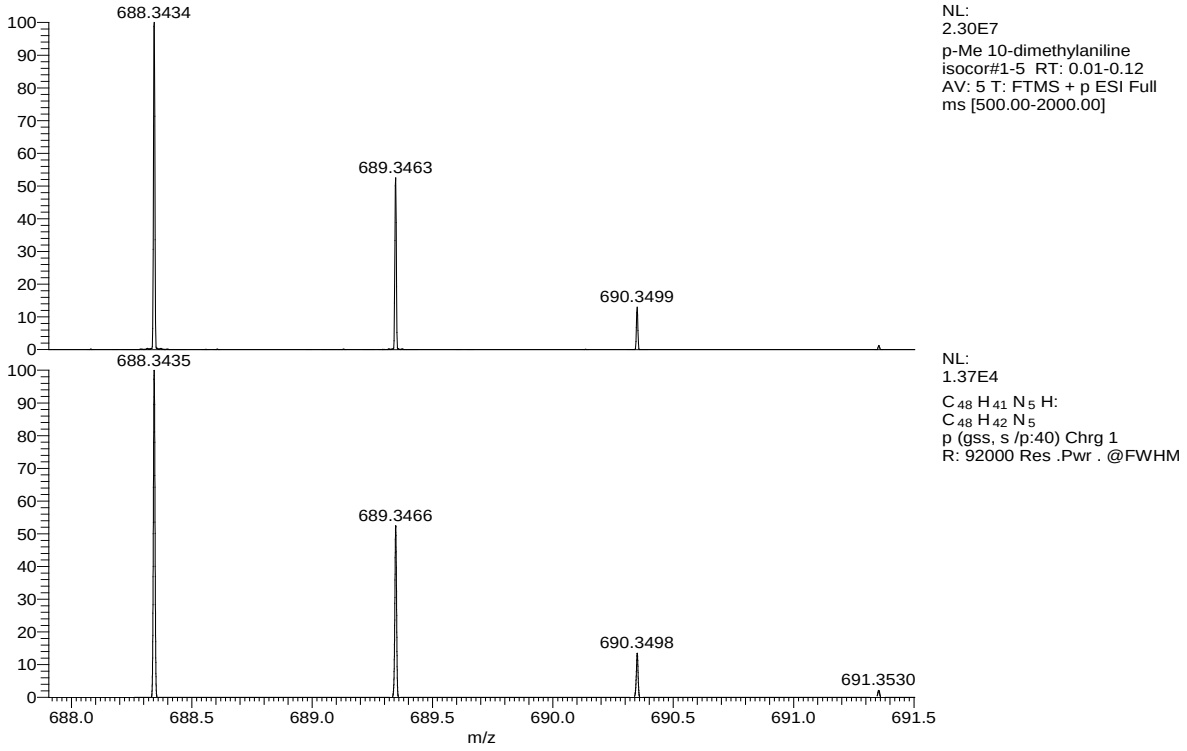

Figure 3.34. ESI-MS spectrum of 10-[4-(*N*,*N*-dimethylaminophenyl)]-5,10,15-tris(4-methylphenyl)isocorrole.

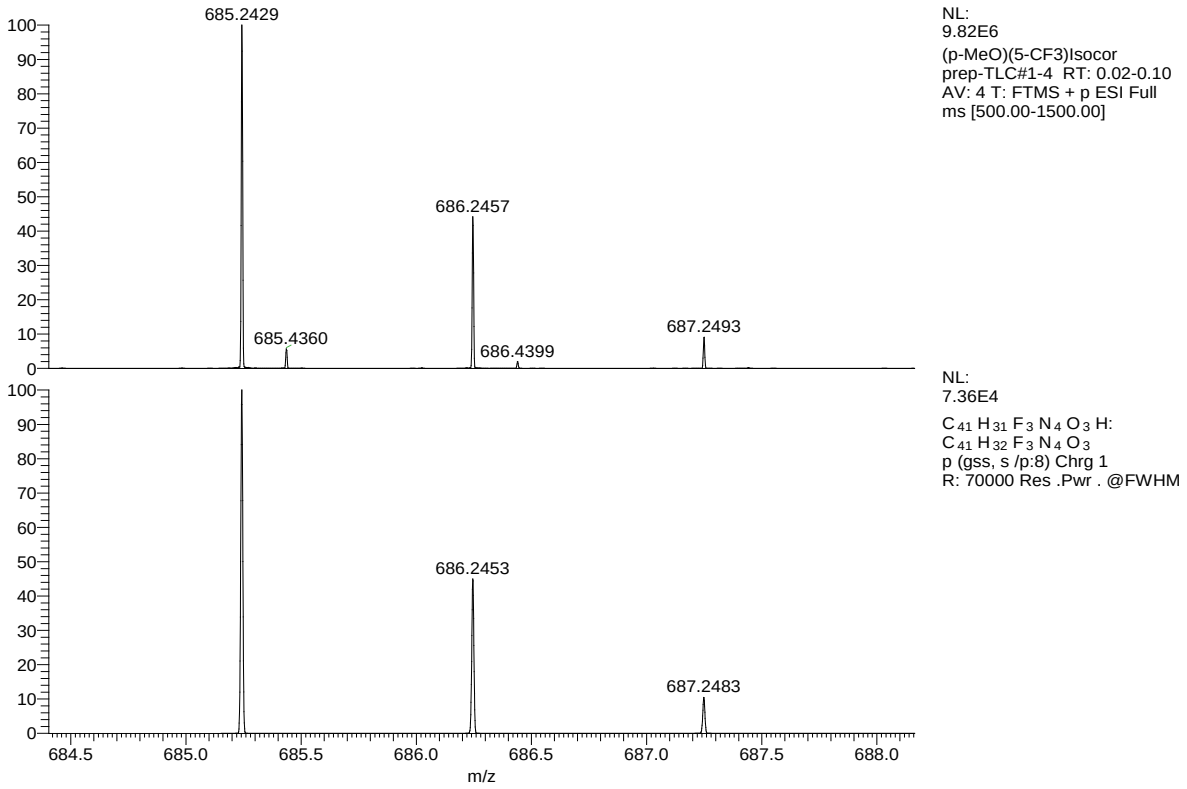

Figure 3.35. ESI-MS spectrum of 5-CF_3-5,10,15-tris(4-methoxyphenyl)isocorrole.

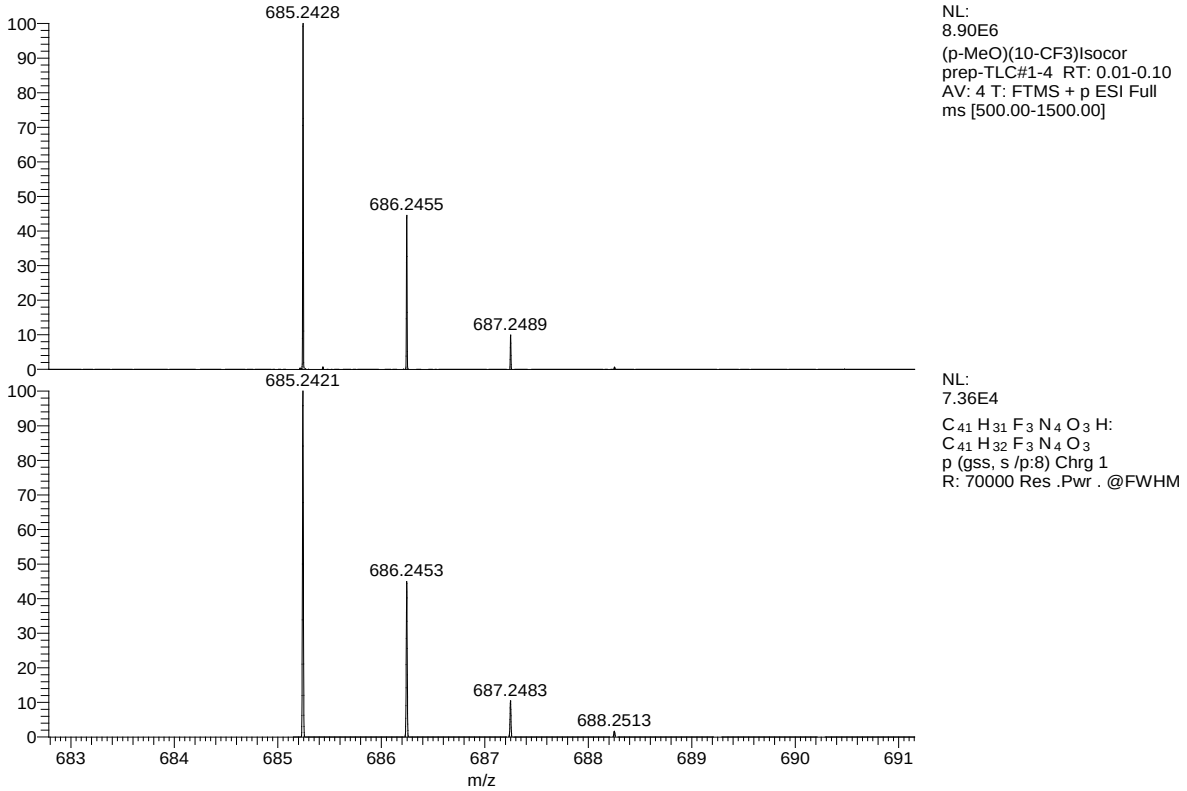

Figure 3.36. ESI-MS spectrum of 10-CF_3-5,10,15-tris(4-methoxyphenyl)isocorrole.

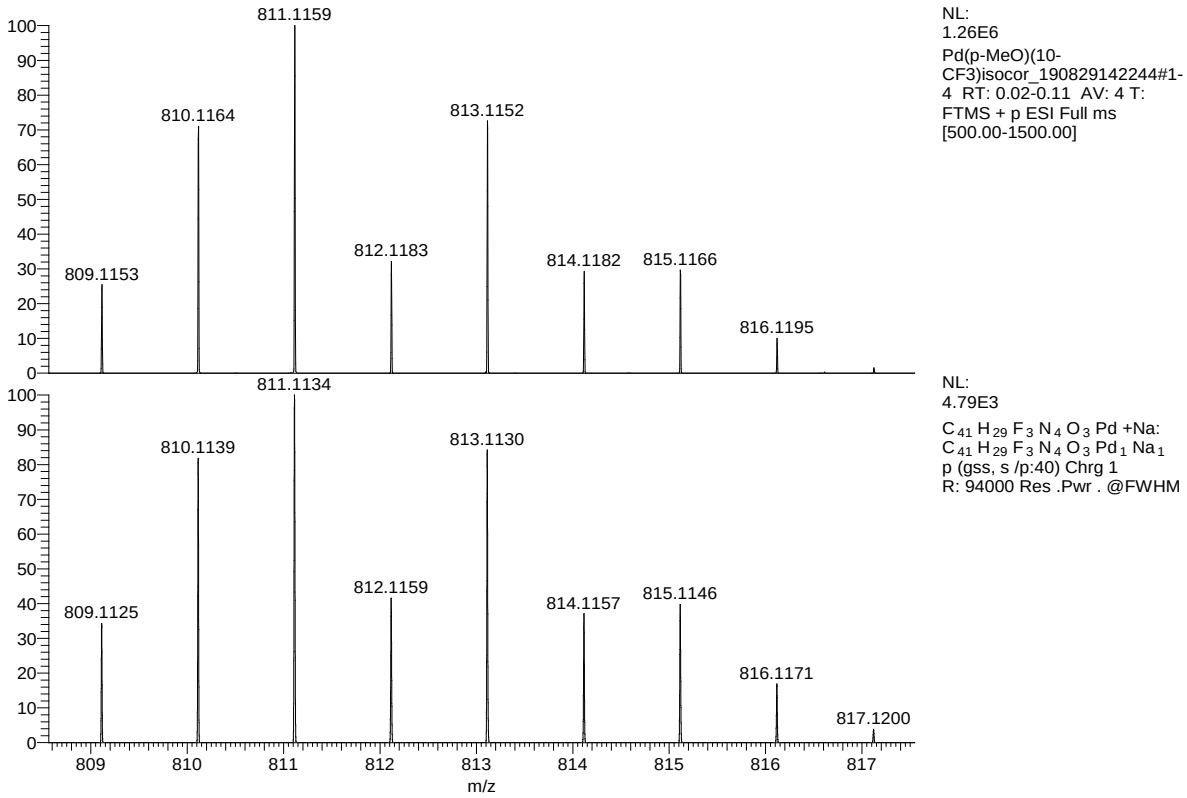

Figure 3.37. ESI-MS spectrum of Pd[10-CF_3-5,10,15-tris(4-methoxyphenyl)isocorrole].

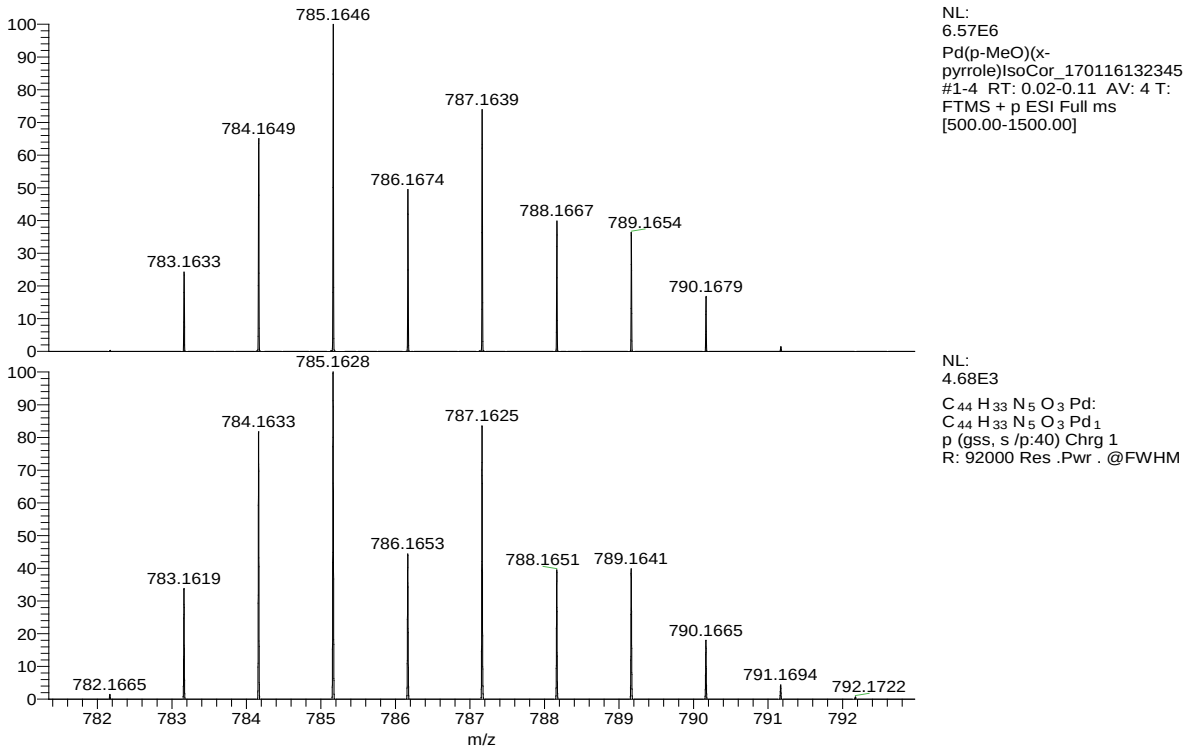

Figure 3.38. ESI-MS spectrum of Pd[5-(2-pyrrolyl)-5,10,15-tris(4-methoxyphenyl)isocorrole].

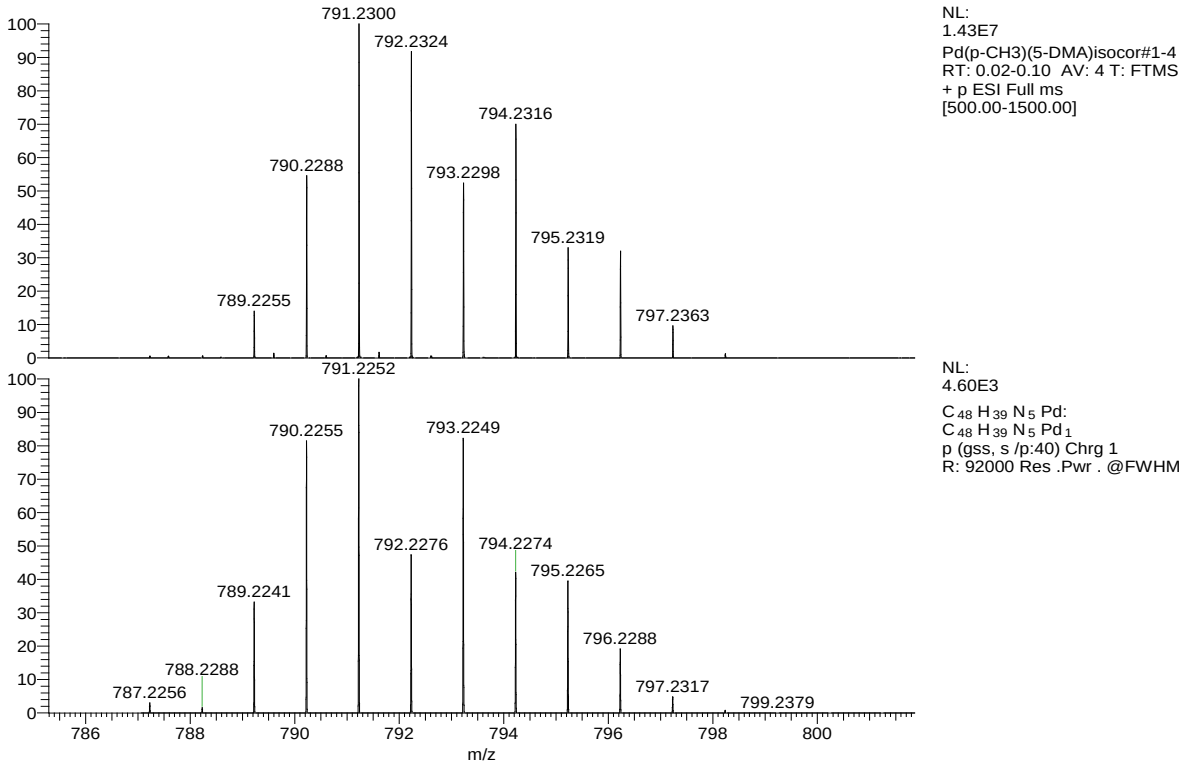

Figure 3.39. ESI-MS spectrum of palladium 5-[4-(*N*,*N*-dimethylaminophenyl)]-5,10,15-tris(4-methylphenyl)isocorrole.

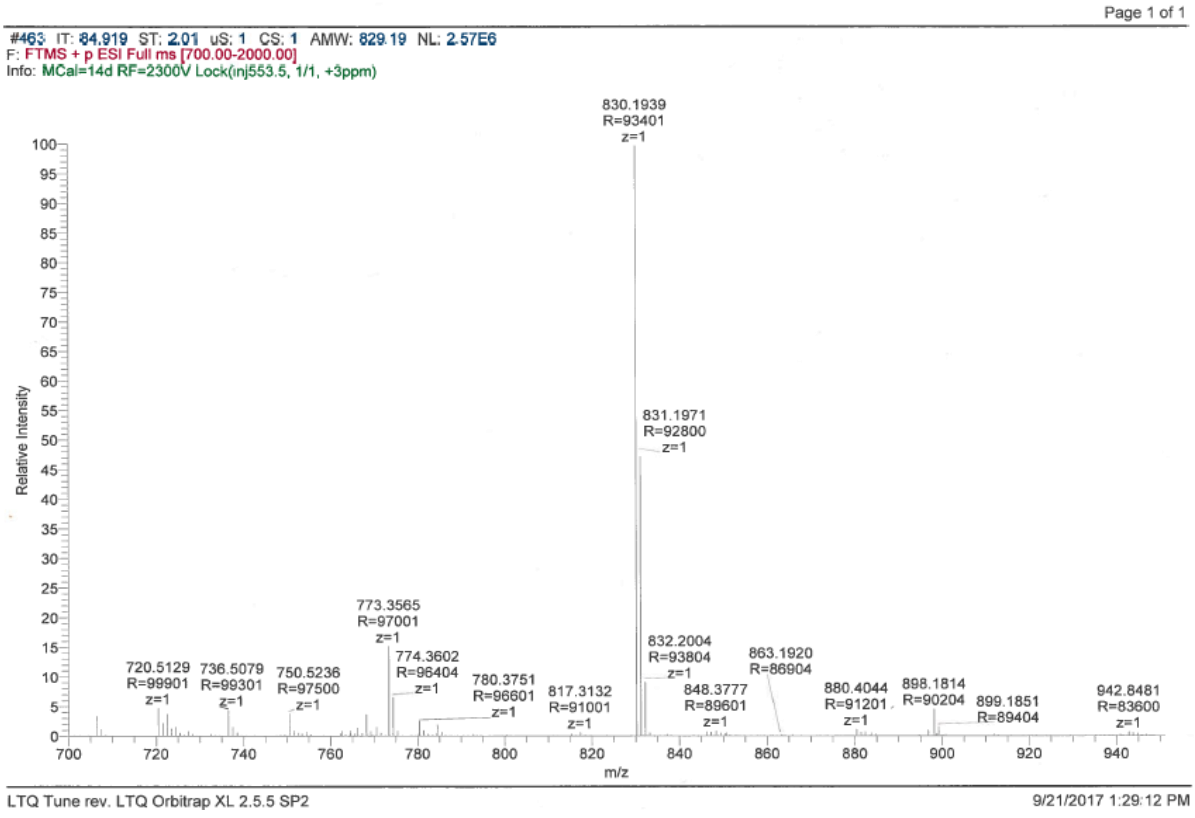

Figure 3.40. ESI-MS spectrum of Au[3-CF3-5,10,15-tris(4-methylphenyl)corrole].

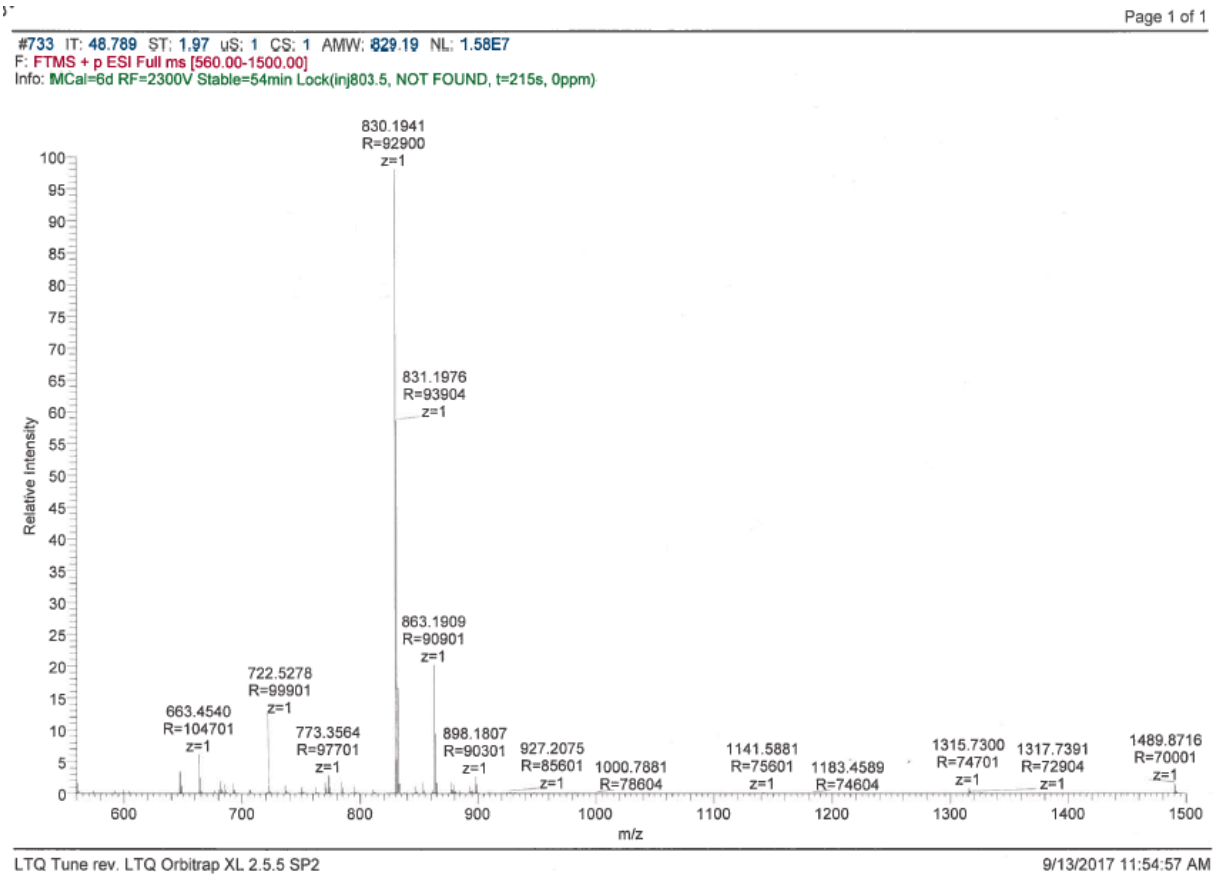

Figure 3.41. ESI-MS spectrum of Au[2-CF3-5,10,15-tris(4-methylphenyl)corrole].

Chapter 4. Azuliporphyrins

4.1. Introduction

Carbaporphyrins are porphyrins where carbacyclic (i.e., non-heterocyclic) moieties replace one or more of the pyrrole subunits. Examples include *N*-confused porphyrin, benziporphyrin, oxybenziporphyrin, benzocarbaporphyrin, tropiporphyrin and azuliporphyrin (**Figure 4.1**).[156] Azuliporphyrin (**Figure 4.2**),[157] where azulene has replaced one of the pyrrole units, is the focus of this chapter. In **Chapter 5** the synthesis of an azulicorrole, where azulene replaces one of the pyrrole units of corrole, will be presented.

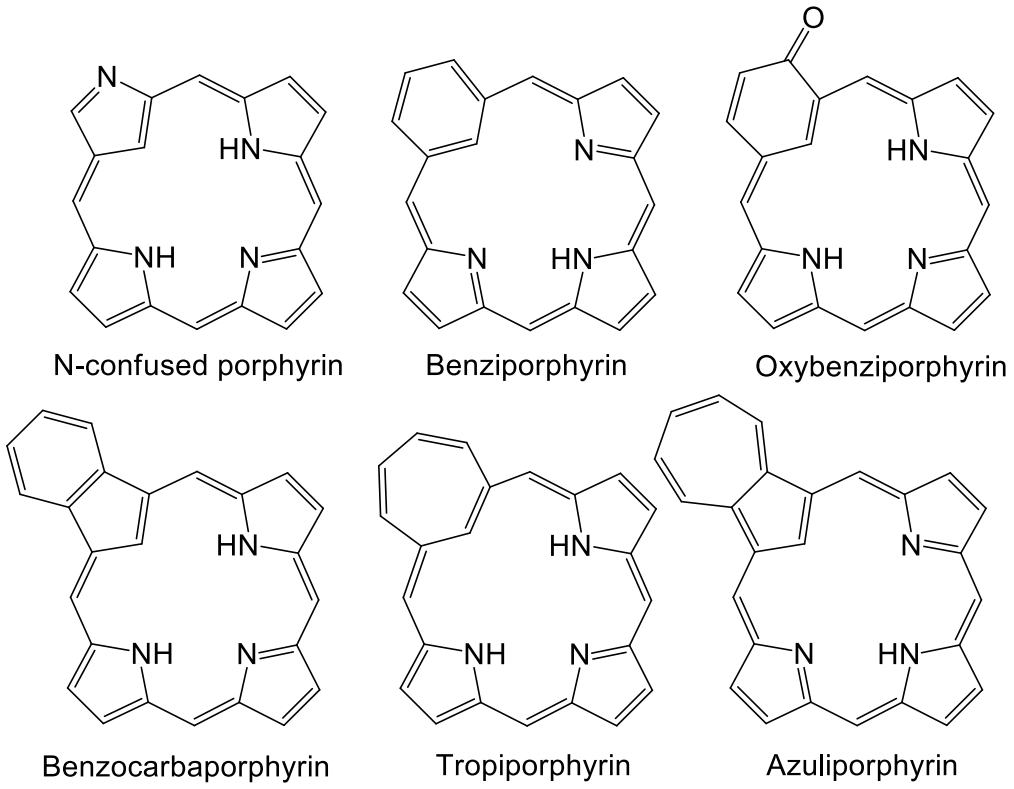

Figure 4.1. Examples of carbaporphyrins.

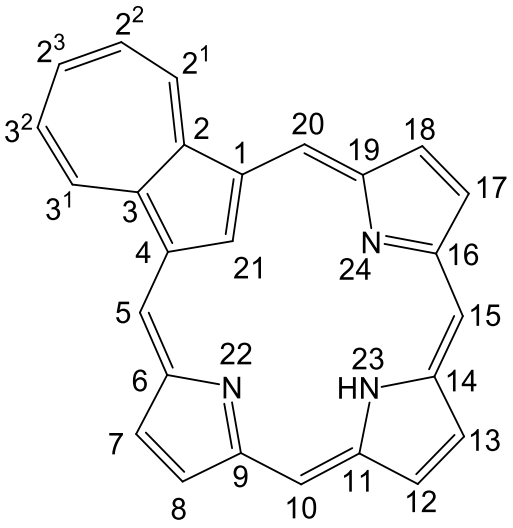

Figure 4.2. General structure of azuliporphyrin with atom numbering.

4.2. Synthesis and properties of free-base azuliporphyrins

Lash and Chaney reported the first synthesis of azuliporphyrin in 1997. By applying the MacDonald "3+1" method, a tripyrrane and 1,3-azulenedicarbaldehyde was condensed in the presence of TFA and oxidized to azuliporphyrin with DDQ (**Figure 4.3**).[158] Initially, the reaction yielded 28 %, this has in recent years been improved to 77%.[159]

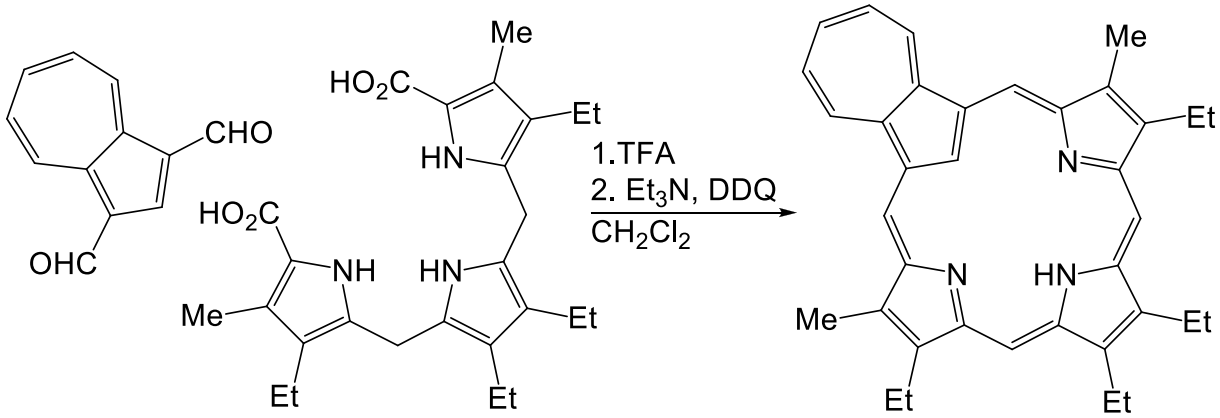

Figure 4.3. Synthesis of the first azuliporphyrin via the MacDonald "3+1" method.

^{1}H NMR revealed a relatively weak macrocyclic ring current. The *meso*-protons appeared as two singlets at δ ~ 8 and 8.9 ppm, which may be compared to a value of ~10.4 ppm for porphine.[160] These data indicate that azuliporphyrins, despite being cross-conjugated, possess intermediate porphyrinoid aromaticity. Addition of trace amounts of TFA shifted the *meso*-protons downfield by about 1.4 ppm, indicative of increased macrocyclic currents.

The macrocyclic aromaticity reflects dipolar resonance forms, where the azulene moiety takes on a tropylium-cation character, while the remainder of the macrocycle resembles a porphyrinoid anion (**Figure 4.4**). The resulting charge separation disfavors the dipolar resonance form in neutral azuliporphyrin, while charge delocalization stabilizes the tropylium resonance form in the protonated azuliporphyrin.

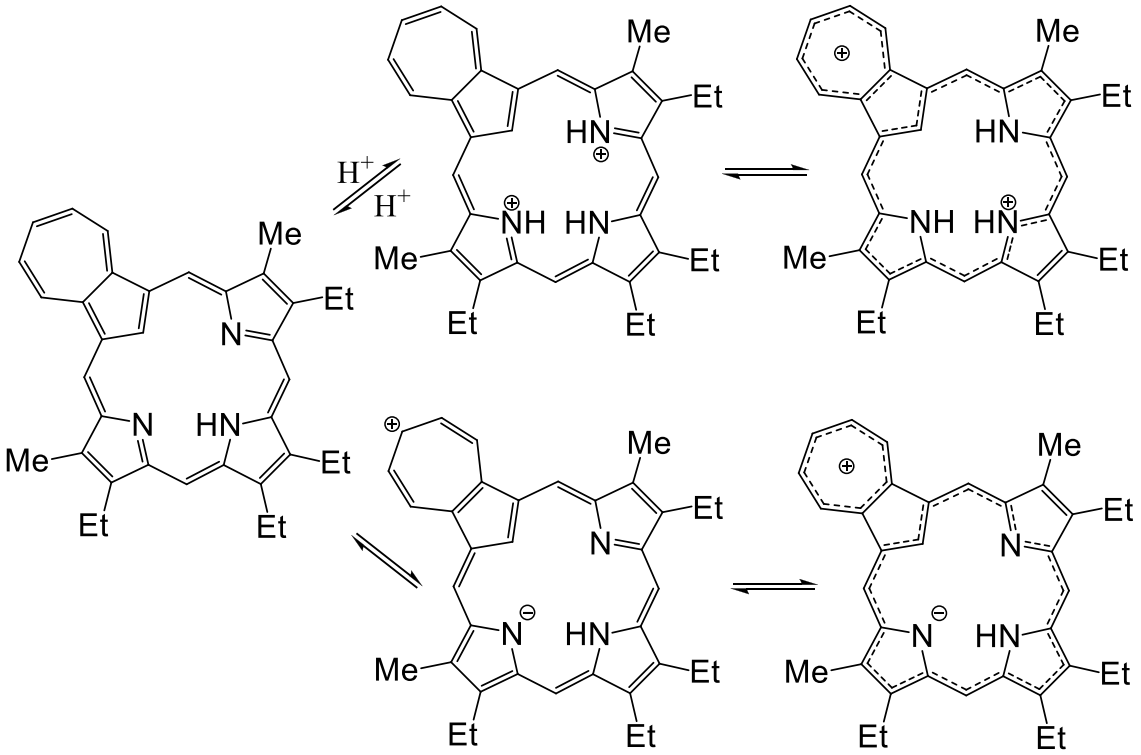

Figure 4.4. The protonated (top) and neutral (bottom) dipolar resonance forms contributing to porphyrinoid-like aromaticity.

UV-vis spectra appear to corroborate the above observations from the NMR spectra. For the neutral form, the UV-vis spectra show a series of moderately strong absorptions between 350 and 500 nm and a broad absorption between 500 and 800nm. When protonated, the UV-vis spectra display two strong Soret bands at 364 and 460 nm, in addition to several Q bands between 580 and 800 nm (**Figure 4.5**), characteristic of porphyrin-like compounds.

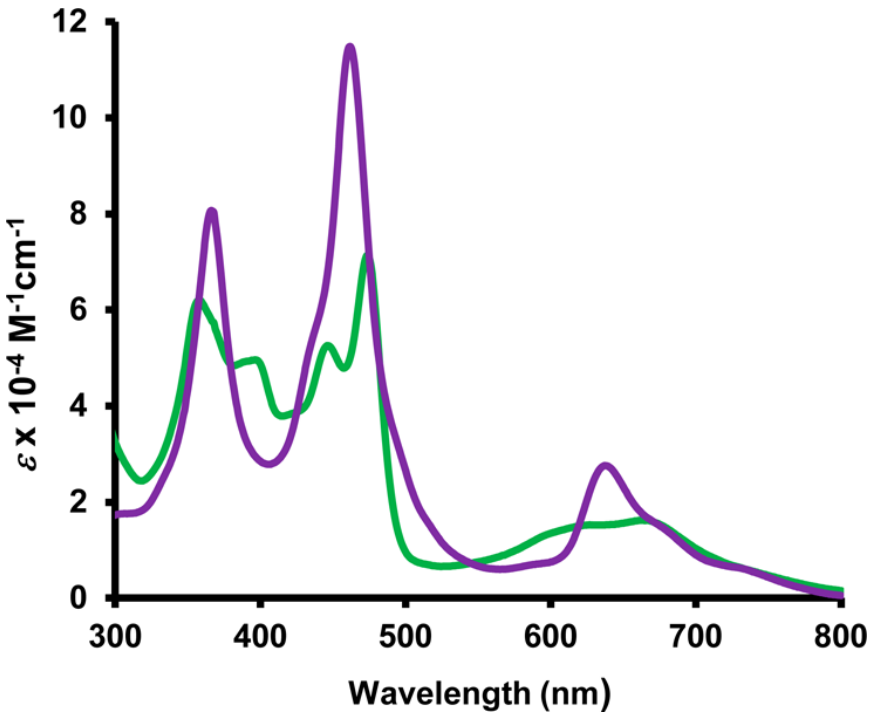

Figure 4.5. UV-vis spectra of azuliporphyrin in 1% Et_3N-$CHCl_3$ (free-base, green line) and 1% TFA-$CHCl_3$ (dication, purple line). Adapted with permission from ref 157. Copyright 2016 American Chemical Society.

Prior to the work of Lash and Chaney, the Breitmaier group condensed tripyrranes with 1,3-azulenedicarbaldehyde, but with a different result. Employing DCM/THF as solvent with HBr in glacial acetic acid as catalyst, the reaction yielded benzocarbaporphyrin instead of azuliporphyrin.[161] While the authors made no effort to explain their findings, Lash provided an explanation when he demonstrated that the 2^3 position of the azulene moiety reacts with nucleophiles.[162] Adding pyrrolidine to a solution of azuliporphyrin caused a shift of the *meso*- and core C-H protons to ~10 and -7 ppm respectively, which was rationalized in terms of the two compounds forming an adduct that allowed the azuliporphyrin to be fully conjugated (**Figure 4.6**). Furthermore, Lash showed that reacting azuliporphyrin with *tert*-butyl hydroperoxide and a strong base resulted in the same benzocarbaporphyrins as that of the Breitmaier group.

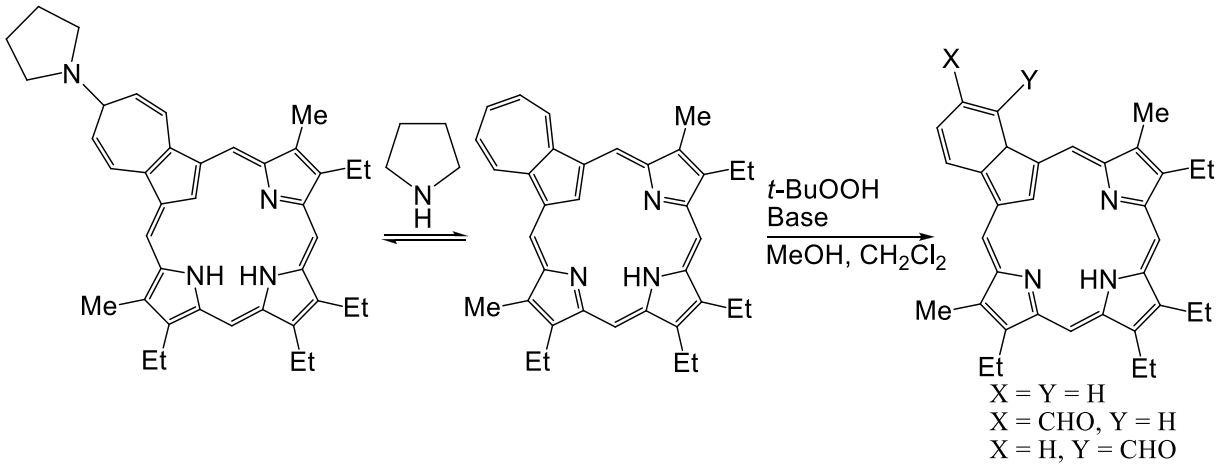

Figure 4.6. Reactions at the 2^3 position of the azulene moiety leading to a pyrrolidine adduct and benzocarbaporphyrins.

By condensing azulene with two equivalents of acetoxymethylpyrrole in refluxing acetic acid/isopropyl alcohol, the Lash group prepared an azulitripyrrane (**Figure 4.7**),[163] which could be condensed with dialdehydes to generate novel azuliporphyrinoid systems. Thus, dialdehydes of pyrrole, thiophene and selenophene produced the corresponding azuli-, thiaazuli- and selenaazuliporphyrins.[159] The azuliporphyrin produced via this pathway differed from the one mentioned earlier only in the relative positions of the methyl and ethyl groups, but their other spectroscopic characteristics were close to identical. The thia- and selenaazuliporphyrins displayed slightly enhanced diatropic ring currents, relative to the azuliporphyrin, evidenced by slightly downfield shifted *meso*-protons. The UV-vis spectra shared the characteristics of the azuliporphyrin with moderately strong absorptions in the 350 to 500 nm region, followed by a broad absorption between 500 and 800 nm. TFA produced dications of both thia- and selenaazuliporphyrins, with similar effects on the UV-vis and NMR spectra as for azuliporphyrins.

Furandialdehyde led not to oxaazuliporphyrin, but rather to a mixture of (ring-contracted) oxacarbaporphyrins, analogous to the benzocarbaporphyrins formed by ring contraction of azuliporphyrins.[163] Condensation with diformylindene led to the first example of a dicarbaporphyrin.[163] The ^{1}H NMR spectrum of the latter revealed a weak diatropic current, while the UV-vis showed only broad absorptions centered around 494 and 675 nm, indicating a nonaromatic macrocycle. Adding TFA led first to a monocation and then to a dication, both of which exhibited enhanced diatropic current in the ^{1}H NMR spectra. The UV-vis did not change much for the monocation, but the dication showed a strong Soret-like absorption at 481 nm and several weaker absorptions at 529, 623 and 670 nm.

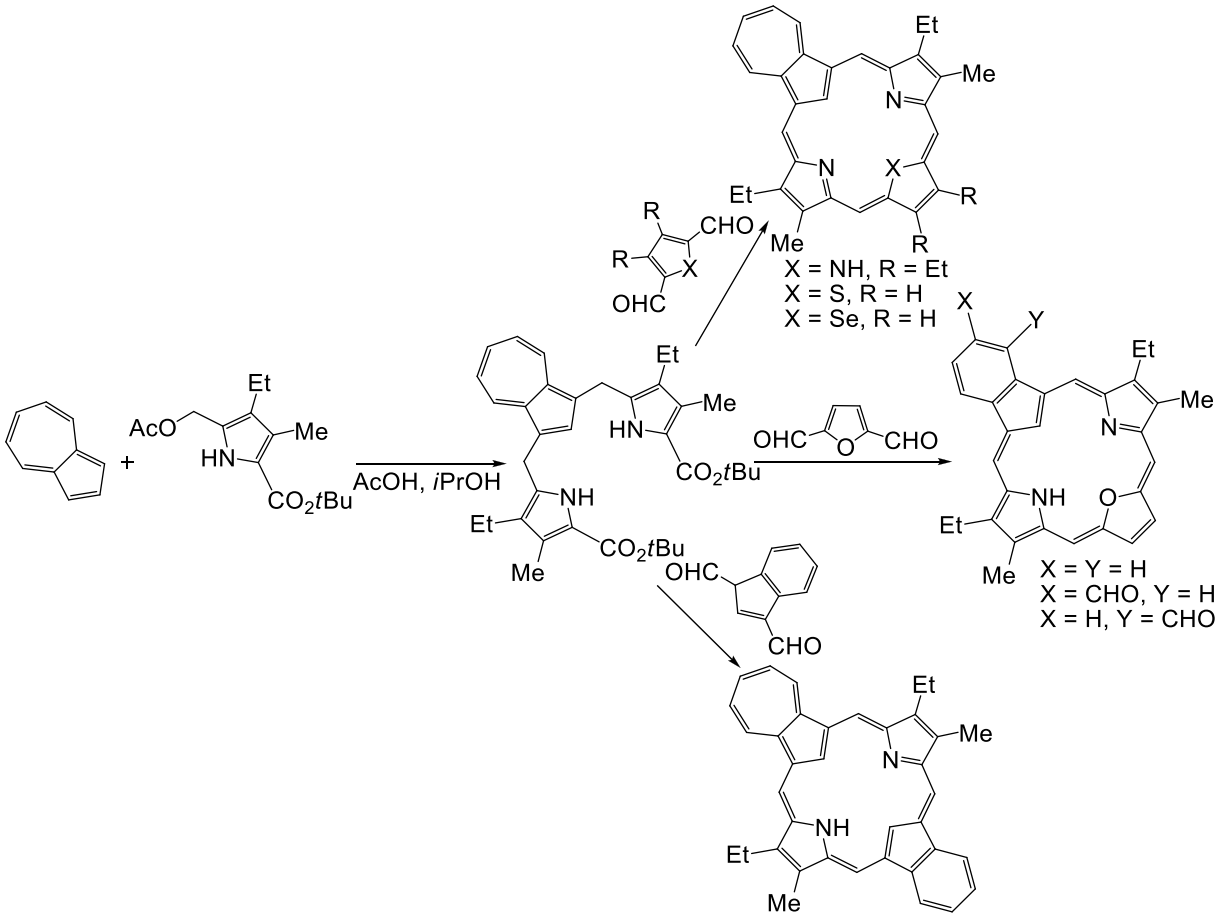

Figure 4.7. Synthesis of azulitripyrrane and condensation with dialdehydes to yield novel porphyrinoid macrocycles.

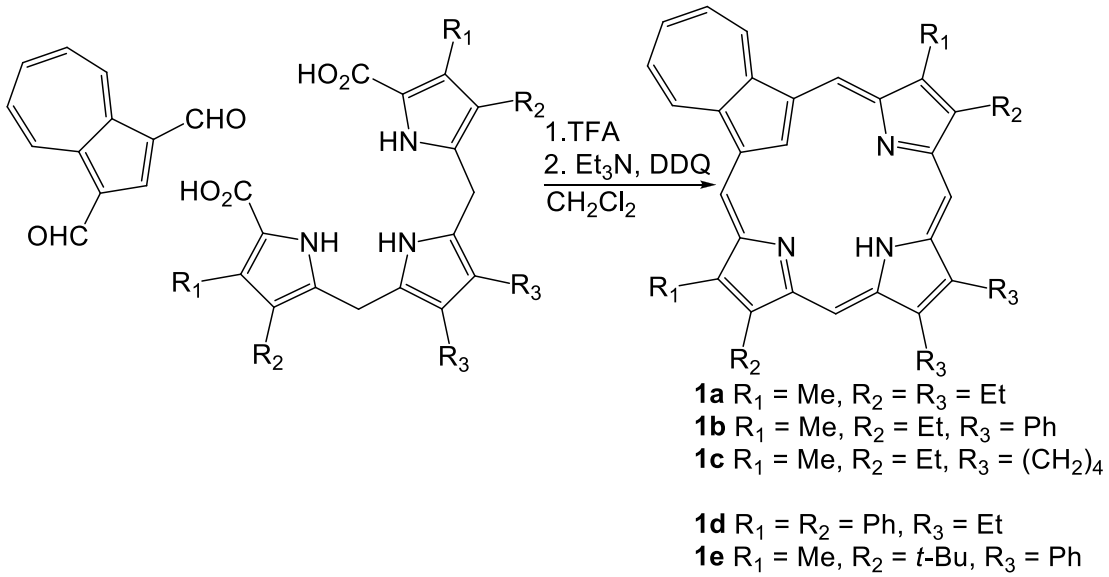

Figure 4.8. Synthesis of azuliporphyrins with varying β-substituents.

The group of Lash synthesized a series of tripyrranes with varying *β*-substituents to ascertain their effect on the aromaticity of the azuliporphyrin (**Figure 4.8**).[159,164] While azuliporphyrins **1a** and **1c** differ only in their R_3-substituents, and have similar spectroscopic properties, **1c** was the first azuliporphyrin sufficiently soluble to allow the study of solvent effects on their chemical shifts.[159] In $CDCl_3$, the *meso*-protons appeared at 7.9 and 8.9 ppm and the doublet from the proton at the 2^1 position of the azulene moiety resonated at 9.2 ppm. Changing to deuterated benzene caused a slight upfield shift to 7.9, 8.8 and 8.8 ppm respectively, while deuterated pyridine caused a downfield shift to 8.3, 9.4 and 9.6 ppm respectively. These shifts correlate with the relative polarity of the solvents. Solvents of higher polarity stabilize the dipolar resonance form, resulting in an increased diatropic ring current. Studies of solvent effect conducted on thia- and selenaazuliporphyrins led to similar results.

Poor resolution, due to aggregation, meant that NMR studies of **1b** were not feasible. The bulky *tert*-butyl substituents of **1e**, however, allowed full assignment of the NMR spectrum. The *meso*-protons resonated slightly downfield relative to **1a** (δ = 8.61 and 8.95 ppm), while the core protons were observed at 2.53 and 2.88 ppm for the CH and NH, respectively. Addition of TFA produced a dication that had similar NMR shifts compared to the dication of **1a**.

The *meso*-protons of azuliporphyrin **1d** resonated at 8.35 and 9.16 ppm while the CH and NH resonated at 2.79 and 2.65 ppm respectively, comparable to that of **1e**. The dication of **1d**, surprisingly, displayed reduced diatropicity relative to the dications of both **1a** and **1e**. To

explain this observation, the authors pointed to the effect of the phenyl groups on the dipolar resonance forms (**Figure 4.4**). The reduced electron-donating character of the phenyl groups contributed to the stability of the anion of the neutral form. In the dication form, however, the phenyl groups would assist in the delocalization of the positive charges, resulting in resonance forms with interrupted macrocyclic conjugation.

To investigate the effect of substituents on the azulene moiety, the Lash group synthesized a series of six 2^3-substituted azuliporphyrins (**Figure 4.9**).[165] T*ert*-butylazulene or phenylazulene was either formylated and condensed with tripyrranes to yield **2a-b** and **3a-b**, or incorporated into the tripyrrane and condensed with a pyrrole dialdehyde to give azuliporphyrins **2c** and **3c**.

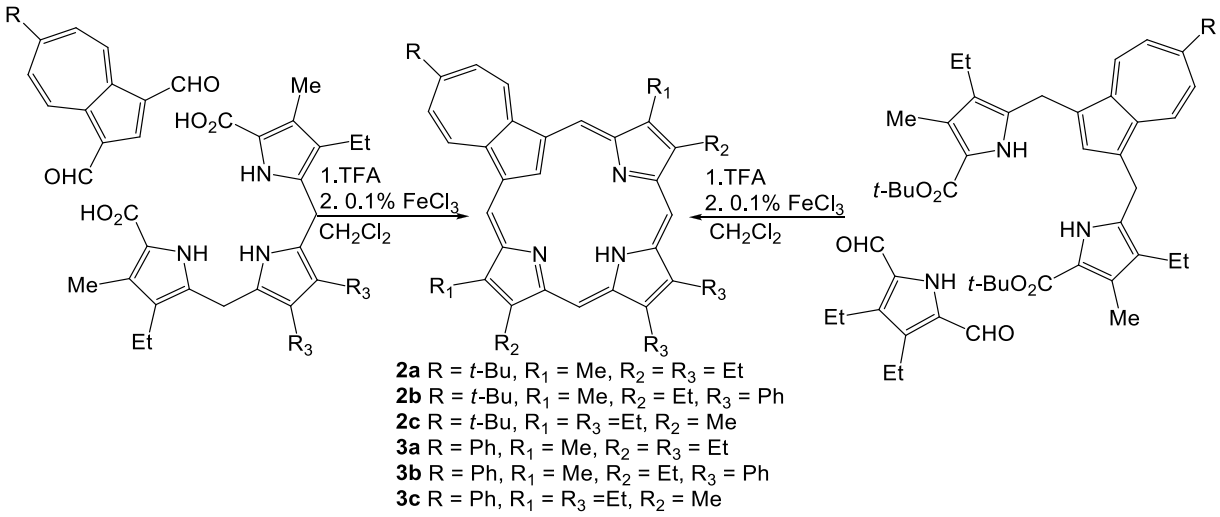

Figure 4.9. Synthesis of 2^3 substituted azuliporphyrins.

Of the six compounds, five were sufficiently soluble to give good NMR spectra. Compound **3b** gave a poorly resolved spectrum due to aggregation. The proton NMR of **2a** showed the *meso*-protons as two singlets at 8.15 and 9.05 ppm, while the azulene protons appeared as two doublets at 7.89 and 9.33 ppm and the core protons appeared between 2.8 and 2.9 ppm. The proton NMR spectrum of **3a** revealed the core protons at 3.23 and 3.30 ppm, significantly downfield compared to **2a**. The *meso*-protons at 8.06 and 8.96 ppm and the azulene doublets at 7.81 and 9.29 were all upfield relative to **2a**. The proton NMR spectrum of **2b** revealed an opposite trend, the core protons resonating at 2.8 and 2.49 ppm and the *meso*-protons and azulene protons all showing minor downfield shifts relative to **2a**. The NMR data for **2c** and **3c** were similar to their isomers **2a** and **3a**. The observed shifts appear to reflect the effect of substituents on the dipolar resonance forms (**Figure 4.4**). The electron-

donating *tert*-butyl group of **2a** stabilizes the positive charge on the azulene moiety more than the phenyl group of **3a**. On the other hand, the less electron-donating phenyl group is better placed at the β-positions, as it is less destabilizing toward a negative charge.

Compound **2a** afforded X-ray quality crystals. The resulting crystal structure revealed an essentially planar macrocycle with the azulene moiety tilting ~7.4° out of the plane (**Figure 4.10**), while electron density maps clearly indicated hydrogens at C21 and N23 in the core. Analysis of the bond lengths indicated a delocalized π-system as depicted in **Figure 4.10**.

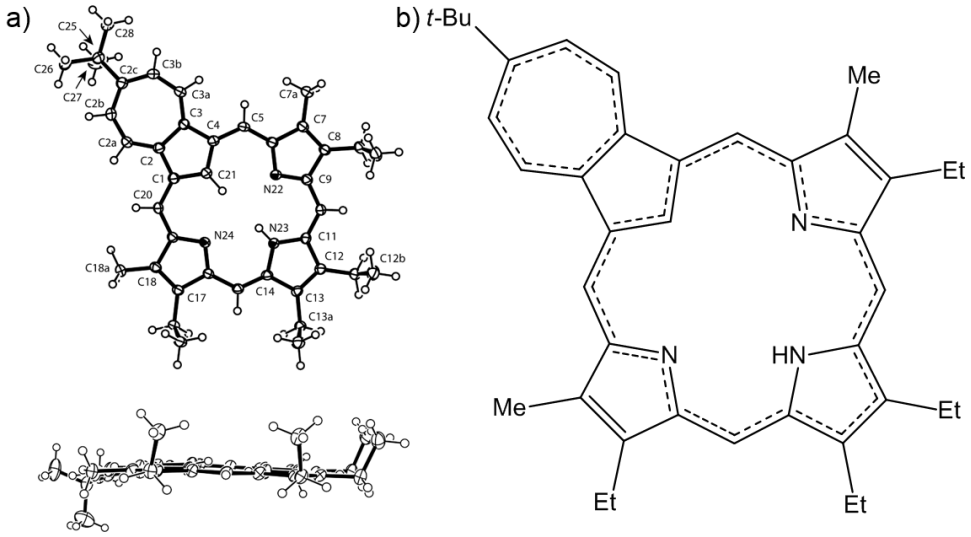

Figure 4.10. a) ORTEP-III drawing of **2a**, adapted with permission from ref 165. Copyright 2007 American Chemical Society. b) Aromatic pathway depicted by analysis of bond lengths.

The presence of substituents at the 2^3-position did not stop nucleophiles from reacting with the azulene moiety. Both **2c** and **3c** formed adducts with pyrrolidine and underwent oxidative ring contractions to the corresponding benzocarbaporphyrins in the presence of *tert*-butyl hydroperoxide and a base. Both the pyrrolidine adducts and benzocarbaporphyrins shared key ^{1}H NMR and UV-vis spectroscopic properties with their analogous azuliporphyrin counterparts.

Lash et al. reported a slightly modified Lindsey[27,28] procedure where azulene, pyrrole and benzaldehyde were condensed in the presence of boron trifluoride etherate to yield, following oxidation, tetraphenylazuliporphyrin.[166] Despite mediocre yield (13%), the simplicity of the one-pot procedure represented a significant breakthrough. Shortly thereafter, the Lash group demonstrated that the procedure also worked with other aromatic aldehydes[167] and substituted azulenes (**Figure 4.11**).[168]

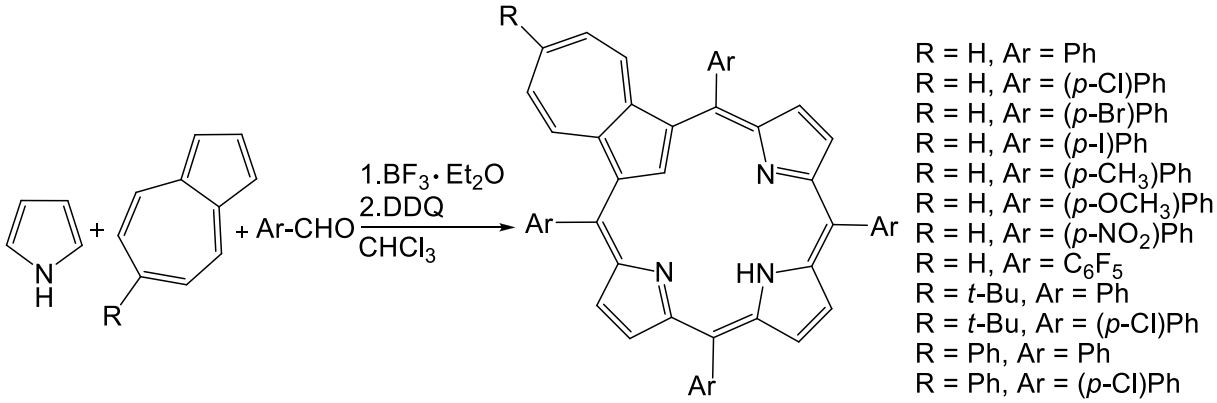

Figure 4.11. One-pot procedure towards tetraarylazuliporphyrins.

^{1}H NMR spectroscopy revealed that tetraarylazuliporphyrins, like their *meso*-unsubstituted counterparts, exhibit intermediate porphyrinoid aromaticity. The chemical shifts also demonstrate that tetraarylazuliporphyrins possess slightly lower diatropic ring currents, compared with the *meso*-unsubstituted azuliporphyrins. This is presumably due to distortions from planarity caused by the increased steric strain from the phenyl groups. The tetraarylazuliporphyrins formed adducts with pyrrolidine and underwent oxidative ring contractions when exposed to hydroperoxides and bases. Again, the resulting adducts and tetraarylbenzocarbaporphyrins exhibited slightly lower diatropic ring currents compared to the analogous *meso*-unsubstituted counterparts. Electron-withdrawing *meso*-aryl groups (e.g., Ar = *p*-NO_2-Ph or C_6F_5) led to increased diatropic ring currents, as they stabilized the negative charge of the dipolar resonance forms (**Figure 4.4**). Likewise, *tert*-butyl substitution of the azulene moiety were found to elicit the same effect, since they stabilized the positive charge on the azulene moiety.

Reactions of azuliporphyrins with $Cu(OAc)_2$ led to copper complexes of 21-oxyazuliporphyrin, i.e., azuliporphyrins with an oxygen attached to its core carbon (**Figure 4.12**).[169] Treating the complexes with TFA removed the copper ion and the free base was isolated, albeit in poor yield. Silver(I) acetate, on the other hand, directly produced 21-oxaazuliporphyrins in good yields, without forming the silver complex.[170] The ^{1}H NMR spectrum of the oxaazuliporphyrins revealed the *β*-protons between 7.38 and 7.84 ppm, similar to those of the parent azuliporphyrin, while the azulene protons resonated between 5 and 6 ppm, about 2 ppm upfield relative to the non-oxygenated azuliporphyrin.

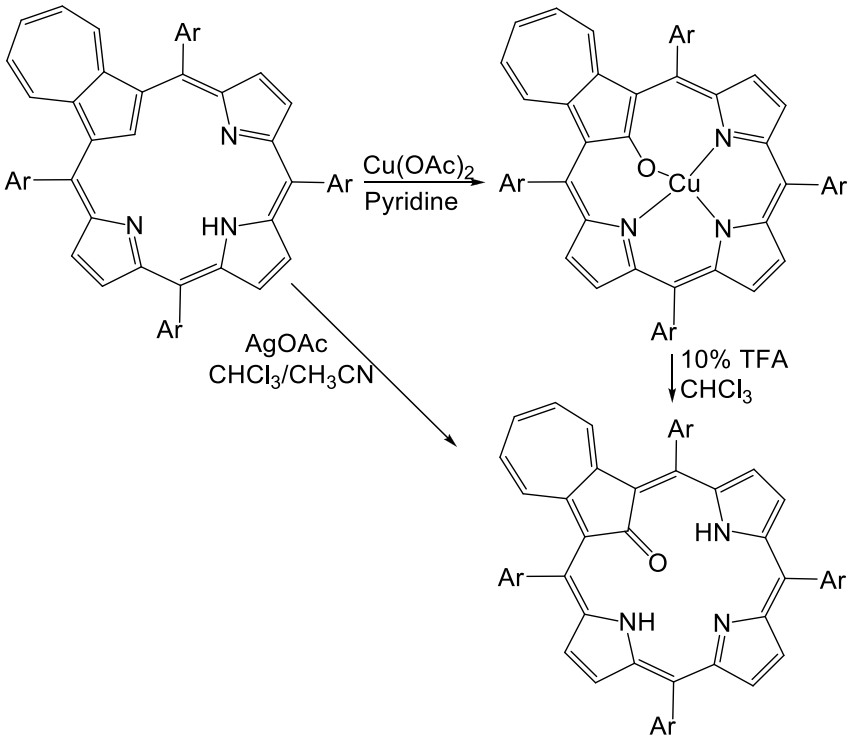

Figure 4.12. Synthesis of 21-oxaazuliporphyrins, directly and via the copper complex.

DFT calculations, specifically NICS, on several azuliporphyrin tautomers have shed light on their aromatic properties, particularly with regard to the global current pathways.[171] The most stable tautomer is depicted in **Figure 4.13**, with the preferred ring current pathway marked in bold. Also depicted is an 18 π-electron pathway that stems from a dipolar resonance form, which rationalizes the aromatic properties. Surprisingly, the calculations did not indicate tropylium cation character of the azulene moiety, in contrast to previous beliefs (**Figure 4.4**).

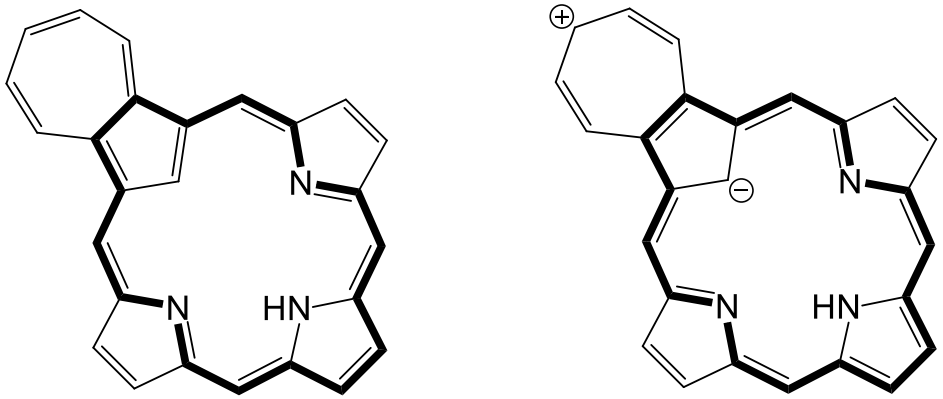

Figure 4.13. The most stable azuliporphyrin tautomer (left) and the dipolar resonance form responsible for its aromaticity (right). The preferred electronic pathway is marked in bold.

Calculations of magnetically induced current densities paint a similar picture. The macrocyclic current bifurcates at each pyrrole unit and prefers the outer route. At the two nonprotonated pyrrole units, however, there is little difference in the current strengths via the inner and outer route. Through the azulene moiety, the current passes via the C2-C3 bond, and in line with the NICS calculations, only a weak current passes along the outer rim of the azulene moiety (**Figure 4.14**). For further details see **Paper D**: "Local versus global aromaticity in azuliporphyrin and benziporphyrin derivatives."

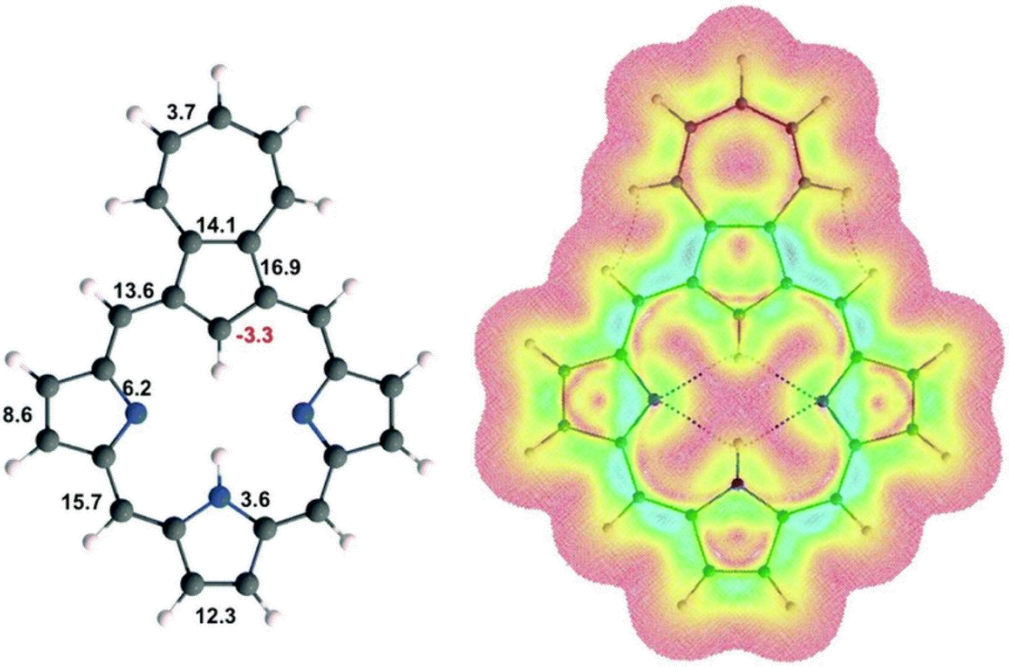

Figure 4.14. Calculated current densities (left, in nAT^{-1}) and current density plot (right) of azuliporphyrin, calculated 1 bohr above the molecular plane. Adapted with permission from ref 172. Copyright 2018 The Royal Society of Chemistry.

4.3. Synthesis and properties of metal azuliporphyrins

The first metal complexes of azuliporphyrins reported were those of nickel(II) and palladium(II),[165,168,173,174] followed shortly by platinum(II).[174] Heating azuliporphyrins in DMF with the appropriate metal salts produced the Ni and Pd complexes in good to excellent yields and the Pt complexes in lower yields. UV-vis spectra of all complexes displayed several absorptions in the 300-500 nm region and broad absorptions at higher wavelengths (500-800 nm).

The complexes of the *meso*-unsubstituted azuliporphyrins are only sparingly soluble in common solvents, resulting in partially resolved ^{1}H NMR spectra. Nevertheless, the *meso*-

protons could be identified, revealing that the chemical shifts of the complexes were all slightly downfield compared to the parent free bases. Among the complexes, Pd exhibited the greatest degree of aromatic character, presumably due to Pd being the best fit for the macrocyclic cavity, allowing the ligand to adopt a more planar conformation. For complexes of *meso*-aryl azuliporphyrins, the β-protons chemical shifts were nearly identical across the different metals, indicating similar diatropic currents. The shifts of the azulene protons varied, suggesting different degrees of tropylium cation character, but this effect may also reflect conformational differences, resulting in varying degrees of shielding from the adjacent aryl groups.

X-ray crystal structures of nickel[173,174] and palladium[173-175] azuliporphyrins revealed that while the nickel ion lies above the center of the macrocyclic cavity, the palladium ion sits in the core, in line with the observations of the NMR spectra. The nickel complex is ruffled while the palladium complex is only mildly saddled and as such more planar.

While the copper complex of tetraphenyloxyazuliporphyrin (**Figure 4.12**) was not suitable for NMR, an X-ray crystal structure confirmed its structure and revealed a saddled macrocycle, in which the oxyazulene moiety was tilted 53 degrees from the mean plane of the remainder of the macrocycle.[169] For comparison, the pyrrole moieties deviated 15.8, 17.8 and 14.3 degrees from the mean plane. Free-base tetraphenyloxyazuliporphyrin was complexed to nickel, palladium and platinum via interactions with the appropriate metal salts.[170] Similar to their non-oxygenated counterparts the complexes exhibited slightly enhanced aromaticity, compared to the parent free bases, with palladium being the most aromatic.

Reacting tetraphenylazuliporphyrin with sub- or equimolar amounts of $[Ru_3(CO)_{12}]$ in refluxing toluene, produced a ruthenium carbonyl tetraphenylazuliporphyrin, while an excess of $[Ru_3(CO)_{12}]$ resulted in a cluster complex where the π-system of the azulene moiety bound an additional $Ru_4(CO)_9$ cluster (**Figure 4.15**).[176] Both complexes exhibited intermediate aromaticity with the β-protons between 7 and 8 ppm. Similar cluster complexes were also prepared from nickel, palladium and platinum tetraphenylazuliporphyrins. All three complexes bound a $Ru_4(CO)_9$ cluster attached to the azulene moiety and displayed similar chemical shifts in the NMR.

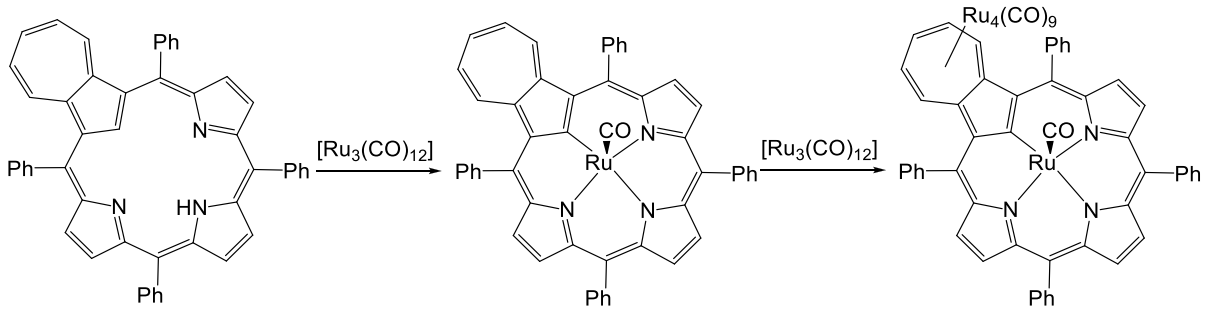

Figure 4.15. Synthesis of Ru(CO)tetraphenylazuliporphyrin and its cluster complex.

Interaction of $[Ru_3(CO)_{12}]$ and tetraphenyloxyazuliporphyrin **1**-OH (**Figure 4.16**) at 80°C led to the corresponding RuCO complex **3**.[177] The latter complex could also be formed via aerial oxidation of RuCO tetraphenylazuliporphyrin, while the reverse reaction (deoxygenation) proved possible at higher temperatures in chlorobenzene. Complex **3** was found to exist in equilibrium with its dimer **4**, unless an additional ligand was added. ^{1}H NMR of **3**-L, where L equals deuterated pyridine, revealed similar shifts to the free-base tetraphenyloxyazuliporphyrin, while ^{1}H NMR of the **4** was complex, indicative of multiple possible conformations.

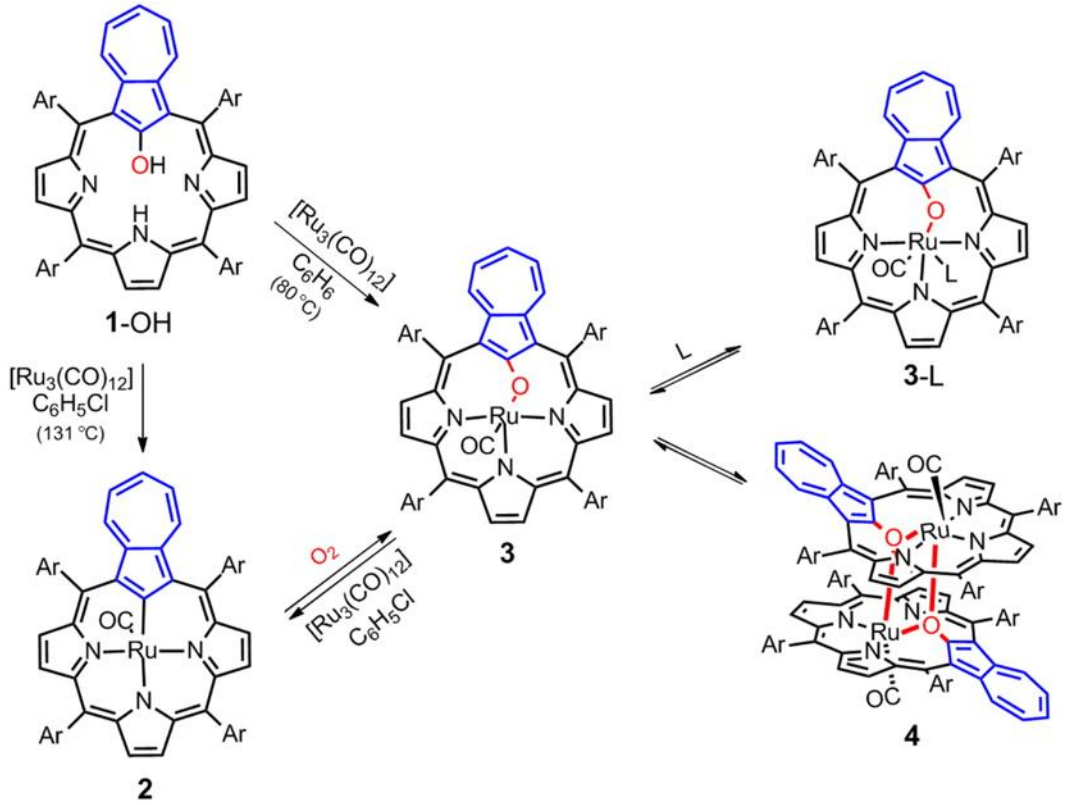

Figure 4.16. Synthesis of Ru(CO)tetraphenyloxyazuliporphyrin. Adapted with permission from ref 177. Copyright 2015 American Chemical Society.

When reacted with $[Ir(COD)Cl]_2$ in refluxing *o*- or *p*-xylene, azuliporphyrins picked up iridium and an oxidized solvent molecule to form methylbenzoyliridium(III) complexes in yields up to 15% (**Figure 4.17**).[178] Similarly, refluxing an azuliporphyrin in *o*-, *m*- or *p*-xylene with $[Rh(CO)_2Cl]_2$ gave rhodium complexes with the appropriate xylyl group as the axial ligand.[179] Both metal complexes showed UV-vis spectra with strong absorptions in the 300-550 nm region and weaker and broader absorptions at higher wavelengths, while ^1H NMR spectroscopy indicated only a slight enhancement of overall aromaticity relative to the free base.

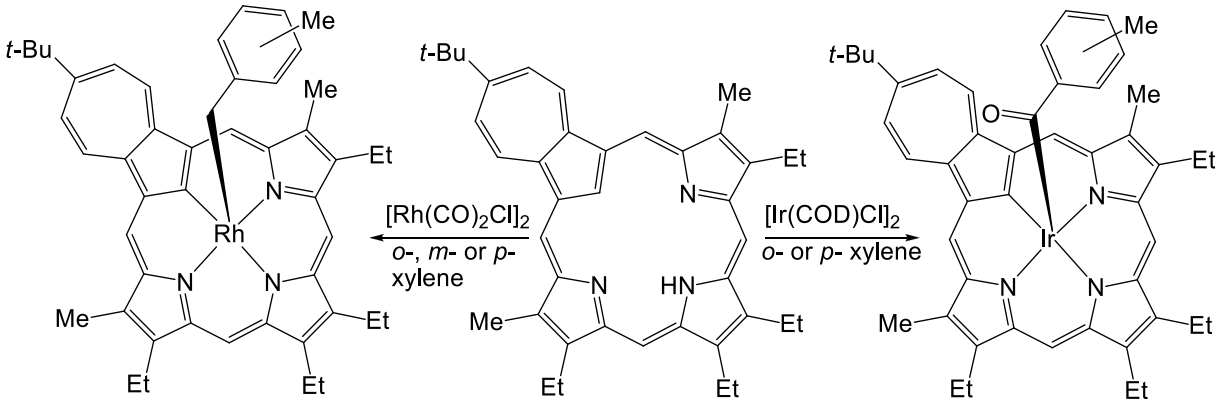

Figure 4.17. Synthesis of rhodium and iridium azuliporphyrins.

Chapter 5. Azulicorrole

Looking for ways to improve the yield of azulitetraphenylporphyrin in order to further explore its coordination chemistry,[166-168] I started to examine the simultaneous interactions of pyrrole, azulene, and various benzaldehydes. To my surprise, adding a drop of TFA to a dichloromethane solution of azulene and benzaldehyde resulted in the instantaneous formation of calix[4]azulene. Intrigued by the speed at which azulene reacted, I added a small amount of azulene to the reaction mixture of a solvent-free, TFA-catalyzed corrole synthesis[37] and, to my delight, I was able to detect azulicorrole in the ESI-MS. Upon careful optimization of the reaction times and the relative amounts of azulene, pyrrole, 4-trifluoromethylbenzaldehyde, and DDQ, I was finally able to isolate 5,10,15-tris(4-trifluoromethylphenyl)azulicorrole (**Figure 5.1**), albeit in very low yields (< 1%). Fortunately, the free base proved readily amenable to both copper and gold complexation.

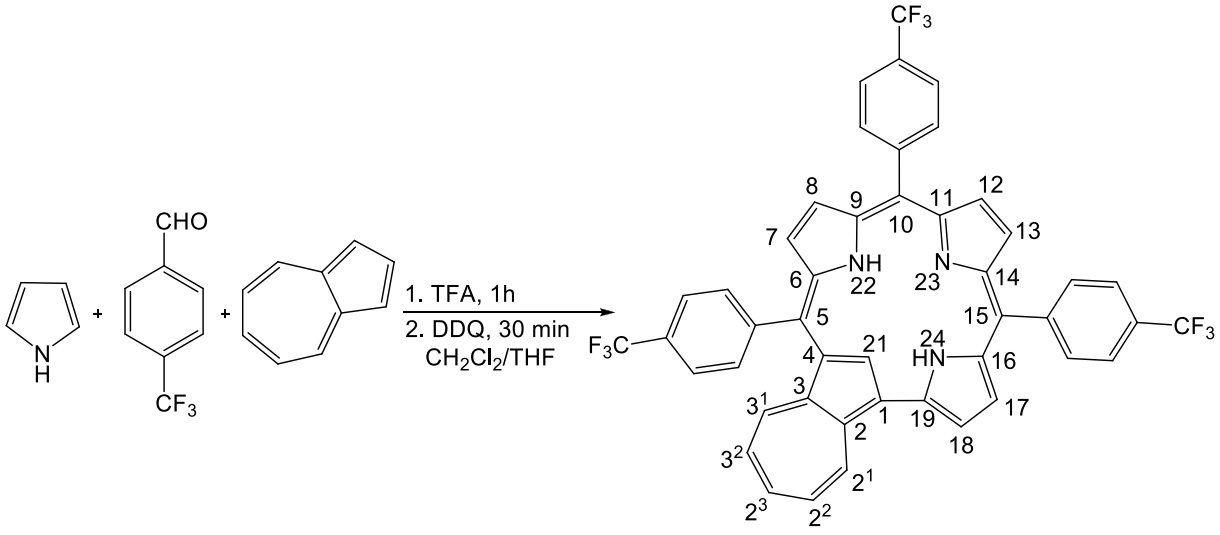

Figure 5.1. Synthesis of azulicorrole, with atom numbering.

Proton NMR spectroscopy afforded insights into the electronic structure of the azulicorrole. From the structural formula, macrocyclic conjugation appears to be interrupted by internal conjugation of the azulene moiety. Nevertheless, the β-protons resonate between 7.21 and 7.95 ppm, placing the azulicorrole in between corrole and isocorrole, in terms of aromaticity. DFT calculations quantified the net diamagnetic macrocyclic current to 15.3 nAT^{-1}, compared to 26.5 nAT^{-1} for gold corrole and 9.8 nAT^{-1} for nickel isocorrole (**Paper B**).

As for azuliporphyrins (**Chapter 4**), the aromaticity of azulicorrole is presumed to reflect a dipolar resonance form, in which the azulene moiety assumes a degree of tropylium-cation character, while the remainder of the macrocycle resembles a corrole anion. I accordingly

sought evidence for this dipolar resonance form by measuring ^{1}H NMR in solvents of increasing polarity, expecting higher-polarity solvents to better stabilize the dipolar resonance form. While low solubility hampered full assignment in solvents other than chloroform-*d*, the azulene protons were identifiable across solvents, and revealed downfield shifts upon increasing solvent polarity, indicating increasing tropylium-cation character and underscoring the importance of the dipolar resonance form.

Recent calculations, both NICS[171] and magnetically induced current densities (**Paper D**), argue for a dipolar resonance structure where the azulene moiety exhibits little or no aromaticity, in both azuliporphyrins and azulicorroles. It is worth noting, however, that the magnetically induced current density calculations were only performed on an azulicorrole complex, and bond length analysis of crystal structures indicates a larger tropylium cation character in free-base azulicorrole.

The optical spectra of the azulicorroles revealed near-IR absorptions. Considering that gold corroles have demonstrated applications in PDT and DSSC,[71] I intended to measure the photophysical properties of gold azulicorrole (enlisting the aid of one of our collaborators) to assess its potential as a photoactive compound. Unfortunately, the low stability of the gold azulicorrole complicated this task.

Further details are available in **Paper C**: "Azulicorrole", and **Paper D**: "Local versus global aromaticity in azuliporphyrin and benziporphyrin derivatives."

Conclusion

The main achievements of this thesis are the facile preparation of new isocorrole ligands, the first isolation of an azulicorrole, and insights gained regarding their electronic structures and aromaticity.

Pyrrole-appended isocorroles were prepared in reasonable yields from *meso*-triarylcorroles, following brief interaction with DDQ and pyrrole. A total of eight free bases, 5- and 10-isomers of isocorroles with four different *meso*-substituents, were prepared, as well as their copper complexes. Optical spectra revealed intriguing near-IR absorptions, while ^{1}HNMR spectroscopy indicated antihomoaromatic character for several compounds. Crystal structures of two of the isocorrole derivatives revealed essentially planar macrocycles.

Replacing pyrrole with *N*,*N*-dimethylaniline or phenylmagnesiumbromide in the above approach afforded *N*,*N*-dimethylaminophenyl- and phenyl-appended isocorroles. The former was found to exhibit similar electronic absorption properties, while the latter exhibited broadened Q bands in the UV-vis-NIR spectra.

Interactions between a corrole and a hypervalent iodine-based Togni reagent resulted in a trifluoromethylated isocorrole. The reaction presumably proceeds via a radical mechanism, potentially showcasing a new method for isocorrole preparation.

Three palladium isocorroles were prepared by refluxing three different free-base isocorroles with $Pd(OAc)_2$ in DMF. All three compounds exhibited strong absorptions in the 800-1000 nm region. Unfortunately, preliminary phosphorescence measurements failed to detect emissions when excited at these wavelengths.

DFT studies (in collaboration with Dr. Cina Foroutan-Nejad and Prof. Jeanet Conradie) demonstrated hyperconjugation through the saturated *meso*-carbon, revealing that isocorroles can vary from homoaromatic to antihomoaromatic, depending on the nature of the substituents at the saturated carbon.

Adding azulene to an otherwise standard solvent-free, TFA-catalyzed corrole synthesis afforded the first example of an azulicorrole. In spite of its cross-conjugated character, proton NMR spectroscopy revealed intermediate aromatic properties for the macrocycle. Proton NMR measurements in solvents of different polarity implicated a dipolar resonance form as the likely cause of aromaticity, much as for azuliporphyrin. DFT studies (in collaboration

with Dr. Cina Foroutan-Nejad and Prof. Jeanet Conradie) confirmed the intermediate degree of aromaticity.

The free-base azulicorrole proved amenable to copper and gold insertion. UV-vis-NIR spectra of the metal complexes revealed strong near-IR absorptions, foreshadowing potential as photosensitizers in PDT.

References

(1) Poulos, T. L. Heme Enzyme Structure and Function. *Chemical Reviews* **2014**, *114*, 3919-3962.

(2) Fliegl, H.; Sundholm, D. Aromatic Pathways of Porphins, Chlorins, and Bacteriochlorins. *The Journal of Organic Chemistry* **2012**, *77*, 3408-3414.

(3) Alemayehu, A. B.; Gonzalez, E.; Hansen, L. K.; Ghosh, A. Copper Corroles Are Inherently Saddled. *Inorganic Chemistry* **2009**, *48*, 7794-7799.

(4) Ganguly, S.; Giles, L. J.; Thomas, K. E.; Sarangi, R.; Ghosh, A. Ligand Noninnocence in Iron Corroles: Insights from Optical and X-ray Absorption Spectroscopies and Electrochemical Redox Potentials. *Chemistry – A European Journal* **2017**, *23*, 15098-15106.

(5) Ganguly, S.; Renz, D.; Giles, L. J.; Gagnon, K. J.; McCormick, L. J.; Conradie, J.; Sarangi, R.; Ghosh, A. Cobalt- and Rhodium-Corrole-Triphenylphosphine Complexes Revisited: The Question of a Noninnocent Corrole. *Inorganic Chemistry* **2017**, *56*, 14788-14800.

(6) Ganguly, S.; Conradie, J.; Bendix, J.; Gagnon, K. J.; McCormick, L. J.; Ghosh, A. Electronic Structure of Cobalt–Corrole–Pyridine Complexes: Noninnocent Five-Coordinate Co(II) Corrole–Radical States. *The Journal of Physical Chemistry A* **2017**, *121*, 9589-9598.

(7) Ganguly, S.; Vazquez-Lima, H.; Ghosh, A. Wolves in Sheep's Clothing: μ-Oxo-Diiron Corroles Revisited. *Chemistry – A European Journal* **2016**, *22*, 10336-10340.

(8) Norheim, H.-K.; Capar, J.; Einrem, R. F.; Gagnon, K. J.; Beavers, C. M.; Vazquez-Lima, H.; Ghosh, A. Ligand noninnocence in FeNO corroles: insights from β-octabromocorrole complexes. *Dalton Transactions* **2016**, *45*, 681-689.

(9) Vazquez-Lima, H.; Norheim, H.-K.; Einrem, R. F.; Ghosh, A. Cryptic noninnocence: FeNO corroles in a new light. *Dalton Transactions* **2015**, *44*, 10146-10151.

(10) Aviv, I.; Gross, Z. Corrole-Based Applications. *ChemInform* **2007**, *38*, no-no.

(11) Birel, Ö.; Nadeem, S.; Duman, H. Porphyrin-Based Dye-Sensitized Solar Cells (DSSCs): a Review. *Journal of Fluorescence* **2017**, *27*, 1075-1085.

(12) Castillero, P.; Roales, J.; Lopes-Costa, T.; Sánchez-Valencia, J. R.; Barranco, A.; González-Elipe, A. R.; Pedrosa, J. M. Optical Gas Sensing of Ammonia and Amines Based on Protonated Porphyrin/TiO_2 Composite Thin Films. *Sensors (Basel, Switzerland)* **2016**, *17*, 24.

(13) Fischer, H.; Zeile, K. Porphyrin syntheses. XXII. Syntheses of hematoporphyrin, protoprophyrin and hemin. *Justus Liebigs Ann. Chem.* **1929**, *468*, 98-116.

(14) Fischer, H.; Zeile, K. Synthese des Hämatoporphyrins, Protoporphyrins und Hämins. *Justus Liebigs Annalen der Chemie* **1929**, *468*, 98-116.

(15) Tschesche, R. Die Chemie des Pyrrols. Von H. Fischer u. H. Orth. II. Band: Pyrrolfarbstoffe. 1. Hälfte: Porphyrine – Hämin – Bilirubin und ihre Abkömmlinge. 764 Seiten. Akademische Verlagsgesellschaft m. b. H., Leipzig 1937. Preis geh. RM. 42, —, geb. RM. 44, —. *Angewandte Chemie* **1938**, *51*, 27-27.

(16) Arsenault, G. P.; Bullock, E.; MacDonald, S. F. Pyrromethanes and porphyrins therefrom. *J. Am. Chem. Soc.* **1960**, *82*, 4384-4389.

(17) Boudif, A.; Momenteau, M. A new convergent method for porphyrin synthesis based on a '3 + 1' condensation. *Journal of the Chemical Society, Perkin Transactions 1* **1996**, 1235-1242.

(18) Boudif, A.; Momenteau, M. Synthesis of a porphyrin-2,3-diacrylic acid using a new '3 + 1' type procedure. *J. Chem. Soc., Chem. Commun.* **1994**, 2069-2070.

(19) Vicente, M. d. G. H.; Smith, K. M. Syntheses and Functionalizations of Porphyrin Macrocycles. *Current organic synthesis* **2014**, *11*, 3-28.

(20) Smith, K. M. Development of porphyrin syntheses. *New Journal of Chemistry* **2016**, *40*, 5644-5649.

(21) Rothemund, P.; Menotti, A. R. Porphyrin studies. IV. The synthesis of α,β,γ,δ-tetraphenylporphine. *J. Am. Chem. Soc.* **1941**, *63*, 267-270.

(22) Rothemund, P. Porphyrin studies. III. The structure of the porphine ring system. *J. Am. Chem. Soc.* **1939**, *61*, 2912-2915.

(23) Rothemund, P. New porphyrin synthesis. Synthesis of porphin. *J. Am. Chem. Soc.* **1936**, *58*, 625-627.

(24) Rothemund, P. FORMATION OF PORPHYRINS FROM PYRROLE AND ALDEHYDES. *Journal of the American Chemical Society* **1935**, *57*, 2010-2011.

(25) Thomas, D. W.; Martell, A. E. Tetraphenylporphine and Some para-Substituted Derivatives1,2. *Journal of the American Chemical Society* **1956**, *78*, 1335-1338.

(26) Adler, A. D.; Longo, F. R.; Shergalis, W. Mechanistic Investigations of Porphyrin Syntheses. I. Preliminary Studies on ms-Tetraphenylporphin. *Journal of the American Chemical Society* **1964**, *86*, 3145-3149.

(27) Lindsey, J. S.; Schreiman, I. C.; Hsu, H. C.; Kearney, P. C.; Marguerettaz, A. M. Rothemund and Adler-Longo reactions revisited: synthesis of tetraphenylporphyrins under equilibrium conditions. *J. Org. Chem.* **1987**, *52*, 827-836.

(28) Lindsey, J. S.; Hsu, H. C.; Schreiman, I. C. Synthesis of tetraphenylporphyrins under very mild conditions. *Tetrahedron Letters* **1986**, *27*, 4969-4970.

(29) Lindsey, J. S.; MacCrum, K. A.; Tyhonas, J. S.; Chuang, Y. Y. Investigation of a Synthesis of meso-Porphyrins Employing High Concentration Conditions and an Electron Transport Chain for Aerobic Oxidation. *The Journal of Organic Chemistry* **1994**, *59*, 579-587.

(30) Johnson, A. W.; Kay, I. T. Synthesis of Corroles and Related Ring Systems. *Proceedings of the Royal Society of London. Series A, Mathematical and Physical Sciences* **1965**, *288*, 334-341.

(31) Johnson, A. W.; Kay, I. T. 306. Corroles. Part I. Synthesis. *Journal of the Chemical Society (Resumed)* **1965**, 1620-1629.

(32) Paolesse, R.; Mini, S.; Sagone, F.; Boschi, T.; Jaquinod, L.; J. Nurco, D.; M. Smith, K. 5,10,15-Triphenylcorrole: a product from a modified Rothemund reaction. *Chemical Communications* **1999**, 1307-1308.

(33) Paolesse, R.; Nardis, S.; Sagone, F.; Khoury, R. G. Synthesis and Functionalization of meso-Aryl-Substituted Corroles. *The Journal of Organic Chemistry* **2001**, *66*, 550-556.

(34) Gross, Z.; Galili, N.; Saltsman, I. The First Direct Synthesis of Corroles from Pyrrole. **1999**, *38*, 1427-1429.

(35) Gross, Z.; Galili, N.; Simkhovich, L.; Saltsman, I.; Botoshansky, M.; Bläser, D.; Boese, R.; Goldberg, I. Solvent-Free Condensation of Pyrrole and Pentafluorobenzaldehyde: A Novel Synthetic Pathway to Corrole and Oligopyrromethenes. *Organic Letters* **1999**, *1*, 599-602.

(36) Wasbotten, I. H.; Wondimagegn, T.; Ghosh, A. Electronic Absorption, Resonance Raman, and Electrochemical Studies of Planar and Saddled Copper(III) meso-Triarylcorroles. Highly Substituent-Sensitive Soret Bands as a Distinctive Feature of High-Valent Transition Metal Corroles. *Journal of the American Chemical Society* **2002**, *124*, 8104-8116.

(37) Gryko, D. T.; Koszarna, B. Refined methods for the synthesis of meso-substituted A3- and trans-A2B-corroles. *Organic & Biomolecular Chemistry* **2003**, *1*, 350-357.

(38) Koszarna, B.; Gryko, D. T. Efficient Synthesis of meso-Substituted Corroles in a H2O−MeOH Mixture. *The Journal of Organic Chemistry* **2006**, *71*, 3707-3717.

(39) Kral, V.; Vasek, P.; Dolensky, B. Green Chemistry for Preparation of Oligopyrrole Macrocycles Precursors: Novel Methodology for Dipyrromethanes and Tripyrromethanes Synthesis in Water. *ChemInform* **2004**, *35*, no-no.

(40) A. Shelnutt, J.; Song, X.-Z.; Ma, J.-G.; Jia, S.-L.; Jentzen, W.; J. Medforth, C.; J. Medforth, C. Nonplanar porphyrins and their significance in proteins. *Chemical Society Reviews* **1998**, *27*, 31-42.

(41) Jentzen, W.; Song, X.-Z.; Shelnutt, J. A. Structural Characterization of Synthetic and Protein-Bound Porphyrins in Terms of the Lowest-Frequency Normal Coordinates of the Macrocycle. *The Journal of Physical Chemistry B* **1997**, *101*, 1684-1699.

(42) Jentzen, W.; Ma, J.-G.; Shelnutt, J. A. Conservation of the Conformation of the Porphyrin Macrocycle in Hemoproteins. *Biophysical Journal* **1998**, *74*, 753-763.

(43) Senge, M. O. Prevention of out-of-plane macrocycle distortion by thallium in the sterically strained 2,3,7,8,12,13,17,18-octaethyl-5,10,15,20-tetranitroporphyrin. *Journal of the Chemical Society, Dalton Transactions* **1993**, 3539-3549.

(44) Barkigia, K. M.; Fajer, J.; Adler, A. D.; Williams, G. J. B. Crystal and molecular structure of (5,10,15,20-tetra-N-propylporphinato)lead(II): a "roof" porphyrin. *Inorganic Chemistry* **1980**, *19*, 2057-2061.

(45) Boyle, N. M.; Rochford, J.; Pryce, M. T. Thienyl—Appended porphyrins: Synthesis, photophysical and electrochemical properties, and their applications. *Coordination Chemistry Reviews* **2010**, *254*, 77-102.

(46) Nurco, D. J.; Medforth, C. J.; Forsyth, T. P.; Olmstead, M. M.; Smith, K. M. Conformational Flexibility in Dodecasubstituted Porphyrins. *Journal of the American Chemical Society* **1996**, *118*, 10918-10919.

(47) Li, X. Y.; Czernuszewicz, R. S.; Kincaid, J. R.; Spiro, T. G. Consistent porphyrin force field. 3. Out-of-plane modes in the resonance Raman spectra of planar and ruffled nickel octaethylporphyrin. *Journal of the American Chemical Society* **1989**, *111*, 7012-7023.

(48) Akiba, K.-y.; Nadano, R.; Satoh, W.; Yamamoto, Y.; Nagase, S.; Ou, Z.; Tan, X.; Kadish, K. M. Synthesis, Structure, Electrochemistry, and Spectroelectrochemistry of Hypervalent Phosphorus(V) Octaethylporphyrins and Theoretical Analysis of the Nature of the PO Bond in P(OEP)(CH2CH3)(O). *Inorganic Chemistry* **2001**, *40*, 5553-5567.

(49) Tozuka, A.; Ohgo, Y.; Ikezaki, A.; Taniguchi, M.; Nakamura, M. Electronic Structure of Highly Ruffled Low-Spin Iron(III) Porphyrinates with Electron Withdrawing Heptafluoropropyl Groups at the meso Positions. *Inorganic Chemistry* **2010**, *49*, 10400-10408.

(50) Senge, M. O.; Ema, T.; Smith, K. M. Crystal structure of a remarkably ruffled nonplanar porphyrin (pyridine)[5,10,15,20-tetra(tert-butyl)porphyrinato]zinc(II). *Journal of the Chemical Society, Chemical Communications* **1995**, 733-734.

(51) Ema, T.; Senge, M. O.; Nelson, N. Y.; Ogoshi, H.; Smith, K. M. 5,10,15,20-Tetra-tert-butylporphyrin and Its Remarkable Reactivity in the 5- and 15-Positions. *Angewandte Chemie International Edition in English* **1994**, *33*, 1879-1881.

(52) Hoshino, A.; Ohgo, Y.; Nakamura, M. Synthesis and inversion barriers of undeca- and dodeca-substituted saddle shaped porphyrin complexes. *Tetrahedron Letters* **2005**, *46*, 4961-4964.

(53) Bhyrappa, P.; Purushothaman, B.; Vittal, J. J. Highly brominated porphyrins: synthesis, structure and their properties. *Journal of Porphyrins and Phthalocyanines* **2003**, *07*, 682-692.

(54) Thomassen, I. K.; Vazquez-Lima, H.; Gagnon, K. J.; Ghosh, A. Octaiodoporphyrin. *Inorganic Chemistry* **2015**, *54*, 11493-11497.

(55) Capar, J.; Conradie, J.; Beavers, C. M.; Ghosh, A. Molecular Structures of Free-Base Corroles: Nonplanarity, Chirality, and Enantiomerization. *The Journal of Physical Chemistry A* **2015**, *119*, 3452-3457.

(56) Thomas, K. E.; Beavers, C. M.; Ghosh, A. Molecular structure of a gold β-octakis(trifluoromethyl)-meso-triarylcorrole: an 85° difference in saddling dihedral relative to copper. *Molecular Physics* **2012**, *110*, 2439-2444.

(57) Luobeznova, I.; Raizman, M.; Goldberg, I.; Gross, Z. Synthesis and Full Characterization of Molybdenum and Antimony Corroles and Utilization of the Latter Complexes as Very Efficient Catalysts for Highly Selective Aerobic Oxygenation Reactions. *Inorganic Chemistry* **2006**, *45*, 386-394.

(58) Einrem, R. F.; Braband, H.; Fox, T.; Vazquez-Lima, H.; Alberto, R.; Ghosh, A. Synthesis and Molecular Structure of 99Tc Corroles. *Chemistry – A European Journal* **2016**, *22*, 18747-18751.

(59) Einrem, R. F.; Gagnon, K. J.; Alemayehu, A. B.; Ghosh, A. Metal–Ligand Misfits: Facile Access to Rhenium–Oxo Corroles by Oxidative Metalation. *Chemistry – A European Journal* **2016**, *22*, 517-520.

(60) Alemayehu, A. B.; Gagnon, K. J.; Terner, J.; Ghosh, A. Oxidative Metalation as a Route to Size-Mismatched Macrocyclic Complexes: Osmium Corroles. *Angewandte Chemie International Edition* **2014**, *53*, 14411-14414.

(61) Alemayehu, A. B.; Vazquez-Lima, H.; Gagnon, K. J.; Ghosh, A. Stepwise Deoxygenation of Nitrite as a Route to Two Families of Ruthenium Corroles: Group 8 Periodic Trends and Relativistic Effects. *Inorganic Chemistry* **2017**, *56*, 5285-5294.

(62) Thomas, K. E.; Conradie, J.; Hansen, L. K.; Ghosh, A. A Metallocorrole with Orthogonal Pyrrole Rings. *European Journal of Inorganic Chemistry* **2011**, *2011*, 1865-1870.

(63) Thomas, K. E.; Vazquez-Lima, H.; Fang, Y.; Song, Y.; Gagnon, K. J.; Beavers, C. M.; Kadish, K. M.; Ghosh, A. Ligand Noninnocence in Coinage Metal Corroles: A Silver Knife-Edge. *Chemistry – A European Journal* **2015**, *21*, 16839-16847.

(64) Thomas, K. E.; Conradie, J.; Hansen, L. K.; Ghosh, A. Corroles Cannot Ruffle. *Inorganic Chemistry* **2011**, *50*, 3247-3251.

(65) Pomarico, G.; Tortora, L.; Fronczek, F. R.; Smith, K. M.; Paolesse, R. Selective nitration and bromination of surprisingly ruffled phosphorus corroles. *Journal of Inorganic Biochemistry* **2016**, *158*, 17-23.

(66) Gouterman, M.; Wagnière, G. H.; Snyder, L. C. Spectra of porphyrins: Part II. Four orbital model. *Journal of Molecular Spectroscopy* **1963**, *11*, 108-127.

(67) Gouterman, M. Spectra of porphyrins. *Journal of Molecular Spectroscopy* **1961**, *6*, 138-163.

(68) Namuangruk, S.; Sirithip, K.; Rattanatwan, R.; Keawin, T.; Kungwan, N.; Sudyodsuk, T.; Promarak, V.; Surakhot, Y.; Jungsuttiwong, S. Theoretical investigation of the charge-transfer properties in different meso-linked zinc porphyrins for highly efficient dye-sensitized solar cells. *Dalton Transactions* **2014**, *43*, 9166-9176.

(69) Ghosh, A.; Wondimagegn, T.; Parusel, A. B. J. Electronic Structure of Gallium, Copper, and Nickel Complexes of Corrole. High-Valent Transition Metal Centers versus Noninnocent Ligands. *Journal of the American Chemical Society* **2000**, *122*, 5100-5104.

(70) Singh, S.; Aggarwal, A.; Bhupathiraju, N. V. S. D. K.; Arianna, G.; Tiwari, K.; Drain, C. M. Glycosylated Porphyrins, Phthalocyanines, and Other Porphyrinoids for Diagnostics and Therapeutics. *Chemical Reviews* **2015**, *115*, 10261-10306.

(71) Alemayehu, A. B.; Day, N. U.; Mani, T.; Rudine, A. B.; Thomas, K. E.; Gederaas, O. A.; Vinogradov, S. A.; Wamser, C. C.; Ghosh, A. Gold Tris(carboxyphenyl)corroles as Multifunctional Materials: Room Temperature Near-IR Phosphorescence and Applications to Photodynamic Therapy and Dye-Sensitized Solar Cells. *ACS Applied Materials & Interfaces* **2016**, *8*, 18935-18942.

(72) Ethirajan, M.; Chen, Y.; Joshi, P.; Pandey, R. K. The role of porphyrin chemistry in tumor imaging and photodynamic therapy. *Chem. Soc. Rev.* **2011**, *40*, 340-362.

(73) Pimenta, F. M.; Jensen, R. L.; Holmegaard, L.; Esipova, T. V.; Westberg, M.; Breitenbach, T.; Ogilby, P. R. Singlet-Oxygen-Mediated Cell Death Using Spatially-Localized Two-Photon Excitation of an Extracellular Sensitizer. *The Journal of Physical Chemistry B* **2012**, *116*, 10234-10246.

(74) Rogers, J. E.; Nguyen, K. A.; Hufnagle, D. C.; McLean, D. G.; Su, W.; Gossett, K. M.; Burke, A. R.; Vinogradov, S. A.; Pachter, R.; Fleitz, P. A. Observation and Interpretation of Annulated Porphyrins: Studies on the Photophysical Properties of meso-Tetraphenylmetalloporphyrins. *The Journal of Physical Chemistry A* **2003**, *107*, 11331-11339.

(75) Sommer, J. R.; Shelton, A. H.; Parthasarathy, A.; Ghiviriga, I.; Reynolds, J. R.; Schanze, K. S. Photophysical Properties of Near-Infrared Phosphorescent π-Extended Platinum Porphyrins. *Chemistry of Materials* **2011**, *23*, 5296-5304.

(76) Koren, K.; Borisov, S. M.; Saf, R.; Klimant, I. Strongly Phosphorescent Iridium(III)–Porphyrins – New Oxygen Indicators with Tuneable Photophysical Properties and Functionalities. *European Journal of Inorganic Chemistry* **2011**, *2011*, 1531-1534.

(77) Borisov, S. M.; Alemayehu, A.; Ghosh, A. Osmium-nitrido corroles as NIR indicators for oxygen sensors and triplet sensitizers for organic upconversion and singlet oxygen generation. *Journal of Materials Chemistry C* **2016**, *4*, 5822-5828.

(78) Borisov, S. M.; Einrem, R. F.; Alemayehu, A. B.; Ghosh, A. Ambient-temperature near-IR phosphorescence and potential applications of rhenium-oxo corroles. *Photochemical & Photobiological Sciences* **2019**.

(79) Palmer, J. H.; Durrell, A. C.; Gross, Z.; Winkler, J. R.; Gray, H. B. Near-IR Phosphorescence of Iridium(III) Corroles at Ambient Temperature. *Journal of the American Chemical Society* **2010**, *132*, 9230-9231.

(80) Alemayehu, A. B.; McCormick, L. J.; Gagnon, K. J.; Borisov, S. M.; Ghosh, A. Stable Platinum(IV) Corroles: Synthesis, Molecular Structure, and Room-Temperature Near-IR Phosphorescence. *ACS Omega* **2018**, *3*, 9360-9368.

(81) Bhuyan, J. Metalloisoporphyrins: from synthesis to applications. *Dalton Transactions* **2015**, *44*, 15742-15756.

(82) Boudiaf, M.; Liang, Y.; Lamare, R.; Weiss, J.; Ibrahim, H.; Goldmann, M.; Bentouhami, E.; Badets, V.; Choua, S.; Le Breton, N.; Bonnefont, A.; Ruhlmann, L. Stable isoporphyrin copolymer: Electrochemical mechanism and behavior and photovoltaic properties. *Electrochimica Acta* **2019**, *309*, 432-449.

(83) Ehudin, M. A.; Senft, L.; Franke, A.; Ivanović-Burmazović, I.; Karlin, K. D. Formation and Reactivity of New Isoporphyrins: Implications for Understanding the Tyr-His Cross-Link Cofactor Biogenesis in Cytochrome c Oxidase. *Journal of the American Chemical Society* **2019**, *141*, 10632-10643.

(84) Garcia-Bosch, I.; Sharma, S. K.; Karlin, K. D. A Selective Stepwise Heme Oxygenase Model System: An Iron(IV)-Oxo Porphyrin πCation Radical Leads to a Verdoheme-Type Compound via an Isoporphyrin Intermediate. *J. Am. Chem. Soc.* **2013**, *135*, 16248-16251.

(85) Evans, J. P.; Niemevz, F.; Buldain, G.; Ortiz de Montellano, P. Isoporphyrin Intermediate in Heme Oxygenase Catalysis: oxidation of α-meso-phenylheme. *J. Biol. Chem.* **2008**, *283*, 19530-19539.

(86) Woodward, R. B.: The total synthesis of chlorophyll. In *Pure and Applied Chemistry*, 1961; Vol. 2; pp 383.

(87) Dolphin, D.; Felton, R. H.; Borg, D. C.; Fajer, J. Isoporphyrins. *J. Amer. Chem. Soc.* **1970**, *92*, 743-745.

(88) Hinman, A. S.; Pavelich, B. J.; Kondo, A. E.; Pons, S. Oxidative voltammetry of some tetraphenylporphyrins in the presence of nucleophiles leading to isoporphyrins. *J. Electroanal. Chem. Interfacial Electrochem.* **1987**, *234*, 145-162.

(89) Kadish, K. M.; Rhodes, R. K. Reactions of metalloporphyrin π radicals. 2. Thin-layer spectroelectrochemistry of zinc tetraphenylporphyrin cation radicals and dications in the presence of nitrogenous bases. *Inorg. Chem.* **1981**, *20*, 2961-2966.

(90) Felton, R. H.; Owen, G. S.; Dolphin, D.; Forman, A.; Borg, D. C.; Fajer, J. OXIDATION OF FERRIC PORPHYRINS*. *Annals of the New York Academy of Sciences* **1973**, *206*, 504-515.

(91) Guzinski, J. A.; Felton, R. H. meso-Tetraphenylmethoxyisoporphyriniron(III) chloride. *Journal of the Chemical Society, Chemical Communications* **1973**, 715-716.

(92) Gold, A.; Ivey, W.; Toney, G. E.; Sangaiah, R. Ferric isoporphyrins from hydroperoxide oxidation of (tetraphenylporphinato)iron(III) complexes. *Inorg. Chem.* **1984**, *23*, 2932-2935.

(93) Yoshihiko, T.; Shigeru, T.; Yoshiko, K.; Hiroaki, M.; Hirochika, S.; Katsumi, T. Isoporphyrins. Near-Infrared Dyes with Noticeable Photochemical and Redox Properties. *Chemistry Letters* **1990**, *19*, 2103-2106.

(94) Lee, W. A.; Bruice, T. C. Transfer of oxygen from percarboxylic acids and alkyl hydroperoxides to (meso-tetraphenylporphinato)cobalt(III) chloride. *Inorganic Chemistry* **1986**, *25*, 131-135.

(95) Balch, A. L.; Latos-Grazynski, L.; Noll, B. C.; Olmstead, M. M.; Zovinka, E. P. Geometric and electronic structure of paramagnetic tetraarylporphyrin complexes of chromium. *Inorganic Chemistry* **1992**, *31*, 1148-1151.

(96) Borah, K. D.; Bhuyan, J. Methoxy-isoporphyrins of water-soluble porphyrins: synthesis, characterization and electrochemical properties. *Journal of Coordination Chemistry* **2019**, *72*, 2251-2260.

(97) Kishii, N.; Shirai, K.; Tamura, S.-i.; Seto, J. e.; Tokumaru, K.; Takagi, S.; Arai, T.; Sakuragi, H. Electron transfer reaction from zinc(II)tetraphenylporphine to dichloromethane. *J. Lumin.* **1995**, *64*, 125-129.

(98) Harriman, A.; Porter, G.; Walters, P. Photooxidation of metalloporphyrins in aqueous solution. *J. Chem. Soc., Faraday Trans. 1* **1983**, *79*, 1335-1350.

(99) Schmidt, E. S.; Bruice, T. C.; Brown, R. S.; Wilkins, C. L. Oxidation of (tetraphenylporphyrin)chromium(III) chloride by styrene ozonide. *Inorganic Chemistry* **1986**, *25*, 4799-4800.

(100) Smith, K. M.; Barnett, G. H.; Evans, B.; Martynenko, Z. Novel meso-substitution reactions of metalloporphyrins. *Journal of the American Chemical Society* **1979**, *101*, 5953-5961.

(101) Evans, B.; Smith, K. M. Novel meso-substitution reactions of zinc(II) octaethylporphyrin. *Tetrahedron Letters* **1977**, *18*, 3079-3082.

(102) Barnett, G. H.; Evans, B.; Smith, K. M.; Besecke, S.; Fuhrhop, J. H. Synthesis of meso-pyridinium porphyrin salts. *Tetrahedron Letters* **1976**, *17*, 4009-4012.

(103) Barnett, G. H.; Smith, K. M. Reactions of some metalloporphyrin and metallochlorin π-cation radicals with nitrite. *Journal of the Chemical Society, Chemical Communications* **1974**, 772-773.

(104) Malek, A.; Latos-Grazynski, L.; Bartczak, T. J.; Zadlo, A. Reactions of the iron(III) tetraphenylporphyrin .pi. cation radical with triphenylphosphine and the nitrite anion. Formation of .beta.-substituted iron(III) porphyrins. *Inorganic Chemistry* **1991**, *30*, 3222-3230.

(105) Shine, H. J.; Padilla, A. G.; Wu, S.-M. Ion radicals. 45. Reactions of zinc tetraphenylporphyrin cation radical perchlorate with nucleophiles. *The Journal of Organic Chemistry* **1979**, *44*, 4069-4075.

(106) Rachlewicz, K.; Latos-Grazynski, L. Novel Reactions of Iron(III) Tetraphenylporphyrin π-Cation Radicals with Pyridine. *Inorg. Chem.* **1995**, *34*, 718-727.

(107) Bhuyan, J.; Sarkar, S. Oxidative Degradation of Zinc Porphyrin in Comparison with Its Iron Analogue. *Chem. - Eur. J.* **2010**, *16*, 10649-10652, S10649/10641-S10649/10648.

(108) Kurtikyan, T. S.; Stepanyan, T. G.; Gasparyan, A. V.; Zhamkochyan, G. A. Interaction of nitrogen dioxide with sublimed films of meso-tetraphenylporphyrinatozinc. *Russ. Chem. Bull.* **1998**, *47*, 644-647.

(109) Johnson, E. C.; Dolphin, D. The reactions of magnesium octaethylporphyrin and its Π-cations with nitrogen dioxide and nitrite. *Tetrahedron Letters* **1976**, *17*, 2197-2200.

(110) Abhilash, G. J.; Bhuyan, J.; Singh, P.; Maji, S.; Pal, K.; Sarkar, S. ·NO2-Mediated meso-Hydroxylation of Iron(III) Porphyrin. *Inorg. Chem.* **2009**, *48*, 1790-1792.

(111) BHUYAN, J.; SARKAR, S. NO2-induced synthesis of nitrato-iron(III) porphyrin with diverse coordination mode and the formation of isoporphyrin‡. *Journal of Chemical Sciences* **2013**, *125*, 707-714.

(112) Xie, H.; Smith, K. M. Stable isoporphyrin chromophores: synthesis. *Tetrahedron Lett.* **1992**, *33*, 1197-1200.

(113) Barkigia, K. M.; Renner, M. W.; Xie, H.; Smith, K. M.; Fajer, J. Structural consequences of porphyrin tautomerization. Molecular structure of a zinc isoporphyrin. *J. Am. Chem. Soc.* **1993**, *115*, 7894-7895.

(114) Fawcett, W. R.; Fedurco, M.; Smith, K. M.; Xie, H. The electrochemistry of a stable zinc isoporphyrin. *J. Electroanal. Chem.* **1993**, *354*, 281-287.

(115) Gentemann, S.; Leung, S. H.; Smith, K. M.; Fajer, J.; Holten, D. Photophysical Consequences of Porphyrin Tautomerization. Steady-State and Time-Resolved Spectral Investigations of a Zinc Isoporphyrin. *J. Phys. Chem.* **1995**, *99*, 4330-4334.

(116) Xie, H.; Leung, S. H.; Smith, K. M. Syntheses and some chemistry of stable isoporphyrin systems. *Journal of Porphyrins and Phthalocyanines* **2002**, *06*, 607-616.

(117) Mwakwari, S. C.; Wang, H.; Jensen, T. J.; Vicente, M. G. H.; Smith, K. M. Syntheses, properties and cellular studies of metallo-isoporphyrins. *J. Porphyrins Phthalocyanines* **2011**, *15*, 918-929.

(118) Mwakwari, C.; Fronczek, F. R.; Smith, K. M. b-Bilene to a,c-biladiene transformation during syntheses of isoporphyrins and porphyrins. *Chem. Commun. (Cambridge, U. K.)* **2007**, 2258-2260.

(119) Schweyen, P.; Hoffmann, M.; Krumsieck, J.; Wolfram, B.; Xie, X.; Bröring, M. Metal-Assisted One-Pot Synthesis of Isoporphyrin Complexes. *Angewandte Chemie International Edition* **2016**, *55*, 10118-10121.

(120) Cong, Z.; Kurahashi, T.; Fujii, H. Formation of Iron(III) meso-Chloro-isoporphyrin as a Reactive Chlorinating Agent from Oxoiron(IV) Porphyrin π-Cation Radical. *J. Am. Chem. Soc.* **2012**, *134*, 4469-4472.

(121) Zhang, A.; Kwan, L.; Stillman, M. J. The spectroscopic impact of interactions with the four Gouterman orbitals from peripheral decoration of porphyrins with simple electron withdrawing and donating groups. *Organic & Biomolecular Chemistry* **2017**, *15*, 9081-9094.

(122) Anabuki, S.; Shinokubo, H.; Aratani, N.; Osuka, A. A meso-Spiro[Cyclopentadiene-Isoporphyrin] from a Phenylethynyl Porphyrin Platinum(II) Pincer Complex. *Angew. Chem., Int. Ed.* **2012**, *51*, 3174-3177, S3174/3171-S3174/3128.

(123) Dogutan, D. K.; Ptaszek, M.; Lindsey, J. S. Direct Synthesis of Magnesium Porphine via 1-Formyldipyrromethane. *The Journal of Organic Chemistry* **2007**, *72*, 5008-5011.

(124) Fan, Y.; Huang, Y.; Jiang, Y.; Ning, X.; Wang, X.; Shan, D.; Lu, X. Comparative study on the interfacial electron transfer of zinc porphyrins with meso-π-extension at a 2n pattern. *Journal of Colloid and Interface Science* **2016**, *462*, 100-109.

(125) Franzke, Y. J.; Sundholm, D.; Weigend, F. Calculations of current densities and aromatic pathways in cyclic porphyrin and isoporphyrin arrays. *Physical Chemistry Chemical Physics* **2017**, *19*, 12794-12803.

(126) Kadish, K. M.: The Electrochemistry of Metalloporphyrins in Nonaqueous Media. In *Progress in Inorganic Chemistry*, 1986; pp 435-605.

(127) Foroutan-Nejad, C.; Larsen, S.; Conradie, J.; Ghosh, A. Isocorroles as Homoaromatic NIR-Absorbing Chromophores: A First Quantum Chemical Study. *Scientific Reports* **2018**, *8*, 11952.

(128) Paolesse, R.; Nardis, S.; Sagone, F.; Khoury, R. G. Synthesis and Functionalization of meso-Aryl-Substituted Corroles. *The Journal of Organic Chemistry* **2000**, *66*, 550-556.

(129) Mandoj, F.; Nardis, S.; Pomarico, G.; Paolesse, R. Demetalation of corrole complexes: an old dream turning into reality. *Journal of Porphyrins and Phthalocyanines* **2008**, *12*, 19-26.

(130) Hohlneicher, G.; Bremm, D.; Wytko, J.; Bley-Escrich, J.; Gisselbrecht, J.-P.; Gross, M.; Michels, M.; Lex, J.; Vogel, E. Spiroconjugation in Spirodicorrolato-Dinickel(II). *Chemistry – A European Journal* **2003**, *9*, 5636-5642.

(131) Hoffmann, M.; Cordes, B.; Kleeberg, C.; Schweyen, P.; Wolfram, B.; Bröring, M. Template Synthesis of Alkyl-Substituted Metal Isocorroles. *European Journal of Inorganic Chemistry* **2016**, *2016*, 3076-3085.

(132) Setsune, J.-i.; Tsukajima, A.; Watanabe, J. Synthesis and chiroptical property of C2-symmetric cyclohexapyrrole. *Tetrahedron Letters* **2007**, *48*, 1531-1535.

(133) Setsune, J.-i.; Tsukajima, A.; Watanabe, J. Synthesis of isocorrole and the higher homologues. *Tetrahedron Letters* **2006**, *47*, 1817-1820.

(134) Setsune, J.-i.; Tsukajima, A.; Okazaki, N. Synthesis and structure of isocorrole metal complexes. *Journal of Porphyrins and Phthalocyanines* **2009**, *13*, 256-265.

(135) Flint, D. L.; Fowler, R. L.; LeSaulnier, T. D.; Long, A. C.; O'Brien, A. Y.; Geier, G. R. Investigation of Complementary Reactions of a Dipyrromethane with a Dipyrromethanemonocarbinol Leading to a 5-Isocorrole. *The Journal of Organic Chemistry* **2010**, *75*, 553-563.

(136) Costa, R.; Geier Iii, G. R.; Ziegler, C. J. Structure and spectroscopic characterization of free base and metal complexes of 5,5-dimethyl-10,15-bis(pentafluorophenyl)isocorrole. *Dalton Transactions* **2011**, *40*, 4384-4386.

(137) Paolesse, R.; Mini, S.; Sagone, F.; Boschi, T.; Jaquinod, L.; J. Nurco, D.; M. Smith, K. 5,10,15-Triphenylcorrole: a product from a modified Rothemund reaction. *Chemical Communications* **1999**.

(138) Gross, Z.; Galili, N.; Saltsman, I. The First Direct Synthesis of Corroles from Pyrrole. *Angewandte Chemie International Edition* **1999**, *38*, 1427-1429.

(139) Nardis, S.; Pomarico, G.; Fronczek, F. R.; Vicente, M. G. H.; Paolesse, R. One-step synthesis of isocorroles. *Tetrahedron Letters* **2007**, *48*, 8643-8646.

(140) Pomarico, G.; Xiao, X.; Nardis, S.; Paolesse, R.; Fronczek, F. R.; Smith, K. M.; Fang, Y.; Ou, Z.; Kadish, K. M. Synthesis and Characterization of Free-Base, Copper and Nickel Isocorroles. *Inorganic chemistry* **2010**, *49*, 5766-5774.

(141) Nardis, S.; Pomarico, G.; Mandoj, F.; Fronczek, F. R.; Smith, K. M.; Paolesse, R. One-pot synthesis of meso-alkyl substituted isocorroles: the reaction of a triarylcorrole with Grignard reagent. *Journal of Porphyrins and Phthalocyanines* **2010**, *14*, 752-757.

(142) Thomas, K. E.; Beavers, C. M.; Gagnon, K. J.; Ghosh, A. β-Octabromo- and β-Octakis(trifluoromethyl)isocorroles: New Sterically Constrained Macrocyclic Ligands. *ChemistryOpen* **2017**, *6*, 402-409.

(143) Capar, J.; Zonneveld, J.; Berg, S.; Isaksson, J.; Gagnon, K. J.; Thomas, K. E.; Ghosh, A. Demetalation of copper undecaarylcorroles: Molecular structures of a free-base undecaarylisocorrole and a gold undecaarylcorrole. *Journal of Inorganic Biochemistry* **2016**, *162*, 146-153.

(144) Stefanelli, M.; Shen, J.; Zhu, W.; Mastroianni, M.; Mandoj, F.; Nardis, S.; Ou, Z.; Kadish, K. M.; Fronczek, F. R.; Smith, K. M.; Paolesse, R. Demetalation of Silver(III) Corrolates. *Inorganic Chemistry* **2009**, *48*, 6879-6887.

(145) Tortora, L.; Nardis, S.; Fronczek, F. R.; Smith, K. M.; Paolesse, R. Functionalization of the corrole ring: the role of isocorrole intermediates. *Chemical Communications* **2011**, *47*, 4243-4245.

(146) Saltsman, I.; Mahammed, A.; Goldberg, I.; Tkachenko, E.; Botoshansky, M.; Gross, Z. Selective Substitution of Corroles: Nitration, Hydroformylation, and Chlorosulfonation. *Journal of the American Chemical Society* **2002**, *124*, 7411-7420.

(147) Bhyrappa, P.; Karunanithi, K.; Varghese, B. 2,3,12,13-Tetramethyl-5,10,15,20-tetraphenylporphyrin. *Acta Crystallographica Section E* **2007**, *63*, o4755.

(148) Zou, J.-Z.; Xu, Z.; Li, M.; You, X.-Z.; Wang, H.-Q. 7,8,17,18-Tetrabromo-5,10,15,20-tetraphenylporphyrin, C44H26Br4N4. *Acta Crystallographica Section C* **1995**, *51*, 760-761.

(149) Nardis, S.; Pomarico, G.; Fronczek, F. R.; Vicente, M. G. H.; Paolesse, R. One-step synthesis of isocorroles. *Tetrahedron Lett.* **2007**, *48*, 8643-8646.

(150) Wiehn, M. S.; Vinogradova, E. V.; Togni, A. Electrophilic trifluoromethylation of arenes and N-heteroarenes using hypervalent iodine reagents. *J. Fluorine Chem.* **2010**, *131*, 951-957.

(151) Umemoto, T.; Ishihara, S. Power-variable electrophilic trifluoromethylating agents. S-, Se-, and Te-(trifluoromethyl)dibenzothio-, -seleno-, and -tellurophenium salt system. *J. Am. Chem. Soc.* **1993**, *115*, 2156-2164.

(152) Thomas, K. E.; Alemayehu, A. B.; Conradie, J.; Beavers, C.; Ghosh, A. Synthesis and Molecular Structure of Gold Triarylcorroles. *Inorganic Chemistry* **2011**, *50*, 12844-12851.

(153) Winstein, S. HOMO-AROMATIC STRUCTURES. *Journal of the American Chemical Society* **1959**, *81*, 6524-6525.

(154) Williams, R. V. Homoaromaticity. *Chemical Reviews* **2001**, *101*, 1185-1204.

(155) Fernández, I.; Wu, J. I.; von Ragué Schleyer, P. Substituent Effects on "Hyperconjugative" Aromaticity and Antiaromaticity in Planar Cyclopolyenes. *Organic Letters* **2013**, *15*, 2990-2993.

(156) Lash, T. D. Carbaporphyrinoid Systems. *Chem. Rev. (Washington, DC, U. S.)* **2017**, *117*, 2313-2446.

(157) Lash, T. D. Out of the Blue! Azuliporphyrins and Related Carbaporphyrinoid Systems. *Acc. Chem. Res.* **2016**, *49*, 471-482.

(158) Lash, T. D.; Chaney, S. T. Conjugated macrocycles related to the porphyrins. Part 8. Azuliporphyrin: a case of borderline porphyrinoid aromaticity. *Angew. Chem., Int. Ed. Engl.* **1997**, *36*, 839-840.

(159) Lash, T. D.; Colby, D. A.; Graham, S. R.; Chaney, S. T. Synthesis, spectroscopy, and reactivity of meso-unsubstituted azuliporphyrins and their heteroanalogues. Oxidative ring contractions to carba-, oxacarba-, thiacarba-, and selenacarbaporphyrins. *J. Org. Chem.* **2004**, *69*, 8851-8864.

(160) Neya, S.; Quan, J.; Hoshino, T.; Hata, M.; Funasaki, N. Convenient synthesis of porphine from β-tetra(tert-butyl)porphyrin. *Tetrahedron Letters* **2004**, *45*, 8629-8630.

(161) Berlin, K.; Steinbeck, C.; Breitmaier, E. Synthesis of Carba-Porphyrinoids from Tripyrranes and Unsaturated Dialdehydes. *Synthesis* **1996**, *1996*, 336-340.

(162) D. Lash, T. The azuliporphyrin-carbaporphyrin connection†. *Chemical Communications* **1998**, 1683-1684.

(163) Graham, S. R.; Colby, D. A.; Lash, T. D. Conjugated macrocycles related to the porphyrins. Part 19. An azulene analogue of the tripyrranes and carbaporphyrinoids therefrom. *Angew. Chem., Int. Ed.* **2002**, *41*, 1371-1374.

(164) Lash, T. D.; Bergman, K. M. Further Observations on Conformational and Substituent Effects in Acid-Catalyzed "3 + 1" Cyclizations of Tripyrranes with Aromatic Dialdehydes. *J. Org. Chem.* **2012**, *77*, 9774-9783.

(165) Lash, T. D.; El-Beck, J. A.; Ferrence, G. M. Syntheses and Reactivity of meso-Unsubstituted Azuliporphyrins Derived from 6-tert-Butyl- and 6-Phenylazulene. *J. Org. Chem.* **2007**, *72*, 8402-8415.

(166) Colby, D. A.; Lash, T. D. Conjugated macrocycles related to the porphyrins, part 23: Adaptation of the Rothemund reaction for carbaporphyrin synthesis: preparation of meso-tetraphenylazuliporphyrin and related benzocarbaporphyrins. *Chem. - Eur. J.* **2002**, *8*, 5397-5402.

(167) Lash, T. D.; Colby, D. A.; Ferrence, G. M. Further studies on the synthesis of meso-tetraarylazuliporphyrins under Lindsey - Rothemund reaction conditions and their conversion into benzocarbaporphyrins. *Eur. J. Org. Chem.* **2003**, 4533-4548.

(168) El-Beck, J. A.; Lash, T. D. Conjugated macrocycles related to the porphyrins, 44. Synthesis and reactivity of 23-tert-butyl- and 23-phenyltetraarylazuliporphyrins: an analysis of the effect of bulky substituents on oxidative ring contractions to benzocarbaporphyrins. *Eur. J. Org. Chem.* **2007**, 3981-3990.

(169) Colby, D. A.; Ferrence, G. M.; Lash, T. D. Oxidative metalation of azuliporphyrins with copper(II) salts: Formation of a porphyrin analogue system with a unique fully conjugated nonaromatic azulene subunit. *Angew. Chem., Int. Ed.* **2004**, *43*, 1346-1349.

(170) Lash, T. D.; Colby, D. A.; El-Beck, J. A.; AbuSalim, D. I.; Ferrence, G. M. Preparation, Structural Characterization, Assessment of Potential Antiaromaticity and Metalation of 21-Oxyazuliporphyrins. *Inorg. Chem.* **2015**, *54*, 9174-9187.

(171) AbuSalim, D. I.; Lash, T. D. Tropylium and Porphyrinoid Character in Carbaporphyrinoid Systems. Relative Stability and Aromatic Characteristics of Azuliporphyrin and

Tropiporphyrin Tautomers, Protonated Species, and Related Structures. *The Journal of Physical Chemistry A* **2019**, *123*, 230-246.

(172) Ghosh, A.; Larsen, S.; Conradie, J.; Foroutan-Nejad, C. Local versus global aromaticity in azuliporphyrin and benziporphyrin derivatives. *Org. Biomol. Chem.* **2018**, *16*, 7964-7970.

(173) Graham, S. R.; Ferrence, G. M.; Lash, T. D. Conjugated macrocycles related to porphyrins. Part 19. Organometallic chemistry of carbaporphyrinoids: synthesis and characterization of nickel(II) and palladium(II) azuliporphyrins. *Chem. Commun. (Cambridge, U. K.)* **2002**, 894-895.

(174) Lash, T. D.; Colby, D. A.; Graham, S. R.; Ferrence, G. M.; Szczepura, L. F. Organometallic Chemistry of Azuliporphyrins: Synthesis, Spectroscopy, Electrochemistry, and Structural Characterization of Nickel(II), Palladium(II), and Platinum(II) Complexes of Azuliporphyrins. *Inorg. Chem.* **2003**, *42*, 7326-7338.

(175) Ferrence, G. M.; Lash, T. D. (23-tert-Butyl-5,10,15,20-tetraphenylazuliporphyrinato)palladium(II) dichloromethane solvate. *Acta Crystallogr., Sect. E: Struct. Rep. Online* **2007**, *63*, m1351-m1353.

(176) Bialek, M. J.; Latos-Grazynski, L. Merging of inner and outer ruthenium organometallic coordination motifs within an azuliporphyrin framework. *Chem. Commun. (Cambridge, U. K.)* **2014**, *50*, 9270-9272.

(177) Bialek, M. J.; Bialonska, A.; Latos-Grazynski, L. Oxidation and Oxygenation of Carbonyl Ruthenium(II) Azuliporphyrin. *Inorg. Chem.* **2015**, *54*, 6184-6194.

(178) Lash, T. D.; Pokharel, K.; Zeller, M.; Ferrence, G. M. Iridium(III) azuliporphyrins. *Chem. Commun. (Cambridge, U. K.)* **2012**, *48*, 11793-11795.

(179) Stateman, L. M.; Ferrence, G. M.; Lash, T. D. Rhodium(III) Azuliporphyrins. *Organometallics* **2015**, *34*, 3842-3848.

Paper A

Organic & Biomolecular Chemistry

PAPER

View Article Online
View Journal | View Issue

Cite this: Org. Biomol. Chem., 2019, 17, 3159

Rapid one-pot synthesis of pyrrole-appended isocorroles†

Simon Larsen, [a] Laura J. McCormick [b] and Abhik Ghosh *[a]

Received 22nd January 2019,
Accepted 26th February 2019

DOI: 10.1039/c9ob00168a

rsc.li/obc

Free-base *meso*-triarylcorroles have been found to undergo oxidative coupling with an excess of pyrrole in dichloromethane in the presence of 2,3-dichloro-5,6-dicyano-1,4-benzoquinone (DDQ) affording 5/10-pyrrole-appended isocorroles in reasonable yields (35–60%) and in a matter of seconds. The free-base isocorrole ligands could all be complexed to copper with $Cu(OAc)_2{\cdot}H_2O$ in chloroform/methanol in 55–80% yields. Single-crystal X-ray structures of two of the new compounds (H_2[5-pyr-T*p*OMePiC] and Cu[10-pyr-T*p*OMePiC]) revealed planar macrocycles with rms atomic displacements of only 0.02 and 0.06 Å relative to their respective best-fit $C_{19}N_4$ planes. Both free-base and Cu(II)-complexed isocorroles exhibit richly featured UV-vis-NIR spectra with red/NIR absorption maxima at ~650 nm and ~725 nm for the free-bases and ~800–850 nm for the copper complexes, suggesting potential applications in photodynamic therapy. Cyclic voltammetric analyses of five of the Cu complexes revealed fully reversible redox cycles with multiple oxidation and reduction features.

Introduction

Over the last quarter-century, during which the chemistry of corroles has grown by leaps and bounds,[1–3] isocorroles have to some extent languished in the shadow of their better-known isomers. Nevertheless, a string of papers over the last decade have highlighted their potential importance.[4–7] They are relatively stable and practical to work with. They are also increasingly accessible, albeit in rather variable yields, *via* simple derivatization of corroles.[4,8,9] Moreover, by combining a porphyrin-like 2– charge with a corrole-like, sterically constrained N_4 core, isocorroles and heteroisocorroles[10,11] provide novel platforms for coordination chemistry.[12,13] Finally, as homoconjugated and potentially homoaromatic[14] compounds, they exhibit surprisingly porphyrin-like electronic absorption spectra that extend well into the near-infrared (NIR), potentially heralding applications in photodynamic therapy.[15,16] Here we report that *meso*-pyrrole–appended isocorroles may be obtained in reasonable yields *via* brief, room-temperature oxidative coupling of a free-base *meso*-triarylcorrole and pyrrole (Scheme 1).[17–19] Both 5- and 10-isocorroles were obtained, with the former predominating. Unambiguous proof of structure came from two single-crystal X-ray diffraction analyses, one for a free-base 5-isocorrole and the other for a Cu(II) 10-isocorrole.

Results and discussion

The free-base compounds described here were first observed as products of pyrrole-aldehyde condensations,[1,20] particularly reaction conditions with a large excess of pyrrole. Mass spectrometric analyses indicated pentapyrrolic products with a

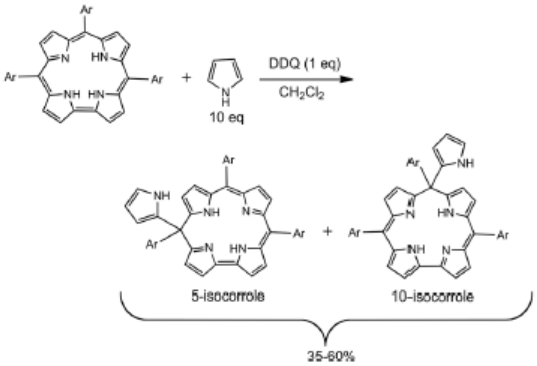

Scheme 1 Synthesis of pyrrole-appended *meso*-tris(*para*-X-phenyl) isocorroles, abbreviated hereafter as H_2[5/10-pyr-T*p*XPiC], where X ⊂ {CF_3, H, Me, OMe}.

[a]*Department of Chemistry, UiT – The Arctic University of Norway, 9037 Tromsø, Norway. E-mail: abhik.ghosh@uit.no*
[b]*Advanced Light Source, Lawrence Berkeley National Laboratory, Berkeley, CA 94720-8229, USA*

† Electronic supplementary information (ESI) available. CCDC 1847337–1847338. For ESI and crystallographic data in CIF or other electronic format see DOI: 10.1039/c9ob00168a

molecular formula equivalent to 'pyrrole + corrole–2H', apparently consistent with an isosmaragdyrin. One of these products fortunately proved amenable to single-crystal X-ray structure determination, clearly indicating a 5-(2-pyrrolyl)isocorole (as opposed to an isosmaragdyrin). With the nature of the products established, we devised an alternative, more convenient route based on the oxidative coupling of a corrole and pyrrole. According to the final protocol, a *meso*-tris(*para*-X-phenyl) corrole, H_3[T*p*XPC], where X ⊂ {CF_3, H, Me, OMe}, and pyrrole underwent immediate coupling in dichloromethane in the presence of 2,3-dichloro-5,6-dicyano-1,4-benzoquinone (DDQ). Both the 5- and 10-(2-pyrrolyl)isocorrole isomers were obtained, denoted hereafter as H_2[5/10-pyr-T*p*XPiC], with the 5-isomer accounting for ≳90% of the combined yield, which ranged from about 35–40% for X = CF_3 and H to about 60% for X = Me and OMe.[21] The free ligands were also complexed to Cu(II) using $Cu(OAc)_2 \cdot H_2O$ (Ac = acetyl) in 4 : 1 v/v mixture of chloroform/methanol as solvent. The 5- and 10-regioisomers of both the free bases and Cu(II) complexes could be separated *via* preparative thin layer chromatography.

The ^{1}H NMR spectra of the eight free-base isocorroles could each be fully assigned, as depicted in Fig. 1 for H_2[5-pyr-T*p*OMePiC]. The chemical shifts of all the β- and *meso*-aryl protons, including the *meso*-pyrrolyl CH protons, were found to range from about 5.9 to 7.5 ppm, while the *meso*-pyrrolyl NH proton was found at ~8.1 ppm. Using the latter peak as a starting point, COSY analysis led to the assignment of the other *meso*-pyrrolyl protons. NOESY analysis then identified the nearby *meso*-aryl and β protons, with the remainder of the peaks identified *via* a combination of COSY and NOESY analysis. The two inner NH protons were located at 14.83 ± 0.3 ppm, suggesting a net global paratropic current. Such a proposition is in line with recent DFT calculations of magnetically induced current densities indicating that, while unsubstituted isocorrole is homoaromatic,[15,16] substituents at the satu-

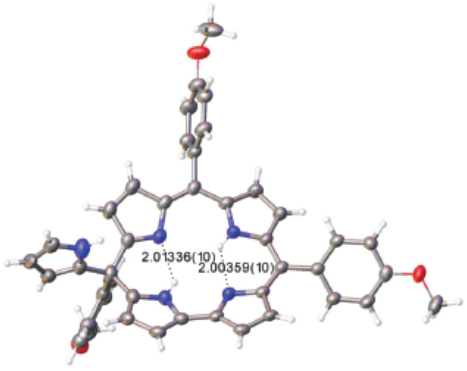

Fig. 2 Thermal ellipsoid plot for H_2[5-pyr-T*p*OMePiC], including key hydrogen bond distances.

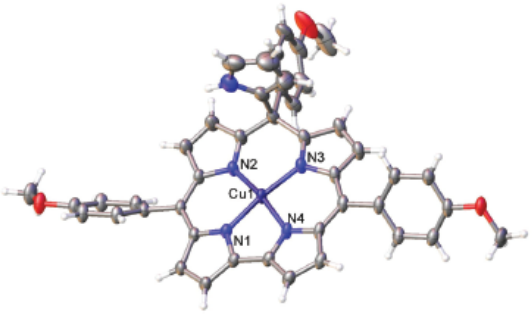

Fig. 3 Thermal ellipsoid plot for Cu[10-pyr-T*p*OMePiC]. Selected distances (Å): Cu1–N1 1.915(3), Cu1–N2 1.925(3), Cu1–N3 1.925(3), and Cu1–N4 1.921(3).

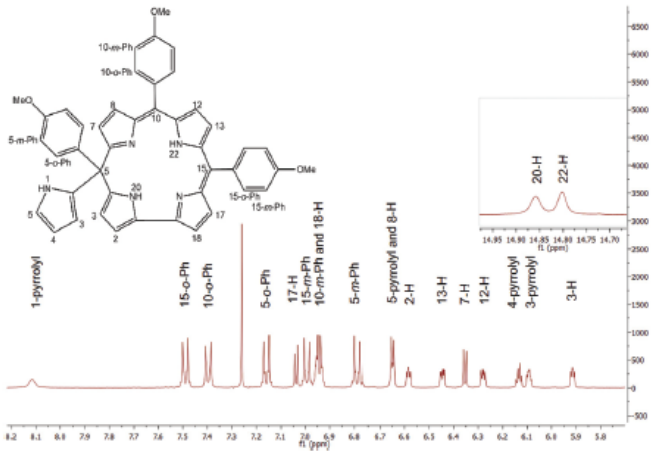

Fig. 1 The ^{1}H NMR spectrum of H_2[5-pyr-T*p*OMePiC].

Table 1 Crystallographic data for H_2[5-pyr-TpOMePiC] and Cu[10-pyr-TpOMePiC]

Sample	H_2[5-pyr-T*p*OMePiC]-dichloromethane	Cu[10-pyr-T*p*OMePiC]-chloroform
Chemical formula	$C_{45}H_{37}Cl_2N_5O_3$	$C_{45}H_{34}Cl_3CuN_5O_3$
Formula mass	766.69	862.66
Crystal system	Triclinic	Triclinic
Crystal size (mm^3)	0.230 × 0.030 × 0.010	0.150 × 0.080 × 0.070
Space group	$P\bar{1}$	$P\bar{1}$
λ (Å)	0.7749	0.7749
a (Å)	9.7321(6	11.1767(16)
b (Å)	12.1142(7)	11.6310(16)
c (Å)	16.7703(10)	15.297(2)
α (°)	85.618(2)	104.788(3)
β (°)	85.655(2)	91.215(3)
g (°)	70.199(2)	96.469(3)
Z	2	2
V ($Å^3$)	1852.20(19)	1907.9(5)
Temperature (K)	100(2)	100(2)
Density (g cm^{-3})	1.375	1.502
Measured reflections	24 592	94 061
Unique reflections	4811	10 084
Parameters	554	570
Restraints	46	56
R_{int}	0.0583	0.0568
θ range (°)	1.330 to 24.614	1.503 to 31.849
R_1, wR_2 all data	0.0970, 0.2092	0.0842, 0.2105
S (GooF) all data	1.133	1.026
Max/min res. dens. (e $Å^{-3}$)	0.474/−0.538	1.383/−1.674

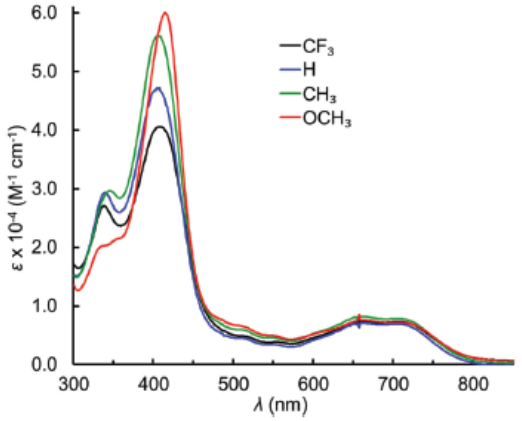

Fig. 4 UV-visible spectra of H_2[5-pyr-T*p*XPiC], where X ⊂ {CF_3, H, Me, OMe}.

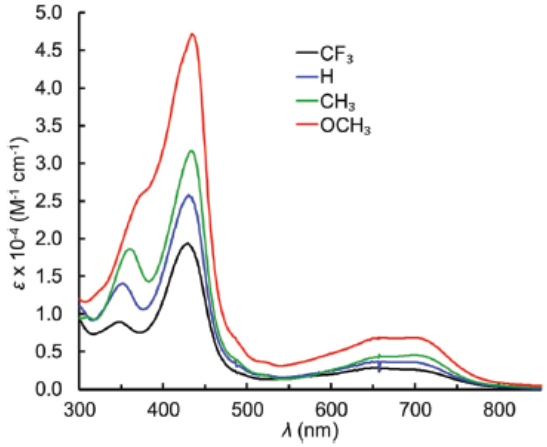

Fig. 5 UV-visible spectra of H_2[10-pyr-T*p*XPiC], where X ⊂ {CF_3, H, Me, OMe}.

rated *meso* carbon can dramatically affect the global ring current. Substituted isocorroles accordingly may range from homoaromatic to antihomoaromatic.

Single-crystal X-ray structures could be obtained for two of the compounds prepared, H_2[5-pyr-T*p*OMePiC] (Fig. 2) and Cu[10-pyr-T*p*OMePiC] (Fig. 3 and Table 1). Like other isocorrole structures reported to date,[4–9] both compounds exhibit remarkably planar macrocycles with rms atomic displacements of only 0.02 and 0.06 Å relative to their respective best-fit $C_{19}N_4$ planes. The relative planarity of the Cu complex may be contrasted with the saddled geometries of Cu corroles, in which the saddling is thought to reflect a noninnocent Cu^{II}-$corrole^{\bullet 2-}$ description.[22–30] Not surprisingly, the observed Cu–N distances (1.915–1.925 Å) are intermediate between those observed for typical Cu triarylcorroles and Cu porphyrins.[2,31] Aside from these, the other bond distances do not warrant much comment, the skeletal C–C and C–N bond distances being typical of those observed for dipyrrins.

Both the free-base and Cu(II)-complexed isocorroles exhibit richly featured UV-vis-NIR spectra (Fig. 4–7 and Table 2). All the compounds exhibit a strong "Soret" band in the

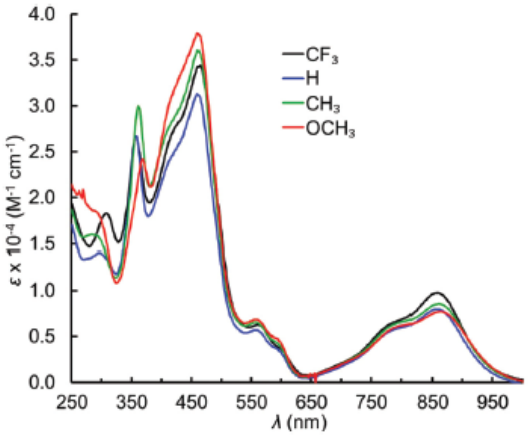

Fig. 6 UV-visible spectra of Cu[5-pyr-T*p*XPiC], where X ⊂ {CF_3, H, Me, OMe}.

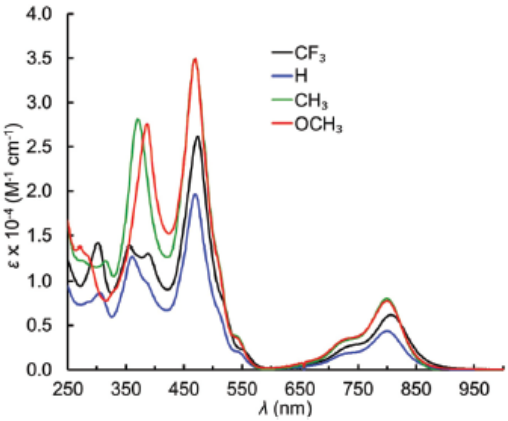

Fig. 7 UV-visible spectra of Cu[10-pyr-T*p*XPiC], where X ⊂ {CF_3, H, Me, OMe}.

400–500 nm region as well as one or more sharp post-Soret features in the near-UV. More notably, compared with their free-base precursors, the Cu isocorrole derivatives exhibit significantly more redshifted Soret maxima, by a margin of a few tens of nm. The compounds also exhibit strong "Q" bands. For the free base isocorroles, these are broad, double-humped features plateauing within approximately 650–725 nm. The Q bands of the Cu complexes are also double humped, but sharper and redshifted into the near-IR, with the most intense peaks occurring at ~855 nm for the 5-regioisomers and ~800 nm for the 10-regioisomers. We tentatively suggest that the considerably redshifted spectra of the Cu complexes relative to the free bases might reflect ligand-to-metal charge transfer transitions. That said, the optical properties of isocorrole derivatives clearly deserve more in-depth study, both *via* the synthesis of new complexes and *via* quantum chemical means.[15] The potential for new isocorrole-based sensitizers for photodynamic therapy is indeed considerable.

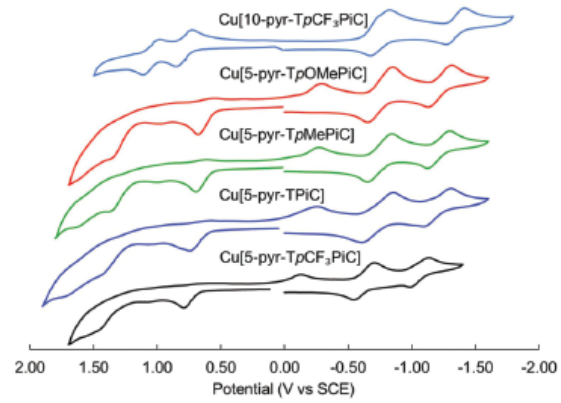

Fig. 8 Cyclic voltammograms of selected Cu isocorrole complexes in CH_2Cl_2 containing 0.1 M TBAP. Scan rate = 100 mV s^{-1}.

Table 2 UV-vis absorption maxima (nm) and molar absorptivities ($\varepsilon \times 10^{-4}$, M^{-1} cm^{-1}) in dichloromethane solution

	<450 nm	450–600 nm	>600 nm
H_2[5-pyr-T*p*OCH_3PiC]	345 (2.05), 415 (6.00)	—	660 (0.76), 708 (0.72).
H_2[5-pyr-T*p*MePiC]	345 (2.97), 406 (5.61)	—	661 (0.82), 705 (0.79)
H_2[5-pyr-TPiC]	339 (2.94), 407 (4.72)	—	661 (0.71), 705 (0.69
H_2[5-pyr-T*p*CF_3PiC]	338 (2.71), 407 (4.06)	—	661 (0.73), 706 (0.74)
H_2[10-pyr-T*p*OCH_3PiC]	375 (2.61), 434 (4.71)	—	656 (0.69), 698 (0.69)
H_2[10-pyr-T*p*MePiC]	359 (1.86), 432 (3.16)	—	658 (0.44), 699 (0.45)
H_2[10-pyr-TPiC]	351 (1.41), 430 (2.58)	—	656 (0.37), 691 (0.36)
H_2[10-pyr-T*p*CF_3PiC]	347 (0.89), 429 (1.94)	—	648 (0.29), 700 (0.26)
Cu[5-pyr-T*p*OCH_3PiC]	368 (2.42)	459 (3.80), 556 (0.69)	786 (0.59), 862 (0.77)
Cu[5-pyr-T*p*MePiC]	285 (1.60), 361 (3.00)	459 (3.61), 557 (0.65)	793 (0.65), 860 (0.85)
Cu[5-pyr-TPiC]	296 (1.41), 357 (2.68)	459 (3.13), 557 (0.57)	792 (0.58), 856 (0.80)
Cu[5-pyr-T*p*CF_3PiC]	308 (1.83), 357 (2.67)	465 (3.44), 560 (0.63)	792 (0.67), 858 (0.98)
Cu[10-pyr-T*p*OCH_3PiC]	271 (1.38), 387 (2.76)	470 (3.50), 544 (0.34)	726 (0.34), 800 (0.78)
Cu[10-pyr-T*p*MePiC]	315 (1.23), 370 (2.81)	468 (3.49), 539 (0.38)	728 (0.33), 800 (0.80)
Cu[10-pyr-TPiC]	305 (0.87), 361 (1.28)	470 (1.96), 540 (0.21)	729 (0.18), 800 (0.44)
Cu[10-pyr-T*p*CF_3PiC]	302 (1.42), 356 (1.39), 388 (1.31)	474 (2.62), 545 (0.24)	734 (0.27), 806 (0.62)

Table 3 Redox potentials (V *vs.* SCE) of selected Cu isocorrole derivatives in CH_2Cl_2 containing 0.1 M TBAP. Scan rate = 100 mV s^{-1}

Compound	$E_{1/2ox\text{-}c}$	$E_{1/2ox\text{-}b}$	$E_{ox\text{-}a}$	$E_{red\text{-}a}$	$E_{1/2red\text{-}b}$	$E_{1/2red\text{-}c}$
Cu[10-pyr-T*p*CF_3PiC]	1.05	0.79	—	—	−0.75	−1.34
Cu[5-pyr-T*p*OCH_3PiC]	—	—	0.68[a]	−0.29[a]	−0.75	−1.23
Cu[5-pyr-T*p*CH_3PiC]	—	—	0.70[a]	−0.27[a]	−0.75	−1.22
Cu[5-pyr-TPiC]	—	—	0.74[a]	−0.26[a]	−0.74	−1.20
Cu[5-pyr-T*p*CF_3PiC]	—	—	0.79[a]	−0.13[a]	−0.63	−1.06

[a] Peak potential.

Cyclic voltammetry on the four Cu(II) 5-isocorroles and on Cu[10-pyr-T*p*CF_3PiC] revealed fully reversible redox cycles with multiple oxidation and reduction features (Fig. 8 and Table 3). Interestingly, the 5-isocorrole series was found to exhibit an isolated oxidation peak 0.74 ± 0.05 V *vs.* SCE with no nearby, corresponding reduction peak and a reduction peak at −0.21 ± 0.9 V *vs.* SCE with no nearby, corresponding oxidation peak. It is reasonable to suppose that oxidation leads to a persistent π-cation radical, potentially involving the pendant pyrrole, which is reduced at a much more negative potential relative to the oxidation peak potential. In contrast, the 10-isocorrole complex Cu[10-pyr-T*p*CF_3PiC] was found to exhibit normal, reversible oxidation and reduction features. Interestingly, the second reduction peak of the 5-isocorrole series (labeled $E_{1/2red\text{-}b}$ in Table 3) occurs at the same potential as the first reduction of *meso*-methoxy isocorrole complexes Cu[5/10-MeO-T*p*CH_3PiC] studied by Pomarico *et al.* and therefore by analogy may be tentatively assigned to a reduction leading to the molecular anion.[4] Detailed spectroelectrochemical and density functional theory-based computational studies are currently in progress, which should result in full assignment of the electrochemical features observed here.[4]

Conclusion

Interaction of free-base *meso*-triarylcorroles with an excess of pyrrole in the presence of DDQ in dichloromethane at room temperature results in moderate yields (35–60%) of 5/10-(2-pyrrolyl)isocorroles in a matter of seconds. Metal coordination to each isocorrole ligand was demonstrated by complexation with Cu(II). Both the free ligands and their metal complexes were found to exhibit strong absorption in the near-infrared, foreshadowing potential applications as sensitizers in photodynamic therapy.

Experimental section

Materials

All free-base corroles were synthesized *via* the now-standard water-methanol method.[32] All reagents, except pyrrole, were purchased from Sigma-Aldrich and used as received. Pyrrole was passed through basic alumina (aluminium oxide 60, active basic activity I, 0.063–0.200 mm particle size, 70–230 mesh, Merck) and stored in the freezer. Silica gel 60 (0.04–0.063 mm particle size, 230–400 mesh, Merck) was employed for flash chromatography. Silica gel 60 preparative thin-layer chromatographic plates (20 cm × 20 cm × 0.5 mm, Merck) were used for final purification of all compounds.

General instrumental methods

UV-visible spectra were recorded on an HP 8453 spectrophotometer. ^{1}H NMR spectra were recorded on a 400 MHz Bruker Avance III HD spectrometer equipped with a 5 mm BB/1H SmartProbe and referenced to either residual CH_2Cl_2 at 5.32 ppm or residual $CHCl_3$ at 7.26 ppm. High-resolution electrospray-ionization (HR-ESI) mass spectra were recorded on an LTQ Orbitrap XL spectrometer, using methanolic solutions and typically in positive ion mode. Elemental analyses were performed by Atlantic Microlab Inc., USA[33]

Cyclic voltammetry was carried out at 298 K with an EG&G Model 263A potentiostat equipped with a three-electrode system: a glassy carbon working electrode, a platinum wire counterelectrode, and a saturated calomel reference electrode (SCE). Tetra(*n*-butyl)ammonium perchlorate (*CAUTION!*), recrystallized twice from absolute ethanol and dried in a desiccator for at least 2 weeks, was used as the supporting electrolyte. Anhydrous CH_2Cl_2 (Aldrich) was used as solvent. The reference electrode was separated from the bulk solution by a fritted-glass bridge filled with the solvent/supporting electrolyte mixture. The electrolyte solution was purged with argon for at least 2 min prior to all measurements, which were carried out under an argon blanket. All potentials were referenced to the SCE.

General procedure for preparation of free-base 5/10-(2-pyrrolyl) isocorroles

A 100 mL round-bottom flask equipped with a magnetic stirring bar was charged with a free-base *meso*-triarylcorrole (20–25 mg) and dichloromethane (10 ml). To the stirred, degassed solution under argon were added DDQ (1 eq.) and pyrrole (10 eq.) in succession, whereupon the color of the solution turned olive-green within seconds. The reaction mixture was then passed through a silica plug with dichloromethane to yield the crude product as a mixture of the 5- and 10-isomer. Separation of the two regioisomers was accomplished with preparative thin-layer chromatography employing the following solvents: dichloromethane/*n*-hexane (8 : 1) for X = *p*-OCH_3, dichloromethane/*n*-hexane (2 : 1) for *p*-CH_3, dichloromethane/pentane (1 : 1) for *p*-H, and dichloromethane/

pentane (1 : 2) for *p*-CF_3. In the event the isomers did not separate, the isocorrole band was divided in fractions and prep-TLC repeated on each individual fraction. The process continued until full separation was achieved. Yields and analytical details for each compound are as follows. Because of the low yields of the 10-isomers, elemental analyses were only carried out for the 5-isomers.

5-(2-Pyrrolyl)-5,10,15-tris(4-methoxyphenyl)isocorrole. Yield 14.8 mg (56%). UV-Vis (CH_2Cl_2) λ_{max} (nm) [$\varepsilon \times 10^{-4}$ (M^{-1} cm^{-1})]: 345 (2.05), 415 (6.00), 660 (0.76), 708 (0.72). ^{1}H NMR (400 MHz, $CDCl_3$, δ): 14.86 (s, 1H, NH), 14.80 (s, 1H, NH), 8.12 (s, 1H, 1-pyrrolyl), 7.49 (d, J = 8.8 Hz, 2H, 15-*o*-Ph), 7.40 (d, J = 8.8 Hz, 2H, 10-*o*-Ph), 7.16 (d, J = 8.9 Hz, 2H, 5-*o*-Ph), 7.04 (d, J = 4.5 Hz, 1H, β-H), 6.99 (d, J = 8.8 Hz, 2H, 15-*m*-Ph), 6.96–6.91 (m, 3H, overlapping 10-*m*-Ph and β-H), 6.79 (d, J = 8.8 Hz, 2H, 5-*m*-Ph), 6.67–6.63 (m, 2H, overlapping β-H and 5-pyrrolyl), 6.58 (dd, J = 3.6, 2.5 Hz, 1H, β-H), 6.45 (dd, J = 4.2, 2.0 Hz, 1H, β-H), 6.35 (d, J = 4.5 Hz, 1H, β-H), 6.28 (dd, J = 4.3, 2.5 Hz, 1H, β-H), 6.15–6.12 (m, 1H, 4-pyrrolyl), 6.10–6.07 (m, 1H, 3-pyrrolyl), 5.91 (dd, J = 3.6, 2.4 Hz, 1H, β-H), 3.89 (s, 3H, 15-*p*-OCH_3), 3.88 (s, 3H, 10-*p*-OCH_3), 3.78 (s, 3H, 5-*p*-OCH_3). MS (ESI) *m*/*z*: 682.2815; calcd for $C_{44}H_{35}N_5O_3H$: 682.2813 [M + H^+]. Elemental analysis: 77.45, H 5.25, N 10.09; calcd for $C_{44}H_{35}N_5O_3$: C 77.51, H 5.17, N 10.27.

10-(2-Pyrrolyl)-5,10,15-tris(4-methoxyphenyl)isocorrole. Yield 1.2 mg (4.5%). UV-Vis (CH_2Cl_2) λ_{max} (nm) [$\varepsilon \times 10^{-4}$ (M^{-1} cm^{-1})]: 375 (2.61), 434 (4.71), 656 (0.69), 698 (0.69). ^{1}H NMR (400 MHz, $CDCl_3$, δ): 14.72 (s, 2H, NH), 7.93 (s, 1H, 1-pyrrolyl), 7.56 (d, J = 8.7 Hz, 4H, 5,15-*o*-Ph), 7.04–6.97 (m, 6H, overlapping 5,15-*m*-Ph and 10-*o*-Ph), 6.82 (d, J = 8.9 Hz, 2H, 10-*m*-Ph), 6.77 (d, J = 4.1 Hz, 2H, β-H), 6.73 (d, J = 4.1 Hz, 2H, β-H), 6.68–6.65 (m, 1H, 5-pyrrolyl), 6.64 (d, J = 4.2 Hz, 2H, β-H), 6.11–6.07 (m, 1H, 4-pyrrolyl), 5.99 (d, J = 4.2 Hz, 2H, β-H), 5.85–5.81 (m, 1H, 3-pyrrolyl), 3.90 (s, 6H, 5,15-*p*-OCH_3), 3.80 (s, 3H, 10-*p*-OCH_3). MS (ESI) *m*/*z*: 682.2814; calcd for $C_{44}H_{35}N_5O_3H$: 682.2813 [M + H^+].

5-(2-Pyrrolyl)-5,10,15-tris(4-methylphenyl)isocorrole. Yield 17.1 mg (58%). UV-Vis (CH_2Cl_2) λ_{max} (nm) [$\varepsilon \times 10^{-4}$ (M^{-1} cm^{-1})]: 345 (2.97), 406 (5.61), 661 (0.82), 705 (0.79); ^{1}H NMR (400 MHz, $CDCl_3$, δ): 14.85 (s, 1H, NH), 14.79 (s, 1H, NH), 8.12 (s, 1H, 1-pyrrolyl), 7.44 (d, J = 8.0 Hz, 2H, 10-*o*-Ph), 7.35 (d, J = 7.9 Hz, 2H, 10-*o*-Ph), 7.28 (d, J = 7.0 Hz, 2H, 15-*m*-Ph), 7.22 (d, J = 7.2 Hz, 2H, 10-*m*-Ph), 7.14 (d, J = 8.2 Hz, 2H, 5-*o*-Ph), 7.09–7.02 (m, 3H, overlapping 5-*m*-Ph and β-H), 6.94 (d, J = 4.5 Hz, 1H, β-H), 6.67–6.62 (m, 2H, overlapping 5-pyrrole and β-H), 6.60 (dd, J = 2.6 Hz, 1H, β-H), 6.43 (dd, J = 4.3, 1.5 Hz, 1H, β-H), 6.37 (d, J = 4.6 Hz, 1H, β-H), 6.25 (dd, J = 4.5, 2.0 Hz, 1H, β-H), 6.15–6.09 (m, 2H, overlapping 3-pyrrolyl and 4-pyrrolyl), 5.92 (dd, J = 3.8, 1.7 Hz, 1H, β-H), 2.45 (s, 3H, 15-*p*-CH_3), 2.44 (s, 3H, 10-*p*-CH_3), 2.32 (s, 3H, 5-*p*-CH_3). MS (ESI) *m*/*z*: 634.2958; calcd for $C_{44}H_{35}N_5H$: 634.2965 [M + H^+]. Elemental analysis: C 82.68, H 5.79, N 10.59; calcd for $C_{44}H_{35}N_5$: C 83.38, H 5.57, N 11.05.

10-(2-Pyrrolyl)-5,10,15-tris(4-methylphenyl)isocorrole. Yield 0.8 mg (2.7%). UV-Vis (CH_2Cl_2) λ_{max} (nm) [$\varepsilon \times 10^{-4}$ (M^{-1} cm^{-1})]: 359 (1.86), 432 (3.16), 658 (0.44), 699 (0.45); ^{1}H NMR (400 MHz, $CDCl_3$ δ): 14.73 (s, 2H, NH), 7.94 (s, 1H, 1-pyrrolyl), 7.49 (d, J = 7.8 Hz, 4H, 5,15-*o*-Ph), 7.28 (d, 4H, 5,15-*m*-Ph), 7.09 (d, J = 8.1 Hz, 2H, 10-*m*-Ph), 6.99 (d, J = 7.9 Hz, 2H, 10-*o*-Ph), 6.76 (d, J = 4.1 Hz, 2H, β-H), 6.72 (d, J = 4.1 Hz, 2H, β-H), 6.67–6.64 (m, 1H, 2-pyrrolyl), 6.62 (d, J = 4.2 Hz, 2H, β-H), 6.11–6.08 (m, 1H, 3-pyrrolyl), 5.98 (d, J = 4.3 Hz, 2H, β-H), 5.87–5.83 (m, 1H, 4-pyrrolyl), 2.46 (s, 6H, 5,15-*p*-CH_3), 2.33 (s, 3H, 10-*p*-CH_3). MS (ESI) *m*/*z*: 634.2968; calcd for $C_{44}H_{35}N_5H$: 634.2965 [M + H^+].

5-(2-Pyrrolyl)-5,10,15-triphenylisocorrole. Yield 11.6 mg (38%). UV-Vis (CH_2Cl_2) λ_{max} (nm) [$\varepsilon \times 10^{-4}$ (M^{-1} cm^{-1})]: 339 (2.94), 407 (4.72), 661 (0.71), 705 (0.69). ^{1}H NMR (400 MHz, CD_2Cl_2 δ): 14.85 (s, 1H, NH), 14.81 (s, 1H, NH), 8.21 (s, 1H, 1-pyrrolyl), 7.59–7.55 (m, 2H, Ph), 7.52–7.43 (m, 8H, overlapping 5-*o*-Ph, 10-*o*-Ph and Ph), 7.33–7.23 (m, 5H, overlapping 15-*o*-Ph and Ph), 7.05 (d, J = 4.5 Hz, 1H, β-H), 7.00 (d, J = 4.5 Hz, 1H, β-H), 6.70–6.62 (m, 3H, overlapping 5-pyrrolyl and β-H), 6.46 (dd, J = 4.3, 1.8 Hz, 1H, β-H), 6.38 (d, J = 4.5 Hz, 1H, β-H), 6.27 (dd, J = 4.3, 2.3 Hz, 1H, β-H), 6.14–6.11 (m, 1H, 4-pyrrolyl), 6.11–6.08 (m, 1H, 3-pyrrolyl), 5.94 (dd, J = 2.9 Hz, 1H, β-H). MS (ESI) *m*/*z*: 592.2495; calcd for $C_{41}H_{29}N_5H$: 592.2496 [M + H^+]. Elemental analysis (%): C 82.60, H 5.41, N 11.15; calcd for $C_{41}H_{29}N_5$: C 83.22, H 4.94, N 11.84.

10-(2-Pyrrolyl)-5,10,15-triphenylisocorrole. Yield 1.2 mg (3.9%). UV-Vis (CH_2Cl_2) λ_{max} (nm) [$\varepsilon \times 10^{-4}$ (M^{-1} $cm^{-1}M^{-1}$ cm^{-1})]: 351 (1.41), 430 (2.58), 656 (0.37), 691 (0.36). ^{1}H NMR (400 MHz, $CDCl_3$ δ): 14.73 (s, 2H, NH), 7.94 (s, 1H, 1-pyrrolyl), 7.63–7.58 (m, 4H, 5,15-*o*-Ph), 7.50–7.44 (m, 6H, overlapping 5,15-*m*-Ph and 5,15-*p*-Ph), 7.34–7.28 (m, 3H, overlapping 10-*m*-Ph and 10-*p*-Ph), 7.13–7.08 (m, 2H, 10-*o*-Ph), 6.77–6.73 (m, 4H, overlapping β-H), 6.69–6.65 (m, 1H, 2-pyrrolyl), 6.61 (d, J = 4.3 Hz, 2H, β-H), 6.10 (q, J = 3.0 Hz, 1H, 3-pyrrolyl), 5.97 (d, J = 4.3 Hz, 2H, β-H), 5.87–5.84 (m, 1H, 4-pyrrolyl). MS (ESI) *m*/*z*: 592.2499; calcd for $C_{41}H_{29}N_5H$: 592.2496 [M + H^+].

5-(2-Pyrrolyl)-5,10,15-tris[(4-trifluoromethyl)phenyl]isocorrole. Yield 6.1 mg (30%). UV-Vis (CH_2Cl_2) λ_{max} (nm) [$\varepsilon \times 10^{-4}$ (M^{-1} cm^{-1})]: 338 (2.71), 407 (4.06), 661 (0.73), 706 (0.74). ^{1}H NMR (400 MHz, $CDCl_3$, δ): 14.75 (s, 2H, NH), 8.11 (s, 1H, 1-pyrrolyl), 7.77–7.69 (m, 4H, overlapping 10-*m*-Ph and 15-*m*-Ph), 7.67 (d, J = 8.0 Hz, 2H, 15-*o*-Ph), 7.61 (d, J = 7.9 Hz, 2H, 10-*o*-Ph), 7.53 (d, J = 8.2 Hz, 2H, 5-*m*-Ph), 7.36 (d, J = 8.2 Hz, 2H, 5-*o*-Ph), 7.01 (d, 2H, 2 overlapping β-H), 6.70–6.67 (m, 2H, overlapping 5-pyrrolyl and β-H), 6.58 (d, J = 4.6 Hz, 1H, β-H), 6.40–6.36 (m, 2H, 2 overlapping β-H), 6.20 (dd, J = 4.3, 2.4 Hz, 1H, β-H), 6.18–6.15 (m, 1H, 4-pyrrolyl), 6.15–6.11 (m, 1H, 3-pyrrolyl), 5.95 (dd, J = 3.6, 2.5 Hz, 1H, β-H). MS (ESI) *m*/*z*: 796.2114; calcd for $C_{44}H_{26}N_5F_9H$: 796.2117 [M + H^+]. Elemental analysis (%): C 66.62, H 3.42, N 8.69; calcd for $C_{44}H_{26}N_5F_9$: C 66.42, H 3.29, N 8.80.

10-(2-Pyrrolyl)-5,10,15-tris[(4-trifluoromehtyl)phenyl]isocorrole. Yield 0.4 mg (2.0%). UV-Vis (CH_2Cl_2) λ_{max} (nm) [$\varepsilon \times 10^{-4}$ (M^{-1} cm^{-1})]: 347 (0.89), 429 (1.94), 648 (0.29), 700 (0.26). ^{1}H NMR (400 MHz, $CDCl_3$ δ): 14.58 (s, 2H, NH), 7.86 (s, 1H, 1-pyrrolyl), 7.71–7.62 (m, 8H, overlapping 5,15-*o*-Ph and 5,15-*m*-Ph), 7.50 (d, J = 8.2 Hz, 2H, 10-*m*-Ph), 7.15 (d, J = 8.2 Hz, 2H, 10-*o*-Ph), 6.72 (d, J = 4.2 Hz, 2H, β-H), 6.67–6.61 (m, 3H, overlapping

β-H and 2-pyrrolyl), 6.50 (d, J = 4.3 Hz, 2H, β-H), 6.06 (q, J = 3.0 Hz, 1H, 3-pyrrolyl), 5.90 (d, J = 4.3 Hz, 2H, β-H), 5.79 (d, J = 3.9 Hz, 1H, 4-pyrrolyl). MS (ESI) m/z: 796.2112; calcd for $C_{44}H_{26}N_5F_9H$: 796.2117 [M + H$^+$].

General procedure for preparation of copper 5/10-(2-pyrrolyl) triarylisocorroles

To a 100 ml round-bottom flask equipped with a magnetic stirring bar was added free-base isocorrole (15–25 mg, mixture of isomers), $Cu(OAc)_2{\cdot}H_2O$ (1.5 eq.), $CHCl_3$ (8 mL) and MeOH (2 mL). The mixture was refluxed for 30 minutes (room temperature for p-CF_3). The solvents were removed under vacuum and the solids passed through silica with dichloromethane. Separation of 5- and 10-isomers required preparative thin-layer chromatography employing DCM for p-OCH_3, DCM/pentane (1 : 1) for p-CH_3, and DCM/pentane (1 : 2) for p-H and p-CF_3. In the event the isomers did not separate, the copper isocorrole band was divided in fractions and prep-TLC repeated on each individual fraction. The process continued until full separation was achieved. Yields and analytical details for each compound are as follows. Because of the low yields of the 10-isomers, elemental analyses were only carried out for the 5-isomers.

Copper 5-(2-pyrrolyl)-5,10,15-tris(4-methoxyphenyl)isocorrole. Yield 9.2 mg (54%). UV-Vis (CH_2Cl_2) λ_{max} (nm) [$\varepsilon \times 10^{-4}$ (M^{-1} cm^{-1})]: 368 (2.42), 459 (3.80), 556 (0.69), 786 (0.59), 862 (0.77). MS (ESI) m/z: 742.1869; calcd for $C_{44}H_{33}N_5O_3Cu$: 742.1874 [M$^+$]. Elemental analysis (%): C 71.19, H 4.70, N 9.03; calcd for $C_{44}H_{33}N_5O_3Cu$: C 71.10, H 4.47, N 9.42.

Copper 10-(2-pyrrolyl)-5,10,15-tris(4-methoxyphenyl)isocorrole. Yield 0.9 mg (5.3%). UV-Vis (CH_2Cl_2) λ_{max} (nm) [$\varepsilon \times 10^{-4}$ (M^{-1} cm^{-1})]: 271 (1.38), 387 (2.76), 470 (3.50), 544 (0.34), 726 (0.34), 800 (0.78). MS (ESI) m/z: 742.1876; calcd for $C_{44}H_{33}N_5O_3Cu$: 742.1874 [M$^+$].

Copper 5-(2-pyrrolyl)-5,10,15-tris(4-methylphenyl)isocorrole. Yield 21.7 mg (77%). UV-Vis (CH_2Cl_2) λ_{max} (nm) [$\varepsilon \times 10^{-4}$ (M^{-1} cm^{-1})]: 285 (1.60), 361 (3.00), 459 (3.61), 557 (0.65), 793 (0.65), 860 (0.85). MS (ESI) m/z: 694.2032; calcd for $C_{44}H_{33}N_5Cu$: 694.2026 [M$^+$]. Elemental analysis (%): C 75.41, H 5.06, N 9.61; calcd for $C_{44}H_{33}N_5Cu$: C 76.00, H 4.78, N 10.07.

Copper 10-(2-pyrrolyl)-5,10,15-tris(4-methylphenyl)isocorrole. Yield 1.5 mg (5.3%). UV-Vis (CH_2Cl_2) λ_{max} (nm) [$\varepsilon \times 10^{-4}$ (M^{-1} cm^{-1})]: 315 (1.23) 370 (2.81), 468 (3.49), 539 (0.38), 728 (0.33), 800 (0.80). MS (ESI) m/z: 694.2031; calcd for $C_{44}H_{33}N_5Cu$: 694.2026 [M$^+$].

Copper 5-(2-pyrrolyl)-5,10,15-triphenylisocorrole. Yield 14.7 mg (73%). UV-Vis (CH_2Cl_2) λ_{max} (nm) [$\varepsilon \times 10^{-4}$ (M^{-1} cm^{-1})]: 296 (1.41), 357 (2.68), 459 (3.13), 557 (0.57), 792 (0.58), 856 (0.80). MS (ESI) m/z: 652.1558; calcd for $C_{41}H_{27}N_5Cu$: 652.1557 [M$^+$]. Elemental analysis (%): C 75.44, H 4.57, N 10.25; calcd for $C_{41}H_{27}N_5Cu$: C 75.38, H 4.17, N 10.72.

Copper 10-(2-pyrrolyl)-5,10,15-triphenylisocorrole. Yield 1 mg (5.0%). UV-Vis (CH_2Cl_2) λ_{max} (nm) [$\varepsilon \times 10^{-4}$ (M^{-1} cm^{-1})]: 305 (0.87), 361 (1.28), 470 (1.96), 540 (0.21), 729 (0.18), 800 (0.44); MS (ESI) m/z: 652.1556; calcd for $C_{41}H_{27}N_5Cu$: 652.1557 [M$^+$].

Copper 5-(2-pyrrolyl)-5,10,15-tris[(4-trifluoromethyl)phenyl] isocorrole. Yield 11.6 mg (48%). UV-Vis (CH_2Cl_2) λ_{max} (nm) [$\varepsilon \times 10^{-4}$ (M^{-1} cm^{-1})]: 308 (1.83), 357 (2.67), 465 (3.44), 560 (0.63), 792 (0.67), 858 (0.98). MS (ESI) m/z: 856.1171; calcd for $C_{44}H_{24}N_5F_9Cu$: 856.1179 [M$^+$]. Elemental analysis (%): C 61.17, H 3.06, N 7.70; calcd for $C_{44}H_{24}N_5F_9Cu$: C 61.65, H 2.82, N 8.17.

Copper 10-(2-pyrrolyl)-5,10,15-tris[(4-trifluoromethyl)phenyl] isocorrole. Yield 1.2 mg (5.0%). UV-Vis (CH_2Cl_2) λ_{max} (nm) [$\varepsilon \times 10^{-4}$ (M^{-1} cm^{-1})]: 302 (1.42), 356 (1.39), 388 (1.31), 474 (2.62), 545 (0.24), 734 (0.27), 806 (0.62). MS (ESI) m/z: 856.1173; calcd for $C_{44}H_{24}N_5F_9Cu$: 856.1179 [M$^+$].

Single-crystal X-ray structure determination. X-ray structure determination. Suitable crystals were obtained by diffusion of methanol vapor into concentrated solutions of H_2[5-pyr-TpOMePiC] in dichloromethane and Cu[10-pyr-TpOMePiC] in chloroform. X-ray data were collected on beamline 11.3.1 at the Advanced Light Source of Lawrence Berkeley National Laboratory, Berkeley, California. The samples were mounted on MiTeGen® kapton loops and placed in a 100(2) K nitrogen cold stream provided by an Oxford Cryostream 700 Plus low temperature apparatus on the goniometer head of a Bruker D8 diffractometer equipped with PHOTONII CPAD detector. Diffraction data were collected using synchrotron radiation monochromated with silicon(111) to a wavelength of 0.7749(1) Å. In each case, an approximate full-sphere of data was collected using 1° ω scans. Absorption corrections were applied using SADABS.[34] The structure was solved by intrinsic phasing (SHELXT)[35] and refined by full-matrix least squares on F^2 (SHELXL-2014)[36] using the ShelXle GUI.[37] All non-hydrogen atoms were refined anisotropically. Hydrogen atoms were geometrically calculated and refined as riding atoms.

Conflicts of interest

There are no conflicts of interest to declare.

Acknowledgements

This work was supported by the Research Council of Norway (grant no. 262229 to AG) and by the Advanced Light Source, Berkeley, California. The Advanced Light Source is supported by the Director, Office of Science, Office of Basic Energy Sciences, of the U.S. Department of Energy under Contract No. DE-AC02-05CH11231.

References

1 R. Orlowski, D. Gryko and D. T. Gryko, *Chem. Rev.*, 2017, **117**, 3102–3137.
2 A. Ghosh, *Chem. Rev.*, 2017, **117**, 3798–3881.
3 R. D. Teo, J. Y. Hwang, J. Termini, Z. Gross and H. B. Gray, *Chem. Rev.*, 2017, **117**, 2711–2729.

4 G. Pomarico, X. Xiao, S. Nardis, R. Paolesse, F. R. Fronczek, K. M. Smith, Y. Fang, Z. Ou and K. M. Kadish, *Inorg. Chem.*, 2010, **49**, 5766–5774.
5 R. Costa, G. R. Geir III and C. J. Ziegler, *Dalton Trans.*, 2011, **40**, 4384–4386.
6 M. Hoffmann, B. Cordes, C. Kleeberg, P. Schweyen, B. Wolfram and M. Bröring, *Eur. J. Inorg. Chem.*, 2016, 3076–3085.
7 K. E. Thomas, C. M. Beavers, K. J. Gagnon and A. Ghosh, *ChemistryOpen*, 2017, **6**, 402–409.
8 S. Nardis, G. Pomarico, F. Mandoj, F. R. Fronczek, K. M. Smith and R. Paolesse, *J. Porphyrins Phthalocyanines*, 2010, **14**, 752–757.
9 S. Nardis, G. Pomarico, F. R. Fronczek, M. G. H. Vicente and R. Paolesse, *Tetrahedron Lett.*, 2007, **48**, 8643–8646.
10 D. Sakow, B. Böker, K. Brandhorst, O. Burghaus and M. Bröring, *Angew. Chem., Int. Ed.*, 2013, **52**, 4912–4915.
11 B. Umasekhar, V. S. Shetti and M. Ravikanth, *RSC Adv.*, 2018, **8**, 21100–21132.
12 M. Bröring, S. Köhler and C. Pietzonka, *J. Porphyrins Phthalocyanines*, 2012, **16**, 641–650.
13 D. Sakow, D. Baabe, B. Böker, O. Burghaus, M. Funk, C. Kleeberg, D. Menzel, C. Pietzonka and M. Bröring, *Chem. – Eur. J.*, 2014, **20**, 2913–2924.
14 S. Winstein, *J. Am. Chem. Soc.*, 1959, **81**, 6524–6525.
15 C. Foroutan-Nejad, S. Larsen, J. Conradie and A. Ghosh, *Sci. Rep.*, 2018, **8**, 11952.
16 C. Foroutan-Nejad and A. Ghosh, *ACS Omega*, 2018, **3**, 15865–15869.
17 Several pyrrole-appended porphyrinoid macrocycles are reported in the literature.[18,19].
18 M. Pawlicki, I. Kańska and L. Latos-Grażyński, *Inorg. Chem.*, 2007, **46**, 6575–6584, and references therein.
19 M. Li, P. Wei, M. Ishida, X. Li, M. Savage, R. Guo, Z. Ou, S. Yang, H. Furuta and Y. Xie, *Angew. Chem., Int. Ed.*, 2016, **55**, 3063–3067.
20 A. Ghosh, *Angew. Chem., Int. Ed.*, 2004, **43**, 1918–1931.
21 The overwhelming preference for the 5-isocorrole regioisomer observed here differs from the much more even 5/10 regioisomer ratio reported in ref. 9. In our hands, however, the conditions used in ref. 9 (*i.e.*, DDQ-promoted addition of methanol) applied to free-base triphenylcorrole also led to a strong preponderance of the 5-isocorrole.[15].
22 I. H. Wasbotten, T. Wondimagegn and A. Ghosh, *J. Am. Chem. Soc.*, 2002, **124**, 8104–8116.
23 M. Bröring, F. Bregier, E. C. Tejero, C. Hell and M. C. Holthausen, *Angew. Chem., Int. Ed.*, 2007, **46**, 445–448.
24 A. B. Alemayehu, E. Gonzalez, L. K. Hansen and A. Ghosh, *Inorg. Chem.*, 2009, **48**, 7794–7799.
25 K. E. Thomas, J. Conradie, L.-K. Hansen and A. Ghosh, *Eur. J. Inorg. Chem.*, 2011, 1865–1870.
26 A. B. Alemayehu, L.-K. Hansen and A. Ghosh, Nonplanar, Noninnocent, and Chiral: A Strongly Saddled Metallocorrole, *Inorg. Chem.*, 2010, **49**, 7608–7610.
27 K. E. Thomas, H. Vazquez-Lima, Y. Fang, Y. Song, K. J. Gagnon, C. M. Beavers, K. M. Kadish and A. Ghosh, *Chem. – Eur. J.*, 2015, **21**, 16839–16847.
28 K. E. Thomas, L. J. McCormick, D. Carrié, H. Vazquez-Lima, G. Simonneaux and A. Ghosh, *Inorg. Chem.*, 2018, **57**, 4270–4276.
29 S. Berg, K. E. Thomas, C. M. Beavers and A. Ghosh, *Inorg. Chem.*, 2012, **51**, 9911–9916.
30 I. K. Thomassen, L. J. McCormick and A. Ghosh, *ACS Omega*, 2018, **3**, 5106–5110.
31 K. E. Thomas, A. B. Alemayehu, J. Conradie, C. M. Beavers and A. Ghosh, *Acc. Chem. Res.*, 2012, **45**, 1203–1214.
32 B. Koszarna and D. T. Gryko, *J. Org. Chem.*, 2006, **71**, 3707–3717.
33 Many metalloporphyrins and metallocorroles, in particular hemes and Mn and Fe corroles do not yield satisfactory elemental analyses. Others, such as coinage metal corroles, do so readily. The present complexes turned out to be intermediate. Although the majority of analyses proved to be within 0.5% of their theoretical values, a few exhibited errors of 1–2%. Although the latter can be accounted for by assuming tightly held solvent molecules, the theoretical analyses quoted here refer to simply the solvent-free molecular formulas.
34 L. Krause, R. Herbst-Irmer, G. M. Sheldrick and D. Stalke, Comparison of silver and molybdenum microfocus X-ray sources for single-crystal structure determination, *J. Appl. Crystallogr.*, 2015, **48**, 3–10.
35 G. M. Sheldrick, SHELXT - Integrated Space-Group and Crystal-Structure Determination, *Acta Crystallogr., Sect. A: Found. Adv.*, 2015, **A71**, 3–8.
36 G. M. Sheldrick, Crystal Structure Refinement with SHELXL, *Acta Crystallogr., Sect. C: Struct. Chem.*, 2015, **C71**, 3–8.
37 C. B. Hübschle, G. M. Sheldrick and B. Dittrich, ShelXle: a Qt graphical user interface for SHELXL, *J. Appl. Crystallogr.*, 2011, **44**, 1281–1284.

Paper B

SCIENTIFIC REPORTS

OPEN

Isocorroles as Homoaromatic NIR-Absorbing Chromophores: A First Quantum Chemical Study

Cina Foroutan-Nejad[1], Simon Larsen[2], Jeanet Conradie[2,3] & Abhik Ghosh[2]

Density functional theory calculations of magnetically induced current densities have revealed high diatropic ring currents in unsubstituted isocorrole consistent with homoaromatic character. An examination of the Kohn-Sham molecular orbitals showed clear evidence of homoconjugative interactions in four occupied π-type molecular orbitals as well as in the LUMO. Remarkably, substituents at the saturated *meso* position were found to exert a dramatic influence on the overall current density pattern. Thus, whereas bis(trimethylsilyl)-substitution strongly enhanced the peripheral diatropic current (consistent with enhanced homoaromaticity), difluoro-substitution engendered a strong, net paratropic current (consistent with antihomoaromaticity). In this respect, isocorroles stand in sharp contrast to benzenoid aromatics, for which substituents typically exert a small influence on the current density distribution.

Isocorroles are fascinating macrocyclic ligands with a sterically constrained N_4 cavity characteristic of corroles and with the 2– charge of porphyrins (Fig. 1)[1–5]. With significant absorption in 700–1000 nm range, they are of considerable interest as near-IR dyes[6]. They also exhibit a Soret-like band in the 400–500 nm range, with an intensity comparable to those of porphyrins and corroles. These characteristics are exemplified in Fig. 2, which depicts the UV-vis spectra of selected 5/10-methoxy-5,10,15-triphenylisocorrole derivatives, H_2[iso-5/10-MeO-TPC] and Ni[iso-5/10-MeO-TPC]. In addition, the ^{1}H NMR spectra of many free-base isocorroles (including H_2[iso-5/10-MeO-TPC]) exhibit moderately upfield-shifted *β*-pyrrole resonances and dramatically downfield-shifted NH resonances (relative to analogous corroles) (Fig. 3). These spectroscopic features are suggestive of either homoaromaticity or antihomoaromaticity, which are associated with the presence of a ring current in organic molecules in which an sp^3 atom interrupts the conjugation[7–9]. Two density functional theory-based approaches have been employed here to examine the potential homoaromaticity of select isocorrole derivatives (Fig. 4), magnetically induced current density analysis and time-dependent density functional theory (TDDFT) calculations.

Results and Discussion

Current density analyses. Figure 5 depicts B3LYP/def2-TZVP current densities for unsubstituted gold corrole (Au[Cor])[10] and free-base (H_2[10-isoCor]) and nickel 10-isocorrole (Ni[10-isoCor]). Because the current density in all fully conjugated porphyrin-type molecules bifurcates at the pyrrole *α*-carbons, we will use the term 'peripheral current' to refer to the current along either the C9-C10 or the C1-C19 bond. The general features of the current density pathways for the molecules examined here are similar to those of other porphyrinoids; diatropic currents circulate along the outer rim of the molecules, while paratropic ones flow around the inner $C_{11}N_4$ framework[11,12]. Figure 5 shows that Au[Cor] sustains a strong diatropic peripheral current of ~26 nA·T^{-1} comparable to that of porphyrins. The current density passing between nitrogens and the central Au atom is almost negligible, reminiscent of current density pathways in porphyrins[11]. By comparison, the peripheral ring current in the unsubstituted metalloisocorrole Ni[10-isoCor] is ~9.8 nA·T^{-1} for the C9-C10 bond, which is about a third of that calculated for Au[Cor]. The reduced peripheral ring current in Ni[10-isoCor] is nevertheless far from insignificant and is just under that calculated for benzene (~11 nA·T^{-1}). Qualitatively similar peripheral currents were also observed for the corresponding free-base isocorrole H_2[10-isoCor] (Fig. 5). These data strongly suggest that Ni[10-isoCor] and H_2[10-isoCor] are homoaromatic. Indeed, an examination of the π-type molecular

[1]CEITEC – Central European Institute of Technology, Masaryk University, Kamenice 5, CZ – 62500, Brno, Czech Republic. [2]Department of Chemistry, UiT – The Arctic University of Norway, 9037, Tromsø, Norway. [3]Department of Chemistry, University of the Free State, 9300, Bloemfontein, Republic of South Africa. Correspondence and requests for materials should be addressed to C.F.-N. (email: cina.foroutannejad@ceitc.muni.cz) or J.C. (email: conradj@ufs.ac.za) or A.G. (email: abhik.ghosh@uit.no)

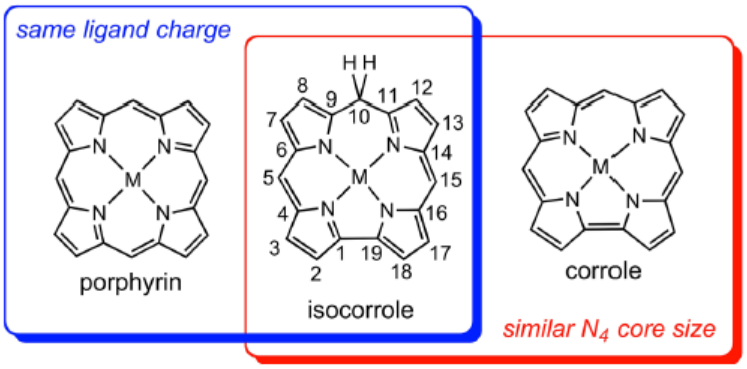

Figure 1. Isocorroles (with atom numbering of the carbon skeleton) as hybrid ligands with characteristics of both porphyrins and corroles.

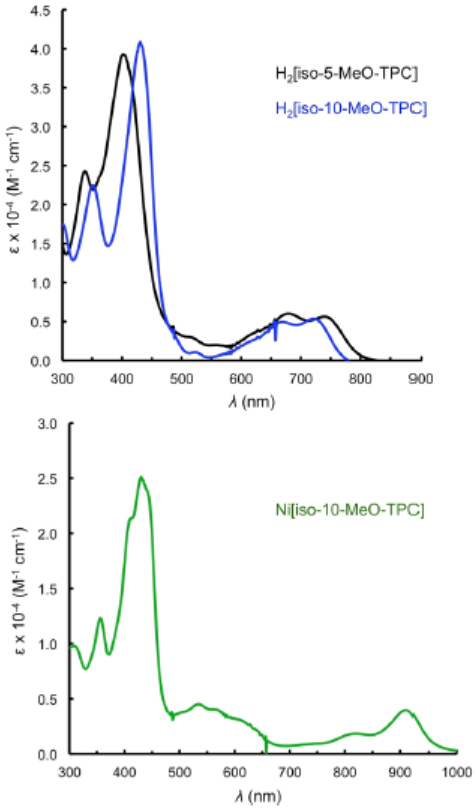

Figure 2. UV-vis spectra of representative isocorrole derivatives.

orbitals of isocorrole derivatives provides conclusive proof of homoconjugation (hyperconjugative interactions); as discussed later in the paper, a total of 4 occupied MOs and the LUMO were found to exhibit with significant amplitudes at the saturated *meso* position.

Remarkably, substituents at the saturated *meso* position C10 by fluoro and trimethylsilyl groups were found to result in striking changes in the calculated current densities (Fig. 6). Thus, fluoro substituents effectively quench the diatropic ring current; indeed, the difluorinated compound Ni[10-F_2-isoCor] sustains a net paratropic peripheral current and is legitimately viewed as antihomoaromatic. The paratropic current in this compound flows largely around the 15-membered inner $C_{11}N_4$ ring, paralleling similar behavior observed for other antiaromatic

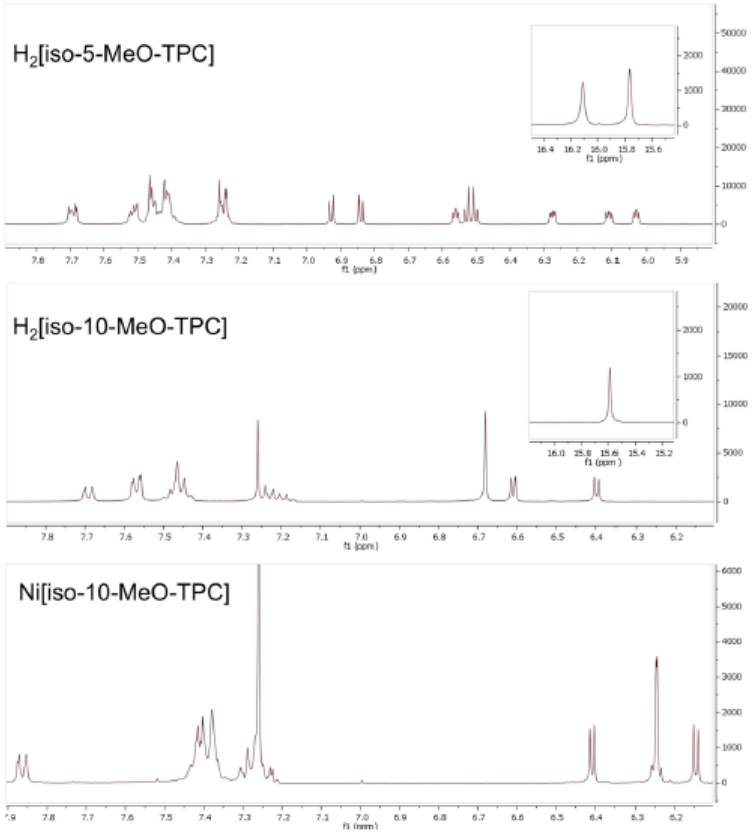

Figure 3. ^{1}H NMR spectra of representative isocorrole derivatives.

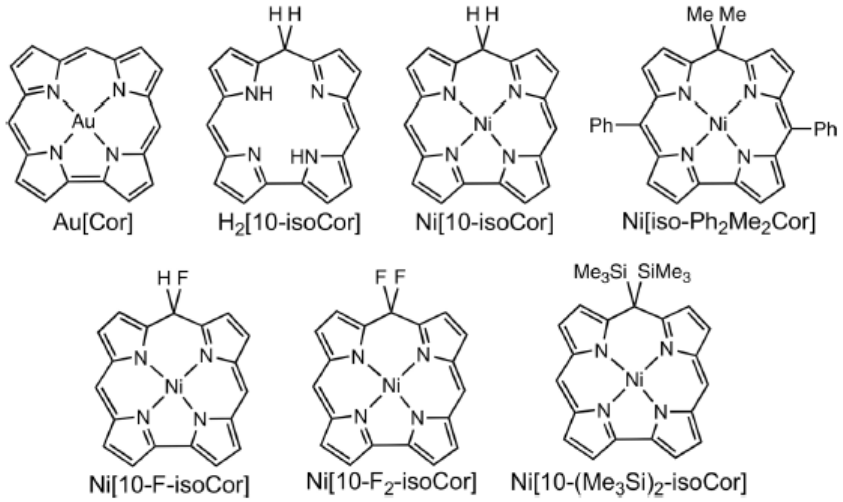

Figure 4. Corrole and isocorrole derivatives examined in this study.

porphyrinoids[13]. Trimethylsilyl groups on the other hand behave oppositely; the hypothetical bis(trimethylsilyl) compound Ni[10-$(Me_3Si)_2$-isoCor] sustains a greatly enhanced diatropic peripheral current and may be regarded as strongly homoaromatic. This diverse range of behavior is relatively simply attributed to the hyperconjugative

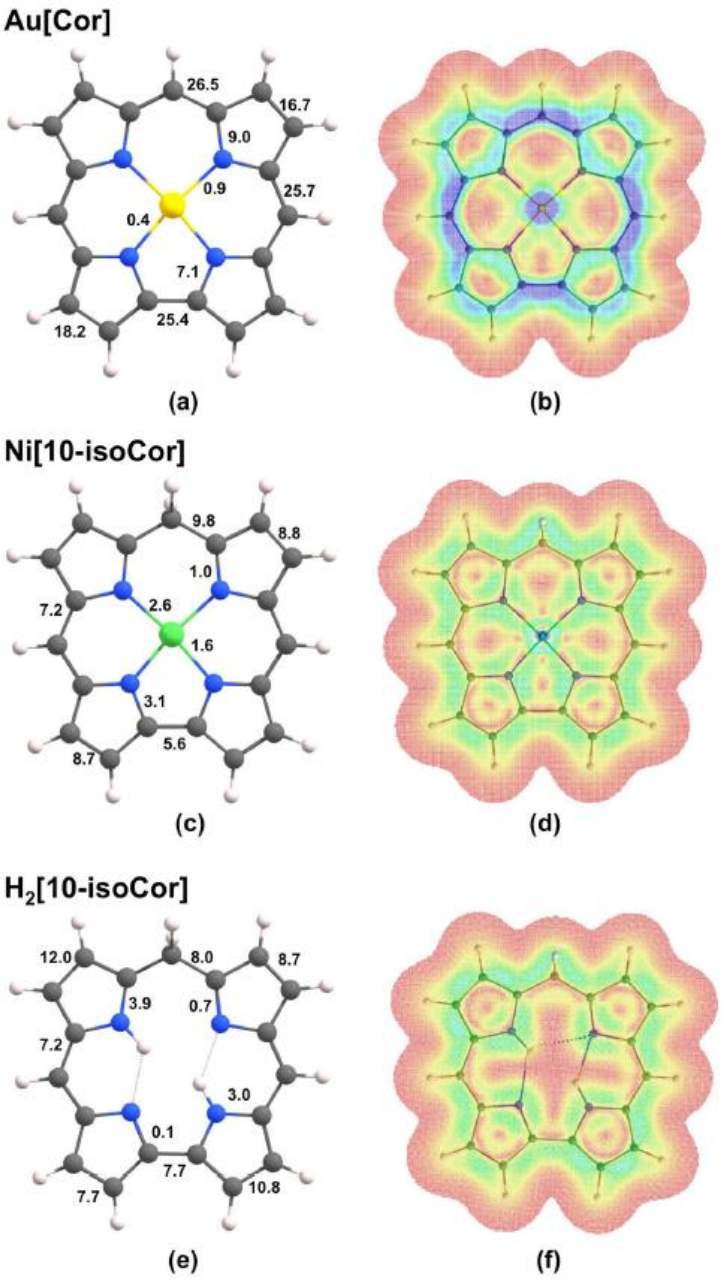

Figure 5. Current density pathways (**a**, **c**, and **e**) and plots (**b**, **d**, and **f**) for Au[Cor], Ni[10-isoCor], and H_2[10-isoCor]. The plots refer to a displacement of 1 bohr above the molecular plane, where the π ring current is most intense. Colors ranging from blue (corresponding to 0.001 au) to red (0.0 au) represent stronger to weaker current densities.

effects of C-F σ* orbitals and of C-Si σ orbitals, as discussed by von Schleyer and coworkers[14,15]. Nevertheless, given that substituent effects on ring currents in aromatic systems are typically quite small[16–20], the present dramatic variations as a function of substituents at the saturated *meso* carbon are unusual indeed.

TDDFT calculations. Molecular orbital and TDDFT[21,22] analyses were carried out on a number of isocorrole derivatives with all-electron OLYP/STO-TZP calculations. The various systems chosen yielded very similar

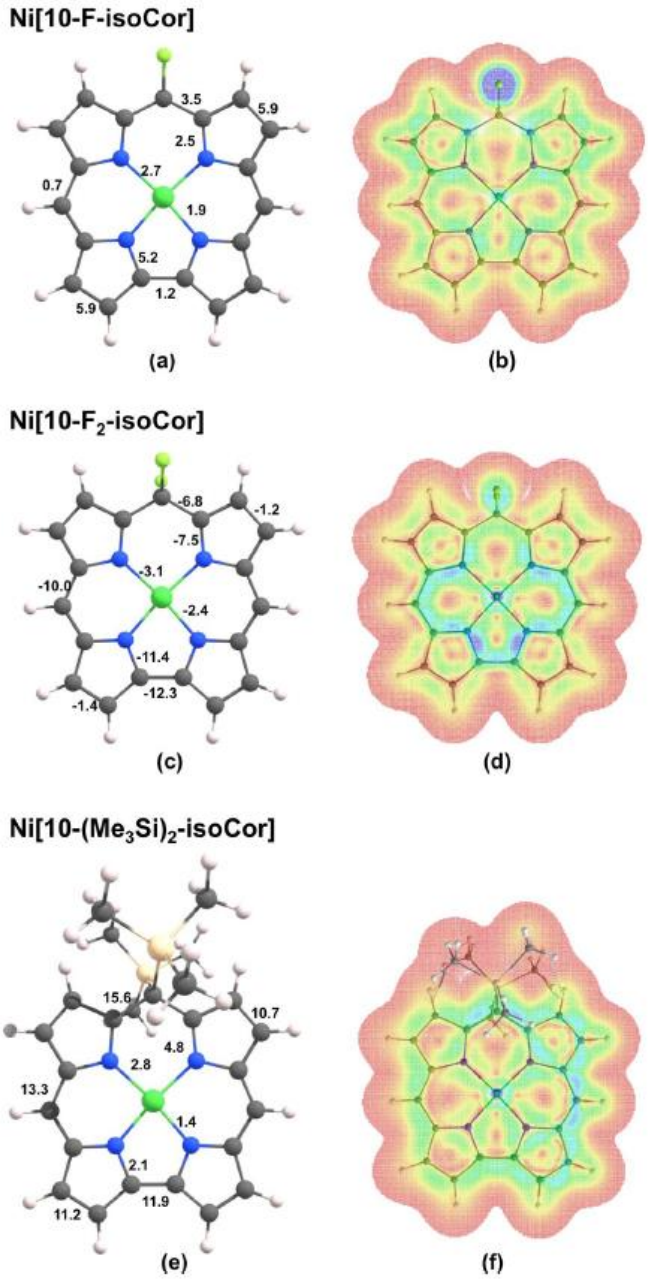

Figure 6. Integrated current densities (**a**, **c**, and **e**) and current density plots (**b**, **d**, and **f**) for Ni[10-F-isoCor], Ni[10-isoCor], and Ni[10-$(Me_3Si)_2$-isoCor]. The plots refer to a displacement of 1 bohr above the molecular plane. Colors ranging from blue (corresponding to 0.001 au) to red (0.0 au) represent stronger to weaker current densities. Negative values in entry (**c**) indicate net paratropic currents.

qualitative insights; the discussion below is based on our results for nickel 10,10-dimethyl-5,15-diphenylisocorrole, Ni[iso-Ph_2MeCor]. The ground-state calculations readily identified four π-type occupied MOs and the LUMO as having significant hyperconjugative interactions, i.e., relatively large amplitudes at the saturated *meso* position (Fig. 7). The TDDFT results (Table 1 and Figs 8 and 9) led to several additional insights. First, the energy spacing of the Kohn-Sham MO eigenvalues clearly does not correspond to Gouterman's four-orbital model[23]. That said, the HOMO-4, HOMO-3, LUMO, and LUMO + 1 do resemble the four frontier orbitals of a porphyrin or corrole

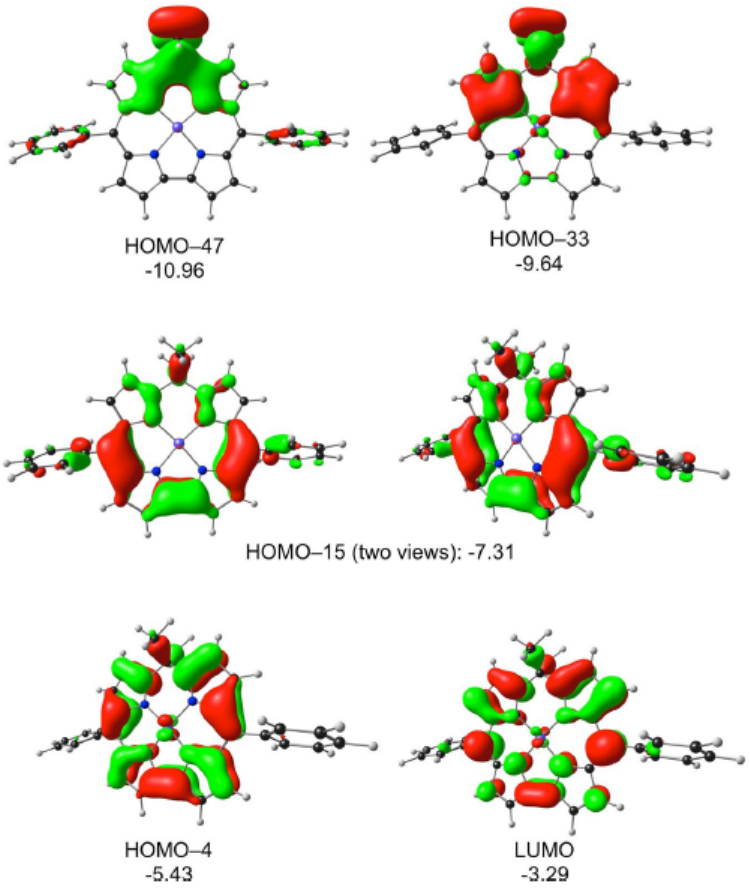

Figure 7. OLYP/STO-TZP π-type MOs of Ni[IsoPh$_2$MeCor], which involve homoconjugative interactions at the C10 *meso* position, along with their orbital energies (eV).

in terms of qualitative shape[24,25]. Of these, the HOMO-4 and LUMO exhibit significant hyperconjugative interactions, i.e., relatively large amplitudes at the saturated *meso* position. The most intense calculated transitions all involve substantial HOMO-1/HOMO → LUMO/LUMO + 1 character as well as smaller amounts of HOMO-4 character. The lowest-energy transition exhibits a Q-like transition energy of ~2.0 eV and has predominantly HOMO-3 → LUMO character. Furthermore, multiple transitions with a similar intensity then cluster in the typical Soret region (~3.0 eV), whose cumulative effect is a deceptively porphyrin-like overall spectrum. Finally, since the LUMO has large amplitudes at the *meso* positions and the majority of the low-energy transitions have significant LUMO character, it stands to reason that the UV-vis-NIR spectra should exhibit a strong dependence on *meso* substituents, as is indeed observed[1–5].

Conclusion

A first detailed DFT investigation has clearly implicated homoconjugation as a critical determinant of the observed spectroscopic features of isocorroles. Thus, the calculations indicated unsubstituted free-base 10-isocorrole and its nickel complex as clearly homoaromatic. That said, substituents at the saturated *meso* carbon were found to dramatically affect the homoconjugation. Thus, while fluoro substituents were found to quench the diatropic peripheral current, leading in some cases to net antihomoaromatic character, trimethylsilyl substituents were found to greatly enhance homoaromatic character. The calculations further revealed homoconjugative/hyperconjugative interactions in four π-type occupied MOs as well as in LUMO. The strong Soret-like feature of isocorroles was found to arise from the clustering of several near-degenerate transitions with individual Q-like intensities. Finally, the large amplitude of the LUMO at the *meso* positions provides a simple rationale for the observed large variations in the UV-vis-NIR spectral profiles of isocorroles as a function of *meso* substituents.

E (eV)	Symmetry	λ (nm)	*f*	From	To	% contribution
1.988	B	624	1.46×10^{-1}	HOMO-3	LUMO	84.0
				HOMO-2	LUMO + 1	6.4
				HOMO	LUMO	3.9
				HOMO	LUMO + 2	2.7
				HOMO-3	LUMO + 2	0.6
3.033	A	409	8.87×10^{-2}	HOMO	LUMO + 4	54.9
				HOMO-4	LUMO	10.0
				HOMO-3	LUMO + 1	8.9
				HOMO-8	LUMO	6.3
				HOMO-9	LUMO	5.4
3.081	A	402	9.63×10^{-2}	HOMO	LUMO + 4	40.1
				HOMO-9	LUMO	27.8
				HOMO-4	LUMO	8.4
				HOMO-3	LUMO + 1	6.2
3.166	B	392	6.84×10^{-2}	HOMO-4	LUMO + 1	37.7
				HOMO-7	LUMO	24.2
				HOMO-11	LUMO	16.0
				HOMO-14	LUMO	9.9
3.169	A	391	8.16×10^{-2}	HOMO-9	LUMO	35.1
				HOMO-10	LUMO	19.4
				HOMO	LUMO + 6	9.4
				HOMO-4	LUMO	7.1
				HOMO-8	LUMO	5.6

Table 1. TDDFT (OLYP/STO-TZP) results for the main "Q" and "Soret" transitions of Ni[Iso10Me$_2$–5,15Ph$_2$C].

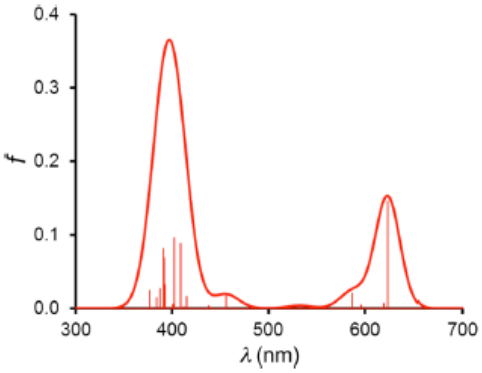

Figure 8. TDDFT oscillator strengths (*f*) plotted against wavelength (λ, nm) and an artificially broadened spectrum with Gaussians with FWHM = 30 nm.

Methods

All structures were fully optimized at B3LYP[26–28]/def2-TZVP[29] computational level by Gaussian 09 rev. D1[30]. (All optimized Cartesian coordinates are listed in the Supplementary information.) Eigenvalues of the Hessian matrix of energy were checked to ensure that all structures correspond to local minima. To obtain current density plots and intensities GIAO NMR computations were performed at the same level of theory by Gaussian 09 rev. D1 and the wave function of the NMR computations were further analyzed by AIMAll (version 16.05.18) suite of programs[31]. The current density were obtained within the context of quantum theory of atoms in molecules as developed by Keith and Bader[32–36]. TDDFT calculations were performed with ADF2017[37,38] on OLYP[27,39]/STO-TZP optimized geometries.

Free-base H$_2$[iso-5/10-MeO-TPC] was synthesized according to the method described by the Kadish and Paolesse groups[2]. Although both isomeric free bases were isolated in reasonable yields, only the 10-methoxy compound (surprisingly) proved readily amenable to nickel insertion.

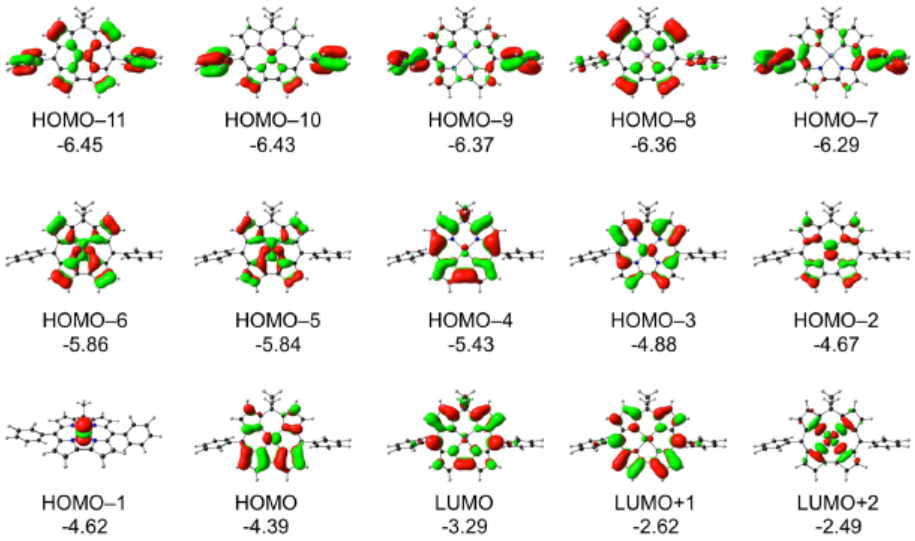

Figure 9. Selected OLYP/STO-TZP MOs relevant to Table 1, along with their orbital energies (eV).

Synthesis of H_2[iso-5/10-MeO-TPC]. To a solution of 5,10,15-triphenylcorrole (46.7 mg) in a mixture of dichloromethane (20 mL) and methanol (10 mL) was added DDQ (20.4 mg, 1 eq) and the resulting solution was stirred for 10 min. The solvents were removed under vacuum and the solids were washed down through a plug of silica with dichloromethane. The two isomers were then separated with preparative thin-layer chromatography on silica plates employing 2:1 dichloromethane/hexane as solvent. Yields: 32 mg of the 5-isomer (64.8 %) and 5.5 mg (11.1%) of the 10-isomer.

Spectroscopic data for H_2[iso-5-MeO-TPC]. ^{1}H NMR (400 MHz, $CDCl_3$, δ): 16.19 (s, 1H, NH), 15.85 (s, 1H, NH), 7.72 – 7.67 (m, 2H, 5-*o*-Ph), 7.53 – 7.48 (m, 2H, 15-*o*-Ph), 7.48 – 7.37 (m, 9H, 10-*o*-Ph and Ph), 7.25 – 7.22 (m, 2H, Ph), 6.93 (d, J = 4.6 Hz, 1H, β-H), 6.84 (d, J = 4.5 Hz, 1H, β-H), 6.56 (dd, J = 3.6, 2.6 Hz, 1H, β-H), 6.53 (d, J = 4.6 Hz, 1H, β-H), 6.50 (d, J = 4.6 Hz, 1H, β-H), 6.27 (dd, J = 4.3, 2.0 Hz, 1H, β-H), 6.11 (dd, J = 4.3, 2.6 Hz, 1H, β-H), 6.03 (dd, J = 3.6, 2.5 Hz, 1H, β-H), 3.43 (s, 3H, 5-MeO). UV-Vis (CH_2Cl_2) λ_{max} [nm; $\epsilon \times 10^{-4}$ ($M^{-1}cm^{-1}$)]: 337 (2.42), 401 (3.93), 678 (0.60), 739 (0.56). MS (MALDI-TOF): m/z calcd for $C_{38}H_{28}N_4O$ 556.2263 [M^+]; found 556.2272.

Spectroscopic data for H_2[iso-10-MeO-TPC]. ^{1}H NMR (400 MHz, $CDCl_3$, δ): 15.58 (s, 2H, NH), 7.69 (d, J = 7.0 Hz, 2H, 10-*o*-Ph), 7.59 – 7.55 (m, 4H, 5,15-*o*-Ph), 7.48 – 7.42 (m, 6H, 5,15-*m*-Ph and 5,15-*p*-Ph), 7.25 – 7.16 (m, 3H, 10-*m*-Ph and 10-*p*-Ph), 6.69 – 6.67 (m, 4H, β-H), 6.61 (d, J = 4.3 Hz, 2H, β-H), 6.40 (d, J = 4.3 Hz, 2H, β-H), 3.49 (s, 3H, 10-MeO). UV-Vis (CH_2Cl_2) λ_{max} [nm; $\epsilon \times 10^{-4}$ ($M^{-1}cm^{-1}$)]: 351 (2.24), 430 (4.09), 668 (0.49), 721 (0.53). MS (MALDI-TOF): m/z calcd for $C_{38}H_{28}N_4O$ 556.2263 [M^+]; found: 556.2272.

Synthesis of Ni[iso-5/10-MeO-TPC]. Free-base isocorrole (12.8 mg, mixture of isomers) and $Ni(OAc)_2 \cdot 4H_2O$ (48.9 mg, 6 eq) were dissolved in dry DMF (5 ml) and refluxed for 1 h. The solvent was removed under vacuum and the solids were washed down with dichloromethane through a silica gel plug. The resulting product, upon preparative thin-layer chromatography on a silica plate with 2:1 dichloromethane/hexane as eluent, yielded a brown band composed of Ni[5,10,15-triphenyl-10-methoxyisocorrole]. Yield 1.2 mg (8.5%).

Spectroscopic data for Ni[iso-10-MeO-TPC]. ^{1}H NMR (400 MHz, $CDCl_3$, δ): 7.86 (d, J = 7.6 Hz, 2H, Ph), 7.45 – 7.35 (m, 13H, Ph), 6.41 (d, J = 4.5 Hz, 2H, β-H), 6.27 – 6.23 (m, 4H, β-H), 6.15 (d, J = 4.5 Hz, 2H, β-H), 3.39 (s, 3H, 10-MeO). UV-Vis (CH_2Cl_2) λ_{max} [nm; $\epsilon \times 10^{-4}$ ($M^{-1}cm^{-1}$)]: 356 (1.23), 430 (2.51), 533 (0.45), 818 (0.18), 909 (0.39); MS (MALDI-TOF): m/z calcd for $C_{38}H_{26}N_4ONi$: 612.1460 [M^+]; found 612.1638.

References

1. Hohlneicher, G. *et al.* Spiroconjugation in Spirodicorrolato-Dinickel(II). *Chem. Eur. J.* **9**, 5636–5642 (2003).
2. Pomarico, G. *et al.* Synthesis and Characterization of Free-Base, Copper, and Nickel Isocorroles. *Inorg. Chem.* **49**, 5766–5774 (2010).
3. Costa, R., III, Geier,G. R. & Ziegler, C. J. Structure and spectroscopic characterization of free base and metal complexes of 5,5-dimethyl-10,15-bis(pentafluorophenyl)isocorrole. *Dalton Trans.* **40**, 4384–4386 (2011).
4. Hoffmann, M. et. al. Template Synthesis of Alkyl-Substituted Metal Isocorroles. *Eur. J. Inorg Chem.* 3076–3085 (2016).
5. Thomas, K. E., Beavers, C. M., Gagnon, K. J. & Ghosh, A. β-Octabromo- and β-Octakis(trifluoromethyl)isocorroles: New Sterically Constrained Macrocyclic Ligands. *ChemistryOpen* **6**, 402–409 (2017).
6. Omori, H., Hiroto, S. & Shinokubo, H. 10-Silacorroles Exhibiting Near-Infrared Absorption and Emission. *Chem. Eur. J.* **23**, 7866–7870 (2017).
7. Winstein, S. Homo-Aromatic Structures. *J. Am. Chem. Soc.* **81**, 6524–6525 (1959).

8. Warner, P., Harris, D. L., Bradley, C. H. & Winstein, S. Further evidence on the nature of the monohomotropylium ion. *Tetrahedron Lett.* **11**, 4013–4016 (1970).
9. Williams, R. V. Homoaromaticity. *Chem. Rev.* **101**, 1185–1204 (2001).
10. Au[Cor] has been chosen as a paradigmatic, innocent metallocorrole: Thomas, K. E., Alemayehu, A. B., Conradie, J., Beavers, C. & Ghosh, A. Synthesis and Molecular Structure of Gold Triarylcorroles. *Inorg. Chem.* **50**, 12844–12851 (2011).
11. Fliegl, H. & Sundholm, D. Aromatic Pathways of Porphins, Chlorins, and Bacteriochlorins. *J. Org. Chem.* **77**, 3408–3414 (2012).
12. Franzke, Y. J., Sundholm, D. & Weigend, F. *Phys. Chem. Chem. Phys.* **19**, 12794–12803 (2017).
13. Fliegl, H., Pichierri, F. & Sundholm, D. Calculations of current densities and aromatic pathways in cyclic porphyrin and isoporphyrin arrays. *J. Phys. Chem. A* **119**, 2344–2350 (2015).
14. Nyulászi, L. & Schleyer, Pv. R. Nucleus-Independent Chemical Shifts: A Simple and Efficient Aromaticity Probe. *J. Am. Chem. Soc.* **121**, 6872–6875 (1999).
15. Fernández, I. & Wu, J. I. & Schleyer, P. v. R. Substituent Effects on "Hyperconjugative" Aromaticity and Antiaromaticity in Planar Cyclopolyenes. *Org. Lett.* **15**, 2990–2993 (2013).
16. Krygowski, T. M. *et al.* Relation between the Substituent Effect and Aromaticity. *J. Org. Chem.* **69**, 6634–6640 (2004).
17. Krygowski, T. M., Dobrowolski, M. A., Zborowski, K. & Cyrański, M. K. Relation between the substituent effect and aromaticity. Part II. The case of *meta*- and *para*-homodisubstituted benzene derivatives. *J. Phys. Org. Chem.* **19**, 889–895 (2006).
18. Krygowski, T. M., Palusiak, M., Płonka, A. & Zachara-Horeglad, J. E. Relationship between substituent effect and aromaticity – Part III: naphthalene as a transmitting moiety for substituent effect. *J. Phys. Org. Chem.* **20**, 297–306 (2007).
19. Curutchet, C., Poater, J., Solà, M. & Elguero, J. Analysis of the Effects of N-Substituents on Some Aspects of the Aromaticity of Imidazoles and Pyrazoles. *J. Phys. Chem. A* **115**, 8571–8577 (2011).
20. Radula-Janik, K., Kopka, K., Kupka, T. & Ejsmont, K. Substituent Effect Of Nitro Group On Aromaticity Of Carbazole Rings. *Chem. Heterocycl. Compd.* **50**, 1244–1251 (2014).
21. Alemayehu, A. B., Conradie, J. & Ghosh, A. A First TDDFT Study of Metallocorrole Electronic Spectra: Copper *meso*-Triarylcorroles Exhibit Hyper Spectra. *Eur. J. Inorg. Chem.* **12**, 1857–1864 (2011).
22. Rhoda, H. M., Crandall, L. A., Geier, G. R. III, Ziegler, C. J. & Nemykin, V. N. Combined MCD/DFT/TDDFT Study of the Electronic Structure of Axially Pyridine Coordinated Metallocorroles. *Inorg. Chem.* **54**, 4652–4662 (2015).
23. Gouterman, M., Wagnière, G. H. & Snyder, L. C. Spectra of porphyrins: Part II. Four orbital model. *J. Mol. Spectrosc.* **11**, 108–115 (1963).
24. Ghosh, A., Wondimagegn, T. & Parusel, A. B. J. Electronic Structure of Gallium, Copper, and Nickel Complexes of Corrole. High-Valent Transition Metal Centers versus Noninnocent Ligands. *J. Am. Chem. Soc.* **122**, 5100–5104 (2000).
25. Ghosh, A. Electronic Structure of Corrole Derivatives: Insights from Molecular Structures, Spectroscopy, Electrochemistry, and Quantum Chemical Calculations. *Chem. Rev.* **117**, 3798–3881 (2017).
26. Becke, A. D. Density-functional exchange-energy approximation with correct asymptotic behavior. *Phys. Rev. A* **38**, 3098–3100 (1988).
27. Lee, C., Yang, W. & Parr, R. G. Development of the Colle-Salvetti correlation-energy formula into a functional of the electron density. *Phys. Rev. B* **37**, 785–789 (1988).
28. Miehlich, B., Savin, A., Stoll, H. & Preuss, H. Results obtained with the correlation energy density functionals of Becke and Lee, Yang and Parr. *Chem. Phys. Lett.* **157**, 200–206 (1989).
29. Weigend, F. & Ahlrichs, R. Balanced basis sets of split valence, triple zeta valence and quadruple zeta valence quality for H to Rn: Design and assessment of accuracy. *Phys. Chem. Chem. Phys.* **7**, 3297–3305 (2005).
30. Frisch, M. J. et al. *Gaussian 09*, Gaussian, Inc., Wallingford CT, 2013.
31. Keith, T. A. *AIMAll*, Gristmill Software: Overland Park KS, USA, 2017.
32. Keith, T. A. & Bader, R. F. W. Calculation of magnetic response properties using atoms in molecule. *sChem. Phys. Lett.* **194**, 1–8 (1992).
33. Keith, T. A. & Bader, R. F. W. Calculation of magnetic response properties using a continuous set of gauge transformations. *Chem. Phys. Lett.* **210**, 223–231 (1993).
34. Keith, T. A. & Bader, R. F. W. Topological analysis of magnetically induced molecular current distributions. *J. Chem. Phys.* **99**, 3669–3682 (1993).
35. Keith, T. A. Calculation of magnetizabilities using GIAO current density distributions. *Chem. Phys.* **213**, 123–132 (1996).
36. Keith, T. A. & Bader, R. F. W. Properties of atoms in molecules: nuclear magnetic shielding. *Can. J. Chem.* **74**, 185–200 (1996).
37. te Velde, G. *et al.* Chemistry with ADF. *J. Comput. Chem.* **22**, 931–967 (2001).
38. Guerra, C. F., Snijders, J. G., te Velde, G. & Baerends, E. J. Towards an order-N DFT method. *Theor. Chem. Acc.* **99**, 391–403 (1998).
39. Handy, N. C. & Cohen, A. J. Left-right correlation energy. *Mol. Phys.* **99**, 403–412 (2001).

Acknowledgements

Financial support from the Research Council of Norway (grant no. 262229 to AG) and the National Research Foundation of South Africa (grant no. 113327 to JC) is gratefully acknowledged. C.F.-N. acknowledges (1) "Projects of Large Research, Development, and Innovations Infrastructures" for access to the computational resources provided by the CESNET LM2015042 and the CERIT Scientific Cloud LM2015085 and (2) project CEITEC 2020 LQ1601 with financial support from the Ministry of Education, Youth, and Sports of the Czech Republic under the National Sustainability Programme II.

Author Contributions

C.F.N. performed the current density calculations and J.C. carried out the TDDFT and MO analyses. S.L. carried out all syntheses and spectroscopic analyses. A.G. planned and coordinated the project. All authors contributed to the writing of the paper.

Additional Information

Supplementary information accompanies this paper at https://doi.org/10.1038/s41598-018-29819-3.

Competing Interests: The authors declare no competing interests.

Publisher's note: Springer Nature remains neutral with regard to jurisdictional claims in published maps and institutional affiliations.

Paper C

Paper D

Organic & Biomolecular Chemistry

PAPER

View Article Online
View Journal | View Issue

Cite this: Org. Biomol. Chem., 2018, 16, 7964

Local *versus* global aromaticity in azuliporphyrin and benziporphyrin derivatives†

Abhik Ghosh, *[a] Simon Larsen,[a] Jeanet Conradie [a,b] and Cina Foroutan-Nejad *[c]

Received 14th July 2018,
Accepted 5th October 2018

DOI: 10.1039/c8ob01672k

rsc.li/obc

Carbaporphyrinoids afford fascinating examples of competition between local and global aromaticity in conjugated, polycyclic systems. Thus, whereas density functional theory calculations reveal only a modest effect of metal complexation on the current density profiles of true carbaporphyrins and azuliporphyrins, the impact is much greater for benziporphyrins, underscoring a strong competition between local and global aromaticity in the latter system. Furthermore, the calculations shed light on the remarkable efficacy of suitably placed electron-donating substituents on the benzene ring in boosting the global diatropic currents in a metallobenziporphyrin.

Introduction

Carbaporphyrins, first reported in the mid-1990s,[1–5] today constitute a broad field of research.[6] From the very beginning, these molecules have attracted considerable interest on account of their aromatic behavior (as reflected in their ^{1}H NMR spectra) and their ability to form organometallic complexes with a variety of transition metals. Unsurprisingly, the molecules have attracted immediate attention from quantum chemists.[7–9] One of us explained the stability of organometallic complexes by invoking the singlet N-heterocyclic carbene character of the coordinated ligands.[6,10] While the carbene analogy is no longer prevalent, other researchers addressed the question of aromaticity by means of density functional theory (DFT)-based nucleus-independent chemical shift (NICS) calculations.[11,12] A key point of interest concerns the competition between local, small-ring aromaticity and global, macrocyclic aromaticity. Naively speaking, high global aromaticity is likely to translate to a high HOMO–LUMO gap, which can be experimentally determined with electrochemical measurements and chemical stability (such as toward atmospheric oxygen). DFT calculations of magnetically induced current densities have addressed this issue to some degree for *N*-confused porphyrins, true carbaporphyrins, and azuliporphyrins.[13,14] Little theoretical insight, however, is available on the impact of metal ion complexation and of peripheral substituents on current pathways, twin themes that we have investigated here with B3LYP gauge-independent atomic orbital (GIAO) calculations, with emphasis on free-base and metal-complexed benziporphyrin (BP)[15,16] and azuliporphyrin (AP)[17] derivatives (Fig. 1). In addition, pursuing our longstanding interest in corroles,[18,19] we have also investigated as yet experimentally unknown azulicorrole (AC) derivatives.

Results and discussion

True carbaporphyrins

The current density plots (always depicted for a surface 1 bohr above the molecular plane) and integrated currents of the two true carbaporphyrin (CP) derivatives H_3[CP] and Au[CP][20–22] (Fig. 2) are similar to those of analogous porphyrins.[23,24] Both the free-base and metal-complexed forms sustain large peripheral ring currents (along the C_α–C_{meso} bonds) of about 25 nA T^{-1}, consistent with a strong global magnetic aromaticity. The ring current bifurcates when passing through the five-membered rings. For the pyrrole rings, a major fraction of the current passes along the exterior of the molecules *via* the β-carbons. In contrast, for the carba-substituted ring, the great majority of the current passes *via* the internal carbon.

Azuliporphyrin and azulicorrole derivatives

As shown in Fig. 3 and 4, the AP and AC derivatives studied exhibit significant differences in their current profiles relative to the CP derivatives. Thus, the azulene moieties channel the great majority of the ring current *via* the ring fusion bond between the five- and seven-membered rings rather than *via*

[a]Department of Chemistry, UiT – The Arctic University of Norway, 9037 Tromsø, Norway. E-mail: abhik.ghosh@uit.no
[b]Department of Chemistry, University of the Free State, 9300 Bloemfontein, Republic of South Africa
[c]CEITEC – Central European Institute of Technology, Masaryk University, Kamenice 5, CZ – 62500 Brno, Czech Republic. E-mail: cina.foroutannejad@ceitc.muni.cz

†Electronic supplementary information (ESI) available. See DOI: 10.1039/c8ob01672k

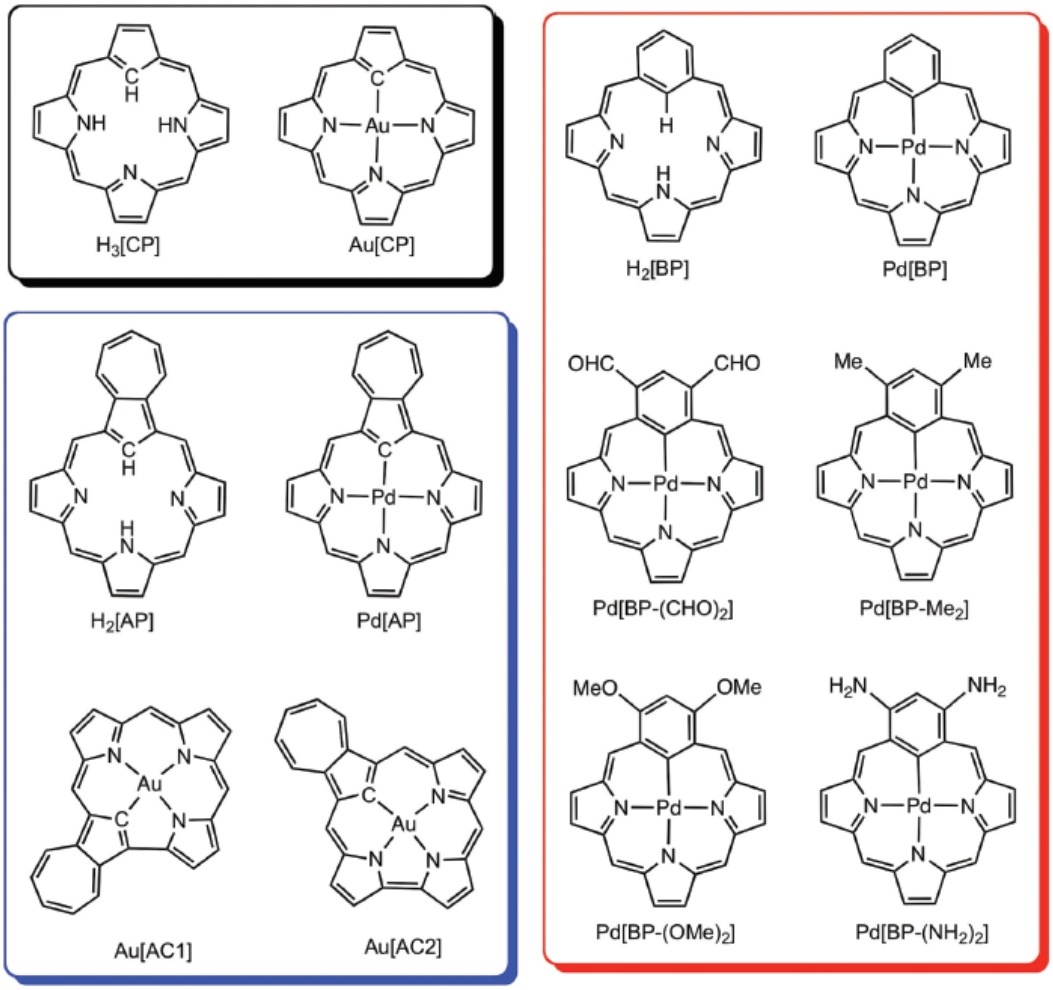

Fig. 1 Carbaporphyrin (CP), benziporphyrin (BP), azuliporphyrin (AP), and azulicorrole (AC) derivatives studied in this work.

the internal carbon. The weak paratropic current along the inner edge of the azulene moieties is thought to reflect a remnant of the ring current of free azulene. In free azulene, the five-membered ring sustains a strong current of 19.1 nA T^{-1}, while the seven-membered ring sustains a current of 11.3 nA T^{-1}, which is similar to that of benzene; the shared bond between the two rings sustains a net current that is the difference between the currents in the five- and seven-membered rings, *i.e.* 7.7 nA T^{-1}. Thus, according to Fig. 3 and 4, the currents in both the five- and seven-membered rings in AP and AC derivatives are lower than those in free azulene. In particular, the current along the outer edge of the seven-membered ring of the azulene-containing macrocycles is sharply diminished relative to free azulene. A second difference relative to the true CP derivatives is that the global ring currents in the AP and AC derivatives are lower by some 10 nA T^{-1}. The two experimentally unknown AC derivatives Au[AC1] and Au[AC2][25] exhibit current profiles that are qualitatively quite similar to that of the stable compound Pd[AP],[26,27] potentially indicating metallo-ACs as stable synthetic targets.

Benziporphyrin derivatives

BP derivatives exhibit a number of novel features relative to the CP and AP derivatives discussed above.

First, the ring current of 10.2 nA T^{-1} in the benzene moiety of H_2[BP] is similar to that of benzene (11.0 nA T^{-1}), while the global ring current hovers at just around 5.5 nA T^{-1}, a reflection of the local aromaticity of benzene dominating over the global aromaticity (Fig. 5).

Palladium(II) complexation brings about major changes to the current profile, in particular, lowering the benzene ring current to 7.9 nA T^{-1}.[28,29] In addition, Pd(II) complexation

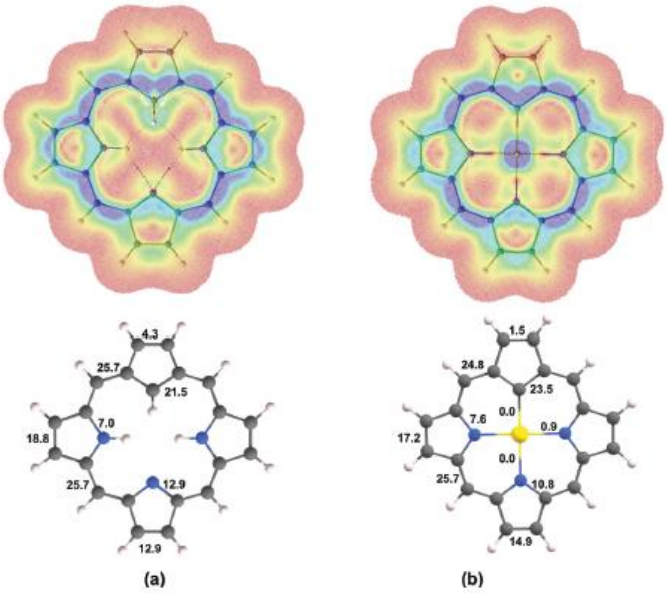

Fig. 2 Current density plots (above) and integrated currents (below, in nA T^{-1}) for (a) H_3[CP] and (b) Au[CP].

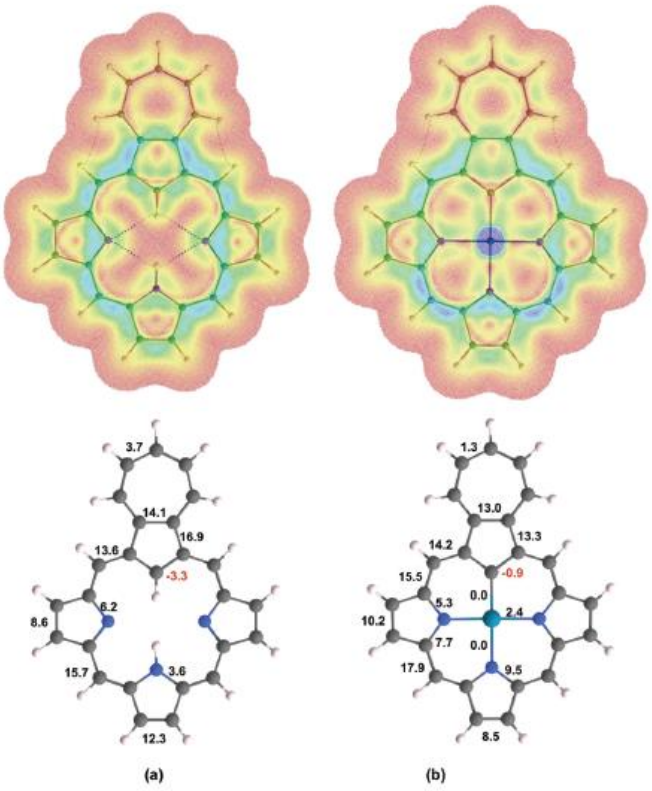

Fig. 3 Current density plots (above) and integrated currents (below, in nA T^{-1}) for (a) H_2[AP] and (b) Pd[AP].

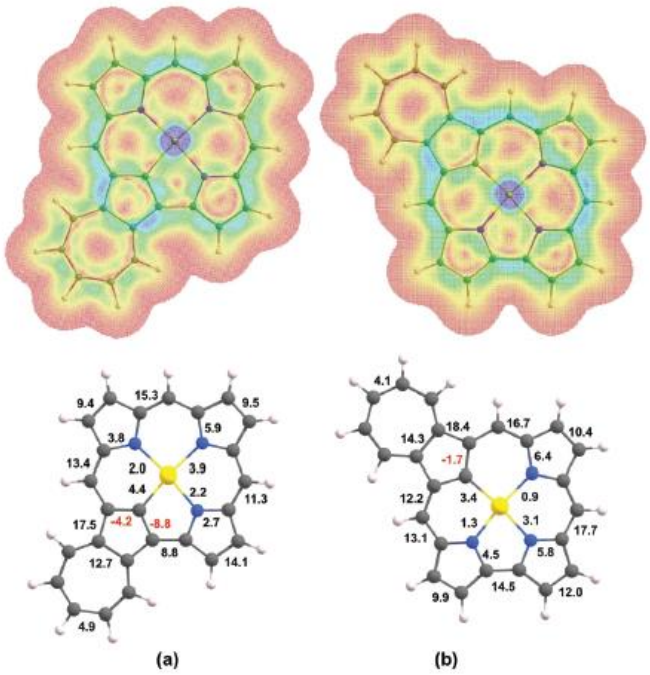

Fig. 4 Current density plots (above) and integrated currents (below, in nA T^{-1}) for (a) Au[AC1] and (b) Au[AC2].

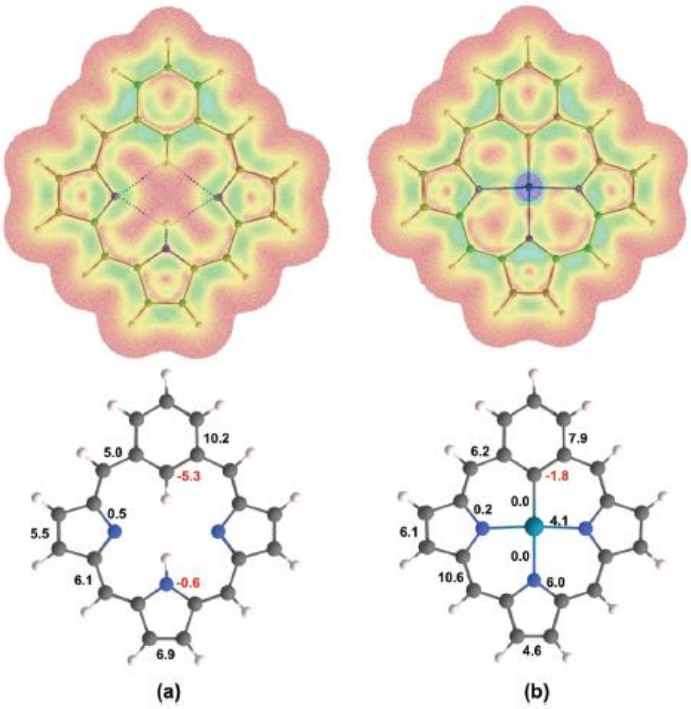

Fig. 5 Current density plots (above) and integrated currents (below, in nA T^{-1}) for (a) H_2[BP] and (b) Pd[BP].

opens a new current path (4.1 nA T^{-1}) *via* the N–Pd–N linkage, effectively bisecting the molecule into two inequivalent parts. Thus, the global current through the *meso* positions on the benzene side of the N–Pd–N linkage is only 6.2 nA T^{-1}, *i.e.*, marginally stronger than that in H_2[BP]. On the other hand, the global current through the *meso* positions on the other side of the N–Pd–N linkage is much higher, 10.6 nA T^{-1}. Overall, metal complexation may be said to enhance the global aromaticity in Pd[BP] at the expense of the local aromaticity of the benzene ring.

Prompted by reports of strong substituent effects on the aromaticity of metallobenziporphyrins, we examined the effects of diformyl, dimethyl, dimethoxy,[30,31] and diamino substitution on Pd[BP]. As shown in Fig. 6, progressively stronger electron-donating substituents extinguish the local ring current in the benzene ring and intensify the global current. The two substituted complexes Pd[BP–$(OMe)_2$] and

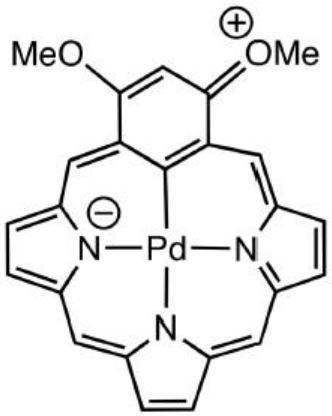

Fig. 7 Resonance form explaining the enhanced global aromaticity in Pd[BP–$(OMe)_2$].

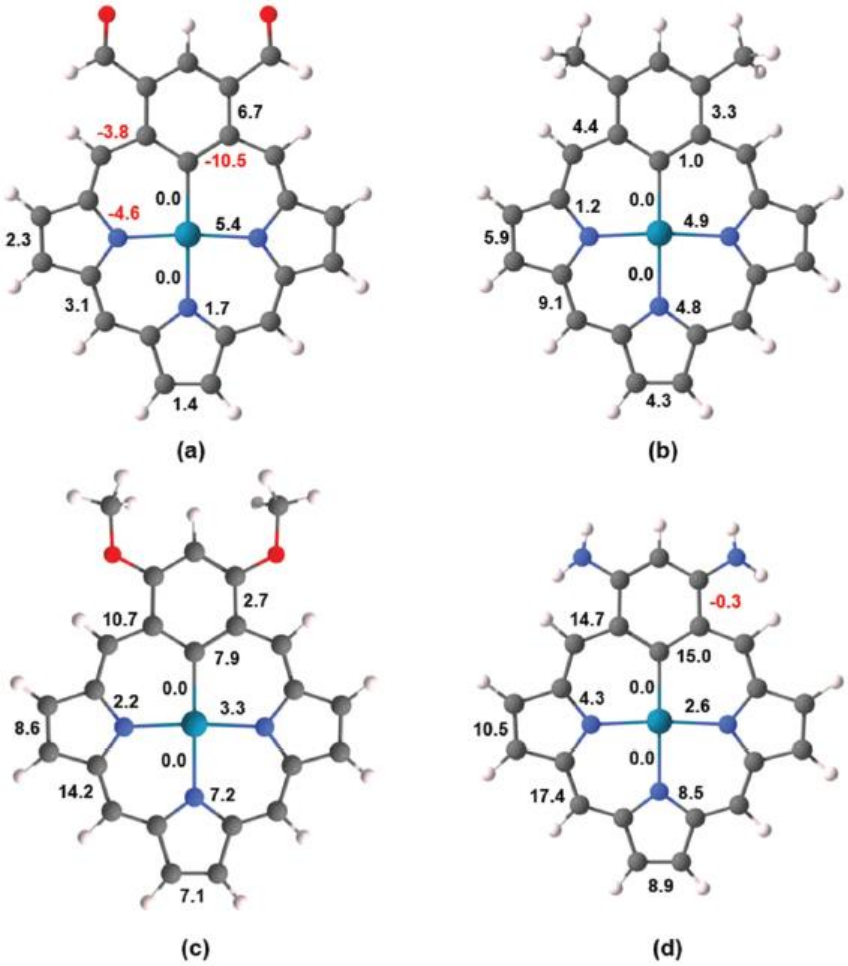

Fig. 6 MICs (in nA T^{-1}) for (a) Pd[BP–$(CHO)_2$], (b) Pd[BP–Me_2], (c) Pd[BP–$(OMe)_2$], and (d) Pd[BP–$(NH_2)_2$].

Pd[BP–$(NH_2)_2$] thus may be said to exhibit substantial global aromaticity. The effect has been qualitatively explained by invoking a resonance form such as that shown for Pd[BP–$(OMe)_2$] (Fig. 7).[30,31]

Conclusion

In summary, we have described a DFT (B3LYP) study of carbaporphyrinoid systems with the goal of elucidating the effects of metal coordination and of peripheral substituents on magnetically induced current density pathways. Thus, whereas metal complexation has only a modest effect on the current density profiles of true carbaporphyrins and azuliporphyrins, the impact is much greater for benziporphyrins, underscoring the competition between the local and global aromaticity in the latter system. The calculations furthermore provide detailed insights into the remarkable effects of suitably placed substituents on the ring currents and aromaticity of a metallobenziporphyrin.

Methods

All structures were fully optimized at the B3LYP[32–34]/def2-TZVP[35] computational level with Gaussian 09 rev. D1[36] and confirmed as local minima by means of frequency analyses. Magnetically induced currents and current density plots were computed by post-analysis of the electron density obtained from GIAO NMR computations by the AIMAll (version 17.01.25) suite of programs.[37] The current magnitudes were obtained within the context of the quantum theory of atoms in molecules developed by Keith and Bader[38–42] in terms of the integral of the current density passing through the zero-flux surface between two neighboring atoms. The current intensities and plots were all obtained for a magnetic field that is applied perpendicular to the ring plane of the molecules.

Conflicts of interest

There are no conflicts of interest to declare.

Acknowledgements

Financial support from the Research Council of Norway (grant no. 262229 to AG) and the National Research Foundation of South Africa (grant no. 113327 to JC) is gratefully acknowledged. C. F.-N. acknowledges (1) the CESNET LM2015042 and the CERIT Scientific Cloud LM2015085, provided under the programme "Projects of Large Research, Development, and Innovations Infrastructures" and (2) project CEITEC 2020 LQ1601 with financial support from the Ministry of Education, Youth, and Sports of the Czech Republic under the National Sustainability Programme II.

References

1 H. Furuta, T. Asano and T. Ogawa, *J. Am. Chem. Soc.*, 1994, **116**, 767–768.
2 P. J. Stępień, L. Latos-Grazynski, K. Rachlewicz and T. Glowiak, *Angew. Chem., Int. Ed. Engl.*, 1994, 33, 779.
3 T. D. Lash, *Angew. Chem., Int. Ed. Engl.*, 1995, 34, 2533–2535.
4 T. D. Lash and M. J. Hayes, *Angew. Chem., Int. Ed. Engl.*, 1997, 36, 840.
5 T. D. Lash and S. T. Chaney, *Angew. Chem., Int. Ed. Engl.*, 1997, 36, 839.
6 T. D. Lash, *Chem. Rev.*, 2017, **117**, 2313–2446.
7 A. Ghosh, *Angew. Chem., Int. Ed. Engl.*, 1995, 34, 1028–1030.
8 L. Szterenberg and L. Latos-Grażyński, *Inorg. Chem.*, 1997, 36, 6287–6291.
9 A. Ghosh, T. Wondimagegn and H. J. Nilsen, *J. Phys. Chem. B*, 1998, **102**, 10459–10467.
10 H. J. Nilsen and A. Ghosh, *Acta Chem. Scand.*, 1998, 52, 827–830.
11 D. Li and T. D. Lash, *J. Org. Chem.*, 2014, 79, 7112–7121.
12 D. I. AbuSalim and T. D. Lash, *Org. Biomol. Chem.*, 2014, **12**, 8719–8736.
13 R. R. Valiev, H. Fliegl and D. Sundholm, *Phys. Chem. Chem. Phys.*, 2015, **17**, 14215–14222.
14 I. Benkyi, H. Fliegl, R. R. Valiev and D. Sundholm, *Phys. Chem. Chem. Phys.*, 2016, **18**, 11932–11941.
15 M. StÈ©pień and L. Latos-Grażyński, *Acc. Chem. Res.*, 2005, 38, 88–98.
16 T. D. Lash, *Org. Biomol. Chem.*, 2015, **13**, 7846–7878.
17 T. D. Lash, *Acc. Chem. Res.*, 2016, **49**, 471–482.
18 K. E. Thomas, A. B. Alemayehu, J. Conradie, C. M. Beavers and A. Ghosh, *Acc. Chem. Res.*, 2012, **45**, 1203–1214.
19 A. Ghosh, *Chem. Rev.*, 2017, **117**, 3798–3881.
20 For corroles and other triprotic tetrapyrroles, Au(III) complexes are expected to conform to an innocent, nonradicaloid state of the macrocycle.[18,19].
21 K. E. Thomas, A. B. Alemayehu, J. Conradie, C. M. Beavers and A. Ghosh, *Inorg. Chem.*, 2011, **50**, 12844–12851.
22 K. E. Thomas, H. Vazquez-Lima, Y. Fang, Y. Song, K. J. Gagnon, C. M. Beavers, K. M. Kadish and A. Ghosh, *Chem. – Eur. J.*, 2015, **21**, 16839–16847.
23 H. Fliegl and D. Sundholm, *J. Org. Chem.*, 2012, 77, 3408–3414.
24 Y. J. Franzke, D. Sundholm and F. Weigend, *Phys. Chem. Chem. Phys.*, 2017, **19**, 12794–12803.
25 At the level of theory used, Au[AC1] has a lower energy than Au[AC2] by a margin of 2.7 kcal mol^{-1}.
26 S. R. Graham, G. M. Ferrence and T. D. Lash, *Chem. Commun.*, 2002, 894–895.
27 T. D. Lash, D. A. Colby, S. R. Graham, G. M. Ferrence and L. F. Szczepura, *Inorg. Chem.*, 2003, 42, 7326–7338.
28 M. StÈ©pień, L. Latos-Grażyński, L. Szterenberg, J. Panek and Z. Latajka, *J. Am. Chem. Soc.*, 2004, **126**, 4566–4580.
29 T. D. Lash, A. M. Young, J. M. Rasmussen and G. M. Ferrence, *J. Org. Chem.*, 2011, 76, 5636–5651.

30 D. T. Richter and T. D. Lash, *Tetrahedron*, 2001, 57, 3657–3671.
31 S. C. Fosu, G. M. Ferrence and T. D. Lash, *J. Org. Chem.*, 2014, 79, 11061–11074.
32 A. D. Becke, *Phys. Rev. A: At., Mol., Opt. Phys.*, 1988, 38, 3098–3100.
33 C. Lee, W. Yang and R. G. Parr, *Phys. Rev. B: Condens. Matter Mater. Phys.*, 1988, 37, 785–789.
34 B. Miehlich, A. Savin, H. Stoll and H. Preuss, *Chem. Phys. Lett.*, 1989, 157, 200–206.
35 F. Weigend and R. Ahlrichs, *Phys. Chem. Chem. Phys.*, 2005, 7, 3297–3305.
36 M. J. Frisch, G. W. Trucks, H. B. Schlegel, G. E. Scuseria, M. A. Robb, J. R. Cheeseman, G. Scalmani, V. Barone, B. Mennucci, G. A. Petersson, H. Nakatsuji, M. Caricato, X. Li, H. P. Hratchian, A. F. Izmaylov, J. Bloino, G. Zheng, J. L. Sonnenberg, M. Hada, M. Ehara, K. Toyota, R. Fukuda, J. Hasegawa, M. Ishida, T. Nakajima, Y. Honda, O. Kitao, H. Nakai, T. Vreven, J. A. Montgomery, Jr., J. E. Peralta, F. Ogliaro, M. Bearpark, J. J. Heyd, E. Brothers, K. N. Kudin, V. N. Staroverov, T. Keith, R. Kobayashi, J. Normand, K. Raghavachari, A. Rendell, J. C. Burant, S. S. Iyengar, J. Tomasi, M. Cossi, N. Rega, J. M. Millam, M. Klene, J. E. Knox, J. B. Cross, V. Bakken, C. Adamo, J. Jaramillo, R. Gomperts, R. E. Stratmann, O. Yazyev, A. J. Austin, R. Cammi, C. Pomelli, J. W. Ochterski, R. L. Martin, K. Morokuma, V. G. Zakrzewski, G. A. Voth, P. Salvador, J. J. Dannenberg, S. Dapprich, A. D. Daniels, O. Farkas, J. B. Foresman, J. V. Ortiz, J. Cioslowski and D. J. Fox, *Gaussian 09*, Gaussian, Inc., Wallingford CT, 2013.
37 T. A. Keith, *AIMAll, Gristmill Software*, Overland Park KS, USA, 2017.
38 T. A. Keith and R. F. W. Bader, *Chem. Phys. Lett.*, 1992, 194, 1–8.
39 T. A. Keith and R. F. W. Bader, *Chem. Phys. Lett.*, 1993, 210, 223–231.
40 T. A. Keith and R. F. W. Bader, *J. Chem. Phys.*, 1993, 99, 3669–3682.
41 T. A. Keith, *Chem. Phys.*, 1996, 213, 123–132.
42 T. A. Keith and R. F. W. Bader, *Can. J. Chem.*, 1996, 74, 185–200.